Slipping into Sleep: neurodynamics of alertness transitions in humans and fruit flies

Sridhar R. Jagannathan

Department of Psychology

Churchill College

University of Cambridge

This dissertation is submitted for the
Doctor of Philosophy

March 2019

Declaration

This dissertation is the result of my original work.

It includes nothing which is the outcome of work done in collaboration except as declared in the Preface and specified in the text.

It is not substantially the same as any that I have submitted, or, is being concurrently submitted for a degree or diploma or other qualification at the University of Cambridge or any other University or similar institution except as declared in the Preface and specified in the text.

This thesis does not exceed the prescribed limit of 60000 words (excluding tables, figures, appendices and references) as specified by the degree committee of the Department of Biology.

Sridhar Jagannathan

March 2019

Summary

Slipping into Sleep: neurodynamics of alertness transitions in humans and fruit flies

Sridhar R. Jagannathan

The ability to react to events in the external world determines the fate of every living organism. Such ability corresponds to the general state of readiness often referred to as 'alertness'. Every night we slip into the realm of sleep while our alertness fades away. What happens to the neural machinery in the brain when alertness fades away? How do such transitions of alertness affect behaviour? These questions have important implications ranging from understanding the organizing principles in the brain to the functions of sleep itself. This dissertation aims to explore the dynamics of behaviour during such alertness transitions and to identify the dynamics of the neural machinery responsible for generating such behaviour.

To answer the above questions, I choose organisms that are at the opposite ends of spectrum of complexity. On one hand, I use the richness in behaviour and complexity of the human brain to understand how alertness transitions affects cognitive processes like attention. And on the other, I use fruit flies that display complex behaviour yet have simpler neural dynamics to understand the effect of alertness on the neural machinery over longer time intervals.

First, in order to probe the dynamics of alertness transitions, we must be able to measure the alertness levels in an accurate manner. I argue that a major problem in psychology and physiology experiments is drowsiness (fluctuating levels of alertness). I first show the existing methods (manual) to control for alertness levels are either subjective or too error prone by using inter-rater reliability. I then develop an objective method (micro-measures algorithm) to track alertness levels in a trial-by-trial manner under eyes-closed settings using Electroencephalography(EEG)[1]. I further validate the method in an independent dataset to test its generalisability (Chapter 2). Thus, I provide a unique tool for

probing alertness transitions which can also be used a control method by the cognitive neuroscience community.

Second, I investigate the dynamics of behaviour in alertness transitions. I use a spatial attention task where participants (right-handers) are asked to localize the direction of auditory tones (left or right side) while falling asleep (Chapter 3). I further classify parts of the experiment into 'alert' or 'drowsy' based on the micro-measures algorithm. Then, I use multilevel modelling to show that the proportion of errors in the tones originating from the left direction increases in drowsy conditions (compared to alert). However the error proportion remains unchanged in the tones originating from the right side in the drowsy condition (compared to alert states). Next, I use psychophysics to quantify the subjective mid-line in both alert and drowsy condition and show that the mid-line shifts to the left side (more left errors). Finally I use a hierarchical drift diffusion model (HDDM) to quantify innate bias (starting point) and drift-rate (evidence accumulation rate) and show that differences in behaviour can be explained by drift-rate alone.

Third, I explore the dynamics of neural activity in alertness transitions. For this purpose, I use the same dataset of right-handers as mentioned above. I further use decoding techniques over time (multivariate pattern analysis - MVPA) to identify patterns in the EEG data that discriminate between conditions (Chapter 4). Then, I project these patterns in the source space to identify the locations in the brain that are critically different across conditions. Next, I use variations in the drift rate (computed above) to regress against variations in event related potential (ERP) data. Finally, the patterns of regression are again projected in the source space, revealing convergent patterns similar to the MVPA.

Fourth, I explore the handedness aspect of alertness transitions. For this purpose, I use the spatial attention task as above where participants (now left-handers) perform the tone localisation task while falling asleep. I perform the behavioural analysis as above to show how the performance of left and right-handers are similar under alert conditions while differing under drowsy conditions. I show that different brain regions are involved in performing the same task under alert condition in left and right-handers by presenting evi-

---

[1]EEG is a technique for recording electrical activity of the brain using electrodes on the scalp.

dence from decoding analysis. Further I show that under drowsy conditions brain regions are differently affected in left and right-handers distinctly mapping to performance. Next, I use the drift rate regression with ERP data to provide converging evidence for the brain regions. This highlights a powerful utility of the alertness transitions that it can be used to identify causal mechanisms (Chapter 5) involved in a particular task. Thus, I highlight the issue regarding the majority of neuroscience studies that exclude left-handers neglecting important understanding of the variability of the cognitive function(s) associated with handedness.

To approach the question of alertness transitions in a system amenable to causal manipulation and reduced neural complexity, I chose the fruit fly (*Drosophila melanogaster*). In the fruit fly, I investigated the dynamics of alertness transition by using behaviour and local field potentials (LFP) (Chapter 6). For this purpose, I use the two-channel differential LFP data collected for 24-hour period from flies falling asleep. I then develop an algorithm (similar to the micro-measures algorithm) that can detect fly sleep based on the LFP data and validate it against gold-standard behavioural data. I further show that transition into sleep can be detected using probabilistic classifiers even before the fly actually falls asleep. Next, I collect multi-channel (half-brain probe) data for a 12-hour period from flies falling asleep. I perform spectrum analysis to show how different parts of the fly brain are affected distinctly across awake and sleep conditions. Finally, I show converging evidence from causal experiments with full-brain probe to validate the brain regions and frequency elements detected by the spectrum analysis.

Chapter 7 discusses the significance of the alertness transitions. I discuss how the mapping of alertness transitions - under natural conditions can help us understand some of the unsolved fundamental questions in neuroscience like functions of sleep and mechanisms of general anaesthesia. I also provide a broad overview of how alertness transitions can help understand mechanisms underlying spatial attention.

Finally, in Chapter 8 I draw attention to some of the major limitations of the studies conducted above. I further propose future experiments/analysis techniques that could resolve these issues while adding strength to the theoretical and experimental framework.

*—Study hard what interests you most,
in the most undisciplined, irreverent,
and original manner possible.*

Feynman, Richard

Acknowledgement

I would like to express my sincere thanks to Tristan Bekinschtein, you have been a mentor, a friend, a father figure - teaching me the most important virtues of patience and kindness.

I want to thank the old guard in the lab: Andrés Canales-Johnson, Anat Arzi, Corinne Bareham (for reviewing this thesis as well), Valdas Noreika, Daniel Bor, Will Harrison, Srivas Chennu and my fellow travellers: Alejandro Ezquerro-Nassar, Barbara Jachs, Maria Niedernhuber.

My friends from the Australian lab: Bruno van Swinderen for teaching me flies, african huts and much more. Rhiannon Jeans, Deniz Ertekin, Leonie Kirszenblat for introducing the aussie way to me. To the countless flies who immensely contributed to my scientific quest.

I want to thank my friends Barath, Shyam, Swathi, Ananth for their kind help, belief and motivation in me. To Pip, for showing how awesome a three legged dog can be.

To my dad for teaching me the value of hard work, my sister and my cousin for always being there for me. To my mom - without you nothing.

Note on Dissertation structure

This thesis is based on a combination of traditional chapter based structure and article-based format recently introduced in the University of Cambridge. The Chapters 2,5 take the form of peer-reviewed and preprint journal articles which are either published, submitted or under review during the preparation of this dissertation. In these article-based chapters, I have added a brief introductory statement followed by statements that detail the contribution made by the co-authors in these papers. Next, I have appended the manuscript itself. Finally, I have added a concluding summary that helps to provide an overall context to the manuscript in this thesis.

The other chapters like Chapters (1,3,4 and 6) are written in the traditional format of the dissertation structure. Chapter 7 provides a broad overview and summary of the research questions that were answered in this thesis. Finally, Chapter 8 provides an overview on the future directions of each element of the research question and also provides suggestions on future experiments and analyses that could be carried out to extend the existing-knowledge in this domain.

Contents

Contents

List of Figures

List of Figures

List of Tables

List of Abbreviations

GABA γ-Aminobutyric acid. 43, 46, 47

GFP Green fluorescent protein. 44, 189

HDDM Hierarchical Drift Diffusion Model. viii, 52, 54, 86, 106, 180

ICA Independent component analysis. 80

IFG Inferior frontal gyrus. 26

IPL Inferior parietal lobule. 25–28, 103, 105, 108

IPS Inferior parietal sulcus. 26–28

l-LNvs Large ventral lateral neurons. 47

LFP Local field potential. ix, xiv, xviii, 48, 49, 151–157, 161–163, 165, 168–172, 183, 184, 189, 190

MFC Medial frontal cortex. 10

MFG Medial frontal gyrus. 26, 27

MRI Magnetic resonance image. 98, 181

MTG Middle temporal gyrus. 27

MVPA Multivariate pattern analysis. viii, 29, 50, 51, 53, 54, 94, 95, 106, 178

NE Norepinephrine. 12, 13, 44

PET Positron Emission Tomography. 27

RBF Radial basis function. 163

Rd1 Resistant to dieldrin. 47

REM Rapid eye movement. 47

rmANOVA Repeated measures analysis of variance. 21, 76, 81, 179

ROC Receiver-operating characteristic. 97

ROI Regions of interest. 194

SDT Signal detection theory. 179

SPL Superior parietal lobule. 27, 103, 105, 178

SSVEP Steady state visual evoked potential. 159, 169

STG Superior temporal gyrus. 25–28, 103

SVM Support Vector Machines. 51, 54, 153, 162–164, 187

SWS Slow wave sleep. 47

TMS Transcranial magnetic stimulation. 27

TPJ Temporoparietal junction. 7, 8, 25, 27, 28, 108, 177, 178

VFC Ventral frontal cortex. 7, 8

1

General Introduction

Figure 1.1: "Noon rest" [1]

---

[1] A painting from Vincent Van Gogh depicting an afternoon siesta. Here Van Gogh symbolizes a restful scene set in the rural France of 1860's.

Short Summary

In this chapter, I will first provide a brief introduction to the concept of alertness (using wakefulness) and develop an operational definition of alertness based on the theoretical and experimental framework of attention. I further provide an overview of alertness transitions and introduce both natural and induced forms of transitions. Then, I show how such alertness transitions can be studied from a neurodynamical point of view in humans. Finally I provide a brief overview and motivation of studying alertness fluctuations with fruit flies.

1.1 Alertness

1.1.1 Concept of Wakefulness

Every morning people wake up from the slumber of the previous night (Brown 1970; Dylan 1970). We regain consciousness and often start snoozing the alarm that is blaring at a distance. It is interesting to note that regaining consciousness is only an end point of the waking up process but not a starting stage as it seems. Several other physiological processes like core body temperature and hormones like cortisol level changes precede and trigger the process of waking up itself. Hence it is necessary to differentiate the distinct sub-processes within wakefulness. Wakefulness (Bekinschtein, Cologan, et al. 2009) can be considered to be composed of:

   (a) arousal/responsiveness.

   (b) circadian rhythms.

   (c) sleep cycle.

   (d) homoeostasis.

Arousal refers to arousability which is the capacity to respond to (consciously or not) ex-

ternal stimuli. Circadian rhythms consist of a set of processes that synchronizes the physiological functions to cyclical changes in the environment (Bekinschtein, Cologan, et al. 2009). Sleep cycle refers to sleep patterns of the organism. Homoeostasis refers to the capacity of the body to regulate its internal state in order to maintain a stable condition in the body (Bekinschtein, Cologan, et al. 2009).

Thus the word alertness is used in this thesis in this general context of arousal and the inherent capacity of the system to respond to the external environment.

1.1.2 Framework of Attention

The word Alertness originates from the Italian word *all'erta*, which means to be 'on the watch' (*Alertness Etymology* 1714). Traditionally alertness is considered to be one of the processes of attention. Hence to define alertness it is first necessary to understand the concept of attention. Attention is generally referred to as any process that selectively enhances processing of a subset of stimuli or in general any specific information in the environment.

1.1.3 Types of attentional processes

The process of attention is usually divided into selective and non-selective components (Robertson, Mattingley, et al. 1998). Selective attention denotes the differential processing of sensory information. It can further be subdivided into Orienting and Executive control. While non-selective attention refers to general state of readiness of the system (which is same as the arousal defined earlier).

The following sections provide a brief overview on the types of attention and the various brain networks involved in the corresponding processes.

1.1.3.1 Orienting

Orienting refers to prioritizing a particular sensory input through selecting a particular modality or location (Petersen&Posner 2012). Imagine the response of a dog to a loud sound. The animal immediately turns its head towards the direction of sound and tries to process the information occurring from that direction with priority. Such a response is called an orienting reflex.

Orienting process could be driven by external factors in the environment (bottom-up) such as saliency produced due to any physical property of the stimulus, which is called as stimulus-driven orienting. It could also be driven by internal factors (top-down), which is called as goal-directed orienting.

For example, consider the process of picking out a green 'T' in a crowd of red 'T's (Figure 1.2a). The visual features of the stimuli immediately allows the brain to 'pop out' the green 'T' from the crowd of red 'T's without having to perform a serial item by item search or match. This is referred to as orienting driven by bottom-up processes or stimulus-driven orienting.

On the other hand, consider the task of picking out a green 'T' that is rotated 90 degrees from a crowd of red 'T's and green 'T's (Figure 1.2b). In this case, the colour alone is not useful, as we need to filter out the green 'T's from the target rotated green 'T'. This requires integration of the features of colour and shape to detect the green 'T'. This process of feature integration prevents the pop out of the stimulus and forces us to direct our attention on a particular target (green 'T'). Hence it is referred to as orienting driven by top-down processes or goal-directed orienting.

(a) Bottom-up attention   **(b)** Top-down attention
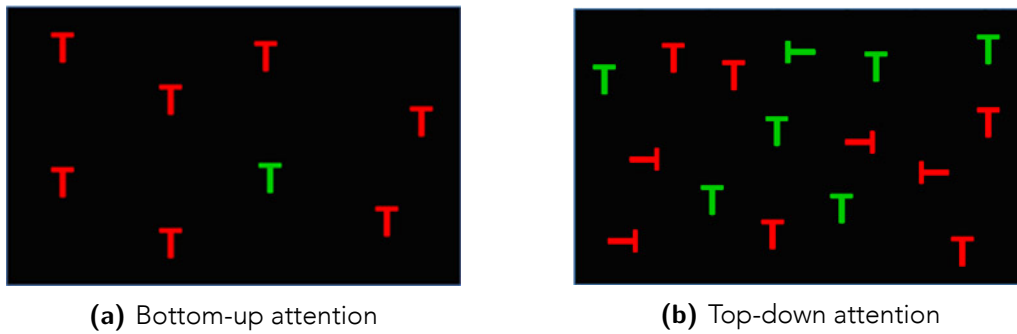
Figure 1.2: Types of Selective attention[2]. Bottom-up attention refers to attention primarily driven by the properties of the stimulus. Top down attention refers to attention primarily driven by internal state of the participant.

Similarly, orienting could also be directed to a particular location in space either by cues generated from the environment (exogenous) or internally (endogenous). For example, think of a target detection task where a cue precedes the appearance of the target in the left or right side. The cue can indicate the direction of the target and hence increase the speed of response. In this case attention is directed to a particular location in space and hence referred to as *spatial attention*. Deficits in certain brain regions can cause individuals unable to direct attention to a particular location in space (typically left side), which is usually referred to as *neglect*.

The next section deals with the brain networks involved in mediating the orienting aspect of attention.

Brain networks:

The influence of fronto-parietal networks in orienting of attention is well established, particularly for visual modality. Several studies with humans (Corbetta, Akbudak, et al. 1998) and primates (Thompson, Biscoe, et al. 2005) have also highlighted the role played by the frontal eye fields (FEF) in mediating the orienting aspect of attention.

The orienting system is divided into dorsal and ventral systems (Figure 1.3). The dorsal system consists of FEF and the intraparietal sulcus, while the ventral system consists of ventral frontal cortex (VFC) and temporoparietal junction (TPJ). Consider a target detec-

---

[2]https://ocw.mit.edu/courses/brain-and-cognitive-sciences/9-00sc-introduction-to-psychology-fall-2011/attention/discussion-attention/

tion task preceded by a cue that has information about the target. Whenever the target is correctly cued, the activity in the dorsal system of FEF and intraparietal sulcus is increased. In case of incorrect cues, the activity in the ventral system allows the participant to switch to the correct target. Specifically, activity in the TPJ of the ventral system is involved in performing the actual switch to the target. In general, the activity in the TPJ is highly right lateralised and deficits in the TPJ interact with the more frontal and dorsal regions to produce *neglect* (lack of attention to the left side of space) syndrome (Corbetta&Shulman 2011).

The mechanism of action of the networks can be analysed (in a causal manner) through pharmacological studies. It has been shown that neuromodulator acetylcholine (Ach) seemed to directly affect the orienting network. For example, studies in monkeys (Davidson&Marrocco 2000) have shown that injecting scopolamine (which is anticholinergic) into the lateral intraparietal region (analogous to the human superior parietal lobe) reduces the ability to orient attention towards a target stimulus.
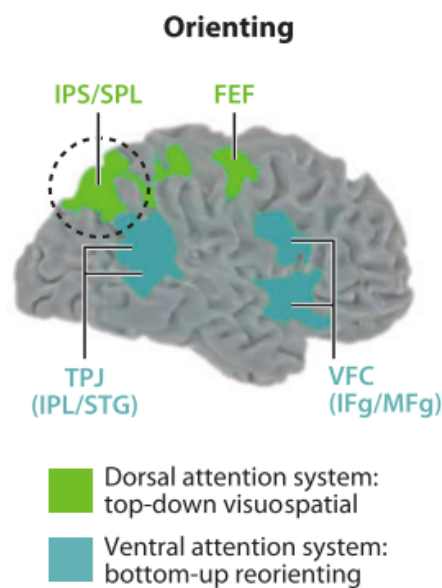
Figure 1.3: Orienting network in humans: Dorsal and Ventral systems [3]. Dorsal attention network is composed of regions in FEF and intraparietal sulcus, while ventral attention network is composed of TPJ and VFC.

To summarise, the dorsal and ventral part of orienting network interact with each other and exert influence on the bottom-up signals to improve the sensitivity of the sensory sys-

---

[3]modified from (Petersen&Posner 2012)

tem, thereby producing faster responses and accurate target detection and thus creating the orienting aspect of attention.

1.1.3.2 Executive Control

Executive control refers to the cluster of the processes comprising of conscious detection of target, response inhibition and conflict monitoring. Detailed explanation for each of these processes is illustrated with examples given below.
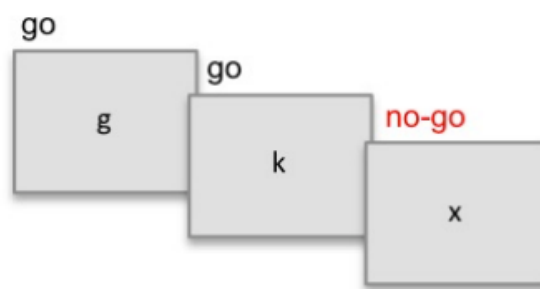
Figure 1.4: Go-NoGo task. Participants need to respond to the task when they see a cue for the 'go' condition (here 'g') and they would need to withhold a response when they see a cue for the 'no-go' condition (here 'k').

Consider the classical *Go-NoGo* task (Figure 1.4), which demonstrates response inhibitory processing. Here participants are asked to respond to the task when they see the 'Go' cue and they are asked to withhold the respond when they see the 'NoGo' cue. This type of task involves withholding a 'habitual' response, that requires executive control. On the other hand, conflict monitoring and resolution refers to the ability to analyse and adjust behaviour in the context of incompatible representations (Hussey&Novick 2012). For example consider the classical stroop task, here participants have to identify the colour of a word displayed on the screen. In some cases though, the words themselves represent another colour. The word 'RED' could be displayed in blue colour, wherein the participants need to identify the colour of the word as blue. Thus the meaning of the word would interfere with the colour being presented on the screen, thereby interfering with the response of the participants. This interference requires resolution of informational conflicts which is provided by executive control.

The next section deals with the brain networks involved in mediating the executive control aspect of attention.

Brain networks:

Studies designed to test for signals involved in top-down task control have revealed two different parts of the executive control network (Figure 1.5). In the first part, these signals reveal a network involved in processing task related instructions that occur in the beginning of the task block. In particular, such signals have been found to reliably activate the fronto-parietal cortex. In the second part, they reveal a network that sustains across the duration of the task. In particular, such signals are found to occur in the cingulo-opercular regions.
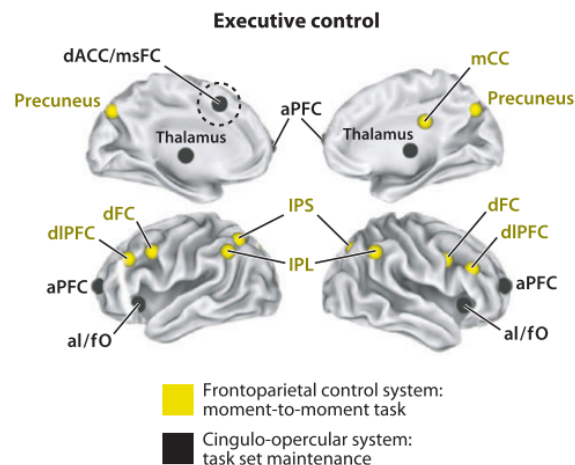
Figure 1.5: Executive control network in humans [4] is composed of two distinct regions. The frontoparietal system is mainly involved in the beginning of the task, while the activity in the cingulo-opercular system is sustained across the duration of the task.

Furthermore, several other studies involved in exploring conscious target detection have reported activation in Medial frontal cortex (MFC), Anterior cingulate cortex (ACC). However the same regions have also been reliably activated in many other tasks associated with cognition, emotion (Botvinick, Braver, et al. 2001),pain and reward processing (Hampton&O'Doherty 2007) which raises the question over specificity of these regions.

---

[4]modified from (Petersen&Posner 2012)

1.1.3.3 Alertness

A more general (non-selective) aspect of attention that allows for enhanced processing of stimuli irrespective of their location or salience is defined as alertness. Alertness is further subdivided into tonic and phasic alertness.

Tonic Alertness:

Tonic alertness (also called as 'intrinsic alertness' or 'sustained vigilance') refers to wakefulness or arousal in the absence of any external cue in the environment i.e. the ability to maintain a 'ready-to-respond' state (Robertson, Mattingley, et al. 1998). This aspect of alertness is usually influenced by factors such as circadian rhythm, body temperature and cortisol levels etc. (Petersen&Posner 2012). This could explain why reaction times (in human studies) usually peak in morning and decrease during the day time and peak again in the night time (showing typical diurnal variation). In laboratory settings, it is often studied with a long uninteresting task where the target occurrence probability is low. Here, the participant could be shown a sequence of stimuli one after the other on a screen. The stimuli could be composed of different geometrical shapes like circle, rectangle, square etc. Correspondingly, there is also a colour associated with the stimuli like red, blue, green etc. A target is said to occur only if two stimuli follow each other that have the same shape but different colour. For example, a red circle followed by a green circle is a target. Whereas, a red circle followed by a red triangle is not a target. Whenever the target appears the participants should indicate with a button press. This example task measures the continuous deployment of attention by the participant over a long range of time. Hence such a kind of alertness is also referred to as sustained attention or vigilance.

Real world examples for tasks requiring tonic alertness could be radar operators scanning the sky for near-threshold changes to detect oncoming objects or security operators in the airports scanning the luggage passing through conveyor belts.

Phasic Alertness:

Phasic alertness refers to the temporary enhancement of alertness due to an external cue in the environment. For example, in a target detection task a warning cue preceding the target can reduce the reaction time compared to a target without a warning cue. The warning cue in essence does not add more information about the incoming target signal, but rather changes the speed with which the orienting aspect of attention can respond. Thus the warning cue typically modulates the resting state prior to the target with an active preparation state that results in faster responses to the target.

The next section deals with the brain networks involved in mediating phasic and tonic alertness.

Brain networks:

In humans, the ability to maintain tonic alertness is dependent on right fronto-parietal systems whereas, the ability to produce phasic alertness is dependent on ascending thalamic-mesencephalic projections (Robertson, Mattingley, et al. 1998). Lesion data from patients with deficits in tonic alertness have confirmed the involvement of the right fronto-parietal systems. Phasic alertness on the other hand has been shown to depend on the neuromodulator norepinephrine (NE). Specifically, whenever a warning cue is presented, activity increases in the *locus coeruleus* (which is a source of NE in the brain). The *locus coeruleus* of a macaque brain is shown in Figure 1.6 which indicates the location of NE pathways. It is crucial to note that in humans, NE pathway traverses the frontal and parietal cortices in the dorsal side but not on the ventral visual pathway, indicating the influence of dorsal fronto-parietal systems on the phasic alerting system.

Several studies have reported differences between tonic and phasic alerting networks. In particular (Coull, Frith, et al. 2000; Fan, McCandliss, Fossella, et al. 2005; Lamb 1998) have found that phasic alerting (triggered by warning cue) relates more to the left cerebral cortex, while tonic alerting is related more with the right cerebral cortex as mentioned above.

In terms of electrophysiological correlates, EEG studies in humans have shown that contingent negative variation (CNV)[5] has been shown to increase (Walter 1964). In general,

the source of the CNV (which is related to NE systems) is found across the anterior cingulate and neighbouring brain regions.
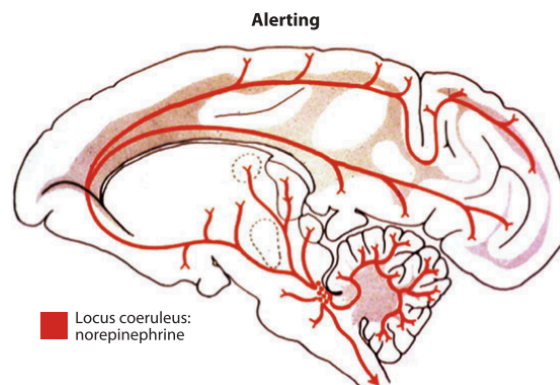
Figure 1.6: Alerting network in a macaque brain [6]. The *locus coeruleus* projections are shown on the macaque brain. The diffuse connections of the alerting systems are known to modulate the more localized connections of other systems.

1.2 Transitions of alertness

The fluctuations or transitions in alertness can usually be divided into two different types based on their triggering cause. Examples of natural transitions include the process of falling asleep. While unnatural transitions include those induced by anaesthetic drugs like propofol etc. Such drugs are used to alleviate pain and sedate patients for surgery. The process of falling asleep produces many interesting neural and behavioural dynamics that provides us with a window to see how the brain reconfigures and prepares itself for reaching deeper sleep states.

The following is a brief introduction to behavioural and physiological changes associated with both transitions to sleep and anaesthesia, after which much more of the focus will be on transitions to sleep.

---

[5]CNV is a slow negative potential in EEG that occurs between a warning cue and an oncoming stimulus which is known to be modulated by NE systems.
[6]modified from (Petersen&Posner 2012)

1.2.1 Transitions to sleep

To understand the transition to sleep, it is first pertinent to define sleep. Sleep is usually defined as the state of reduced or lack of activity. Behaviourally, sleep should satisfy the following criteria (Goupil&Bekinschtein 2012):

 (a) state of inactivity.

 (b) reduced response to stimulus or increased arousal threshold.

 (c) specific posture (like lying down in humans).

 (d) reversible (ability to come out of sleep naturally).

Sleep is driven by two interacting processes namely homoeostatic and circadian (Borbély 1982). The homoeostatic process refers to the drive to sleep that is mainly triggered by the accumulations of sleep-inducing chemicals in the brain. The circadian process on the other hand controls the timing of sleep, which in turn corresponds to the light-dark cycle. For example, when someone is sleep deprived today, the total sleep duration tomorrow would compensate for the duration of sleep lost today. This compensation is mainly driven by the sleep-wake homoeostasis process. Whereas, the trigger to sleep at night is determined by the circadian process. The central clock that controls this circadian process is located in the anterior hypothalamus. While the sleep onset itself is triggered by mutual inhibition of arousal system in the brainstem, posterior hypothalamus and basal forebrain (Goupil&Bekinschtein 2012).

The physiological aspects of sleep onset include the following activities. Core body temperature gets reduced while the peripheral temperature gets increased (Van den Heuvel, Noone, et al. 1998). Slow rolling eye movements occurring at the sleep onset is also reflected in the changes in the EEG activity (Tanaka, Hayashi, et al. 1996; Ogilvie 2001). The respiratory activity also gets reduced, followed by decreased heart rate (Baharav, Kotagal, et al. 1995; Pivik&Busby 1996). Several studies have also observed decrease in skin potential negativity (Tanaka, Hayashi, et al. 1996; Šušmáková&Krakovská 2008).

1.2.2 Transitions with anaesthesia

Anaesthesia is usually defined as the state of loss of consciousness. Behaviourally, Anaesthesia encompasses the following aspects (Kopp Lugli, Yost, et al. 2009):

(a) immobility.

(b) amnesia or loss of memory.

(c) unconsciousness.

(d) reversible (ability to come out of anaesthesia).

The above-mentioned change in behaviour is created by various changes in the physiology is mentioned below.

Immobility is produced by the interaction of the anaesthetics with the spinal cord. The evidence for this includes studies (Antognini&Schwartz 1993; Rampil, Mason, et al. 1993; King&Rampil 1994; Rampil&M.S. 1994) wherein they showed the effect of anaesthetics on sub-cortical structures to inhibit the motor responses, which would otherwise be produced for painful stimuli. Amnesia is produced by the effect of anaesthetics on several regions (Kandel 2001) like hippocampus, amygdala, prefrontal cortex etc. Different types of memory are also affected in distinct ways. Explicit memory (consciously acquired information) is affected in clinical levels of anaesthesia. However implicit memory (unconsciously acquired) seems to be less affected under clinical concentrations (Alkire, Gruver, et al. 2008; Bennett, Davis, et al. 1985; Ali, Ghoneim, et al. 1991; Biebuyck, Ghoneim, et al. 1992; Iselin-Chaves, Willems, et al. 2005). Hence several tools based on EEG such as the Bi-spectral index (BIS), entropy level monitoring, auditory evoked potential measurements have been developed to explicitly quantify the effect of the anaesthetic.

In the following sections we cover the behavioural and neural dynamics of natural transitions i.e. transition into sleep in a detailed manner.

1.3 Behavioural aspects of transitions

As participants transition into sleep, they lose the ability to respond to stimuli in the external environment. This loss of response could be measured by two kinds of paradigms. Active paradigms, where the participant has to respond with a button press after every stimuli (for e.g. auditory tone). Passive paradigms, where participants exert a continuous pressure on a button box. In the case of active paradigms, sleep onset can be measured with the lack of responses to the stimuli. For the passive task, the release of pressure corresponds to sleep onset. While there has been debate about the choice of task to measure the transition (active or passive), the active tasks offer much more flexibility and variety (in terms of stimuli and responses) while being a bit more intrusive (Ogilvie 2001) to the participant.

For example, consider a typical EEG experiment wherein a participant responds to an auditory stimulus while falling asleep (Kouider, Andrillon, et al. 2014). In the start of the experiment (wherein the participant has high alertness level), they respond reliably to the stimulus as shown by green dots in Figure 1.7. As time elapses, the participant starts to fall asleep (wherein the alertness levels drop) and intermittently fails to respond as shown by red dots. The mechanism behind the cessation of responses is thought to be interplay between stimuli perception and response production. When this behavioural transition starts to happen we can also notice changes in the spectral profile of the EEG collected from occipital sites. The frequency spectrum of the pre-trial periods shows that power in the alpha range (8-12 Hz) reduce and the power in the theta range (6-8 Hz) increases. More detailed description of these spectral changes are described in the next section.

In another study (Noreika, Canales-Johnson, et al. 2017), a target sound was presented which was followed by a masking noise. Participants were asked to indicate via button press if they detected the target sound. They were also allowed to fall asleep as above and EEG data was again collected to measure changes in the spectral profile. Psychometric fitting indicated that threshold of detection of stimuli was not modulated by alertness while the slope of hit rate (which indicates variability in neural processes) changed in a sig-

nificant manner. These results point to the fact that different aspects of decision making are modulated by transition to sleep in a distinct manner.
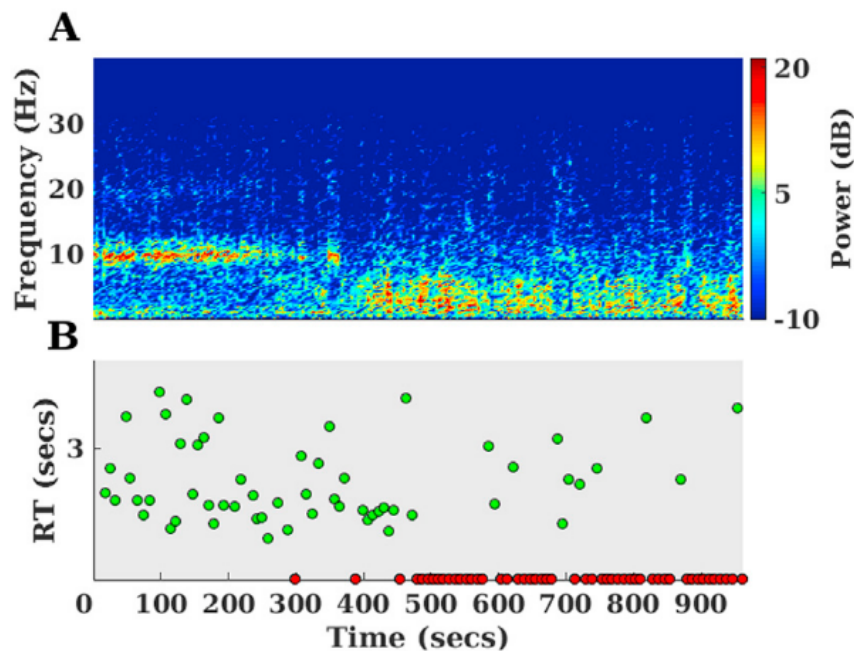
Figure 1.7: Transitions of Alertness[7]. Example of a participant falling asleep, which shows changes in frequency profile and variability in reaction times. (A) depicts changes in spectral power over the occipital sites in the pre-trial period. (B) Reaction times for trials presented at different time points in the same experiment. Red dots indicate cessation of response, while green dots indicate responses.

To summarise, the transition to sleep is followed by increased variability in reaction times (Ogilvie 2001) whereas in more complex tasks the accuracy of responses is also compromised. In the next section we try and understand how specific aspects of selective attention (spatial attention) is modulated by such variation in alertness levels.

1.3.1 Spatial attention & alertness

A recent study (Bareham, Manly, et al. 2014) has provided first evidence (by using direct physiological measures of alertness) that variation in alertness levels produces a modulation of behaviour in a auditory spatial attention task. In this study, right-handed individuals under eyes closed condition performed an auditory tone localization task while falling asleep. The participants showed very little bias (misclassification of tones) when

---

[7]adapted from (Jagannathan, Ezquerro-Nassar, et al. 2018)

they were fully alert. But when they began to fall asleep they produced more misclassification of tones from the left direction (left-errors) compared to the right direction tones (right-errors).

In order to contextualize this spatial attention task and to understand the behavioural dynamics of this task across varying alertness levels, we need to first review the effect of alertness on spatial attention both from clinical and cognitive perspectives.

1.3.2 Unilateral Spatial neglect

Some patients that have cerebral lesions face difficulties in detecting and localising information coming from the side of the space opposite to the lesion (Brain 1941). This debilitating condition is called as *unilateral spatial neglect*. Several studies(Bisiach&Luzzatti 1978; Marshall&Halligan 1988; Karnath, Christ, et al. 1993) have considered neglect to be a deficit of attention and not a primary sensory dysfunction. This is mainly because such deficits can be reduced by presenting salient sensory stimuli (Robertson, Mattingley, et al. 1998). It has been further shown (Bowen, McKenna, et al. 1999) that patients with damage in the right hemisphere (hence left inattention) is markedly more persistent than those with damage in the left hemisphere (right inattention).

Neglect patients most of the time are impaired in shifting their attention to one half of the space and also claim that they are unaware of the presence of stimuli on that side of space. Hence it would be pertinent here to understand the important theoretical differences between attention and awareness. Consider the case of change-blindness in healthy individuals, here observers fail to notice changes in visual scenes when the change happens too fast or if the change co-occurs with a distracting stimulus (even though the changes are obvious). It was argued that observers do not detect changes as they are not paying attention to the changed object. Hence, it may seem intuitive to us that attending to an object and being aware of the object are the same thing. However, consider the case of blind-sight, here patients that have lesions in the primary visual cortex (V1) can respond to stimuli (detect, localize and discriminate aspects of stimuli) even though

they claim to be not aware of them. Furthermore, recent evidence using psychophysics in healthy populations has shown that attention and awareness are distinct entities that can be modulated separately. While attention boosts neural signals (measured with Blood Oxygen Level Dependent - BOLD imaging) in the primary visual cortex, awareness does not seem to modulate the same (Watanabe, Cheng, et al. 2011). In this thesis the main focus is on attention with awareness (as in the case of the auditory spatial attention task from (Bareham, Manly, et al. 2014)). Spatial neglect also falls under this category and hence it is a suitable model from the cognitive perspective of both attention and awareness absent together and as well as from the behavioural perspective of lack of attention to one side of space.

Translation/Rotation of subjective mid-line

Several neuropsychological studies have aimed to quantify the lack of attention in the contralesional side. Most of these studies have aimed at quantifying the subjective mid-line and its corresponding shift from the veridical center. Studies (Vallar, Guariglia, et al. 1995) led by Vallar first investigated whether spatial bias in neglect patients involved a translation of the subjective mid-line or rotation of the body's vertical axis both in the front and back coordinates of space. Using an auditory localization task on patients with right hemisphere damage, they showed the existence of rightward bias in both the front and back space. Thus indicating evidence for translation of subjective mid-line. On the other hand, studies (Karnath 1997) led by Karnath asked patients to direct an LED light to the subjective mid-line and showed that the mid-line is rotated in the earth-vertical body axis. However both studies agree that the mid-line in the front space of the subject is shifted to the right (for which both a translation and rotation explanation hold good).

Alertness & Spatial bias

As mentioned before, it has been shown that left inattention (neglect) following right hemisphere damage is much more persistent than right inattention following left hemisphere damage. One of the main explanations given to this is that, the right hemisphere is specialized for spatial attention. Consequently, when the left hemisphere is affected, the right hemisphere can compensate for the spatial function. However, when the right hemisphere is affected, the left hemisphere cannot compensate, thus producing left-neglect.

However in patients with spatial neglect the location of the lesions is heterogeneous and also affects a variety of cortical and sub-cortical structures. Thus the lesion evidence points to a more diffuse set of processes causing left neglect. Neuropsychological studies (Robertson, Manly, et al. 1997) showed that performance in sustained attention task (that require alertness) predicted persistent neglect bias. Further (Robertson, Mattingley, et al. 1998) showed that phasic alerting (increase in alertness levels) reduced the neglect. All of these studies point to an increasing body of evidence linking alertness with spatial neglect.

To summarise, we have so far established a link between spatial bias (left neglect) and alertness in patients with right hemispheric damage. However, in these studies we could not compare the performance of individuals before and after lesion to establish the causal nature of the link. This leads us to the question, if this link can be probed in healthy populations. In the next section we take the cognitive perspective to try and understand the phenomenon of spatial bias in healthy populations.

1.3.3 Pseudoneglect

When healthy adults participate in a line bisection task, they are asked to judge the middle of a horizontal line. In these cases they tend to show a small bias towards the left side of the actual mid-line (Jewell&McCourt 2000). The right hemisphere dominance in visuospatial attention is thought to be the main factor in this phenomenon. Further the two hemispheres produce two competing attentional gradients on their contra-lateral side of space (Kinsbourne 1970). In such cases pseudoneglect is simply produced by greater activation in the right hemisphere thereby directing attention towards the left side of the line, which makes the mid-line appear to the left of the actual centre (Fink, Marshall, et al. 2001). Apart from attention, there is a range of other factors like hand used in bisection task (Chokron&Imbert 1993; Dellatolas, Coutin, et al. 1996), gaze direction (Chokron&De Agostini 1995) etc. that influence and modulate activity in one or both the hemispheres.

In this context, (Bareham, Manly, et al. 2014) was one of the first study (by using direct

measures of alertness levels) to establish the existence of alertness induced spatial bias in healthy right-handed participants. In this task attention was modulated by changing levels of alertness by allowing participants to fall asleep while localizing tones coming from left and right side of the mid-line. Alertness levels of individual participants were measured using EEG based techniques like alpha-theta ratio and Hori scoring, it was shown (Figure 1.8) that error rate on left tones became higher as the participants became drowsier.
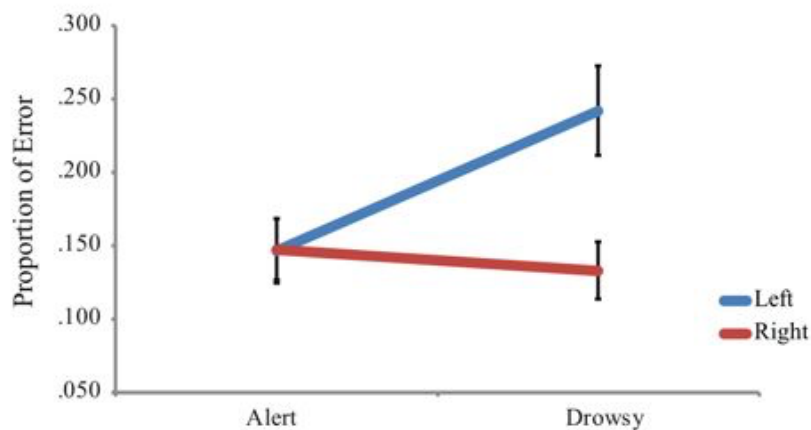
Figure 1.8: Error rates in auditory spatial attention task [8]. Under alert conditions, the error rates of participants are similar across left and right tone. Under drowsy conditions, the error rates of left tone were significantly higher than right tones. Error bars represent standard error of the means.

However, there were several shortcomings associated with this study. First, the method for measuring alertness in this task was based on alpha-theta ratio or Hori scoring. Alpha-theta ratio method (see next section) assumes equal number of trial as 'alert', 'drowsy' (per participant). We know that this is not true, as different participants fall asleep differently (some more drowsy, some less drowsy). Hori scoring (see next section) suffers from the subjective nature of the scorer and hence it has high degree of variability between different scorers. Second, there was no separate baseline task to measure the bias of the individual participant before the experiment. if such a bias was measured before hand, then it could be compared with the bias in the drowsy session to measure the change in bias. Third, some tones (1.86° to 35°) were presented more times than others (40° to 60°), which could potentially bias the results. Fourth, the methods used to analyse the relationship between bias and alertness (repeated measures ANOVA -rmANOVA) assume

---

[8]adapted from (Bareham, Manly, et al. 2014)

individual participants had equal number of trials in 'alert' and 'drowsy' condition, which is not true as different participants fell asleep in different ways. Fifth, the quantification of subjective mid-line as proportion of left tone errors versus right tone errors ignores the variability afforded by tones from -60° to +60°. Such variability could be captured by psychometric fitting in individual participants. Sixth, distribution of reaction times could be used in a much more prudent way to capture the decision making process using sequential sampling models like drift diffusion modelling.

1.3.4 Research Question

The above mentioned reasons led us to our first research question.

Does variation in alertness levels systematically produce bias in spatial attention?

The above question can be further subdivided as:

(a) *Can a more objective method be used to measure alertness levels lead to same spatial bias?*

(b) *Would the spatial bias change if there was a separate baseline session to measure alertness prior to the drowsiness session?*

(c) *Can we utilize methods like multi-level modelling that take advantage of uneven trial numbers per participant per condition? Would the spatial bias results still hold good?*

(d) *Can the shift in subjective mid-line be estimated systematically using psychometric fits? Would the subjective mid-lines shift with drowsiness?*

(e) *Can we use measures that capture the process of evidence accumulation (like drift-diffusion modelling)? Would that show any systematic change in response bias? or evidence accumulation rate?*

(f) *Can these behavioural dynamics be used to understand the underpinning mechanisms of alertness induced spatial bias in these right-handed participants?*

To summarise, so far we have explored the behavioural aspects of transitions into sleep that led us to our first research question of understanding the behavioural dynamics of alertness induced spatial bias. In the next section we briefly review the neural aspects of transitions to sleep that would lead us to our second research question.

1.4 Neural aspects of transitions

The changes in neural activity in the transition to sleep can be explored with neuroimaging. The above mentioned variability in reaction times when a participant transitions into sleep is produced due to an interplay between the thalamus (the thalamus is the hub that transmits information from the sensory systems to the cortex) and fronto-parietal regions (Noreika, Kamke, et al. 2017). The reduced ability to perceive stimuli during this transition is created by thalamic deactivation as evidenced by (Magnin, Rey, et al. 2010). This was again verified by the ability to detect a target which is measured using the response of P300[9]. When a participant moves into lower stages of alertness it was shown that P300 evoked by a deviant stimulus gradually reduced (Cote, de Lugt, et al. 2002). The evidence for impairment of higher cognitive processes (decision making, motor action execution etc.) comes from the reduced activity in prefrontal cortex and *locus coerulus* (Usher, Cohen, et al. 1999; Kaufmann, Wehrle, et al. 2005; Magnin, Rey, et al. 2010). While results from (Noreika, Kamke, et al. 2017) has shown that it is the rapid re-organization of fronto-parietal networks which results in impairment in decision making. The variability in anatomical locations could be possibly due to the variation in the cognitive demands elicited by the different tasks across these studies.

As explained in the previous section the variability in reaction times when a participant transitions into sleep is also reflected in the EEG spectrum. Classically EEG data was studied using sleep stages, which were defined on the basis of 20-30 seconds of data, however changes in the EEG happen in a much finer range which is also reflected from the timing of the cognitive processes (Tanaka, Hayashi, et al. 1996). Hence, this has led

---

[9]P300 is a positive deflection in event related potential (ERP) recorded with EEG, which occurs after 250-500ms of stimulus presentation.

to the formulation of a new system by Hori and collaborators that resulted in more fine-grained measure of alertness compared to the classical N1/N2/REM system. The Hori scale is based on elements like alpha and theta waves, vertex sharp waves, spindles etc. The Figure 1.9 depicts different elements found in EEG across Hori stages. The validity of these different Hori stages has been verified by an ordinal relationship between the reaction times and the corresponding stages. The mean reaction time was found to increase with the 9 stages in a linear manner (Ogilvie 2001).
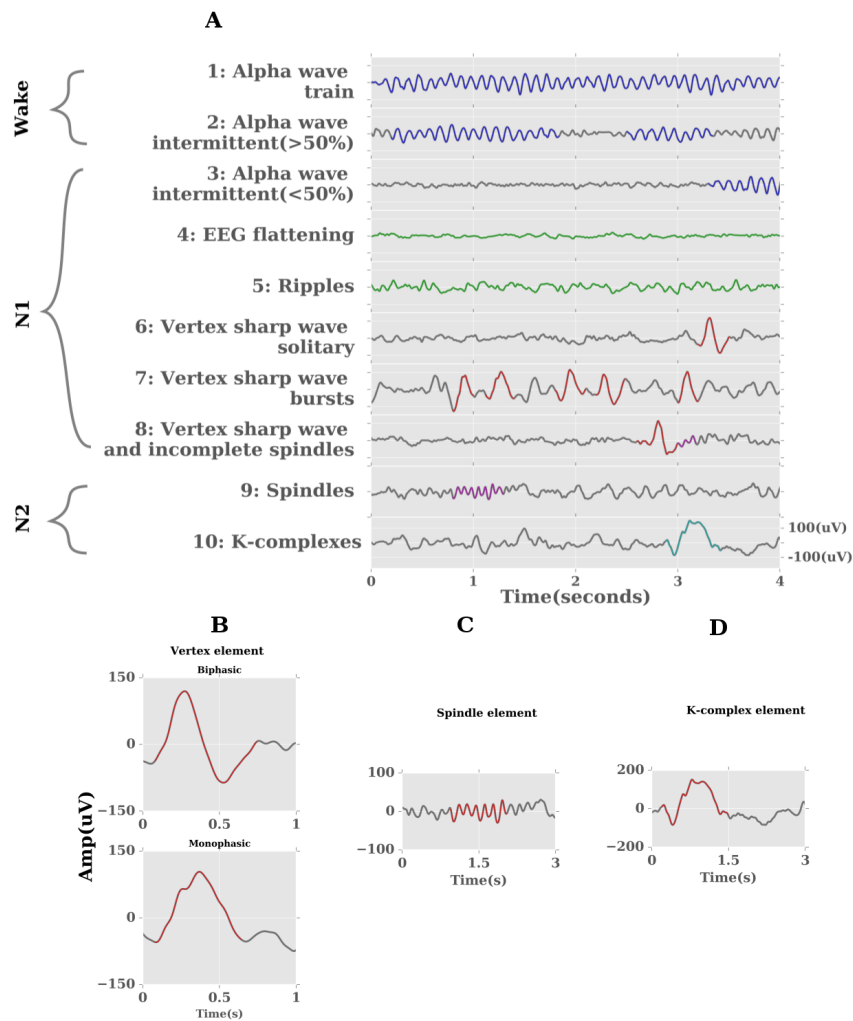
Figure 1.9: Modified Hori stages [10]. (A) Modified Hori scale for detecting differing alertness levels using EEG. Graphoelements of Hori scale in detail (B) Vertex sharp waves are either Biphasic or Monophasic. (C) Spindles are transient patterns with frequency (12 to 16 Hz). (D) K-complex elements are sharp positive deflection followed by a larger negative one.

---

[10]adapted from (Jagannathan, Ezquerro-Nassar, et al. 2018)

The classical Hori scale were limited to 9 stages and the rationale behind addition of the 10th stage is explained in the next chapter.

The classical sleep stage N1 corresponds to the stages 3-8 in the Hori scale, while the stage N2 corresponds to the stage 9 in the Hori system. Though Hori stages are categorized from 1 to 9 rarely participants pass through these stages in an orderly manner. Some subjects that have suppressed alpha (due to structural differences in the occipital cortex) do not usually show the Hori stages 1-3. While some subjects do not show Hori stages 4-6 (Tanaka, Hayashi, et al. 1996; Oken, Salinsky, et al. 2006).

So far we have seen the use of Hori scale to systematically measure the neural dynamics of transition to sleep. In the next step, I establish a framework to understand the neural dynamics behind the alertness induced spatial bias mentioned in the previous section. In order to contextualize the neurodynamics involved in the alertness modulated spatial attention task, we need to first review the existing neuroanatomical models on neglect, spatial attention, alertness, pseudoneglect.

1.4.1 Neuroanatomical models on neglect

Studies with stroke patients have supported that damage to the following areas in the brain to be involved in neglect: anterior, posterior cortical regions (Vallar&Perani 1986) caused by middle cerebral artery stroke (Bartolomeo, Thiebaut de Schotten, et al. 2007), basal ganglia and thalamus (Vallar 2003) caused by posterior artery stroke (Bartolomeo, Thiebaut de Schotten, et al. 2007). These results point to regions that could be considered as 'critical' to generate neglect. This prompted large scale studies to be conducted to identify such 'neglect critical' areas. Findings from (Mort, Malhotra, et al. 2003) point to common areas in the TPJ and Inferior parietal lobule(IPL). However findings from (Karnath, Fruhmann Berger, et al. 2004) showed common areas in the superior temporal gyrus (STG). Perfusion studies from (Hillis, Newhart, et al. 2005) have implicated right STG in allocentric neglect (where left side of objects are ignored, even when they are located in both sides of space). While egocentric neglect (neglect of stimuli located to the left side)

was implicated (Hillis, Newhart, et al. 2005) to right angular gyrus. While personal neglect (supramarginal gyrus in the parietal lobe), extrapersonal neglect (STG and inferior frontal gyrus (IFG)) were implicated by (Committeri, Pitzalis, et al. 2007).

An alternative approach developed by (Corbetta, Kincade, et al. 2005) focussed on the dorsal and ventral systems of attentional processing systems (mentioned before). The dorsal pathway (involving FEF and IPS) consisting of fronto-parietal areas were responsible for spatial orienting and visuomotor control (hand-eye coordination), tasks which are chiefly affected in neglect. However Corbetta and colleagues argue that brain regions typically affected in neglect belong to the ventral processing system (IPL, STG, MFG, and anterior insula). These ventral system regions (associated with alertness, vigilance) feed dorsal systems with potentially important signals. Thus, damage to the ventral system can produce impairment in functional connectivity in the fronto-parietal regions that could cause a bias in spatial attention (He, Snyder, et al. 2007). Further a region near IFG was identified (He, Snyder, et al. 2007) as a key connecting point between ventral and dorsal systems. Similarly, functional connectivity between frontal and parietal regions was found to be disrupted in studies (Thiebaut de Schotten, Urbanski, et al. 2005) leading to neglect-like effects. Similarly lesions in sub-cortical areas like superior longitudinal fasciculus (Doricchi&Tomaiuolo 2003) were also found to be affected in neglect patients. This lead them to think that neglect produces disconnection between frontal and parietal regions and hence coined the term 'disconnection syndrome' for neglect.

1.4.2 Neuroanatomical models on spatial attention

Studies by (Corbetta&Shulman 2002) have shown that two distinct types of attention (top-down, bottom up as mentioned before) map onto distinct regions in the brain that interact with each other to direct attention. Top-down or goal oriented attention activates regions in superior frontal cortex and intra-parietal cortex. While bottom up attention (exogenous; detection of relevant stimuli) activate regions in right hemisphere like inferior frontal cortex and temporo-parietal cortex. Studies from (Silver&Kastner 2009) using

topographical maps in fMRI have shown that right superior parietal lobe (SPL), IPS, supplementary and FEF were involved in attentional processing.

Again Studies by (Corbetta&Shulman 2002) have shown that TPJ was activated when attending to behaviourally relevant stimuli. They showed that the right TPJ was activated in both directions of attentional shift. While STG was found to be activated in studies (Danckert&Ferber 2006) involving spatial memory. Further studies by Corbetta and colleagues (Shulman, Pope, et al. 2010) have shown that activation in the ventral stream (TPJ) was required to shift attention. Further studies by (Szczepanski&Kastner 2013) using transcranial magnetic stimulation (TMS) have shown that when activating the right or left posterior parietal lobule, attention shifted to the ipsilateral direction.

To summarise, the capacity to shift attention relies on areas that are both bilateral in the dorsal stream (fronto-parietal regions) while primarily right lateralised in the ventral stream (TPJ, IPL etc.)

1.4.3 Neuroanatomical models on alertness

One of the first studies (Kinomura, Larsson, et al. 1996) that investigated the brain regions involved in alertness used Positron Emission Tomography (PET). In short, participants were asked to perform an attentionally demanding visual and somatosensory detection task which was compared to the activity of brain at rest. Compared to rest, activity in right thalamic nuclei and midbrain reticular formation system was found to be increased. Further studies by (Sturm, de Simone, et al. 1999) showed that intrinsic alertness (ready to respond state) was associated with increase in brain activity of a number of right hemispheric regions like anterior cingulate, MFG, MTG and STG, brainstem and thalamic regions. This led Sturm and colleagues (Sturm, de Simone, et al. 1999) to propose a network of brain regions composed of frontal-parietal-thamalus-brainstem involved in the deployment of intrinsic alertness. Further studies by (Fan, McCandliss, Sommer, et al. 2002) attempted to disentangle brain regions involved in alerting, orienting, executive control network. They found that distinct brain regions were involved in the above mentioned processes. The

orienting process activates the FEFs and some parietal locations. While executive control process activates several cortical regions indicating the complex nature of processing. While, alerting process involved thalamus and fronto-parietal regions (mainly right TPJ).

To summarise, neglect seems to involve a variety of brain regions mainly TPJ, IPL, STG etc. While spatial attention seems to involve a set of bilateral dorsal (IPS, FEF) regions, right lateralised ventral (TPJ, IPL) regions. Alertness seems to involve mainly regions in thalamus, fronto-parietal regions like right TPJ.

1.4.4 Neuroanatomical models on pseudoneglect

The following are the potential candidate models that could be considered for pseudoneglect (occurring in healthy participants) based on the neglect based studies (conducted with patients) mentioned earlier.

Right hemisphere specialization

Studies from (Vallar&Perani 1986) propose that attention is a right hemisphere specialized function. This is conceptually similar to how aspects of language production is now proposed to be a left hemisphere lateralised function (Ojemann 1991). Further, as discussed earlier alertness is also considered a right hemisphere lateralised system. This makes the right hemisphere highly active in the spatial attention task, whereby directing attention more to the left side of the space. Hence any damage to the right hemisphere would produce co morbid deficits in alertness and attention (Corbetta&Shulman 2011; Robertson, Mattingley, et al. 1998).

Inter-hemispheric competition

Studies from (Kinsbourne 1977; Cohen, Romero, et al. 1994) propose that both the hemispheres compete with each other for attention directed to the contra-lateral space. This finely balanced system allocates attention on the basis of mutual inhibition. The right hemisphere pulling attention to left side of space, while the left hemisphere pulling attention to the right. Hence any damage to the right hemisphere results in the system

being unbalanced and tilts the balance in favour of the left hemisphere, thus directing attention disproportionately to the right side of space (Mesulam 1981).

In both the models, as the participants lose alertness, the right-hemisphere activity gets reduced thereby leading the left-hemisphere to take over. This potentially pulls attention attention to the contra-lateral space (right side), thereby attending more to the right side and not to the left side.

In this context, (Bareham, Manly, et al. 2014) (detailed in the previous section) where participants show spatial bias while falling sleep provides a healthy model to understand the neural mechanisms underlying spatial neglect.

Before we try and understand the neural mechanisms behind neglect, we need to define the characteristics of analysis methods that are best suited to tackle this problem. First, the neural machinery involved in spatial attention, alertness, neglect is composed of a variety of regions that are heavily dependent on the corresponding task being performed by the participant. Hence we need a technique that doesn't depend on *a-priori* definitions of regions involved. Techniques like multivariate pattern analysis (MVPA) satisfy this requirement by involving a data-driven approach that can further be used to identify the temporal and spatial signatures involved in spatial bias induced by low alertness. Second, as we have established in the previous section, we need a computational model of decision making that can explain the behaviour of participants in a trial-by-trial manner. Drift-diffusion model (in previous section) can be used to estimate parameters like evidence accumulation rate (v) and response bias (z) in a trial-by-trial manner. But the crucial aspect would be to connect this decision making model with the neural markers. This would establish converging evidence between the MVPA based analysis and behaviour based drift-diffusion model.

1.4.5 Research Question

The above mentioned framework sets up our quest to investigate the neural dynamics involved with spatial biases during sleep onset, which can be summarised in our second research question.

What changes in neural dynamics (that occur due to variation in alertness levels) can systematically lead to bias in spatial attention?

The above question can be further subdivided as:

(a) *What are the neural patterns that are crucial for performing the spatial attention task when participants are alert?*

(b) *How does these neural patterns change when the participants become drowsy?*

(c) *What are the neural patterns that are involved in generation of spatial bias when participants become drowsy?*

(d) *Can we estimate the spatial and temporal signatures that encode parameters in a decision making model like drift-diffusion?*

(e) *Would these spatial and temporal signatures generated with the computational model on behaviour concur with our neural patterns identified earlier?*

(f) *What neuroanatomical model of spatial bias would these patterns support: Inter-hemispheric competition or Right hemisphere specialization?*

1.5 Handedness aspects of transitions

It is crucial to note that the majority of patients suffering from neglect (and fail to recover) have damage in the right hemisphere (Bowen, McKenna, et al. 1999; Farne, Buxbaum, et al. 2004; Karnath 2007). Hence it was interesting to understand how the models of pseudoneglect in healthy participants (*Right hemisphere specialization,Inter-hemispheric*

competition) could explain the left neglect suffered by patients. However the main confounding factor in these models of neglect is that majority of patients that suffer neglect are right handed individuals. This leads to an interesting question on whether handedness plays an important role in biasing spatial attention. Before we try and understand how handedness influences spatial attention, it would be prudent to understand the definition and origin of handedness in humans.

1.5.1 Handedness

Approximately 10% of the population in the world is left-handed (Hardyck&Petrinovich 1977) while the rest identify themselves as right-handers. Theories of handedness can be divided into environmental and genetic factors that are chiefly responsible for its origin. It is important to understand the origin of handedness so that it can also later be connected to the differences in neuroanatomy between left and right-handed individuals.

Environmental factors

One line of thought is that handedness is mainly caused by evolutionary adaptation. This could explain why the proportion of ambidextrous people are low in the general population, however it fails to explain the highly disproportionate number of right-handers compared to left-handers (Bishop 1990). Another potential explanation is that handedness is a learned behaviour that is created due to cultural and societal pressures. However, this argument also fails to explain why right-handers are prevalent everywhere irrespective of geographical and cultural factors (Connolly&Bishop 1992; Marchant, Mcgrew, et al. 1995). Thus the abundance of right handers crossing cultural and geographical diversity points to potential biological factors influencing it (Bishop 1990).

Genetic factors

Studies using twins (both monozygotic, dizygotic) have investigated the heritability of handedness as a trait. Some reports have argued that Left handedness is more prevalent in twins than singletons (indicating genetic factors), however evidence from (McManus 1980) have questioned the measures on which both twins and singletons were evaluated.

A higher prevalence of left handedness in twins may be related to common pre-natal and environmental factors rather than genetic factors. (Bishop 1990) also point to the fact that incidence of one of the twins being left and other being right handed is high and equally common across mono and dizygotic twins, thus challenging the idea of simple genetic factors. Another influential theory accounting for handedness is right-shift theory developed by Annett (Annett 1975). According to this theory, handedness genotypes are usually biased to the right or unbiased. Though handedness is influenced by chance, the right-shift provides an advantage to the right hand. Also, for individuals born with no preference of hands, the cultural factors play a role in making them more right-handed. Further as handedness is influenced by right-shift allele, this would also mean lateralisation (left hemisphere specialization) of language function. However this argument fails when individuals that are right handed present with lateralisation in language in the right hemisphere itself.

Overall it is interesting to note that both the environmental and genetic factors on their own cannot explain the origin of handedness and the abundance of right-handed individuals in the general population. In the next section, I aim to understand how handedness could influence hemispheric lateralisation in the brain. This is highly relevant to understand the potential behavioural differences (if any) between right and left-handed individuals in the spatial attention task modulated by alertness. Thereby enabling us to understand how handedness influences alertness induced spatial bias.

1.5.2 Handedness & hemispheric lateralisation

One of the first functions tested for laterality in the brain was language. Studies from (Alekoumbides 1978) used data from 29 patients with aphasia (language impairment caused by lesion). These data suggested that the right-handers had language functionality represented only in one hemisphere, whereas left-handers had language represented more bilaterally, which provided them with the ability to compensate for unilateral lesion.

In recent years, neuroimaging of healthy volunteers has served to identify regions of the

brain that are differentially activated, hence enabling to identify functional differences between right and left-handers. Studies by (Knecht, Drager, et al. 2000) used functional transcranial doppler sonography (fTCD) in 326 right and left-handers to identify changes in blood flow while performing a word generation task. They showed that blood flow in right hemisphere increased in 27% of strong left-handers, 15% of ambidextrous participants. While only 4% of right-handers demonstrated increase in right hemisphere activity and 96% demonstrated left hemisphere dominance.

Further functional magnetic resonance imaging (fMRI) was used by (Pujol, Deus, et al. 1999) to investigate the cerebral lateralisation in language function. They used 50 healthy left-handers and 50 right-handers to perform a silent word generation task. In both the groups, the left hemisphere was activated in the task, while in the left-handers (about 24% of them) also activated the right hemisphere. They concluded by saying that 14% of left-handers showed bilateral activation, 10% showed right hemisphere lateralisation, while only 4% of right-handers showed bilateral activation. Other studies (Whitehouse&Bishop 2008) on language function showed that 95% of right-handers showed activation in left hemisphere, while only 75% of left-handers showed activation in left hemisphere. In studies involving spatial memory, it has been shown (Whitehouse&Bishop 2009) that both 75% of right and left-handers have spatial function lateralised in the right hemisphere.

It has also been (Whitehouse&Bishop 2009) shown that language lateralisation, spatial function lateralisation compared across groups of left-handed, right-handed, ambidextrous individuals are not a result of a common underlying process but occur due to independent probabilistic biases. This directly follows analysis made by (Bryden, Hecaen, et al. 1983) in 270 unilateral lesion patients with aphasia and spatial function disorder. They indicated that both language and visuospatial function could occur within the same hemisphere for both left and right-handed individuals. Thus suggesting that cerebral lateralisation exists only as a statistical norm that could be accounted for by individual differences in cognitive skills.

To understand systematic differences in lateralisation of spatial attention and language generation, (Floel, Buyx, et al. 2005) investigated this issue in groups of left (N = 37),

right (N = 38) handers. They used fTCD to monitor blood flow in a word generation task (language) and line bisection (visuospatial attention). The right-handers, showed a typical pattern with left hemisphere lateralisation for language (97%) and right hemisphere lateralisation for spatial attention (95%). The left-handers on the other hand, showed a pattern with left hemisphere dominance for language (74%) and right hemisphere dominance with spatial attention (81%). They summarised that left-handers are more likely to show an uncommon pattern of brain organization for these tasks. They conclude that all combinations of cerebral lateralisation could exist for language and attention in the brain of healthy individuals. It is also interesting to note that 1/3rd of right hemisphere dominant (language) participants were left hemisphere dominant for spatial attention. Further 2/3rd of right hemisphere dominant (language) participants were right hemisphere dominant for spatial attention. This diverges from the 50/50 prediction of right-shift theory, which proposes that, individuals with bilateral or right hemisphere language specialization lack the right-shift factor (allele), hence they would be equally like to have spatial attention in the left and right hemisphere.

1.5.3 Handedness & neglect

There are few and far between studies investigating the interaction of handedness with neglect and cerebral lateralisation. As mentioned before, handedness has shown to affect the lateralisation of cerebral hemispheres in language and spatial memory and hence it is crucial to consider its effect on neglect (which is primarily a disorder of spatial attention). Single case studies (Baxter&Warrington 1986) have reported that language impairment and left spatial neglect following a right hemisphere lesion. This is contradictory to the view that if language lateralisation is reversed (it moves from right hemisphere to left hemisphere), then spatial attention would also reverse (it moves from left hemisphere to right hemisphere). However many studies (Mosidze, Mkheidze, et al. 1994; Kleinman, Newhart, et al. 2007; Binder, Marshall, et al. 1992) have excluded left-handed patients in neglect recovery or they do not report handedness (Farne, Buxbaum, et al. 2004; Becker&Karnath

2007; McIntosh, Brodie, et al. 1997). Thus making it difficult to conclude the effect of handedness on neglect.

The lack of evidence for neglect among left-handed individuals could also mean that left-handers are specifically not vulnerable to neglect. Handedness is known to produce an impact of allocation on attention in space (Buckingham&Carey 2009). In right-handers, it is well known that right hemisphere is specialised for functions of spatial attention and alertness (Robertson, Mattingley, et al. 1998; Corbetta&Shulman 2011; Malhotra, Coulthard, et al. 2006). Hence any lesion occurring in the right hemisphere for right-handers would produce a triple precipitating factor for neglect. That is being right-handed produces right lateralisation of attention and alertness, further right lateralisation of attention, alertness makes the right hemisphere focal point in producing (when lesioned) neglect. For left-handers, this could mean that the severity of the vulnerability to neglect could be reduced, if such hemispheric laterality is not present or reversed (alertness, attention in opposite hemispheres etc.). However, such a study in left-handers with clinical neglect would need to include a large population (at least nine times the usual patients, to match the number of left handers to other studies with right handers).

1.5.4 Research Question

As we have seen before, in healthy individuals (predominantly right-handed), left inattention is increased under conditions of low alertness, however no such evidence is available for whether right-neglect is produced under conditions of low alertness. Evidence for the left neglect in fact comes from *Pseudoneglect* occurring under conditions of low alertness in healthy populations as reported by (Bareham, Manly, et al. 2014; Manly, Cornish, et al. 2005; Fimm, Willmes, et al. 2006). This leads us to ask if healthy left-handers also display such neglect like behaviours and if they do, would they demonstrated left inattention or right inattention? To generalise, this leads us to ask the next question on whether handedness produces a modulation in the direction of effect of spatial bias.

In this context, (Bareham, Bekinschtein, et al. 2015) was one of the first study to establish

the existence of rightward bias with low alertness in healthy left-handed participants. The participants performed the same auditory spatial attention task as (Bareham, Manly, et al. 2014) while falling asleep. Further alertness levels were measured using EEG based techniques like alpha-theta ratio and Hori scoring, it was shown (Figure 1.10) that error rate on left tones became lower, as the error rates in right tones became higher as the participants became drowsier. This pattern is opposite to that of the results from right-handers performing the same task.
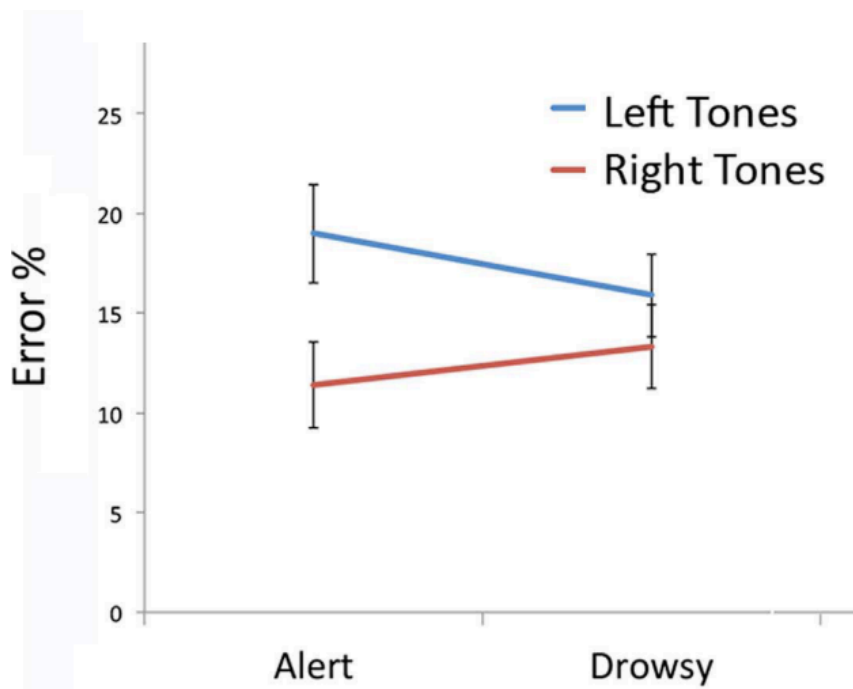
Figure 1.10: Error rates in auditory spatial attention task in left-handers [11]. Under alert conditions, the error rates of participants are significantly different across left and right tone. Under drowsy conditions, the error rates of left tone were similar to right tones. Error bars represent standard error of the means.

However, the shortcomings of the study (Bareham, Manly, et al. 2014) (mentioned in the previous section) were also applicable to (Bareham, Bekinschtein, et al. 2015). This sets us up for the third research question.

(a) *Does variation in alertness levels systematically produce bias in spatial attention in left-handed participants?*

---

[11]modified from (Bareham, Bekinschtein, et al. 2015)

(b) *What changes in neural dynamics in left-handers (that occur due to variation in alert-ness levels) can systematically lead to bias (if any) in spatial attention?*

(c) *How do left and right-handers differ in behavioural and neural dynamics across both 'alert' and 'drowsy' periods?*

(d) *What neuroanatomical model (Inter-hemispheric competition or Right hemisphere specialization) would these patterns support and how does this model depend on handedness of the individual?*

(e) *What does this neuroanatomical model convey about cerebral lateralisation and in-fluence of handedness on spatial attention and other cognitive functions in general?*

1.6 Alertness fluctuations in fruit-flies

To address the question of alertness fluctuations in a system with reduced neural com-plexity and amenable to causal manipulations, I turn to using the fruit-fly (*Drosophila melanogaster*). There are several factors (apart from reduced neural complexity) that served as a motivation to choose the fruit-fly over other animal models which are detailed in the upcoming sections.

1.6.1 Animal models

Studying sleep and attention in smaller animal models has the potential to unravel molec-ular and physiological processes associated with these states, further providing an under-standing of the functional nature of these states (Kirszenblat&van Swinderen 2015). In this context research in invertebrates ranging from the nematode *Caenorhabditis ele-gans* to the fruit fly *Drosophila melanogaster* has acquired importance in recent years. However the choice of the system to study sleep is dependent on several factors. The most important of these factors is the similarity the animal model exhibits with respect to mammalian sleep. In the next section, I motivate how the fruit fly satisfies several of these

requirements and also provides further abilities to dissect the molecular and physiological processes associated with sleep.

1.6.2 *Drosophila Melanogaster*

As mentioned in the section before, sleep is considered to be a behaviour that is produced as an interaction between circadian rhythm and homoeostatic process. The main elements of sleep or associated processes shares the following characteristics (Ly, Pack, et al. 2018; Gilestro 2012; Shaw, Cirelli, et al. 2000; Hendricks, Finn, et al. 2000):

 (a) specific posture and/or place of rest

 (b) periods of immobility.

 (c) increased arousal threshold.

 (d) homeostatic regulation for sleep deprivation.

 (e) reversible to wakefulness or active state.

Several studies have provided evidence for increased arousal threshold in flies following a period of prolonged immobility (van Alphen, Yap, et al. 2013; Yap, Grabowska, et al. 2017). Further it has also been shown (Dissel, Angadi, et al. 2015) that sleep deprivation causes behavioural deficits in learning and restoration of sleep reintroduces behavioural plasticity in flies. However, the nematode *Caenorhabditis elegans* with only 302 neurons also displays sleep-like behaviour (quiescence, reduced arousal, homoeostatic regulation etc.) (Raizen, Zimmerman, et al. 2008). Though in the case of *C. elegans* it has been argued that sleep is merely a state of reduced activity that is needed to cope with the environmental stress or developmental needs of the organism (Kirszenblat&van Swinderen 2015). Hence an alternative definition of sleep also includes its ability to support important functions like attention.

Selective attention (as described before) is an example of such a cognitive function that

can be probed in more complex nervous systems (compared to *C. elegans*) like flies, while it is difficult to quantify in organisms with a limited behavioural repertoire like *C. elegans*. The further advantage of using animals like fruit flies to study sleep and transition to sleep is its simplicity in neuronal architecture. The fly brain has an approximately 135,000 neurons compared to the human brain that has 86 billion neurons. This allows easier identification and manipulation of sleep promoting neural circuits (Donlea, Thimgan, et al. 2011; Pimentel, Donlea, et al. 2016) identified by genetics. Further allowing us to probe the causal mechanisms (using optical and thermal techniques) and understand the functions of sleep and its transition dynamics. For example, sleep induction in flies has been implicated with learning in mutant flies (Dissel, Angadi, et al. 2015) and altered synaptic physiology(Liu, Liu, et al. 2016). Further, *Drosophila* has become an interesting model for understanding the molecular processes associated with sleep in healthy and diseased conditions (van Alphen, Yap, et al. 2013).

In the following sections we cover the behavioural and neural dynamics of natural transitions i.e., transition into sleep in fruit-flies and methods to study them in a detailed manner.

1.6.3 Behavioural dynamics of sleep in flies

In general, a fly is considered to be asleep if it has been inactive for more than 5 minutes or more (Shaw, Cirelli, et al. 2000; Huber, Felice Ghilardi, et al. 2004). This inactivity threshold has been verified by increased arousal threshold using a mechanical stimulus after 5 minutes of inactivity (Shaw, Cirelli, et al. 2000). Further this threshold has been useful for understanding sleep processes and also provided insight on the intensity of sleep in flies (Huber, Felice Ghilardi, et al. 2004). Evidence from early studies (Andretic&Shaw 2005) have also indicated that the overall duration of fly inactivity refers to accumulated sleep processes . Thus fly sleep seems to satisfy most of the definitions of sleep processes like immobility, increased arousal threshold, homoeostasis etc. Sleep in flies can be studied at both individual or at population (group of flies) level. Thus in order to study sleep it

is important to develop methods to analyse behaviour (mainly locomotion or movement) both at population and at an individual level.

1.6.3.1 Population level

Historically sleep in groups of flies has been studied by using the locomotor activity of flies in tubes. For example, a device commonly used to study sleep in flies is called as Drosophila Activity Monitor (DAM). It consists of several tubes each of which house an individual fly. Flies walk back and forth in the length of the tube as the food is usually stored in one end of the tube as shown in Figure 1.11. This locomotion results in the breaking of the infra-red beam (placed in the centre of the tube) on every crossing (Triki-netics, Waltham, MA). The advantage of this approach is that population level studies can be performed in groups of flies with very little effort.
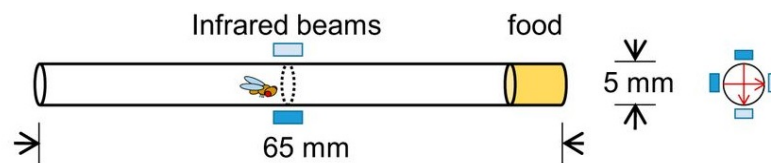
Figure 1.11: Infra-red beam detector [12]used to study sleep in flies. Here, the dark blue bars represent infra-red transmitters and light blue bars indicate receivers. Flies move back and forth in the tube and locomotion activity is measured by the number of infra-red beam crossings.

However,if we are to measure more information about the fly sleep than just number of crossing (activity) per hour we need to move to designs that can probe the behavioural responsiveness and sleep intensity in flies. This has resulted in the development of Drosophila ARousal Tracking (DART) system (Faville, Kottler, et al. 2015). Here the flies are hosted individually in glass tubes as before. Video data is recorded continuously through day and night using a USB-web cam interface as shown in Figure 1.12. Furthermore, to probe the sleep intensity of the flies, vibration stimuli is delivered every hour at specific intensities using shaft-less vibrating motors glued underneath to the tray of flies. This modified design provides us with an ability to measure multiple parameters that include,

---

[12]adapted from (Liu, Haynes, et al. 2015)

positional preferences, behavioural responsiveness, intensity of sleep, homoeostatic effects, general activity levels etc.
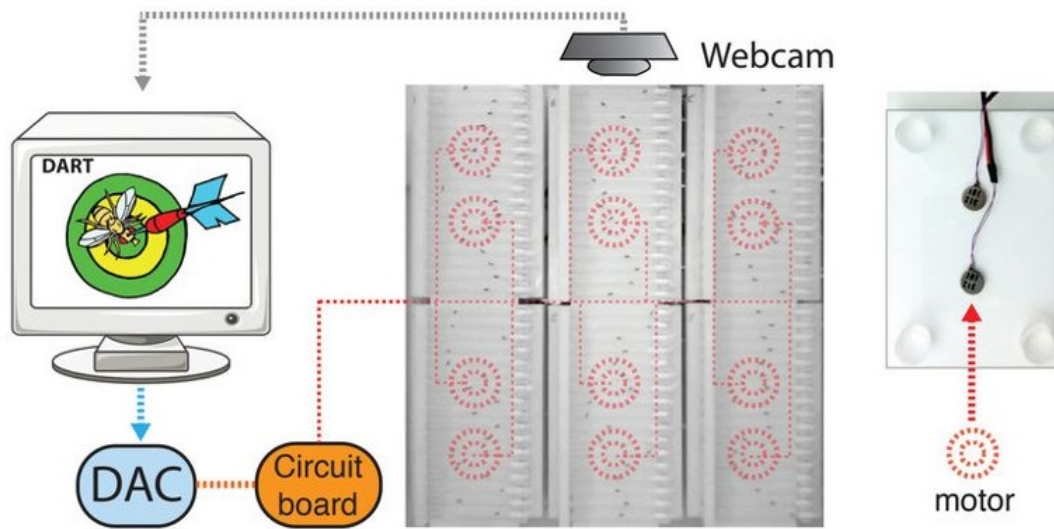
Figure 1.12: Drosophila ARousal Tracking (DART) system [13]. Here the activity of flies is recorded through a web camera. Motor stimuli is periodically applied by using a digital to analog converter (DAC). Each platform consists of two motors as shown (far right) above. Further multiple motors (red circles) are connected to the DAC through a simple circuit board.

1.6.3.2 Individual level

If individual flies are to be studied in much more detail, they are usually tethered to a tungsten rod attached to the thorax of the fly which is then placed on an air supported ball as shown in Figure 1.13. The air-supported ball is usually a polystyrene ball painted with black and white patterns. The ball is allowed to float using a continuous flow of air through a tube situated at its bottom. The use of such a ball allows the fly to walk with least resistance mimicking its environment in natural surroundings. In some cases, where flies are recorded overnight for 24-hr periods, humidified air is also passed through the bottom of the ball to prevent desiccation which can lead to the death of the fly.

---

[13]adapted from (Faville, Kottler, et al. 2015)

Figure 1.13: Fly on the ball set-up[14]. Here the fruit-fly is allowed to walk on the ball, while the motion of the ball can be used to track the movement of the fly including its walking speed, turning direction etc.

From this set-up, we can measure the walking speed of the fly by tracking the rate of change of the black and white patterns, direction of fly walk by tracking the rotational change in the black and white patterns. This set-up also provides for the reliable delivery of olfactory or mechanical stimuli (vibration etc.) and measurement of the corresponding behaviour of the fly.

To summarise, so far we have explored the techniques to study the behavioural aspects of transitions into sleep in fruit-flies. In the next section we briefly review the neuroanatomy of sleep in flies before understanding the techniques to study neural aspects of transitions to sleep in fruit-flies.

1.6.4 Neuroanatomy of sleep in flies

One of the main advantages of using small animal models like fruit flies is that the mapping of neural circuits responsible for generating specific behaviour is easier due to the smaller number of cells, cell types and connections compared to other animal models. In this context it is relevant to study the neurotransmitters involved in wake and sleep

---

[14]adapted from https://news.stanford.edu/news/2011/september/reverse-phi-motion-091211.html

promoting activity for mapping circuits that are involved in maintaining wake and triggering sleep processes. There are seven neurotransmitters involved in sleep and wake regulation in the fly brain. Dopamine, Octopamine and Histamine are involved in wake-promoting activity, while Serotonin and γ-Aminobyuric acid(GABA) are involved in sleep-promoting processes. Further, Acetylcholine (Ach) and Glutamate are involved in both wake-promoting and sleep-promoting processes. The following is a short summary of wake and sleep promoting circuits mediated by the above mentioned neurotransmitters.

1.6.4.1 Dopamine mediated circuits

Dopaminergic cells are present in most of the protocerebrum and innervate many neuropils [15]in the central nervous system (Friggi-Grelin, Coulom, et al. 2003; Mao&Davis 2009). Further, these cells project to the mushroom body and the central complex which are important sleep regulating areas in the fly brain (Pitman, McGill, et al. 2006; Joiner, Crocker, et al. 2006; Donlea, Thimgan, et al. 2011; Liu, Liu, et al. 2016). Mutant flies that directly interfere with the Dopamine production/uptake have produced causal evidence for the interference of dopamine in sleep/wake cycle. Studies (Kume, Kume, et al. 2005) have identified a mutant fly that sleeps less called *fumin* (Japanese word for 'sleepless'). The mutation responsible for generating the sleep loss is said to be present in the dopamine transported (dDAT) gene. dDAT is mainly responsible for dopamine uptake in the pre-synaptic regions (Porzgen, Park, et al. 2001), hence loss of this gene produces prolonged dopamine signals in the specific synapses that results in *fmn* mutants sleeping less. Further studies (Makos, Kim, et al. 2009) have directly confirmed the reduction in levels of dopamine clearance in vivo in *fmn* mutants.

---

[15]area in the nervous system that is mainly composed of un-myelinated axons and dendrites.
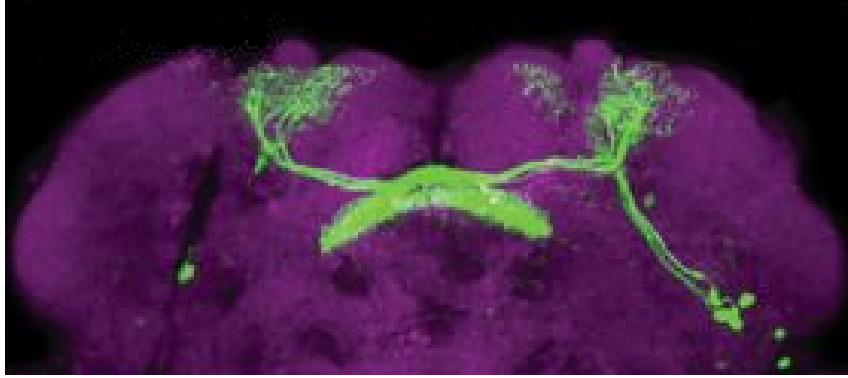
Figure 1.14: Dorsal fan shaped body - Sleep promoting neurons [16]. The neurons in the dFSB are visualized here by green fluorescent protein (GFP) expression using a genetic driver line (23E10-Gal4).

A part of the circuitry of wake-promoting dopamine signal has been isolated to individual neurons in the PPL1 and PPM3 clusters in the posterior protocerebrum that in turn innervate the dorsal fan shaped body (dFSB) (shown with green fluorescent label in Figure 1.14) with dDA1 receptors (Liu, Placais, et al. 2012; Ueno, Tomita, et al. 2012). The location of this circuitry has further been confirmed by the opto-genetic activation of the dopaminergic cells in conjunction with electrophysiological recording of the dFSB neurons (Pimentel, Donlea, et al. 2016).

1.6.4.2 Octopamine mediated circuits

Octopamine is a wake-promoting neurotransmitter similar in structure to NE in mammals (mentioned earlier). In the fly brain approximately 100 octopaminergic cells send projections to distinct regions in the brain like calyx of mushroom bodies, parts of central complex, protocerebrum, optic lobes (Sinakevitch&Strausfeld 2006; Busch, Selcho, et al. 2009). The octopaminergic cells are also similar to NE cells in that they have widespread projections in the central nervous system (of the fly brain).

The arousal promoting effects of octopamine have been verified by pharmacological and genetic manipulations. The oral administration of octopamine in flies resulted in significant reduction of night-time sleep (as it is wake promoting). While mutants carrying

---

[16]adapted from (Yap, Grabowska, et al. 2017)

disruption in key genes in octopamine pathways, slept longer in the day and had reduced latency to sleep at night (indicating increased sleep pressure) (Crocker&Sehgal 2008). The circuitry of the octopamine signals have also been isolated to a cluster of neurons in the medial protocerebrum. These neurons further activate the octopamine receptor in the mushroom body of the fly brain (Crocker, Shahidullah, et al. 2010).

1.6.4.3 Histamine mediated circuits

Evidence from studies (Oh, Jang, et al. 2013) have suggested that histamine promotes arousal in drosophila. 18 cell bodies have been identified to be histaminergic using immunohistochemistry (Nässel 1999). These cell bodies send projections to the ventral and lateral protocerebrum in the fly brain. Further evidence from pharmacological studies have shown that administration of histamine receptor antagonist hydroxyzine decreases latency to sleep (increased sleep pressure as mentioned before) (Pollack&Hofbauer 1991; Nässel 1999).

1.6.4.4 Serotonin mediated circuits

Serotonin is known to be widely expressed in the central nervous system of the fly brain (Nässel 1988; Valles&White 1988; Lundell&Hirsh 1994; Sitaraman, Zars, et al. 2008) and promotes sleep functions (Yuan, Joiner, et al. 2006). Pharmacological studies have shown that increase in serotonin levels via treatment with 5-hydroxytryptophan (5-HTP) which is a precursor to serotonin bio-synthesis is known to increase sleep (Yuan, Joiner, et al. 2006). Further studies have shown that serotonin acts through multiple receptors and brain regions that acts on both baseline sleep (Yuan, Joiner, et al. 2006; Haynes, Christmann, et al. 2015; Qian, Cao, et al. 2017) and sleep rebound due to homoeostatic pressure (Qian, Cao, et al. 2017). Mutants that contain a loss of function gene in 5-HT1a receptors show significant sleep reductions (Yuan, Joiner, et al. 2006). However in the same mutant, transgenic expression of 5-HT1a in the mushroom bodies reverses the sleep pattern (Qian, Cao, et al. 2017) in short-sleeping phenotype of 5-HT1a Drosophila null mutants. This indicates

mushroom bodies as a possible site of action for 5-HT1a sleep regulation. Other studies (Haynes, Christmann, et al. 2015) have indicated that expression of tryptophan hydroxylase (TRH) RNAi in the dorsal paired medial (DPM) neurons that project to the mushroom body significantly reduces sleep. Studies (Qian, Cao, et al. 2017) have also implicated the involvement of 5-HT2b in the dFSB in homoeostatic sleep rebound. To summarise, serotonin mediates sleep and sleep homoeostasis through distinct circuits in the fly brain.
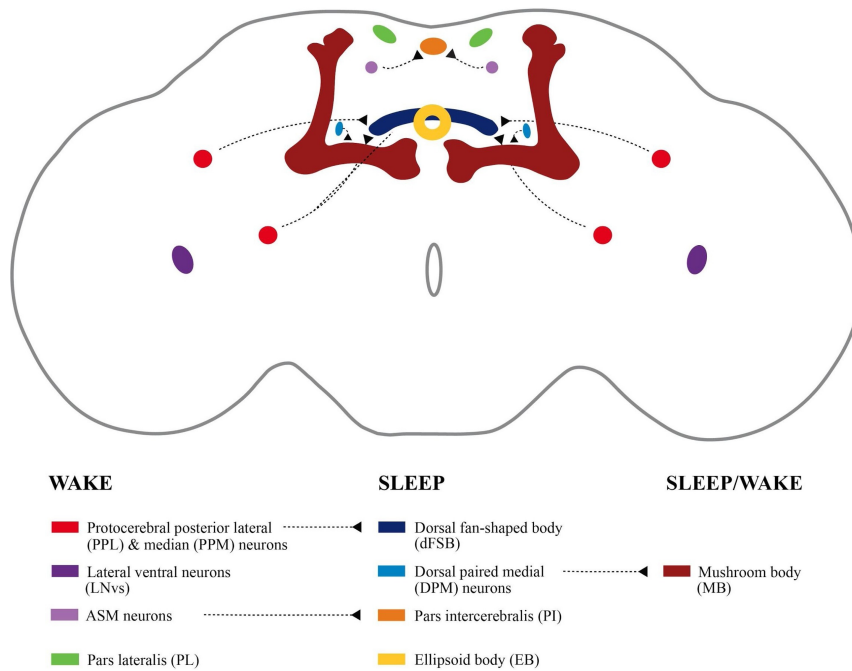
Figure 1.15: Fruit-fly sleep networks [17] involved in regulation of sleep and wake activity. The dashed lines here indicate functional connections between different regions that have been established in the literature.

1.6.4.5 GABA mediated circuits

γ-Aminobutyric acid (GABA) which is one of the primary inhibitory neurotransmitters in both vertebrates and invertebrates occurs in small clusters that innervate large number of cells throughout the fly brain (Enell, Hamasaka, et al. 2007; Okada, Awasaki, et al. 2009). GABAergic transmission in turn promotes sleep and advances sleep onset (Agosto, Choi, et al. 2008) by expressing the transgene for hyper-polarising the potassium channel (in GABAergic neurons). In addition, the administration of THIP (a GABA-A agonist) significantly increases sleep in wild-type flies (Dissel, Angadi, et al. 2015). Clock cells (Parisky,

---

[17] adapted from (Ly, Pack, et al. 2018)

Agosto, et al. 2008) (that control sleep rhythm; also critical for learning and memory (Haynes, Christmann, et al. 2015)) are also regulated by GABA for both sleep and sleep onset.

In the fly brain, the large ventral lateral neurons (l-LNvs) which contain the Resistant to dieldrin (Rd1) ionotropic GABA-A receptor are composed of a network of 150 neurons that are critical to the generation of circadian rhythm (Peschel&Helfrich-Förster 2011). l-LNvs are considered to the principal circadian pacemaker cells in the fly brain with Rd1 as one of the three GABA-A subunits which are present in the optic lobes, antenna lobes, mushroom bodies and central complex (Enell, Hamasaka, et al. 2007). Electrophysio-logical recordings of l-LNvs have also shown that GABA inhibits the activity of l-LNvs, thus suggesting that inhibition of l-LNvs promotes sleep processes (Chung, Kilman, et al. 2009).

The major sleep promoting neurotransmitter mediated circuits in the drosophila brain mentioned above are summarised in the Figure 1.15.

To summarise, so far we have seen a brief overview of the neuroanatomy involved in wake and sleep networks in the fly brain. Next we aim to understand the dynamics of such networks recorded through electrophysiological methods.

1.6.5 Neural dynamics of sleep in flies

Analysis of brain activity in humans using EEG recordings have revealed distinct sleep patterns (Ogilvie 2001; Moser, Anderer, et al. 2009) that are associated with different arousal thresholds. Studies (Ogilvie 2001; Moser, Anderer, et al. 2009) have found that during slow wave sleep (SWS), behavioural responsiveness to stimuli gets reduced, whereas rapid eye movement (REM) sleep was associated with increased responsiveness. Furthermore, SWS has been implicated in memory consolidation and maintaining synaptic homoeostasis (Diekelmann&Born 2010; Tononi&Cirelli 2003; Tononi&Cirelli 2006). These studies have shown the value of performing electrophysiological recordings on a population of neural assemblies. Recently studies (van Alphen, Yap, et al. 2013) have shown using local field

potentials (LFP) recorded from the fly brain, that flies possibly sleep in different stages associated with distinct electrophysiological patterns and different arousal thresholds.

In this context (Yap, Grabowska, et al. 2017) investigated the process of spontaneous falling asleep in flies. LFPs were recorded by implanting two glass electrodes into the two brain hemispheres (Detailed methods in Chapter 6) and an amplified differential voltage was extracted from the electrodes. In this set up, the flies were tethered to a pole and placed on a ball (described before). The behaviour of the flies (mainly locomotion) was recorded for 24-hours using infra-red enabled camera. If the fly was immobile for a period of more than 5 minutes, it is considered to be sleep (as mentioned before). Immobility period was quantified using the pixel subtraction technique (van Alphen, Yap, et al. 2013).Here the change in pixel value between subsequent frames was quantified by subtracting the adjacent frames in a video to create a difference image (Δ pixels) across time. The change in pixels is summed to create a movement value. The fly is said to have moved only if this movement value exceeds a certain threshold. Thus periods of no movement for more than 5 minutes were considered as sleep (sleep from 5th minute). For example, consider a fly that stops moving at 0 minutes and moves back again at 15 minutes. Here the time period from 0 - 5 minutes is considered as transition and any period after the 5th minute (till 15th minute) is considered as sleep.

They showed that (Figure 1.16) 'sleep' and 'awake' periods were characterised by change in the frequency spectrum of the LFP. Furthermore, they associated a frequency band (7-10 Hz) in the central brain as a transitional sleep stage. However, there were several shortcomings associated with the study. First, the transition to sleep (period from 0 minute to 5th minute) was not investigated. Which is co-incidentally one of the prime focus of this dissertation. Second, the sleep in flies was categorized based on the time of sleep induction (day or night). However, it is well known that the depth of the sleep (sleep duration) modulates arousal threshold and hence it would be interesting to dissect the changes in frequency patterns across sleep of different depths. Third, the changes in frequency spectrum across awake and sleep periods were not characterised to identify important elements in the spectrum that can generalise the findings to a new fly (this could be done by building classifiers based on frequency spectrum to identify 'awake'

and 'sleep' periods). Fourth, the two channel differential LFP is not able to provide spatial information on how regions in the brain differ across 'awake' and 'sleep periods.
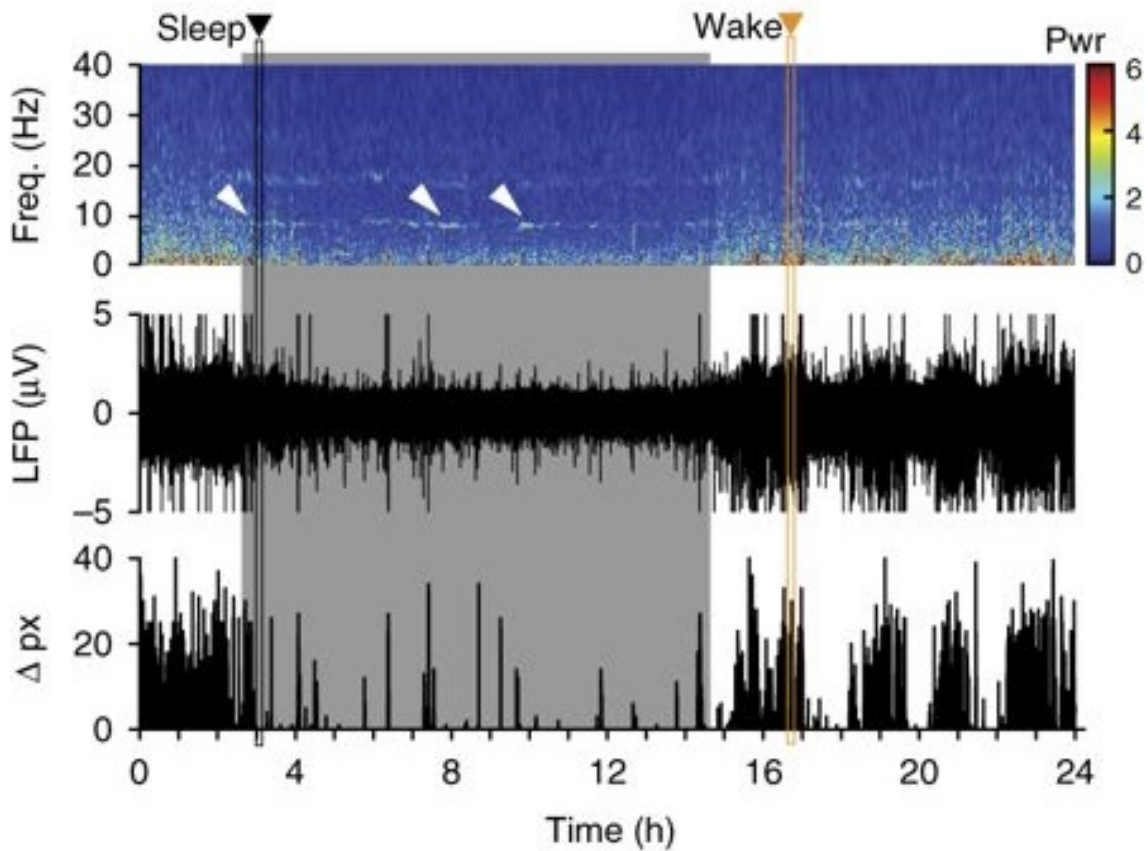
Figure 1.16: Spectogram of 24-hr LFP [18]

1.6.6 Research Question

This sets us up for the fourth research question to understand the process of transition to spontaneous sleep.

(a) *Can we build a data driven approach to analyse the LFP data based on elements of frequency spectrum as done for humans?. For example this could be a classifier (with features like frequency spectrum) and classify the LFP data across 'awake' and 'sleep' periods independent of movement data?*

---

[18]adapted from (Yap, Grabowska, et al. 2017)

(b) *What happens to the frequency spectrum elements (or classifier patterns) when the fly is transitioning into sleep (0 to 5 minutes)?*

(c) *How do the classifier patterns depend on the sleep depth? Does longer sleep duration (deep sleep) differ from smaller sleep duration (light sleep)?*

(d) *Can we uncover the spatial information in the transition to sleep across awake and sleep periods using multichannel recordings as used in (Paulk, Zhou, et al. 2013) or in other words what brain regions change (and in what frequency bands) across awake and sleep periods?*

(e) *How does the spontaneous sleep measured with multichannel recordings differ from artificially inducing sleep. For example thermogenetically activating the dFSB as in (Yap, Grabowska, et al. 2017)?*

1.7 Outline of this dissertation

To summarise, so far we have seen a brief literature overview of alertness, transitions of alertness and both the behavioural and neural dynamics of such transitions in healthy adults and patients. Further, we also reviewed the circuits involved in the transition to spontaneous sleep in flies. We also detailed several unanswered questions and potential problems that need to overcome to understand the behavioural and neural dynamics of alertness induced spatial bias. To be able to solve them, first we need to develop an objective method capable of tracking alertness levels on a fine grained scale (as Hori system of scoring is highly subjective and time consuming). Second, the tracking of behavioural dynamics in attentional biases with low alertness has only been done with simpler measures (like signal detection theory) based on error proportions etc. However, computational modelling of behaviour could lead us to uncover much richer dynamics. Third, the neural dynamics in such alertness induced spatial biases has only been done with univariate analysis techniques. However, MVPA could lead us in understanding the dynamics between

different brain regions in a model free manner. Fourth, the neural dynamics in simpler systems like fruit-flies has not been explored in detail using computational techniques.

Thus, the core aspect of this dissertation consists of addressing the above mentioned problems. I do this systematically by developing a method to track alertness levels, followed by which I use well-established measures for tracking the behavioural and neuro-dynamics of biases in attention (during alertness transitions). For tracking and quantifying behaviour across different alertness levels, I use multilevel modelling, psychophysics, drift diffusion modelling. For tracking and quantifying the neural dynamics across different alertness levels, I use MVPA to identify patterns in the EEG data. Followed by which I connect the drift diffusion parameters with EEG data by performing trial-by-trial regression, thus providing convergent evidence for understanding the dynamics across behaviour and neural data. Finally, I apply machine learning techniques in fruit flies to explore the neural dynamics of spontaneous falling asleep over longer time periods ($12 hours$).

1.7.1 Measurement of alertness levels

This part of the dissertation mainly deals with developing an alternative method to the Hori system. The alternative method should be objective and automated to provide for wide spread application across different domains.

In the first step, I develop a method for tracking levels of alertness in humans with EEG data. I use machine learning methods based on Support Vector Machines (SVM) to develop tools that can track alertness levels in a trial-by-trial manner. I further validate this in a primary dataset with 64-channel EEG using gold standard Hori scores (generated by 3 independent scorers) in Chapter 2. Next, I test the generalisability of this tool by using an independent 128-channel EEG dataset that has been Hori scored by an independent scorer under the supervision of an experienced scorer. Finally, I conclude by highlighting the utility of the method to the general cognitive neuroscience community. This tool can be used to track trial-by-trial alertness levels in their experiments with EEG under eyes closed settings.

1.7.2 Behavioural dynamics of transitions

This part of the dissertation mainly answers the first research question of analysing the behavioural dynamics in spatial bias (across transitions of alertness) using computational modelling.

In this second step, I investigate the behavioural dynamics in alertness induced spatial bias across an auditory spatial attention task. This task is based on an augmented version of the same spatial attention task published earlier (Bareham, Manly, et al. 2014). In this task, right-handers localize the direction of tones originating from the left or right direction (Chapter 3). The participants are also allowed to fall asleep to modulate the alertness levels. First, I use multi-level modelling to show that the proportion of errors committed by the participants in the left direction is disproportionately high when they become drowsy. Second, I use psychophysics to quantify the subjective mid-line by fitting a psychometric function to the proportion of rightward responses. I show that for majority of the subjects the mean of the psychometric function shifts to the left, indicating that the subjects produce more left errors. Third, I use HDDM to quantify the bias (starting point) and drift-rate (evidence accumulation rate). The prime reason to use drift diffusion model is to quantify the different elements of the decision-making process using distribution of reaction time measures, which are independent of the accuracy of the responses. Using HDDM, I show that between left and right stimuli, the drift rate changes largely when the participant becomes drowsy while the change in bias is comparatively small, thereby providing indications of a possible mechanism responsible for the left-side errors (alertness induced spatial bias). Fourth, I discuss how the possible mechanisms help us provide evidence for or against the different neuronatomical models that can explain the spatial bias in right-handers.

1.7.3 Neural dynamics of transitions

This part of the dissertation mainly answers the second research question of analysing the neural dynamics in spatial bias (across transitions of alertness) using multivariate pattern analysis.

In this third step, I investigate the neural dynamics of alertness induced spatial bias across the same auditory spatial attention task as mentioned above. First, I use temporal decoding (MVPA) to identify patterns in data that can discriminate between different conditions (Chapter 4). For example, I start with the basic decoding of left and right stimuli using scalp topography under alert conditions. I show that the decoding of the presented stimulus starts at 200 ms, which is well before the average reaction times (about 400-600 ms) indicating that the neural patterns in the classifier actually capture the process of decision making. Second, I project these patterns to show that brain regions like parietal and temporal cortex may be involved in performing this task. Third, I use trial-by-trial variations in the drift-rate and perform regression against the ERP data to compute the discrimination ability of sensor locations across left and right stimuli. Fourth, I discuss how the different brain regions help us provide evidence for or against the different neuronatomical models that can explain the spatial bias in right-handers.

1.7.4 Handedness aspect of pseudoneglect

This part of the dissertation mainly answers the third research question and deals with understanding the difference in performance (if any) in the auditory spatial attention task between left and right-handers and the neural mechanisms responsible for generating this behavioural difference.

In this fourth step, I use the same spatial attention task as above, but now left-handers perform the tone localization task while falling asleep (Chapter 5). First, I show how the behavioural dynamics of the left-handers are different from right-handers. Using multi-level modelling, I show how handedness modulates the proportion of errors, dependent

on the side of the tone as participants become drowsy. Second, I use MVPA to show that despite left and right-handers showing same behaviour under alert conditions, different regions of the brain seemed to be involved in performing the same task. Next, I show how handedness affects the different regions in the brain involved in performing this task while under drowsy conditions. Third, I use regression of the drift-rate (computed with HDDM) with the ERP data to show how different brain regions can distinguish between left and right tones. Fourth, I show how the evidence from the drift-rate regression converges with the results from MVPA. These results further highlights the mechanisms in the brain responsible for generating behavioural difference across left and right-handers. Fifth, I discuss how the different mechanisms of spatial bias across left and right-handers help us provide evidence for a generic neuronatomical model of alertness induced spatial bias for both left and right-handers. Finally, I also highlight one of the major issues of neuroscience studies: ignoring left-handers provides only models based on the brain and behaviour of right-handers, which removes variability in neural processes and generalisability in cerebral lateralisation that can be caused by natural factors like handedness.

1.7.5 Alertness transitions in the fruit-flies

This part of the dissertation mainly answers the fourth research question of exploring the neural dynamics in the alertness transitions in fruit flies using machine learning techniques.

In this fifth step, I use the fruit fly (*Drosophila melanogaster*) to probe the questions of spontaneous falling asleep in a system amenable to causal manipulations. First, I use single-channel LFP data from flies falling asleep in a 24-hour period (Yap, Grabowska, et al. 2017). I use wavelet decomposition as features and develop an SVM to classify segments of data (1 minute in length) into 'awake' and 'sleep' periods. Next, I validate the same against ground truth computed using video data (pixel subtraction technique). Second, I show that using probabilistic classifier, we can actually detect the probability of fly sleep in the transition from 0th to 5th minute. Further, the classifier also predicts the duration of fly sleep (sleep depth) after the 5th minute. More crucially, the fly sleep can

be actually predicted at -2 minute (before the start of the immobility period). Third, I use multi-channel LFP data using half-brain probe from flies falling asleep in a 12-hour period. I perform power spectrum analysis to show the differences in brain regions across awake and sleep conditions. I further show converging evidence from experiments performed with thermogenetic manipulations using full-brain probe in a previously published dataset (Yap, Grabowska, et al. 2017).

2

Tracking alertness transitions

2.1 Brief introduction

Before exploring the transitions of alertness in both behaviour and neural dynamics, we need to develop a method to be able to track the alertness levels in an accurate manner. As mentioned in the introduction the state of the art methods (like Hori scoring for measuring finer levels of alertness) are subjective and error prone. Hence this necessitates the development of an automatic method that is objective and measure alertness levels in an accurate manner.

This manuscript develops such an automated method for tracking alertness levels with EEG in a trial-by-trial manner. The prime reason for measuring alertness levels (apart from using it to study alertness transitions) is that drowsiness has proved to be confounding factor (Tagliazucchi&Laufs 2014) in several cognitive experiments especially in eyes-closed and resting state settings. Further evidence from studies (Bareham, Manly, et al. 2014; Chennu&Bekinschtein 2012) have shown that alertness is found to modulate attention and many other cognitive sub-processes.

The current methods that are used for measuring alertness to track drowsiness has sev-

eral disadvantages. In task based settings, techniques use pre-trial periods to categorize data segments into different levels of alertness based on manual or automatic methods. Manual techniques like sleep scoring (Berry, Budhiraja, et al. 2012) rely on data segments of 30 seconds in length, however most cognitive experiments have pre-trial periods ranging from 4-5 seconds which make them unsuitable for our purpose. Automated techniques developed elsewhere (Tagliazucchi, von Wegner, et al. 2012) also use American Association of Sleep Medicine (AASM) based sleep stages like wakefulness, N1, N2 etc. which do not have the sufficient temporal resolution to capture dynamics in alertness transitions. Other techniques that use continuous measures like alpha-theta ratio (Šušmáková&Krakovská 2008) to capture variations in alertness classify trials into alert and drowsy based on the assumption that each participant had equal number of alert and drowsy periods, which is not true.

2.2 Declaration of contribution of co-authors

The following paper was published in 2018 in *NeuroImage*. The micro-measures algorithm was mainly developed using dataset #1 consisting of 64 channel EEG data which was already published in (Kouider, Andrillon, et al. 2014). I developed the criteria and code for the automated algorithm, while the ground truth labels of Hori scores were rated by 3 experienced scorers. Next, to test the generalisability of the algorithm, I validated this in another independent dataset #2 consisting of 128 channel EEG data which was already published in (Noreika, Kamke, et al. 2017). I further developed the methods to test the algorithm using an independent behavioural measure of Coefficient of variation in reaction times. The creation of the figures, manuscript were my own work, which underwent revisions based on comments by co-authors and reviewers before its published form below.

2.3 Manuscript, *NeuroImage*
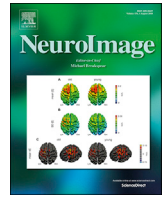
Tracking wakefulness as it fades: Micro-measures of alertness

Sridhar R. Jagannathan [a,*], Alejandro Ezquerro-Nassar [a], Barbara Jachs [a], Olga V. Pustovaya [b,c], Corinne A. Bareham [d], Tristan A. Bekinschtein [a,c]

[a] Department of Psychology, University of Cambridge, Cambridge, United Kingdom
[b] Academy of Biology and Biotechnologies, Southern Federal University (SFU), Rostov-on-Don, Russia
[c] Cognition and Brain Sciences Unit, Medical Research Council, Cambridge, United Kingdom
[d] Department of Clinical Neurosciences, University of Cambridge, Cambridge, United Kingdom

ARTICLE INFO

ABSTRACT

A major problem in psychology and physiology experiments is drowsiness: around a third of participants show decreased wakefulness despite being instructed to stay alert. In some non-visual experiments participants keep their eyes closed throughout the task, thus promoting the occurrence of such periods of varying alertness. These wakefulness changes contribute to systematic noise in data and measures of interest. To account for this omnipresent problem in data acquisition we defined criteria and code to allow researchers to detect and control for varying alertness in electroencephalography (EEG) experiments under eyes-closed settings. We first revise a visual-scoring method developed for detection and characterization of the sleep-onset process, and adapt the same for detection of alertness levels. Furthermore, we show the major issues preventing the practical use of this method, and overcome these issues by developing an automated method (micro-measures algorithm) based on frequency and sleep graphoelements, which are capable of detecting micro variations in alertness. The validity of the micro-measures algorithm was verified by training and testing using a dataset where participants are known to fall asleep. In addition, we tested generalisability by independent validation on another dataset. The methods developed constitute a unique tool to assess micro variations in levels of alertness and control trial-by-trial retrospectively or prospectively in every experiment performed with EEG in cognitive neuroscience under eyes-closed settings.

Introduction

Electroencephalography (EEG) has played a pivotal role in the non-invasive study of brain function (Niedermeyer and Silva, 2004). Typically in an EEG experiment the electrophysiological activity of the brain is recorded from the scalp of the participant while they are performing a cognitive task or under task-free conditions (e.g. resting state). In some task-based experiments, typically in the auditory or tactile domain, the participant performs the task with eyes-closed. Previous studies have shown that such eyes-closed settings can create periods of momentary lapses of alertness (Barry et al., 2007). These periods are usually attributed to variable and long inter-trial intervals (Hackley and Graham, 1987; Kosslyn and Andersen, 1995). The prevalence of this problem can be attested by studies mining large databases, which show that about a third of participants momentarily fall asleep in resting state conditions (Tagliazucchi and Laufs, 2014). Further, task-free settings such as mind wandering or simple non-active instructions can also lead to drowsiness

and sleep (Goupil and Bekinschtein, 2012).

The above mentioned variations in alertness can be inferred using variability in reaction times (Ogilvie, 2001). However, the direct application of reaction time measures in detecting alertness in a trial-by-trial manner is hampered by the following reasons. Firstly, variation in reaction times are also generated due to varying task difficulty, thus making it difficult to disentangle task difficulty with alertness. Secondly, there are no established methods to relate such reaction time measures among different participants in the same study while overcoming individual differences. Thirdly, they cannot be applied for non-active tasks such as resting state studies. Thus, in most of the cognitive neuroscience experiments such alertness lapses are ignored (Olbrich et al., 2009; Tagliazucchi and Laufs, 2014) and data confounded with drowsiness (or low alertness) are used for studying brain functions like attention and cognition. However, attention and many other cognitive sub-processes are known to be directly modulated by lack of alertness in normal (Bareham et al., 2014; Chennu and Bekinschtein, 2012) as well as clinical

populations (Dobler et al., 2005). Hence, fluctuations in alertness need to be measured, to include or exclude trials of low/high alertness to adequately test predefined hypotheses. This argument is illustrated with an experiment in Fig. 1.

Fig. 1(B) shows a typical EEG experiment (Kouider et al., 2014) where the participant responds to auditory stimuli while having their eyes closed. In the beginning of the experiment the participant responds to the stimuli in a reliable manner (green dots) by less variation in reaction times. As time progresses the reaction times become more variable and the participant intermittently fails to respond (red dots). This variation is also captured in the frequency profile of the EEG (occipital sites) during the pre-trial periods of the task as depicted in Fig. 1(A). When the participant responds reliably, the frequency profile predominantly shows power in the alpha range (8–12 Hz) and as they become drowsy the alpha power disappears and low frequency power in the theta range (6–8 Hz) increases. Thus the frequency profile preceding the trial could predict the variability in the responses. In other words, such spectral changes can be used to detect the momentary lapses in alertness that causes variability in the reaction times.

The typical techniques that are used to clean or remove the data from such drowsiness contaminated episodes can be either manual or automatic. Manual methods tend to score the above mentioned pre-trial periods using traditional sleep scoring techniques (Berry et al., 2012). Automatic methods are either continuous (ratio between alpha-theta frequency range) or discrete, which can further be validated with the manual labels described earlier. However, both the techniques face multiple problems. Firstly, sleep scoring techniques rely on having at least 30 s of data (Berry et al., 2012), whereas in most cognitive experiments the pre-trial periods last at most 4–5 s. Secondly, automated methods (Tagliazucchi et al., 2012) that are validated using such sleep scoring techniques classify data into American Association of Sleep medicine (AASM) based sleep stages like wakefulness, N1, N2 etc. But such momentary lapses of alertness require more fine grained scoring techniques that operate on a smaller time range with different features capable of capturing micro variations in alertness levels. Thirdly, continuous measures such as alpha-theta ratio (Šušmáková and Krakovská, 2007) divide the entire set of trials into quartiles and label the trials in the lower quartile (lower alpha-theta ratio) as drowsiest and upper quartiles as most alert (Bareham et al., 2014). Such measures assume every participant had an equal number of alert and drowsy periods, thereby implying that the depths of drowsiness attained by each

participant was the same, which is not necessarily true. Finally, some techniques use the simple variation in reaction times to capture moments of low alertness. But this suffers from the problem of longer reaction times being confounded by other factors such as task difficulty as mentioned earlier (Bareham et al., 2014).

Thus the above mentioned problem of fluctuations in alertness requires a novel solution. Our proposal is to tackle the problem in the following manner: Firstly, we identify these alertness contaminated episodes, through the use of the Hori scale (Tanaka et al., 1996) that captures micro variations in alertness. Though the prime purpose of the Hori system is to identify and characterise the sleep onset process, it contains features that enable us to identify variations in levels of alertness in more fine grained durations (4 s) compared to traditional sleep scoring using wakefulness, N1 and N2. In particular the strength of the sleep graphoelements and other EEG signatures associated with Hori scale have been shown to be more reliable in capturing the drowsiness substages (Goupil and Bekinschtein, 2012). Secondly, we use human scorers to identify different levels of alertness using the Hori scale on a dataset where the participants are allowed to fall asleep while performing the task. Thirdly, we show that despite the clarity of the Hori scale, it is impractical to perform, time consuming and difficult to learn, as elucidated by the low degree of agreement among human scorers. Fourthly, we produce a practical solution to this problem using an automated technique (micro-measures algorithm) that involves using Support Vector Machine (SVM) and individual graphoelement detectors. Further we computed performance measures by training and testing the algorithm on a dataset labelled by gold standard ratings (converging Hori ratings from multiple scorers). Finally, to estimate the reliability and generalisability of the micro-measures algorithm, we tested the same in another independent dataset to show its utility.

As a first step, we introduce the Hori system of scoring and inform the readers about the augmentations made in the system to suit the current purpose of measuring changes in alertness levels.

Hori scale

Hori and colleagues subdivided the sleep onset process into 9 different substages (Tanaka et al., 1996). The first two Hori stages (1,2) correspond to wakefulness. The next six Hori stages (3–8) correspond to the sleep stage N1. The last stage of Hori (9) corresponds to the beginning of N2 sleep (Iber et al., 2007).

Here we decided to augment classical Hori stages with another stage (10) that would correspond to the appearance of K-complexes. The rationale behind this addition is the appearance of K-complexes definitively mark the entrance to N2 sleep. While spindles can still serve this purpose, their variability in duration and disagreement among human raters (Warby et al., 2014) motivates the use of K-complex. The following is a brief description of the elements in the hori scale based on (Ogilvie, 2001) and are shown in Fig. 2.

Alert elements

Alpha waves. Alpha waves are elements that occur in the range of 8–12 Hz during relaxed wakefulness. They are more pronounced in the eyes-closed condition, when the participant is transitioning from alert to relaxed wakefulness (Hori 1–2). Alpha elements are usually more pronounced in EEG from occipital regions.

> *Hori 1*: Epoch is composed of only alpha wave trains (at least 20 μV).
> *Hori 2*: Alpha wave trains occupy more than 50% (but less than 100%) of the activity in the epoch.

Drowsy elements

Alpha waves. Alpha activity usually decreases when the participant

Fig. 1. Differing alertness levels indicated by frequency profile changes and reaction time variability during an auditory experiment in a sample participant falling asleep. (A) Depicts the changes in the power level in different frequency bands in the Occipital electrodes in the pre-trial period of an auditory experiment at different time points. (B) Reaction times at trials presented along the different time points in the same experiment, red dots represent failure to respond and green dots represent responses. The variability in the reaction times (B) and thus reduction in alertness levels closely follows the change in the frequency profile (A) from alpha (8–12 Hz) to theta (6–8 Hz).\

A

B

C

D

Fig. 2. (A) Modified Hori scale for detecting differing alertness levels using EEG. The grey waves indicate background activity and coloured regions indicate characteristic elements for respective Hori stages. AASM based sleep stage classification is also represented for compatibility to classical sleep scoring. Graphoelements of Hori scale in detail: (B) Vertex sharp waves: Biphasic consists of a sharp negative deflection followed by a positive one, whereas Monophasic consists of only a sharp negative deflection. (C) Spindles: transient patterns with frequency (12–16 Hz) and minimum duration of 0.5 s (D) K-complex elements: sharp positive deflection followed by a larger negative one with a duration of at least 0.5 s.

transitions from relaxed wakefulness to drowsy (Hori 3).

Theta waves. Theta waves are elements that occur in the range of 3–8 Hz. They have relatively higher amplitudes than the alpha elements and characterise the transition to N1. Theta activity is usually pronounced in the central and temporal regions (Hori 5).

> *Hori 3*: Alpha wave trains occupy less than 50% of the activity in the epoch.
> *Hori 4*: Activity flattening without any clear element (amplitude < 20 µV).
> *Hori 5*: Low voltage theta waves (ripples) with amplitude between 20 µV and 50 µV.

Graphoelements

Vertex sharp waves. Vertex waves are graphoelements that occur in the beginning of the transition to sleep (Hori 6–8). Appearance of them indicates an altered state of responsiveness in the cerebral cortex (Rodenbeck et al., 2006). The vertex waves can be either monophasic or biphasic. In both cases there is usually a sharp negative discharge followed by a positive one. In the case of biphasic waves, the amplitude of the positive components should be at least 50% of the negative component and at most equal to the level of the negative component. The amplitude of the vertex sharp waves is found to be maximal in parietal and frontal regions (Cz based reference).

> *Hori 6*: Epoch containing only one well defined vertex sharp wave.
> *Hori 7*: Epoch containing more than one vertex sharp wave.

Spindles. Spindles are graphoelements that occur in the beginning of the transition to stage N2 of sleep (Hori 9). They are regarded as transient patterns of EEG activity with a frequency of 12–16 Hz with a minimum duration of 0.5 s (complete spindles). Spindles in general should be distinguishable from the background activity. The typical waxing and waning of spindle shape is vital to distinguish the pattern from high alpha activity. The spindles were found to be prominent in temporal and frontal regions (Cz based reference).

> *Hori 8*: Contains at least one vertex wave and an incomplete spindle (<0.5 s).
> *Hori 9*: Contains one well defined spindle (>0.5 s).

K-complexes. K-complexes are graphoelements that occur in the N2 stage of sleep (modified Hori 10). It starts with a sharp positive wave followed by a large negative wave. The duration of the initial negative wave should be smaller than the positive wave. The overall duration of the K-complex must be at least 0.5 s. The K-complexes were found to be prominent in frontal, temporal and parietal regions (Cz based reference).

Hori 10: Contains at least one well defined K-complex.

In summary, spectral features based on alpha and theta waves can be used to discriminate between alert and drowsy states. Graphical elements such as vertex, spindles and K-complexes can be used to detect deeper states of drowsiness. These are the candidate elements which both manual as well as the micro-measures algorithm would be utilizing for classification.

Materials and methods

Participants and datasets

The first dataset (herein Dataset#1) consisted of 20 native English speakers (12 males; mean age 25.25; age range 20–33), all right handed, who performed a semantic categorization task while falling asleep (Kouider et al., 2014). Participants were screened with the Epworth Sleepiness scale (Johns, 1991) and only easy sleepers (score ≥ 7) were recruited. They were asked not to consume stimulants like Coffee/Tea and to sleep 1–2 h less than usual the night preceding the experiment. The participants also had no auditory, neurological, psychiatric abnormalities. The task consisted of listening to words that belonged to a particular semantic category (e.g. animals or objects) and classifying them accordingly using a left or right button press. Each trial consisted of an auditory stimulus (spoken word: animal or object) presented binaurally with an intertrial interval of 6–9 s. The maximal duration of the experiment was 35 min. On average, 163 trials were presented to each participant (SD = 43.77, Min = 100, Max = 229) resulting in a total of 3269 trials.

The second dataset (herein Dataset#2) consisted of 31 healthy participants, all right handed (assessed with Edinburgh Handedness Scale (Oldfield, 1971)), who performed a auditory masking task while falling asleep (Noreika et al., 2017a). Participants were screened with the Epworth Sleepiness scale (Johns, 1991) and only easy sleepers (score ≥ 7) were recruited. They were also asked not to consume stimulants like Coffee/Tea during the few hours before the experiment. One participant was excluded as the original trial order could not be recovered from raw data resulting in 30 participants (8 males; mean age 27.2; age range 20–39). The task consisted of listening to a target sound (e.g. beep) that was randomly masked by different noise durations. Participants reported whether they heard the target using a button press. Each trial consisted of an auditory stimulus (target) sometimes masked by noise, presented binaurally. The next trial was presented after a pause of 8–12 s after the response or 13–17 s (in case of no response). The maximal duration of the experiment was 120 min. On average, 543 trials were presented to each participant (SD = 62.77, Min = 402, Max = 631) resulting in a total of 16289 trials.

In both experiments subjects were seated on a reclining chair in a dark room and were permitted to fall asleep during the task.

EEG acquisition

Dataset#1: EEG was recorded using 64 Ag/AgCl electrodes (Neuro-Scan labs) with Cz as reference. The electrode impedances were kept below 10 KΩ. The signal was acquired at a sampling rate of 500 Hz.

Dataset#2: EEG was recorded using 128 Ag/AgCl electrodes (Electrical Geodesics Inc) with Cz as reference. The electrode impedances were kept below 100 KΩ. The signal was acquired at a sampling rate of 500 Hz. As the input impedance of the amplifier was high (~200 MΩ), the high electrode impedance (100 KΩ) did not affect the signal quality (Ferree et al., 2001).

Pre-processing

EEG data was pre-processed with custom made scripts in MATLAB (MathWorks Inc. Natick, MA, USA) using EEGLAB toolbox (Delorme and Makeig, 2004).

Dataset#1: The data was bandpass filtered with zero phase shift between 1 and 30 Hz using hamming windowed-sinc FIR filter and was then resampled to 250 Hz. Further, it was epoched from −4000ms to 0ms to the onset of the stimuli. Bad channels were then detected using a two-step fashion: firstly, channels are considered bad if channel variance is below 0.5 and for the remaining channels normalized power spectrum of all channels are computed in the range of 1–30 Hz. Any channel that exceeds the mean power spectrum by ±4 standard deviations is marked as bad. The detected bad channels were then interpolated using spherical interpolation. Finally, the trials that exceed the amplitude threshold of ±250 μV were removed in a semi automatic fashion. The amplitude threshold was liberal as K-complexes usually exceed ±150 μV. The pre-processing steps resulted in 3201 trials (~2% of trials rejected).

Dataset#2: The first pre-processing step for this dataset was to remove peripheral channels in the EEG that covered the regions of forehead, cheeks and neck to minimise eye and muscle related artifacts, thus retaining only 93 channels that covered the scalp. The rest of the pre-processing steps are the same as for dataset#1. The pre-processing steps resulted in 15532 trials (~5% of trials rejected).

Electrode choices

For manual hori-scoring

For the purpose of manually scoring each epoch according to the Hori scale, the EEG data of both datasets was further low pass filtered below 20 Hz using hamming windowed-sinc FIR filter. Only 21 electrodes depicted in Fig. 3(A) derived using the standard 10–20 system were used by the scorers.

For micro-measures algorithm

For the purpose of the micro-measures algorithm, we used the electrodes depicted in Fig. 3(B). The electrodes were chosen in such a way that we sample the Occipital, Frontal, Central, Parietal, Temporal regions. Furthermore, the choices were motivated for maximising the signal to noise ratio for the given reference electrode (Cz). This resulted in using 14 electrodes per dataset for the algorithm. The following are the electrodes used in the algorithm.

Dataset#1: Occipital: Oz, O1, O2; Frontal = F7, F8, Fz; Central = C3, C4; Parietal = Pz; Temporal = T7, T8, TP8, FT10, TP10

Dataset#2: Occipital: E75, E70, E83; Frontal = E33, E122, E11; Central = E36, E104; Parietal = E90; Temporal = E45, E108, E102, E115, E100;

Manual hori-scoring

Dataset#1: Each pre trial epoch (−4000 to 0ms) was rated independently by 3 raters. Of which one was an experienced electrophysiologist (rater C) and 2 of the other raters (A, B) had learnt the technique immediately prior to scoring them independently. The raters in dataset#1 scored each trial based on a manual algorithm depicted in Fig. 3(C). All participants were scored by the 3 raters, except for one participant that was scored only by raters A and B. As data from all participants was used based on group consensus rule (details below) this did not affect the results in anyway.

Group consensus rule: creation of gold standard dataset

In order to create consistency in the labels (manual hori scores) in our input data (Dataset#1), we decided to create a gold standard label for each trial that is based on a group consensus rule. For this purpose, we first subdivided the Hori ratings of each epoch per rater into Alert (Hori: 1,2), Drowsy-mild (Hori: 3,4,5), Drowsy-severe (Hori: 6,7,8,9,10). The gold standard label was computed using a simple majority among the raters. If there was no consensus, then the corresponding trials were ignored from further analysis. This group consensus rule was used in Dataset#1 and each trial was labelled into 'Alert', 'Drowsy (mild)',
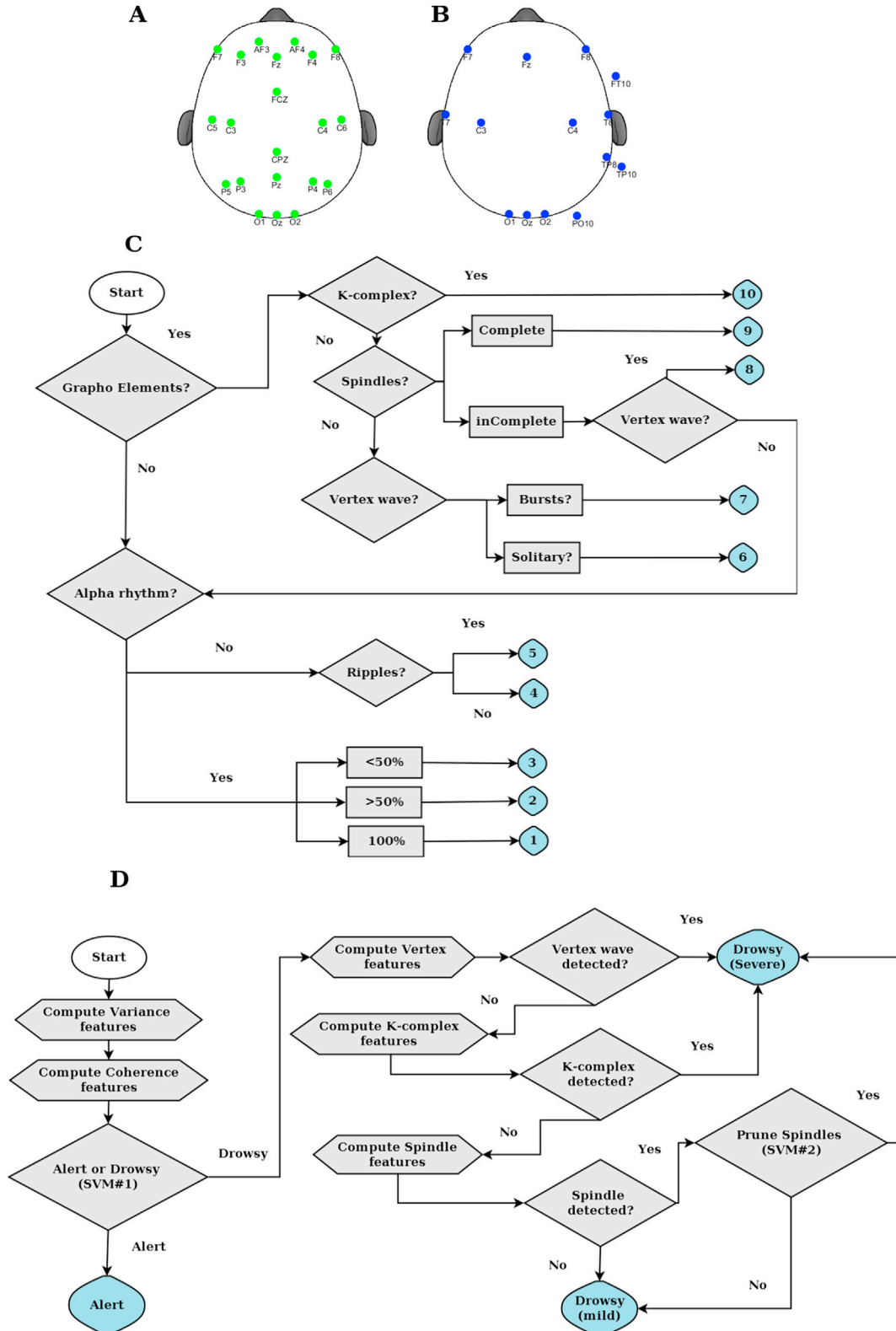
Fig. 3. (A) Electrode sites used for manual Hori scoring based on 21 channels of the locations mainly derived from 10 to 20 electrode sites. (B) Electrodes used for micro-measures algorithm based on sampling from locations in Occipital, Central, Temporal, Parietal, Frontal regions. (C) Step by step technique to manually score each trial using the Hori scale. The preliminary step involves identifying presence of graphoelements followed by specific identification of K-complexes, spindles and vertex waves. In the absence of graphoelements, the trials are scored with identification of alpha rhythms. (D) Brief flow chart of the micro-measures algorithm. The preliminary step involves computation of the predictor variance and coherence features, followed by identification of alert and drowsy trials using SVM (#1). Further, drowsy trials are identified into specific graphoelements using detectors of elements like vertex, K-complex, spindles. Spindles are further pruned using an SVM (#2).

'Drowsy (severe)'. The creation of this gold standard dataset ensured that the micro-measures algorithm was trained and tested with trials that were unambiguous and non-spurious.

After the group consensus rule was applied on Dataset#1, the number of trials in the gold standard dataset in each class were: Alert:478, Drowsy(mild):1121, Drowsy(severe):281. Thus we had 1880 trials which had a consensus rating among the 3 scorers (which is about 60% of the total pre-processed trials of 3201). Thus the gold standard ratings (1880 trials) in dataset#1 were used for training and testing the algorithm.

Dataset#2: Each pre trial epoch (-4000 to 0ms) was rated independently by 1 rater and was further verified with another experienced rater. The rater in dataset#2 scored each trial based on the description provided in (Ogilvie, 2001). The group consensus rule could not be applied to Dataset#2 as it only had one rater. Thus the number of trials in each class were: Alert: 6064, Drowsy(mild): 7229, Drowsy(severe): 481. Thus the total ratings (13774) were used for independently validating the algorithm.

Micro-measures algorithm

The micro-measures algorithm was first developed and tested using Dataset#1 and then independently validated using Dataset#2.

A brief flow chart of the algorithm is shown in Fig. 3(D). The first step in the algorithm involves the computation of predictor variance and coherence features. The second step involves using the variance and coherence features to classify data between alert (Hori:1–2) and Drowsy (Hori: 3–10) using an SVM (#1). The alert data from the output of SVM#1 are classed as 'Alert'. In the third step, the drowsy data from the output of the SVM#1 is passed onto individual element detectors to detect vertex, K-complex and spindles. In the fourth step, detected spindles are further pruned using a separate SVM (#2) to detect true spindles using the variance and coherence features. In the fifth step, the vertex, K-complex and true spindles are grouped as 'Drowsy(severe)' and the rest of the Drowsy data are classed into 'Drowsy(mild)'. Thus a combination of SVMs (#1, #2) and individual element detectors are used to produce a multiclass label of Alert, Drowsy(mild), Drowsy(severe).

Support vector machines

The SVMs are used for two tasks: a) SVM#1: To classify data into 'Alert' and Drowsy. b) SVM#2: To classify spindles detected by the spindle detector in the Drowsy data (from SVM#1) into true and spurious. We decided to use SVMs for the above tasks as the optimization problem in SVM is convex and hence a global minimum is guaranteed to be found (Platt, 1998; Tagliazucchi et al., 2012).

SVM are a class of supervised learning models. Formally, SVM consists of building a hyperplane or a set of hyperplanes in a high dimensional space with the criteria to maximise the distance of separation between the closest data (train-data) point of any class (functional margin) (Cortes and Vapnik, 1995). The choice of such a functional margin would lower the generalization error for new data points (test-data). The motivation to map the data onto higher dimensional space is driven by the fact that most often the classes are inseparable in the lower dimensional space (Boser et al., 1992). The mapping to higher dimensional space is achieved by the use of a kernel function. $k(x, y)$.

The kernel function avoids the need to compute individual data points in the transformed data space (computationally expensive) by using the euclidean inner product (kernel trick). In our paper, we used the MATLAB interface of the open source machine learning library (LIBSVM) (Chang and Lin, 2011) that supports use of kernel SVMs for nonlinear mappings. We used the Radial Basis Function (RBF) as our kernel $k(x, y) = e^{(-\gamma\|x-y\|^2)}$. The choice of the kernels was mainly based on those used in previous studies performing similar classification (Tagliazucchi et al., 2012).

Parameter space. For training the classifier to produce optimal

performance (accuracy) we need to select the optimal value of hyperparameters (γ, C). γ controls the curvature of the hyperplane and C represents the penalty parameter for the soft-margin. Parameter selection for SVM#1 is achieved by performing a grid search in (γ, C) in the space 2^{-1}, $.., 2^{25}$ (Tagliazucchi et al., 2012). For SVM#2, the grid space was narrowed down to $2^{-1}, .., 2^5$. The narrower space for SVM#2 was mainly to prevent overfitting.

Parameter optimization. In order to avoid biasing the tuning of the hyperparameters to the training dataset, we performed a 3-fold nested cross validation for both SVM#1, #2.

SVM#1: In the first step, data from all participants in Dataset#1 was collated. The gold standard labels are grouped into: Alert and Drowsy (mild, severe). The main goal of this classifier is to perform binary classification of Alert, Drowsy. The collated data was then divided into 5 disjoint subsamples, chosen randomly but with equal size. This process was achieved using the 'cvpartition' function in MATLAB. Each subsample consists of four folds grouped into a train set and the fifth fold considered as the test set. Each of the folds within a subsample was made using stratified sampling such that the overall representation of subclasses remained similar in each fold. This will avoid the problems of over-representation prevalent while using random-sampling. In the second step, one of the subsamples is selected. In the third step, half of the trails were randomly chosen from the train set of this subsample and these trials are used for parameter optimization. In the fourth step, we performed a 3-fold nested cross-validation for choosing the optimal parameters from the grid space. Nested cross-validation ensures that parameter selection and validation are independent, thus preventing the over fit of tuning the parameters to the train set. In the fifth step, the best parameter pair is now used and the best model is trained based on the train set. Further a five-fold cross validation is used for estimating the validation metrics for the train set and the best model is used on the test set to produce validation metrics on the same. In the sixth step, the same procedures from the second to the fifth step are repeated on the next subsample. Thus, 5 different subsamples yield 5 separate test and train set validation metrics. The detailed trial numbers and parameter optimization and validation procedure for SVM#1 is shown in Fig. 4(A).

SVM#2: Firstly, the first five steps of SVM#1 are executed as described above. The Drowsy data from the output of SVM#1 was run on the spindle detector and all the probable spindle trials are collated. The true spindles from the output of SVM#1 are computed using the gold standard label of Drowsy (mild). The train set now consists of the detected spindles (true and spurious spindles). The goal of the SVM#2 is now to classify data into spindle, and non-spindle. 3-fold nested cross validation as described in SVM#1 is performed to optimize the hyperparameters. Further a five-fold cross validation was performed and train set validation measures are further computed after running the vertex and K-complex element detectors. The best model of SVM#2 is again used on the test set to produce validation metrics on the same. The same steps are again repeated for the next subsample. Thus, 5 different subsamples yield 5 separate test and train set validation metrics. The detailed trial numbers and validation procedure for SVM#2 is shown in Fig. 4(B). One of the main reasons for using an SVM (#2) to separate true and spurious spindles is because most spindle detectors are used only in N2, however our detector is used on data from N1 also and hence this step is necessary to improve its specificity.

The variation of hyper-parameters in SVM#1, #2 in the grid-search procedure are shown in Fig. 5.

In both the SVMs the test and train sets are produced by collating data from all subjects in Dataset#1, however the usual procedure would be to perform a leave one participant out cross validation for generation of test sets. We were unable to do this, as this would produce a bias of validation metrics as different people fell asleep in different ways (proportion of alert, drowsy(mild), drowsy(severe) trials).

The performance of the classifier is evaluated using sensitivity,

Fig. 4. (A) Flowchart depicting Parameter optimization, model selection and validation metric generation for SVM#1. Trial numbers are presented in braces for the relevant steps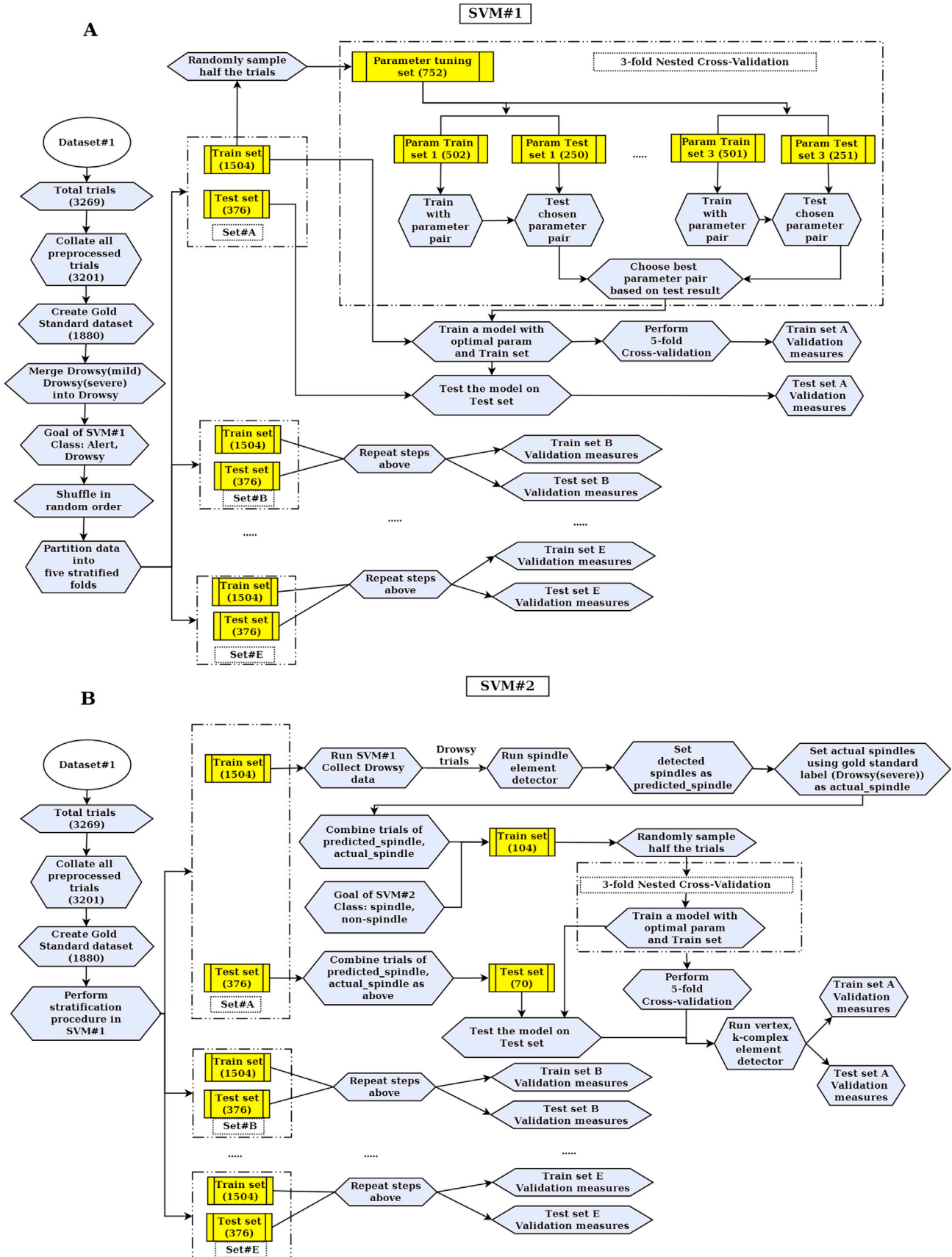. (B) Flowchart depicting Parameter optimization, model selection and validation metric generation for SVM#2. Trial numbers are presented in braces for the relevant steps.
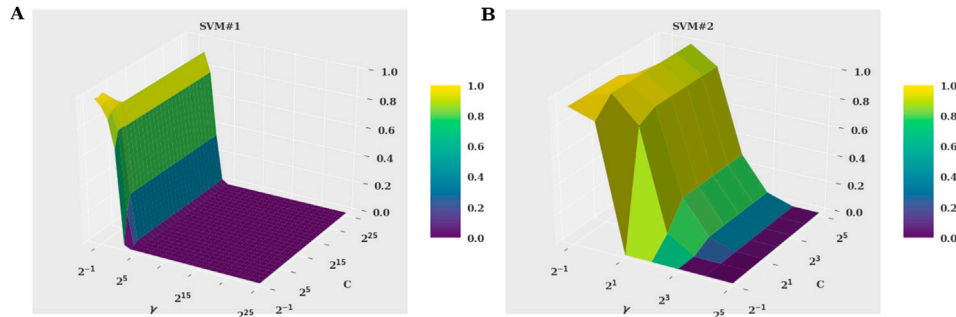
Fig. 5. (A) Hyper-parameter grid space (γ, C) and normalized accuracy for parameter search and optimization in SVM#1. (B) Hyper-parameter grid space (γ, C) and normalized accuracy for parameter search and optimization in SVM#2.

specificity, f1-score as validation metrics.

The definition of the validation metrics used are as follows:

Accuracy: This is defined as the number of correctly classified data points divided by the overall number of classifications made.

Sensitivity: This refers to the ability of a classifier to correctly detect the true class among the classifications made. It is obtained by the (TP/TP + FN). It is also known as recall. TP: True Positives, FN: False Negatives.

Specificity: This refers to the ability of a classifier to correctly ignore the classes that don't belong to the true condition. It is obtained by (TN/TN + FP). TN: True Negatives, FP: False Positives.

F1-score: This is the harmonic mean between precision and recall. Precision refers to measure of exactness of classifier. It is obtained by (TP/TP + FP). Recall refers to the sensitivity of the classifier.

Feature computation

The choice of the features of predictor variance and coherence used in the SVMs(#1,#2) was mainly motivated by previous studies utilizing similar features in automated methods to characterise sleep onset process (Ogilvie, 2001).

Predictor variance. The EEG data in the occipital region was first decomposed into time-frequency for each spatial sample (electrode) per epoch (-4000 to 0ms pre-trial). Predictors for each epoch were then generated based on the variations in the spectral power of the frequency bins A:[2–4 Hz], B:[8–10 Hz], C:[10–12 Hz], D:[2–6 Hz] per epoch. The predictors were then fit to the data per electrode-epoch and the variance explained is computed per electrode-epoch.

The first step is to transform the data $x[n]$ into time-frequency representation (predictors) using the formula below, where n represents time domain with $1 \leq k \leq N$

$$X(k) = \sum_{n=1}^{N} x(n) e^{\frac{-j2\pi(k-1)(n-1)}{N}}$$

The next step is to compute the power in the transformed representation

$$Power = X(k).X^*(k)$$

Followed by computing the predictor variance

$$PredictorVariance_i = 100 - 100 * \frac{Var(Power - X(k_i))}{Var(X(k_i))}$$

Where i the frequency band index (A, B,C,D) and *Var* represents the residual variance. Intuitively, the predictor variance tries to capture the variance in the signal explained by different frequency bands.

Coherence. Coherence was computed per trial in the electrodes in the occipital, frontal, central, temporal regions in the frequency bins: Delta:[1–4 Hz], Theta:[4–7 Hz], Alpha:[7–12 Hz], Sigma:[12–16 Hz], Gamma:[16–30 Hz]

$$C(t,f) = \frac{\left| S_{ij} (t,f) \right|^2}{S_{ii} (t,f).S_{jj} (t,f)}$$

Where $C(t,f)$ represents the coherence value at trial t and frequency band. fS_{ij} represents cross power spectral density between signal i and j S_{ii}, S_{jj} represents auto power spectral density.

In summary a total of 32 features (12 from predictor variance; 20 from coherence) are used in the first stage detection of alert trials from drowsy trials. After the drowsy trials are parsed by the element detectors, the spindle elements are pruned again by a separate SVM (#2) using the same 32 features as above (depicted in Fig. 3(D)). As the input data contains different kinds of features, it was scaled using the minimum value and range before applying the SVM.

Graphoelement detectors

Vertex-wave-detectors. Both monophasic and biphasic waves were detected using the EEG data from parietal electrodes.

Monophasic waves: In the first step, the data was resampled to a uniform rate of 100 Hz. In the second step, the data was further filtered from 0.25 to 6 Hz using inverse fast Fourier transform ('eegfiltfft' from EEGLAB). In the third step, the data was further scaled with respect to its minima. In the fourth step, peaks that are separated by a minimum distance of 1.5 s are computed. In the fifth step, only peaks above a threshold of 40 are retained. In the sixth step, the duration of the peaks is computed and only those below a duration of 1.5 s are retained. In the final step, only positive peaks greater than absolute amplitude of 30 μV and corresponding negative peaks of below -15 μV are considered as monophasic waves.

Biphasic waves: In the first step, the data was resampled to a uniform rate of 100 Hz. In the second step, the data was further filtered from 2.5 to 6 Hz using inverse fast Fourier transform ('eegfiltfft' from EEGLAB). In the third step, the data was further scaled with respect to its minima. In the fourth step, peaks that are separated by a minimum distance of 1.5 s are computed. In the fifth step, only peaks above a threshold of 40 are retained. In the sixth step, the duration of the peaks is computed and only those below a duration of 1.5 s are retained. In the final step, only positive peaks greater than absolute amplitude of 40 μV and corresponding negative peak (following the positive) of below -40 μV are considered as monophasic waves.

Further algorithmic and parametric details are described in the supplementary methods.

Spindle detectors. Spindles were detected using the EEG data from temporal electrodes. In the first step, the data was resampled to a uniform rate of 100 Hz. In the second step, a continuous wavelet transform using

the morlet function as the mother wavelet was applied. In the third step, the absolute amplitude of the wavelet transform was computed. In the fourth step, the coefficients of this transform were normalized using the sum of the absolute amplitude computed in the previous step. In the fifth step, the rank of each scale in the wavelet transform was sorted in ascending order. The rank of the scales belonging to the frequencies between 12 and 16 Hz was summed and normalized by the maximum possible rank that can be obtained. The normalized rank computed is regarded as the probability of spindle occurrence at each time point. In the sixth step, a sliding window of 12 samples were used to compute the probability of spindle occurrence (sliding window). In the seventh step, the maximum probability of spindle occurrence is computed by choosing the greater of the value between the probabilities computed in the sixth and seventh step. In the eight step, the probable spindle locations are short listed using a threshold of 0.6 on the maximum probability computed in the previous step. In the last step, the mean amplitude of the negative and positive peaks within the probable spindle locations is computed and only those exceeding 9 μV are retained as spindles.

Further validation details of our rank method are described in supplementary methods.

K-complex detectors. K-complexes were detected using the EEG data from all the electrode sites in Fig. 3(B). In the first step, the data was resampled to a uniform rate of 100 Hz. In the second step, the data was further filtered from 0.25 to 6 Hz using inverse fast Fourier transform ('eegfiltfft' from EEGLAB). In the third step, the data was further scaled with respect to its maxima. In the fourth step, negative peaks that are separated by a minimum distance of 1.5 s are computed. In the fifth step, only negative peaks below a threshold of −40 are retained. In the sixth step, the duration of the negative peaks is computed and only those below a duration of 1.5 s are retained. In the final step, the following criteria is used for further refining the detection: a) negative peaks should be lower than the absolute amplitude of −45 μV b) the corresponding positive peak associated with this negative peak should be at least half the amplitude of the negative peak c) the difference between the negative and positive peak should be at least 100 μV. The approach developed here is similar (in terms of minima detection) to detectors developed elsewhere (Lajnef et al., 2015).

Further validation details of our peak method are described in supplementary methods.

The rationale behind choosing specific parameters are validated by using external databases as described in supplementary methods and sec External Validation: Spindle, K-complex detectors.

Results

Manual hori-scoring

In order to measure the reliability of scores given by the 3 different raters on different subjects in Dataset#1 we used two different measures of inter-rater agreement (Fig. 6).

Firstly, we used Krippendorff's alpha to compute the agreement between the 3 raters (A, B, C) per subject of Dataset#1. In general alpha scores of above 0.8 are reliable and those between 0.8 and 0.667 can only be used to draw tentative conclusions (Giannantonio, 2010). We can observe from Fig. 6(A) that at least 9 subjects are below 0.667 (mean 0.65) indicating the unreliable nature of scoring each subject among raters. Secondly, we used Cohen's kappa score (weighted) to measure the degree of inter-rater agreement between pairs of raters (AB, AC, BC) of Dataset#1. In general kappa values of above 0.8 are considered strong, between 0.8 and 0.4 as strong to weak, below 0.4 as poor (McHugh, 2012). We can observe from Fig. 6(B) that at least 12 subjects are below 0.4 in the various scorer pairs again indicating the unreliable nature of scoring per subject among raters.

In particular the degree of disagreement was high for subjects that
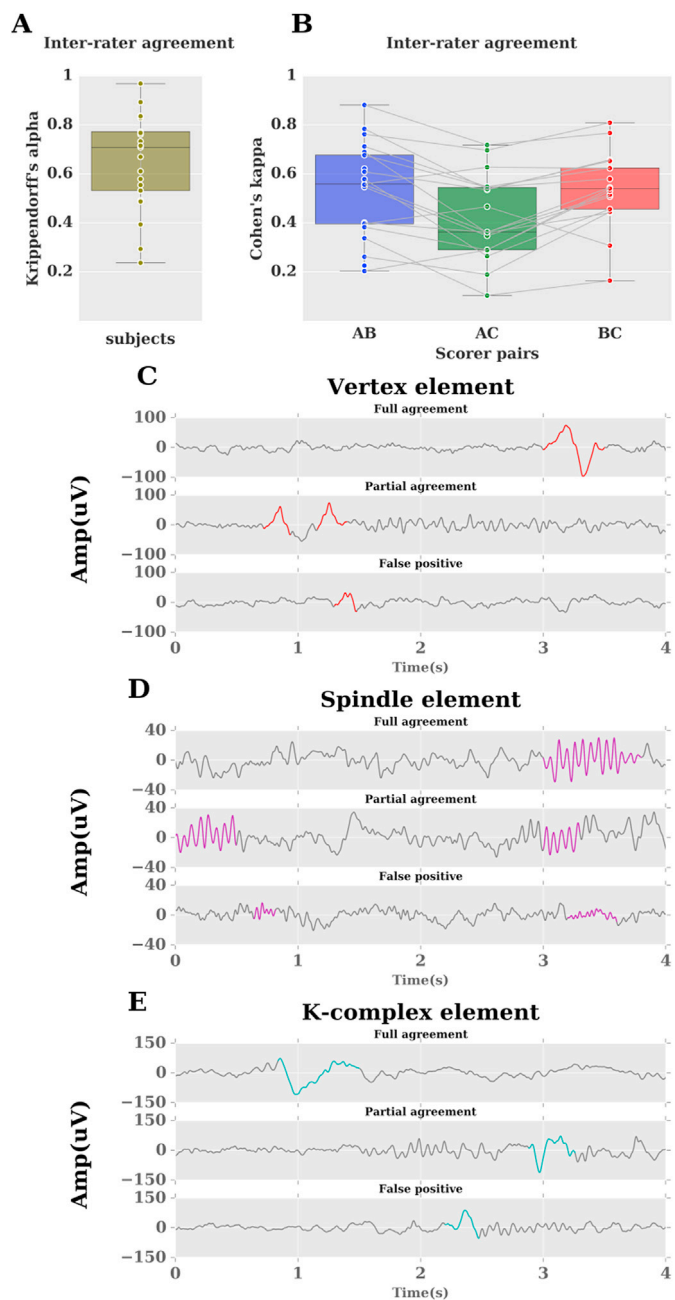
Fig. 6. Inter-rater agreement among different scorers (A,B,C). (A) depicts agreement measured using Krippendorff's alpha. Each data point refers to score from a single subject. (B) depicts agreement measured using Cohen's kappa. Each data point refers to kappa scores from a single subject based on a pair of two different scorers. Inter-rater disagreement is typically caused due to misclassification of Graphoelements: (C) depicts typical Vertex wave agreement/disagreement among scorers highlighted in red. (D) depicts typical Spindle element agreement/disagreement among scorers highlighted in magenta. (E) depicts typical K-complex agreement/disagreement among scorers highlighted in cyan. Full agreement refers to cases where all 3 raters agree, Partial agreement refers to cases where 2 of them agree, and false positives refer to cases where at least one of the rater misclassifies an element.

didn't have a dominant alpha, thereby affecting the ability to rate the Hori scores as (1,2,3). For other subjects the degree of disagreement mainly arose due to the mislabelling of graphical elements. Examples of such typical cases of graphoelements are shown in Fig. 6(C, D, E).

Micro-measures algorithm

External validation: spindle, K-complex detectors

The Spindle, K-complex detectors were validated externally using the DREAMS database along with other state of the art algorithms (Devuyst et al., 2011, 2010; Tsanas and Clifford, 2015) (detailed validation method in supplementary material). The validation results are shown in Fig. 7. This validation ensured the element detectors perform on par with the state of the art methods. The parameters used in spindle, K-complex detectors (like spindle duration, K-complex amplitude etc.) were fixed with respect to the external databases and the same parameters were used in the validation of both Dataset #1, #2.

Validation: Dataset#1

The application of the group consensus rule on Dataset#1 resulted in a total of 1880 trials as mentioned in section Manual Hori-scoring. This shows that about 40% of the overall trials didn't have any consensus among the 3 different raters, further adding evidence to the disagreement among scorers mentioned in section Manual Hori-scoring.

The validation measures like sensitivity, specificity, f-1 scores were generated as described in Fig. 4 and the results are shown in Fig. 9(A, B, C).

Independent validation: Dataset#2

We decided to validate the algorithm (trained using dataset#1) on an independent dataset#2 (participants not seen by the algorithm) to test its generalisability. This would mean that the hyper parameters (γ, C), support vectors trained using dataset#1 were directly applied on the dataset #2 without retraining.

The total number of trials in dataset#2 were 13774 as mentioned in section Manual Hori-scoring. Alert: 6064, Drowsy(mild): 7229, Drowsy(severe): 481. In the first step, the dataset#2 was divided into 5 folds (A,B,C,D,E) using stratified sampling as before. In the second step, one of the subsamples (For e.g. A) is selected. In the third step, the first 4 folds of the selected subsample is merged to create set#1 and set#2 consisted of the 5th fold. The best model (which was trained using dataset#1) is now applied on both sets to produce validation measures for set#1(A), set#2(A). The same procedure is repeated for all the other subsamples as depicted in Fig. 8. The validation measures like sensitivity, specificity, and f-1 scores generated are shown in Fig. 9(D, E, F).

The above mentioned validation measures tend to validate the micro-measures algorithm against the human scorer in Dataset#2. However, to claim that the micro-measures algorithm out performs the human scorer and other automated measures like alpha-theta ratio, we decided to further validate them against an independent measure of drowsiness in

Fig. 7. Performance validation of graphoelement detectors with online database (DREAMS). The spindle detector was validated with state of the art algorithms from (Devuyst et al., 2011; Tsanas and Clifford, 2015). The rank* algorithm developed in this paper performs comparably to the above mentioned algorithms. The K-complex detector was validated with state of the art algorithms from (Devuyst et al., 2010). The peak* algorithm developed in this paper performs comparable to the above mentioned algorithms.

Dataset#2.

Coefficient of variation (C_v) in reaction times has been used previously to measure drowsiness and is independent of both the observer and the algorithm's pre-trial information (Bareham et al., 2014). However, the usage of C_v to directly measure drowsiness is limited by several factors. Firstly, the C_v is not a single trial measure, hence it can only be computed on a group of trials. Secondly, C_v cannot be directly used to separate group of trials based on drowsiness as this would require setting up of arbitrary thresholds. Thirdly, it suffers from all the limitations of reaction time based measures as mentioned in the introduction. However, C_v can be used to validate group of trials already separated by other methods. We separated the trials among different classes of drowsiness using the micro-measures algorithm, alpha-theta ratio and the manual method. For the alpha-theta ratio, we used the methods described in (Bareham et al., 2014). Furthermore, each trial for each participant was classed as 'Alert' if the ratio was within the highest 33% of all trials in that participant and Drowsy(mild) if it belonged to middle 33% and Drowsy(severe) if it belonged to lowest 33%. C_v was computed for the group of reaction times of trials in each class (Alert, Drowsy(mild), Drowsy(severe)) in all methods. Further, we performed an asymptotic test for equality of C_v from k populations based on (Feltz and Miller, 1996) using the package 'cvequality' from R (Marwick and Krishnamoorthy, 2016). The test statistic D'AD produced by the asymptotic test measures the deviation of each sample C_v from the population C_v. Accordingly, the micro-measures algorithm produced D'AD of 13.12 ($p < 0.005$) in comparison with 12.39 ($p < 0.005$) for the manual method and 1.97 ($p > 0.05$) for the alpha-theta based method. These measures shown in Fig. 9(G), clearly indicate the utility of the micro-measures algorithm.

Discussions and conclusions

In this paper, we have first described the pervasive problem of varying levels of alertness during cognitive experiments, particularly during eyes-closed experiments. Such a scenario is further exacerbated in resting state EEG recordings. In many cases data from such experiments are used to compute measures like connectivity etc. that may further be contaminated by participants falling asleep (Tagliazucchi et al., 2012). This situation potentially contributes to wider problems faced by the scientific community such as the replication crisis.

In the past the problem of extreme relaxation and drowsiness has been sometimes ignored by cognitive scientists, who only take this confound into account by looking at reaction times and removing the sections where the participant was not responding or was too slow. Apart from visible changes in reaction times, there are changes in important processes like attention and perception as the participant drifts across varying levels of alertness (Goupil and Bekinschtein, 2012). Hence it is of paramount importance to control for varying levels of alertness. We have tried to solve this problem in an objective manner as follows. We first described the use of Hori scale that has been validated previously to detect the levels of alertness during the sleep onset process. However, the Hori scoring with 4 s epochs is impractical to perform as it is highly subjective and time consuming (Ogilvie, 2001). In a typical experiment of about 600 trials well trained scorers take at least a day to score a single subject, and training new scorers takes atleast a month before they can be used for scoring. Using 3 independent raters on Dataset#1 we further quantified the inter-rater agreement using Krippendorff's alpha and Cohen's kappa metrics to show poor levels of agreement among the raters. This motivated us to develop an algorithmic solution that can be used to measure the level of alertness in a reliable manner.

Other attempts in the past to detect varying level of alertness using algorithms have suffered from several disadvantages. Firstly, such rule based algorithms (Stein, 2007) have validated their system using physiological measures like heart-rate variability etc. This further adds a layer of confound as measures of alertness need to be related again with physiological measures. Secondly, other algorithms (Crisler et al., 2008;
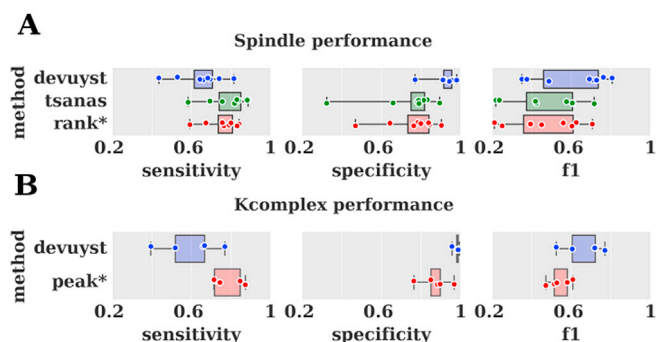
Fig. 8. Flowchart depicting generation of validation measures for independent validation of the micro-measures algorithm in Dataset#2. Trial numbers are presented in braces for the relevant steps.

Gudmundsson et al., 2005; Tagliazucchi et al., 2012) have been developed using traditional sleep stage based scoring. Such systems suffer from lack of resolution as they are validated with sleep scoring techniques that use 30 s epochs. Thus they are unsuitable to match the micro dynamics in alertness observed during cognitive tasks. To our knowledge this is the first time an algorithmic solution has been attempted to measure varying levels of alertness and simultaneously verified using a previously well validated system like Hori.

In the current work we have shown that the micro-measures algorithm using predictor variance, coherence and graphoelement detectors allow us to measure the level of alertness. We have constructed a classifier based on SVM and individual element detectors and have achieved sensitivity, specificity, f1-score of more than 0.8 in all subclasses (alert, drowsy (mild), drowsy (severe)) with respect to manual Hori scoring (gold standard from different raters). We have also validated our algorithm with a second independent dataset using different task conditions and recording electrode sites (using the same hyper parameters and support vectors trained using the first dataset). This produced a sensitivity, specificity of more than 0.7 in all subclasses. The main reason the performance (f1-score) reduces for drowsy (severe) subclass in dataset#2 is due to the lack of a gold standard comparison and fewer trials in this category. As the dataset#2 is scored only by one person it is prone to error (in a fashion similar to dataset#1 as depicted by varying levels of interrater agreement in Fig. 6). This motivated us to use another independent measure of drowsiness and show that our algorithm outperforms the manual scorer as well as other measures like alpha-theta ratio. Hence we employed a previously established independent behavioural measure of drowsiness using C_v in reaction times. We further showed that the micro-measures algorithm captures the variations in C_v better than the manual scorer and alpha-theta ratio in Fig. 9(G). This stands testament to the generalisability of our method in detecting alertness levels across new datasets.

However, the use of Hori scale as validator has some disadvantages.

Firstly, it is difficult to detect Hori stages (1–3) on participants who lack prominent alpha waves (Ogilvie, 2001). This would make these participants difficult to score manually, thereby explaining the lower sensitivity of the algorithm in the Drowsy (mild) subclass compared to the other classes in some participants. However, this is only a problem for the human scorer, as the micro-measures algorithm is relatively immune to this problem, as it operates on relative variances across different bands rather than raw amplitude. Secondly, it has also been reported that the Hori stage (4) also doesn't last long and hence is difficult to score (Ogilvie, 2001). Such samples would have had a high level of disagreement among scorers and hence would have been ignored while computing the gold standard dataset. Consequently, the difficult trials would not have been used for training the algorithm and hence it may not be able to detect any such trials in a new dataset. Thirdly, one of the main reasons for validating the algorithm with 3 subclasses is mainly due to lack of consensus in individual graphoelements. In order to truly validate the graphoelements we would need a dataset rich in those elements and also scorers who are able to consistently detect the graphoelements in a correct fashion.

The micro-measures algorithm devised here could be improved in several ways. Firstly, the current algorithm uses SVM with RBF kernels; other kernel choices like polynomial functions could be evaluated for making the optimal choice. Secondly, we performed only basic preprocessing of the pre trial data. However, it is well known that artifacts like eye movement, sweating, and muscle artifacts can contribute to noise in the data. Hence the performance of the algorithm would improve if noise reduction measures are employed. However, we didn't employ such measures as they are not standardized and we wanted to establish that the performance of the algorithm is robust under all conditions and hence performing specific pre-processing steps should not be an impediment for users of our method. Thirdly, we could also try to reduce the duration of epochs considered for labeling e.g. we can check the classification accuracies of signal durations of 1, 2, 3 s etc. However, validating the same
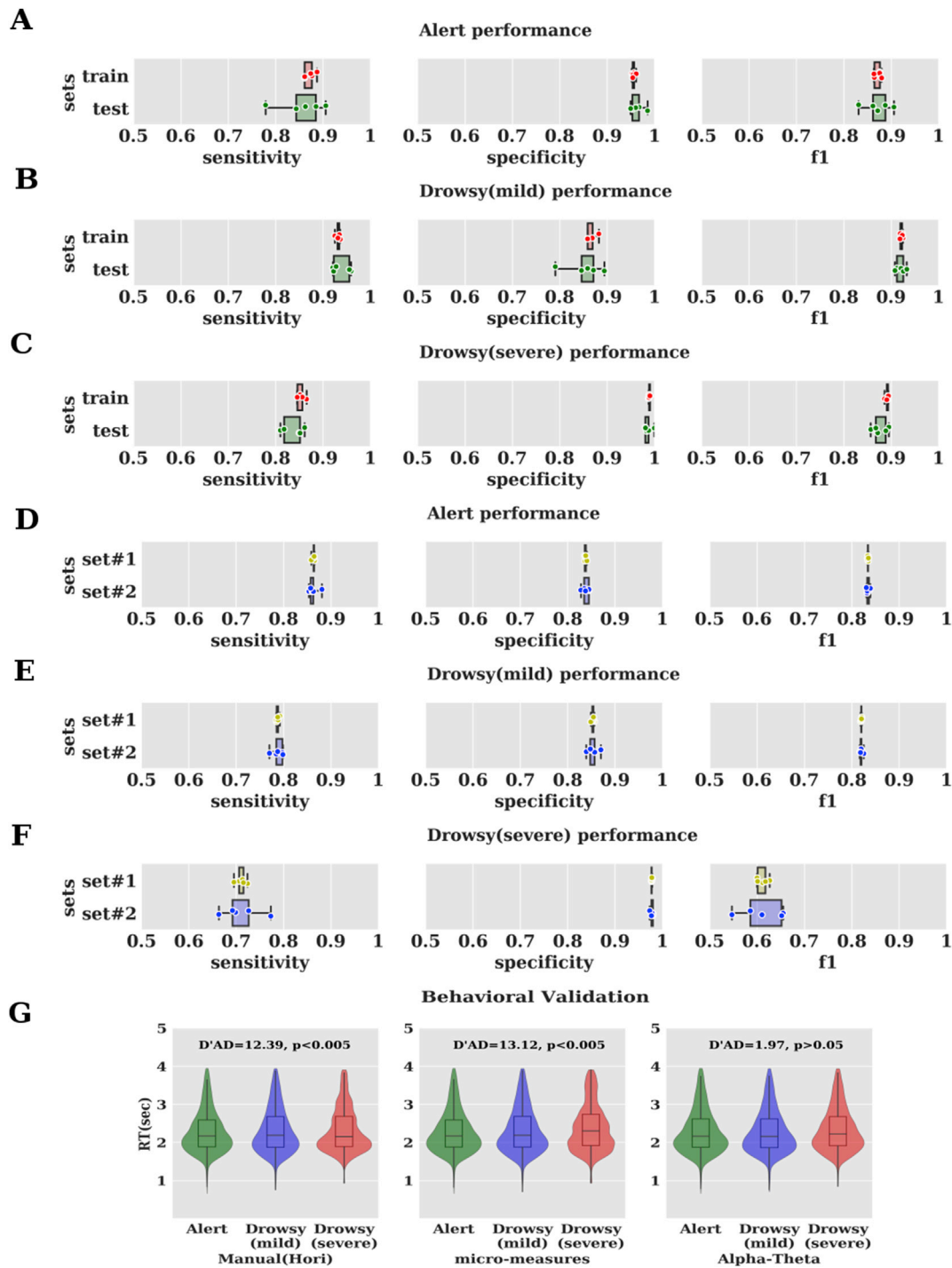
Fig. 9. Validation measures of the micro-measures algorithm. Validated with Dataset#1 using steps described in Fig. 4(A and B). Results are depicted in the Figure (A,B,C). The algorithm was validated in an independent manner using Dataset#2 using steps described in Fig. 8. Results are depicted in the Figure (D,E,F). The distribution of the reactions times (in seconds) are plotted against the different classes obtained using different methods in Dataset#2 is presented in Figure (G). Asymptotic test for equality of C_v (Coefficient of variation in reaction times) shows the micro-measures algorithm performing better than other methods. D'AD represents the asymptotic test statistic.

would be difficult as we also need to redo the human scoring with the corresponding reduced length of epochs. Fourthly, the algorithm has been developed only for eyes-closed condition. But many cognitive experiments have eyes open conditions and participants are also known to fall asleep under such active paradigms. The algorithm could be adapted for such paradigms; however detailed validation needs to be performed with other parallel measures of drowsiness like eye-tracking (as the Hori scale has not been validated for such purposes). Fifthly, the algorithm

could further be refined to produce stages analogous to individual Hori stages. This would be helpful for researchers studying the sleep onset process in an objective manner as many complex non-linear changes in behaviour are known to occur in individual Hori stages (Noreika et al., 2017b). Sixthly, for quick paced experiments (short pre-trial periods), the parameters for detecting certain graphoelements (vertexes, K-complexes) are flexible to account for the shorter duration of the signal. Finally, the usage of three scorers for manual hori scoring in dataset#1 achieved only

consensus ratings in close to 60% of the trials. However, the robustness of the algorithm could be improved if it is trained on large datasets that are scored by the neuroscience community using consensus achieved among a large number of scorers.

The applications of the micro-measures algorithm include the following. Firstly, pre-trial data can be computed from task data (cognitive experiments) and the non-alert trials can be removed thus controlling for the effects of change in alertness levels. Secondly, we can detect and remove non-alert periods of data from resting state EEG experiments in a reliable manner. Thirdly, we can measure alertness as an independent variable and measure its effect on measures of interest. Fourthly, the method circumvents the subjective nature of the manual Hori scoring and thus enables to study the transition to sleep in an objective way. One of the most interesting aspects is the generalisability of the SVM classifier and other element detectors to the independent dataset#2, showing the high degree of transferability of this method, without having to retrain the classifier. Fifthly, when combined with online stimulus delivery techniques, the ability of our method to detect graphoelements (vertex, spindles, K-complexes) also allows us to investigate the effects of these elements on cognitive processes, for example by modulating the stimulus delivery according to the occurrence of these elements. Finally, sleep researchers can use this method for detecting N1 periods in the beginning of the night as well as awakenings and N1 periods during the full night period; further, they can also validate the detection of N2 periods by using the appearance of specific graphoelements (spindles, K-complexes).

All of the above mentioned facets make our method a powerful solution that can be used to micro-measure varying alertness levels and thereby providing a valuable contribution to the study of both cognitive and resting state EEG experiments at large.

Algorithm & data availability

The micro-measures algorithm and its corresponding code are available at: https://github.com/SridharJagannathan/microMeasAlertness_HumanEEG.

The Datasets #1, #2 along with the Hori ratings is available at: https://doi.org/10.17863/CAM.18707.

Recommended usage steps for any dataset

The GitHub repository mentioned above houses the trained algorithm and has detailed pre-processing instructions to obtain drowsiness measures for any EEG dataset. Any potential user needs to perform only 2–3 simple steps to obtain trial by trial drowsiness measures, thereby avoiding the laborious task of manually scoring the EEG.

Reproducing figures

The code for reproducing the main figures in this paper is available in the following GitHub repository: https://github.com/SridharJagannathan/Jagannathan_Neuroimage2018

Conflicts of interest

None.

Author contributions

Conceptualization: SRJ, TAB.
Data Curation: SRJ, TAB.
Formal Analysis: SRJ, BJ, AEN, OVP, TAB.
Funding Acquisition: TAB.
Methodology: SRJ.
Project Administration: TAB.
Resources: TAB.

Software: SRJ.
Supervision: TAB.
Validation: SRJ, CAB, BJ, AEN.
Visualization: SRJ.
Writing – original draft: SRJ.
Writing – review & editing: SRJ, CAB, BJ, AEN, OVP, TAB.

Appendix A. Supplementary data

Supplementary data related to this article can be found at https://doi.org/10.1016/j.neuroimage.2018.04.046.

References

Bareham, C.A., Manly, T., Pustovaya, O.V., Scott, S.K., Bekinschtein, T.A., 2014. Losing the left side of the world: rightward shift in human spatial attention with sleep onset. Sci. Rep. 4, 1–5. https://doi.org/10.1038/srep05092.

Barry, R.J., Clarke, A.R., Johnstone, S.J., Magee, C.A., Rushby, J.A., 2007. EEG differences between eyes-closed and eyes-closed resting conditions. Int. J. Psychophysiol. 118, 2765–2773. https://doi.org/10.1016/j.clinph.2007.07.028.

Berry, R.B., Budhiraja, R., Gottlieb, D.J., Gozal, D., Iber, C., Kapur, V.K., Marcus, C.L., Mehra, R., Parthasarathy, S., Quan, S.F., Redline, S., Strohl, K.P., Ward, S.L.D., Tangredi, M.M., 2012. Rules for scoring respiratory events in sleep: update of the 2007 AASM manual for the scoring of sleep and associated events. J. Clin. Sleep. Med. https://doi.org/10.5664/jcsm.2172.

Boser, B.E., Guyon, I.M., Vapnik, V.N., 1992. A training algorithm for optimal margin classifiers. In: Proceedings of the Fifth Annual Workshop on Computational Learning Theory, COLT '92. ACM, New York, NY, USA, pp. 144–152. https://doi.org/10.1145/130385.130401.

Chang, C.-C., Lin, C.-J., 2011. LIBSVM: a library for support vector machines. ACM Trans. Intell. Syst. Technol. 2 (27), 1–27. https://doi.org/10.1145/1961189.1961199, 27.

Chennu, S., Bekinschtein, T.A., 2012. Arousal modulates auditory attention and awareness: insights from sleep, sedation, and disorders of consciousness. Front. Psychol. 3, 1–9. https://doi.org/10.3389/fpsyg.2012.00065.

Cortes, C., Vapnik, V., 1995. Support-Vector networks. Mach. Learn 20, 273–297. https://doi.org/10.1023/A:1022627411411.

Crisler, S., Morrissey, M.J., Anch, A.M., Barnett, D.W., 2008. Sleep-stage scoring in the rat using a support vector machine. J. Neurosci. Methods 168, 524–534. https://doi.org/10.1016/j.jneumeth.2007.10.027.

Delorme, A., Makeig, S., 2004. EEGLAB: an open source toolbox for analysis of single-trial EEG dynamics including independent component analysis. J. Neurosci. Methods 134, 9–21. https://doi.org/10.1016/j.jneumeth.2003.10.009.

Devuyst, S., Dutoit, T., Stenuit, P., Kerkhofs, M., 2011. Automatic sleep spindles detection–overview and development of a standard proposal assessment method. Conf. Proc. IEEE Eng. Med. Biol. Soc. 1713–1716. https://doi.org/10.1109/IEMBS.2011.6090491, 2011.

Devuyst, S., Dutoit, T., Stenuit, P., Kerkhofs, M., 2010. Automatic K-complexes detection in sleep EEG recordings using likelihood thresholds. In: 2010 Annu. Int. Conf. IEEE Eng. Med. Biol. Soc. https://doi.org/10.1109/IEMBS.2010.5626447. EMBC'10 4658–4661.

Dobler, V.B., Anker, S., Gilmore, J., Robertson, I.H., Atkinson, J., Manly, T., 2005. Asymmetric deterioration of spatial awareness with diminishing levels of alertness in normal children and children with ADHD. J. Child. Psychol. Psychiatry 46, 1230–1248. https://doi.org/10.1111/j.1469-7610.2005.00421.x.

Feltz, C.J., Miller, G.E., 1996. An asymptotic test for the equality of coefficients of variation from k populations. Stat. Med. 15, 647–658. https://doi.org/10.1002/(SICI)1097-0258(19960330)15:6<647::AID-SIM184>3.0.CO;2-P.

Ferree, T.C., Luu, P., Russell, G.S., Tucker, D.M., 2001. Scalp electrode impedance, infection risk, and EEG data quality. Clin. Neurophysiol. 112, 536–544. https://doi.org/10.1016/S1388-2457(00)00533-2.

Giannantonio, C.M., 2010. Book Review: Krippendorff, K. (2004). Content Analysis: an Introduction to its Methodology, second ed., vol. 13. Thousand Oaks, CA, pp. 392–394. https://doi.org/10.1177/1094428108324513. Sage. Organ. Res. Methods.

Goupil, L., Bekinschtein, T. a, 2012. Cognitive processing during the transition to sleep. Arch. Ital. Biol. 150, 140–154. https://doi.org/10.4449/aib.v150i2.1247.

Gudmundsson, S., Runarsson, T.P., Sigurdsson, S., 2005. Automatic sleep staging using support vector machines with posterior probability estimates. Int. Conf. Comput.

Intell. Model. Control Autom. 2, 366–372. https://doi.org/10.1109/CIMCA.2005.1631496.

Hackley, S.A., Graham, F.K., 1987. Effects of attending selectively to the spatial position of reflex-eliciting and reflex-modulating stimuli. J. Exp. Psychol. Hum. Percept. Perform. 13, 411–424.

Iber, C., Ancoli-Israel, S., Chesson, A.L., Quan, S.F., 2007. The AASM manual for the scoring of sleep and associated events American Academy of Sleep Medicine. American Academy of Sleep Medicine, Westchester, IL, pp. 48–49.

Johns, M.W., 1991. A new method for measuring daytime sleepiness: the Epworth sleepiness scale. Sleep 14, 540–545. https://doi.org/10.1093/sleep/14.6.540.

Kosslyn, S.M., Andersen, R.A., 1995. Frontiers in Cognitive Neuroscience. Mit Press.

Kouider, S., Andrillon, T., Barbosa, L.S., Goupil, L., Bekinschtein, T.A., 2014. Inducing task-relevant responses to speech in the sleeping brain. Curr. Biol. 24, 2208–2214. https://doi.org/10.1016/j.cub.2014.08.016.

Lajnef, T., Chaibi, S., Eichenlaub, J.-B., Ruby, P.M., Aguera, P.-E., Samet, M., Kachouri, A., Jerbi, K., 2015. Sleep spindle and K-complex detection using tunable Q-factor wavelet transform and morphological component analysis. Front. Hum. Neurosci. 9, 1–17. https://doi.org/10.3389/fnhum.2015.00414.

Marwick, B., Krishnamoorthy, K., 2016. Cvequality: Tests for the Equality of Coefficients of Variation from Multiple Groups.

McHugh, M.L., 2012. Interrater reliability: the kappa statistic. Biochem. Med. 276–282. https://doi.org/10.11613/BM.2012.031.

Niedermeyer, E., Silva, F.H.L. Da, 2004. Electroencephalography: Basic Principles, Clinical Applications, and Related Fields, fifth ed. Lippincott Williams & Wilkins, Philadelphia , London. Lippincott Williams and Wilkins.

Noreika, V., Canales-Johnson, A., Harrison, W.J., Johnson, A., Arnatkevičiūtė, A., Koh, J., Chennu, S., Bekinschtein, T.A., 2017a. Wakefulness State Modulates Conscious Access: Suppression of Auditory Detection in the Transition to Sleep, pp. 1–34 bioRxiv.

Noreika, V., Kamke, M.R., Canales-Johnson, A., Chennu, S., Mattingley, J.B., Bekinschtein, T.A., 2017b. Neurobehavioral Dynamics of Drowsiness, pp. 1–36. https://doi.org/10.1101/155754 bioRxiv.

Ogilvie, R.D., 2001. The process of falling asleep. Sleep. Med. Rev. 5, 247–270. https://doi.org/10.1053/smrv.2001.0145.

Olbrich, S., Mulert, C., Karch, S., Trenner, M., Leicht, G., Pogarell, O., Hegerl, U., 2009. EEG-vigilance and BOLD effect during simultaneous EEG/fMRI measurement. Neuroimage 45, 319–332. https://doi.org/10.1016/j.neuroimage.2008.11.014.

Oldfield, R.C., 1971. The assessment and analysis of handedness: the Edinburgh inventory. Neuropsychologia 9, 97–113. https://doi.org/10.1016/0028-3932(71)90067-4.

Platt, J., 1998. Sequential Minimal Optimization: a Fast Algorithm for Training Support Vector Machines.

Rodenbeck, A., Binder, R., Geisler, P., Danker-Hopfe, H., Lund, R., Raschke, F., Weeß, H.G., Schulz, H., 2006. A review of sleep EEG patterns. Part I: a compilation of amended rules for their visual recognition according to Rechtschaffen and Kales. Somnologie 10, 159–175. https://doi.org/10.1111/j.1439-054X.2006.00101.x.

Stein, M., 2007. Visual and computer-aided identification of vigilance differences in resting EEG between patients with obsessive-compulsive disorder, patients with borderline personality disorder and healthy controls. [German original title: Visuelle und computergestützt. Thesis Acquis. Ph.D. degree. Ludwig-Maximilians-University Munich, Munich. Med. Fac.

Šušmáková, K., Krakovská, a, 2007. Classification of waking, sleep onset and deep sleep by single measures. Meas. Sci. Rev. 7, 34–38.

Tagliazucchi, E., Laufs, H., 2014. Decoding wakefulness levels from typical fMRI resting-state data reveals reliable drifts between wakefulness and sleep. Neuron 82, 695–708. https://doi.org/10.1016/j.neuron.2014.03.020.

Tagliazucchi, E., von Wegner, F., Morzelewski, A., Borisov, S., Jahnke, K., Laufs, H., 2012. Automatic sleep staging using fMRI functional connectivity data. Neuroimage 63, 63–72. https://doi.org/10.1016/j.neuroimage.2012.06.036.

Tanaka, H., Hayashi, M., Hori, T., 1996. Statistical features of hypnagogic EEG measured by a new scoring system. Sleep 19, 731–738.

Tsanas, A., Clifford, G.D., 2015. Stage-independent, single lead EEG sleep spindle detection using the continuous wavelet transform and local weighted smoothing. Front. Hum. Neurosci. 9, 181. https://doi.org/10.3389/fnhum.2015.00181.

Warby, S.C., Wendt, S.L., Welinder, P., Munk, E.G.S., Carrillo, O., Sorensen, H.B.D., Jennum, P., Peppard, P.E., Perona, P., Mignot, E., 2014. Sleep-spindle detection: crowdsourcing and evaluating performance of experts, non-experts and automated methods. Nat. Methods 11, 385–392. https://doi.org/10.1038/nmeth.2855.

2.4 Discussion

In this manuscript, for the first time we have developed an objective method to control for alertness fluctuations in a trial-by-trail manner and validated the same with an independent measure like Hori scale. I have also highlighted the problem of fluctuating alertness levels in various cognitive experiments, especially during eyes closed settings. Evidence from mining large datasets (Tagliazucchi&Laufs 2014) have also revealed the wide spread nature of this problem, particularly under resting state conditions. Further computing measures of brain activity like connectivity between different brain regions during such drowsiness contaminated episodes can lead to incorrect inferences, potentially contributing to larger problems faced by the scientific community like replication crisis etc. Hence the objective method provided by our micro-measures algorithm to control for such varying levels of alertness is of paramount importance.

Currently effort is under way in our lab to extend this method to Magnetoencephalography (MEG) as well as EEG under eyes open settings. The principle approach being followed is conceptually similar to the approach used here (process of computing features in the data like variance, coherence etc. and using it in a SVM). Apart from this, the micro-measures algorithm can also be used for other purposes. For example, it can be combined with online stimulus delivery techniques to detect graphoelements (vertex, spindles, K-complex etc) and hence to deliver specific stimulus under certain graphoelements. This can be used to probe the effect of these individual elements on specific cognitive processes. Further, sleep researchers can use this tool to detect periods of N1 and also validate periods of N2 with the occurrence of graphoelements (spindles, K-complexes).

The micro-measure algorithm developed here forms an important methodological advancement in this dissertation. It will first be used (in Chapter 3, Chapter 4, Chapter 5) to detect trial-by-trial alertness levels in participants performing auditory tone localisation task. These trial-by-trial measures will further be used to understand the neural mechanism responsible for the generation of spatial bias induced by alertness transitions (as

mentioned in the previous chapter). Finally, this principled approach will also be used later (in Chapter 6) to detect alertness levels in flies undergoing transition to spontaneous sleep.

3

Behavioural dynamics of transitions

3.1 Brief Introduction

In this chapter, I investigate the behavioural dynamics in alertness transitions using an auditory spatial attention task. Briefly, participants hear tones from the left and right of the mid-line and need to localize the direction of the tone with a button press. Participants perform this task with eyes closed condition and are allowed to fall asleep, thus modulating their levels of alertness.

3.2 Background Information

A recent study (Bareham, Manly, et al. 2014) has provided first evidence (by using direct physiological measures of alertness) that variation in alertness levels produces a modulation of behaviour in an auditory spatial attention task. In this study, right-handed individuals under eyes closed condition performed an auditory tone localization task while falling asleep. The participants showed very little bias (misclassification of tones) when they were fully alert. But when they began to fall asleep they produced more misclassifi-

cation of tones from the left direction (left-errors) compared to the right direction tones (right-errors). This process of inattention to the left-side space is similar to neglect (where patients who suffered lesions in right hemisphere lack attention to the left-side space) and is referred herein as alertness induced spatial bias.

3.3 Shortcomings

Though (Bareham, Manly, et al. 2014) was one of the first studies to provide evidence of alertness modulated attention in healthy right-handers there were several shortcomings with the study (as mentioned in the Introduction chapter). First, the method for measuring alertness in this task was based on alpha-theta ratio or Hori scoring. Alpha-theta ratio method assumes equal number of trials as 'alert', 'drowsy' per participant which is not true, as different participants fall asleep differently (some more drowsy, some less drowsy). Hori scoring again suffers from the subjective nature of the scorer. Hence the micro-measures algorithm was developed in the previous chapter, which would provide the best objective measure of trial-by-trial alertness. Second, there was no separate baseline task to measure the bias of the individual participant before the experiment. if such a bias is measured beforehand, then it could be compared with the bias in the drowsy session to measure the change in bias. Third, some tones (1.86° to 35°) were played for more times than others (40° to 60°), which could potentially bias the results. Fourth, the methods used to analyse the relationship between bias and alertness (rmANOVA) assume individual participants had equal number of trials in 'alert' and 'drowsy' condition, which is not true as different participants fall asleep in different ways. Fifth, the quantification of subjective mid-line as proportion of left tone errors versus right tone errors ignores the variability afforded by tones from -60° to +60°. Such variability could be captured by psychometric fitting in individual participants. Sixth, distribution of reaction times could be used in a much more prudent way to capture the decision making process using sequential sampling models like drift diffusion modelling.

3.4 Research Question

The above mentioned shortcomings led us to the following questions which could be answered by an augmented spatial attention experiment (in the next section).

Does variation in alertness levels systematically produce bias in spatial attention?

The above question can be further subdivided as:

(a) *Does using a more objective method like micro-measures algorithm to measure alertness levels still lead to same spatial bias?*

(b) *Would the spatial bias change if there was a separate baseline session to measure alertness prior to the drowsiness session?*

(c) *Can we utilize methods like multi-level modelling that take advantage of uneven trial numbers per participant per condition? Would the spatial bias results still hold good?*

(d) *Can the shift in subjective mid-line be estimated systematically using psychometric fits? Would the subjective mid-lines shift with drowsiness?*

(e) *Can we capture the process of evidence accumulation using methods like drift-diffusion modelling? Would that show any systematic change in response bias? or evidence accumulation rate?*

(f) *Can these behavioural dynamics be used to understand the underpinning mechanisms of alertness induced spatial bias in these right-handed participants?*

3.5 Experiment

Stimuli and Protocol

Each participant in this study underwent two sessions: a) Awake b) Drowsy.

Awake session:

Participants were presented with 124 complex harmonic tones (created from guitar picks) that fell on the left or right of their mid-line (0°) varying from -59.31° to +59.31° as shown in Figure 3.1. The tones were recorded previously in free-field using in ear microphones (Bareham, Manly, et al. 2014). Six tones from -59.31° to -39.26° were presented two times each; twelve tones from -35.24° to -1.86° were presented four times each. The same pattern was repeated on the right side, with twelve tones from 1.86° to 35.24° were presented four times each, six tones from 39.26° to 59.31° presented two times each. The tones in the mid-line (0°) were presented four times. This resulted in a total of 124 tones. The order of stimulus presentation was randomized per participant. Participants were instructed to keep their eyes closed and respond (as quickly and as accurately as possible) with a button press (by left/right thumb) indicating the direction of the tone (left or right). Each trial began after a random interval of 2-3 seconds and if the participant did not respond for 5 seconds, the next trial was started. The participants were also instructed to stay awake throughout the task.

Drowsy session:

Participants were presented with 740 complex harmonic tones (as above) that fell on the left or right of their mid-line (0°) varying from -59.31° to +59.31°. Six tones from -59.31° to -39.26° were presented twenty times each; twelve tones from -35.24° to -1.86° were presented twenty times each. The same pattern was repeated on the right side, with twelve tones from 1.86° to 35.24° were presented twenty times each, six tones from 39.26° to 59.31° were presented twenty times each. The tone in the mid-line (0°) was presented twenty times. This resulted in a total of 740 tones. The order of stimulus presentation was randomized per participant as above. Participants were instructed to keep their eyes closed and respond (as quickly and as accurately as possible) with a button press (by left/right thumb) indicating the direction of the tone (left or right). Each trial began after a random interval of 4-5 seconds and if the participant did not respond for 5 seconds, the next trial was started. The participants were allowed to fall asleep (and become drowsy) and were woken up if they didn't respond to more than 3 trials continuously.

Before the awake and drowsy session, the participants were allowed a practice session to familiarise with the task.
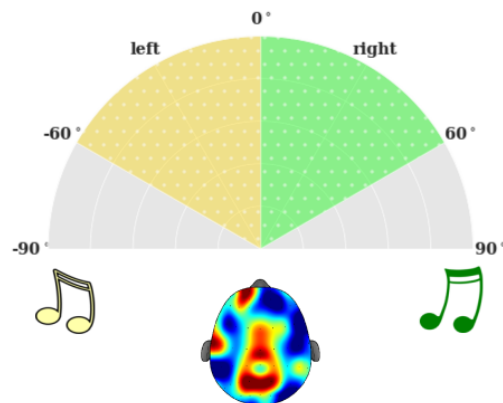
Figure 3.1: Auditory Spatial attention task. Participants had to localize the direction of auditory tones coming from left and right side of the mid-line. The tones fell on the left or right of their mid-line (0°) varying from -59.31° to +59.31°.

Participant details

Forty-one healthy right-handers were recruited for this study. Data from nine participants were removed due to a) technical issues with the headphone amplifier that delivers the auditory stimuli (8). b) Not following instructions (1). This resulted in data from thirty-two participants (24.46 ± 3.72 years old, 14 males) to be considered for further analysis. As this study involved participants falling asleep, only self described easy sleepers were invited to participate in this study. On the day of the experiment, the participants were administered with the Epworth Sleepiness scale (Johns 1991), Edinburgh Handedness Scale (Oldfield 1971). Twenty-nine participants had a sleepiness score >= 7 (easy sleepers) and 3 of them had a sleepiness score >=4. All participants had handedness score of above 0 (right-handed) with mean 80.26 ± 23.59.

All participants had no auditory, neurological, psychiatric abnormalities. They were also asked not to consume stimulants like Coffee/Tea on the day of the experiment. Further, they gave written informed consent and were compensated with 30£ for the study.

3.6 Methods

3.6.1 Preprocessing

EEG data was acquired using 129 Ag/AgCl electrodes (Electrical Geodesics Inc) with Cz as reference. The electrode impedances were kept below $\sim 100 K\Omega$ and signal was acquired at a sampling rate of 500 Hz. EEG data was pre-processed with custom made scripts in MATLAB (MathWorks Inc. Natick, MA, USA) using EEGLAB toolbox (Delorme&Makeig 2004). First, the peripheral channels in the EEG that covered the regions of forehead, cheeks and neck were removed to minimise eye and muscle related artifacts, thus retaining only 92 channels that covered the scalp. Second, the data was bandpass filtered with zero phase shift between 1 and 40 Hz using hamming windowed-sinc FIR filter and was then resampled to 250 Hz. Third, pre-trial and post-trial epochs were created as follows. For the pre-trial epochs, the data was epoched from -4000 ms to 0 ms to the onset of the stimuli in the Drowsy session. Pre-trial epochs were not created in the Awake session (details in next section). For the post-trial epochs, the data was epoched from -200 ms to 800 ms to the onset of the stimuli for both the Awake and Drowsy sessions. Fourth, the trials that exceeded the amplitude threshold of ±250 μV were removed in a semi-automatic fashion. Fifth, the bad channels were detected in two steps: a) channels are considered bad if channel variance is below 0.5. b) The normalized power spectrum of the remaining channels was computed and any channel that exceeds the mean power spectrum by ±3 standard deviations was marked bad. Sixth, Independent component analysis (ICA) was performed on the channels that were not marked as bad in the previous step. ICA components that correspond to artifacts (eye-blinks, muscle) were rejected by manual inspection. Seventh, the bad channels were now interpolated using spherical interpolation. Eighth, the bad trials detection was performed again (amplitude threshold of ±250 μV) and bad electrodes in such trials were interpolated in a trial-by-trial fashion. Ninth, the post-trial epochs were re-referenced to the average of all channels (pre-trial epochs were maintained with the same Cz reference).

3.6.2 Alertness levels

The first step in the analysis involved classifying periods of the experimental session into 'alert' and 'drowsy'. The pre-trial period before each tone was used in classifying the corresponding trial as alert or drowsy. However, in the awake session all participants were explicitly asked to stay alert. Hence the pre-trial epochs were not computed in the awake session and all 124 trials in the awake session in each participant were classified as 'alert'. In the drowsy session, the participants were allowed to fall asleep and hence in some trials they would be alert and in some they would be drowsy. Pre-trial epochs in the drowsy session (computed from the previous section) were analysed using the micro-measures algorithm developed in the previous chapter (Jagannathan, Ezquerro-Nassar, et al. 2018) and each trial was classified was 'alert', 'drowsy(mild)', 'drowsy(severe)'. Only trials that were classified as 'drowsy(mild)' were used as 'drowsy' trials. The other trials were ignored because usually participants don't respond when under 'drowsy(severe)' trials and we also wanted to compare the drowsy trials of the drowsy session to the alert session, so we ignored the 'alert' trials in the drowsy session.

3.7 Results

3.7.1 Multi-level modelling

In the next step we decided to employ statistical models to understand how the behaviour of the participants change across different levels of alertness in this spatial attention task. For this purpose, we decided to use multi-level model (mixed models) wherein the parameters are made to vary at more than one level. This is in contrast to measures like rmANOVA where the parameters are only estimated at one level (group). The main advantages of multi-level models include: a) less strict assumptions: When assumptions of homogeneity of variances, constant covariances, sphericity are violated we cannot use rmANOVA, however multi-level model overcomes such violations. b) Missing data can

be handled directly by multi-level models, however in rmANOVA, subjects with missing data are usually dropped from the analysis.

We first computed the proportion of errors made by each subject under each condition ('alert', 'drowsy') under each stimulus ('left', 'right' to the midline). If the number of trials for any participant under a particular condition is less than 5 then the corresponding error proportion is ignored in the analysis. Next, we investigated whether the proportion of error is influenced by state of the participant ('alert' or 'drowsy'), stimulus ('left' or 'right') or an interaction of both. For this purpose, we defined 4 models. In the null model, the error proportion depends only on its mean (fixed effect) and the individual participant (subject id is used a random effect). In the second model (state model), the error proportion depends only on the state of the participant ('alert' or 'drowsy' as fixed effect) and individual participant (subject id is used as random effect). In the third model (stimulus model), the error proportion depends only on the stimulus being presented ('left' or 'right' as fixed effect) and individual participant (subject id is used as random effect). In the fourth model (state-stimulus model), the error proportion depends on a combination (interaction) of state of participant ('alert' or 'drowsy') and the stimulus being presented ('left' or 'right'), both used as fixed effects and individual participant (subject id is used as random effect). These 4 models are fit using the 'lmer' function in R (Bates, Maechler, et al. 2015b; Bates, Maechler, et al. 2015a) and the winning model is identified as the one with the highest log-likelihood by comparing it with the null model and further performing a likelihood ratio chi-square test (χ^2). Finally, the top two winning models are compared against each other using 'anova' function in R (Fox&Weisberg 2011), to validate whether the winning model (if it is more complex) is actually better than the loosing model (if it is simpler). The models along with log-likelihood values are shown in Table 3.1. The state-stimulus model emerged as the winning model based on higher log-likelihood score.

Model comparison			
Model	Parameters	Log-likelihood	$Pr(>\chi^2)$
Null	Fixed: mean, Random: subject id	61.24	-
State	Fixed: state, Random: subject id	66.62	<0.001
Stimulus	Fixed: stimulus, Random: subject id	68.45	<0.001
State-Stimulus	Fixed: state*stimulus, Random: subject id	77.98	<0.001

Table 3.1: Comparison of various multi-level models in right-handers using log-likelihood

As seen above from the winning model, there was a significant effect of state on error-proportion with $F(1, 95.07) = 14.04$, $p<0.001$. Stimulus type also significantly affected error-proportion with $F(1,95.07) = 18.80$, $p<0.001$. The interaction between state and stimulus also significantly affected error-proportion with $F(1,95.07) = 6.88$, $p<0.05$. This indicates that as right-handers became drowsy the error proportion of some stimulus was affected more than others. Further estimated marginal means were computed (using 'emmeans' package in R) for simple contrast of both left and right stimulus through which error-proportion across alert and drowsy conditions could be compared. This revealed a significant difference between alert and drowsy conditions for left stimuli with mean = -0.13 with standard error = 0.03 and $t(98.11) = -4.45$, $p<0.0001$, whereas for the right stimuli there was no significant difference across alert and drowsy periods with mean = -0.02 with standard error = 0.03 and $t(98.68) = -0.77$, $p>0.05$. To summarise, as right-handers become drowsier they tend to make left errors as shown in Figure 3.2.

3.7.2 Psychophysics

Next, we aimed to quantify the change in the subjective mid-line per participant as they become drowsier. For this purpose, we decided to fit psychometric functions to the responses produced by each participant under alert and drowsy conditions. The proportion of rightward response under each stimulus condition from -60° to +60° was fitted with a cumulative normal function using the generalized linear model 'glm' function in R. The link function used for the fit was 'probit' which asymptotes to 0 (Knoblauch 2014). The 'probit' function is in essence is the cumulative Gaussian function and is constrained within the
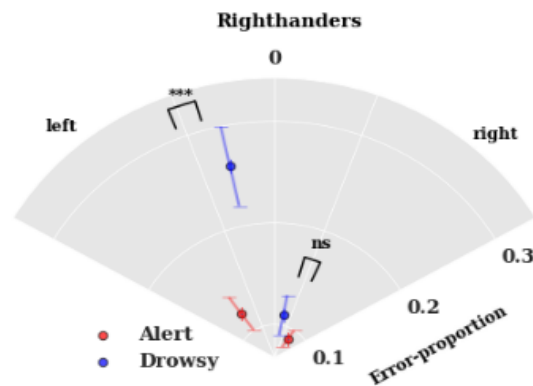
Figure 3.2: Average Proportion of errors committed by right-handers in alert and drowsy periods across left and right stimuli. Error-proportion depends on stimulus type (left,right), state of participant (alert,drowsy) and interaction between stimulus and state. Estimated marginal means (computed for alert and drowsy periods) indicate the error proportion is significantly different across left stimuli, but is not significant across right stimuli. *** indicates p<0.001, ns indicates not significant, error bars indicate standard error of the mean.

range of $[0, 1]$ which is suitable to model the proportion of responses. The mean of the cumulative normal function (the point where the curve cross 0.5 in the y-axis) is referred to as the subjective mid-line ('bias'). This is because the subjective mid-line is the stimulus where the participant performs at chance (0.5). The Bias was calculated separately per participant per condition (alert, drowsy). The standard deviation of the curve (slope or steepness of the curve) represents the 'sensitivity' of the system. Increase in standard deviation reduces the sensitivity of the system. Participants that had a bias point (mean) of more than 60° were ignored in the drowsy condition (this is because overall stimulus angle varied from -60° to +60°).

Thus Bias (mean of the function), Sensitivity (inverse of standard deviation) was computed per participant per condition. For some participants, the bias point shifted to the left as they become drowsier (they started pressing more rightward responses and hence making more left errors). For some other participants, the bias point shifted to the right as they become drowsier (they started pressing more leftward responses and hence making more right errors). If the bias point moved leftwards, the participant is called as 'left-shifters', whereas if the bias point moved rightwards, the participant is called as 'right-shifters'. The

fits of the psychometric functions for example participants who were left and right-shifter is shown in Figure 3.3.
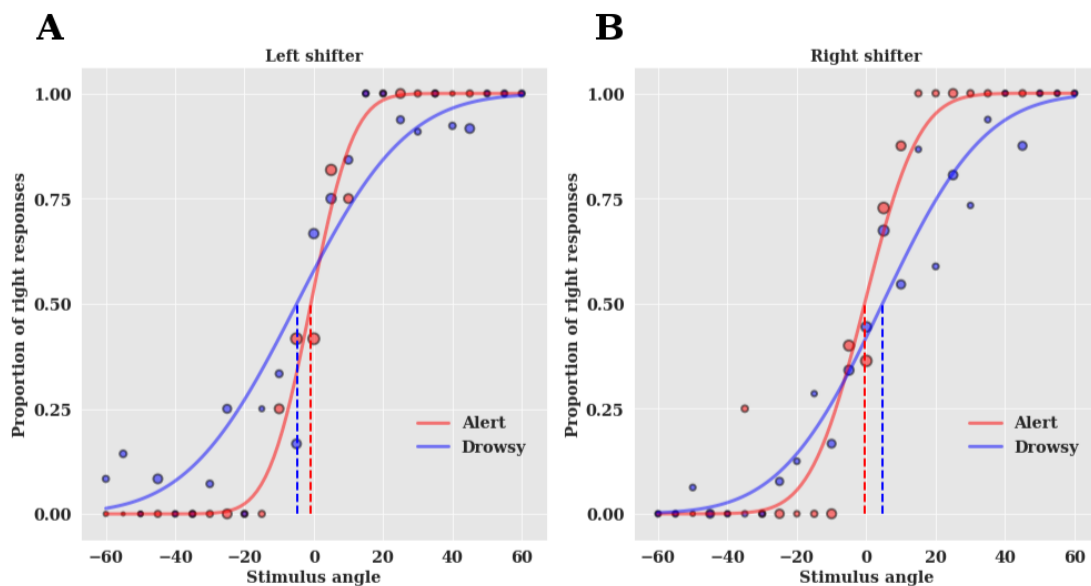
Figure 3.3: Psychometric fits indicating shifts in subjective mid-line. Data from two sample participants (A,B) are shown here. The proportion of right responses were fit across stimuli from -60° to +60° in both alert and drowsy periods. The mean of the fitted function ('probit') indicates the subjective mid-line ('bias'). A) Bias point shifts towards the left as the participant becomes drowsier. B) Bias point shifts towards the right as the participant becomes drowsier.

Twenty-four participants were identified as 'left-shifters' as their subjective mid-line shifted to the left when they became drowsy as shown in Figure 3.4. Seven participants were identified as 'right-shifters' as their subjective mid-line shifted to the right when they became drowsy. One participant was ignored from the analysis as their bias point in drowsy condition exceeded ±60°. This shows that most right-handers make left errors as they become drowsy, which is consistent with the multi-level modelling analysis (in the previous section).

3.7.3 Hierarchical drift diffusion modelling

Next, we aimed to quantify the different elements of decision-making process using the drift-diffusion model. The drift-diffusion model captures the optimal procedure involved in performing a 2-alternative forced choice (2AFC) task. It assumes that the observer accumulates evidence for one or other alternative in every other time step, until that inte-
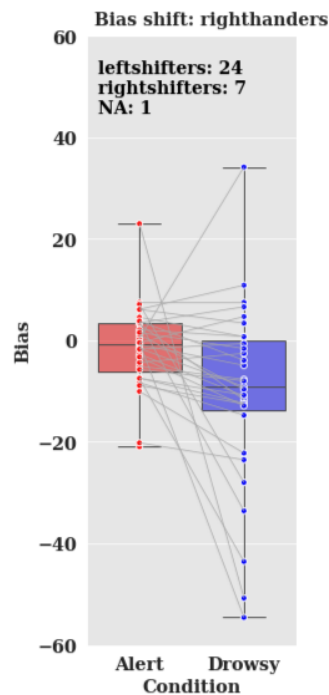
Figure 3.4: Bias points across alert and drowsy periods for right-handers. The bias points move predominantly towards the left (more negative) compared to the right (more positive) as participants become drowsier. This indicates that right-handers are predominantly left-shifters and hence make more left errors as they become drowsier.

grated evidence reaches a threshold to make a decision. This model is known to describe accuracy and reaction time distributions in 2-choice tasks (Ratcliff, Smith, et al. 2016). The primary elements of this model are shown in Figure 3.5 which include i) drift-rate - 'v' which is the evidence accumulation rate ii) bias point - 'z' indicating the starting point of the decision making process iii) boundary separation distance - 'a' which is the distance between the two decision boundaries. iv) non-decision time - 'Ter' usually accounting for processes like stimulus encoding (prior to evidence accumulation), time for response execution (after evidence accumulation).

It is important to note that as different participants would have differing levels of alertness, this would mean that we have varying number of trials per condition per participant. Hence it is crucial to use an approach that would provide a robust estimation of model parameters with the limited amount of trials available (Zhang, Rittman, et al. 2016). Hence, we decided to use the hierarchical drift diffusion model (HDDM) to provide for a hierarchical Bayesian procedure to estimate the model parameters involved in our task (Wiecki,
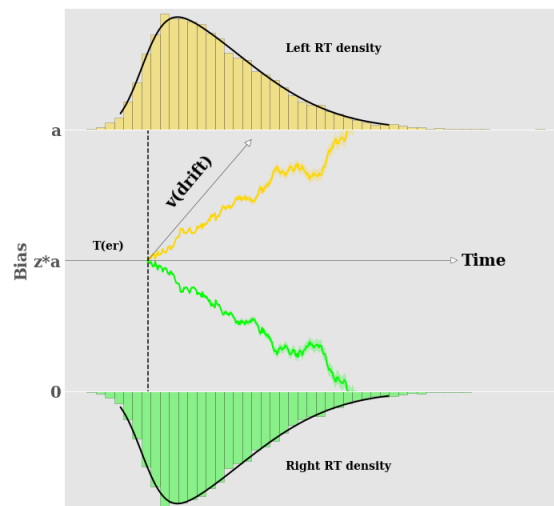
Figure 3.5: Schematic indicating evidence accumulation expressed by driftdiffusion model. The model accounts for the reaction time distributions of responses across left and right stimuli ('Stimulus Coding'). 'V(drift)' indicates the drift rate (evidence accumulation rate), 'a' indicates the boundary separation across left and right responses, 'z' indicates the bias point, usually z = 0.5 for unbiased responses.

Sofer, et al. 2013) (version 0.6.0). For the HDDM we fit the response of each participant ('left' or 'right') instead of accuracy ('correct' or 'incorrect'). This procedure is referred to as Stimulus-coding and is critical to uncover response bias (de Gee, Colizoli, et al. 2017) in the decision making process.

For our purpose, we examined 8 different variants of the drift diffusion models where each model varies on the following parameters: drift-rate (v) depending on state ('alert', 'drowsy') or stimulus ('left', 'right') or combination of both. bias-point (z) was also varied depending on state ('alert', 'drowsy') or stimulus ('left', 'right') or combination of both.

For individual models, we created 15000 samples from the posterior distribution of the model parameters using Markov chain Monte Carlo methods. Further 5000 samples were discarded as burn-in to reduce the effect of initial values on the estimation of the posterior. The winning model in each case was chosen by the lowest deviance information criterion (DIC). The DIC provides a measure for the accuracy of the model, while penalising for model complexity (Spiegelhalter, Best, et al. 2002). To check the convergence of the winning model, Gelman-Rubin statistic was compared for 5 model runs and the winning model was found to have values close to 1 and not larger than 1.2 thus indicating convergence (Gelman 2013). The DIC scores along with model specifications are

shown in Table 3.2. The winning model composed of: Drift-rate (v) varied according to state ('alert','drowsy') and stim ('left','right'). Bias-point (z) varied according to stim ('left','right')

Model comparison			
Model#	Drift-rate(v)	Bias-point(z)	DIC score
1	'state'	'state'	22515.22
2	'state'	'stim'	22474.04
3	'state'	'state','stim'	22274.47
4	'stim'	'state'	24057.05
5	'stim'	'stim'	23903.25
6	'stim'	'state','stim'	22112.33
7	'state','stim'	'state'	21712.48
8	**'state','stim'**	**'stim'**	**21698.74**

Table 3.2: Comparison of various drift-diffusion models in right-handers using DIC scores. The winning model (8) is composed of: Drift-rate (v) varied according to state ('alert','drowsy') and stim ('left','right'). Bias-point (z) varied according to stim ('left','right')

In the next step, the winning model (8) was analysed for the comparison of posterior densities. The traditional way to compare the distribution of population of two groups is using hull-hypothesis testing (frequentist methods). However, we used Bayesian estimate which is fundamentally more informative and avoids the arbitrary choices like significance level, statistical test etc. used by the frequentist based methods (Kruschke 2013).

It was found that the proportion of posterior overlap (between left and right stimuli) in the bias point was 25.1% (Figure 3.6(A)). It was also found that the proportion of posterior overlap (between left and right stimuli) in the drift rate under alert condition was 14.8%(Figure 3.6(B)) this reduces to 3.4%(Figure 3.6(C)) under drowsy condition. This indicates a change in drift-rate (evidence accumulation) between left and right stimuli as right-handers become drowsier. To summarise, as right-handers become drowsier the difference in rates of evidence accumulation between left and right stimuli increases. The difference in drift-rates provides a potential explanation of why right-handers make disproportionally more left-errors as they become drowsier.
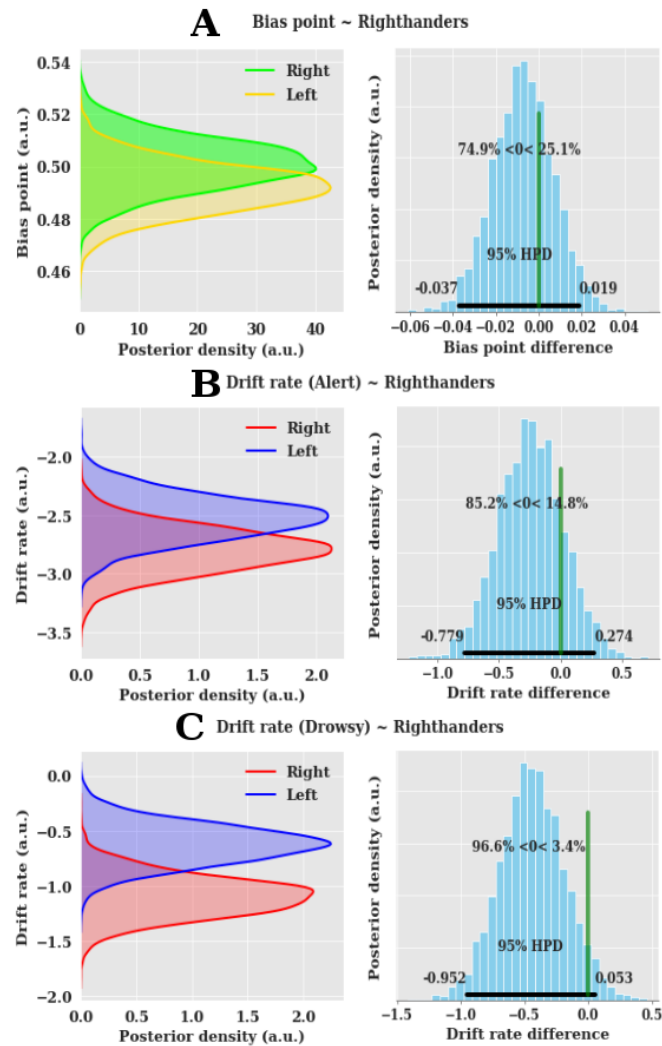
Figure 3.6: A) Group-level posterior distributions for bias-point (z) across left and right stimuli. In right-handers, the difference of traces is plotted indicating proportion of overlap between estimates as 25%. C) Group-level posterior distributions for drift-rate (v) across left and right stimuli in in alert trials. In right-handers, the difference of the traces is plotted indicating proportion of overlap between estimates as 14.8%. C) Group-level posterior distributions for drift-rate (v) across left and right stimuli in drowsy trials. In right-handers, the difference of the traces is plotted indicating proportion of overlap between estimates as 3.4%. HPD stands for highest posterior density representing credible interval for a particular parameter.

3.8 Discussion

In this chapter I decided to investigate the behavioural dynamics of spatial bias induced by alertness transitions. By using a separate baseline 'alert' session, I quantified the inherent bias in individual participants before they become 'drowsy'.

Next, I used multilevel modelling to understand the relationship between the proportion of errors and the state of participant ('alert,'drowsy') and location of auditory stimuli ('left','right') presented. The error proportion was best explained by the model which contained both state of participant and stimulus being presented and a term involving interaction of both. Usage of multilevel model allows us to take full advantage of the variability among participants (number of trials per condition). When, the estimated marginal means were computed across different states, they show that as right-handers become drowsy they tend to make more left errors. These results replicate (Bareham, Manly, et al. 2014) and further show evidence for left-neglect as suggested by (Fink, Marshall, et al. 2001; Jewell&McCourt 2000) in other modalities.

Next, I computed the subjective mid-line by fitting the psychometric functions to the proportion of right responses in individual participants per condition ('alert', 'drowsy'). I have shown that for majority (24) of the participants the mid-line shifts to the left (more left errors). Usage of psychometric functions to estimate the mid-line takes full advantage of the systematic variability afforded by tones from -60° to +60°. These results again replicate the error bias metric ($lefterrors - righterrors/totalerrors$) computed in (Bareham, Manly, et al. 2014) and further show evidence for subjective mid-line shift similar to the observations in patient studies (Vallar, Guariglia, et al. 1995; Karnath 1997).

Finally, I modelled the decision making process by using drift diffusion model. This allowed for the separation of the response bias (z) from evidence accumulation rate (v). I have shown that the bias point (z) varies with respect to the stimuli ('left', 'right') whereas the drift rate (v) varies with respect to both stimuli ('left', 'right') and state ('alert', 'drowsy'). Upon analysing the posterior distributions it can be seen that the drift rate between 'right' and 'left' stimuli changes in a significant manner. These results point towards a process of evidence accumulation that can help disentangle whether drowsiness induced spatial bias is a process of attentional deficit or sensory dysfunction. It has been shown by studies (Nunez, Vandekerckhove, et al. 2017) that trial to trial variability in speed of evidence accumulation (v) is directly linked to attentional processes. Thus our results move closer to the drowsiness induced spatial bias being considered an attentional deficit instead of sensory dysfunction. This also provides potential candidate locations in the brain that

could be responsible for alertness induced spatial bias. As our evidence accumulation process points to signals that are involved in attention, regions like parietal cortex could be possibly involved. Also, as the evidence accumulation rate (drift rate) of right stimuli is different from left stimuli, this could provide support for models that include differential processing of stimuli from the left and right side. In particular models like Right hemisphere dominance could be potential candidates to explain the alertness induced spatial bias.

This leads us to the next stage, wherein the behavioural measures could be connected to neuro-anatomical models of spatial bias by understanding the neural dynamics of the spatial attention task across alertness transitions.

4

Neural dynamics of transitions

4.1 Brief introduction

In this chapter, I investigate the neural dynamics in alertness transitions in the same spatial attention task described in detail in the previous chapter. Further, I evaluate support for various neuroanatomical models of spatial attention described in the literature based on our findings.

4.2 Background Information

In the previous chapter I replicated the main behavioural findings of right-handers making more left errors under drowsy condition while performing the auditory spatial attention task (Bareham, Manly, et al. 2014). Further, I showed that drowsiness produced a rightward shift in spatial bias. In the next step I seek to understand the neural mechanisms behind this spatial bias.

4.3 Motivation

Before we explore the neural mechanisms behind shifts in spatial attention with reduced alertness, we need to define the characteristics of analysis methods that are best suited for this problem (as explained in Chapter 1). First, the neural machinery involved in spatial attention, alertness, neglect is composed of a variety of regions that are heavily dependent on the corresponding task being performed by the participant. Hence we need a technique that doesn't depend on *a-priori* definitions of regions involved. Techniques like multivariate pattern analysis (MVPA) satisfy this requirement by involving a data-driven approach that can further be used to identify the temporal and spatial signatures involved in spatial bias. Second, as we have established in the previous section, we need a computational model of decision making that can explain the behaviour of participants in a trial-by-trial manner. Drift-diffusion model can be used to estimate parameters like evidence accumulation rate (v) and response bias (z) in a trial-by-trial manner. Changes in drift-rate (v) are usually associated with attentional processing and modulations of bias-rate (z) are usually associated with more sensory processing. Hence connecting these model parameters with neural markers would provide an alternative way of identifying spatial and temporal signatures in the brain that are associated with these processes. Hence, this could possibly establish converging evidence between the MVPA based analysis and behaviour based drift-diffusion model.

4.4 Research Question

The above mentioned framework sets up our quest to investigate the neural dynamics involved with drowsiness related spatial biases, which can be summarised in the following research question.

What changes in neural dynamics (that occur due to variation in alertness levels) can systematically lead to bias in spatial attention?

The above question can be further subdivided as:

(a) *What are the neural patterns that are crucial for performing the spatial attention task when participants are alert?*

(b) *How do these neural patterns change when the participants become drowsy?*

(c) *What are the neural patterns that are involved in generation of spatial biases when participants become drowsy?*

(d) *Can we estimate the spatial and temporal signatures that encode parameters in a decision making model like drift-diffusion?*

(e) *Would these spatial and temporal signatures generated with the computational model on behaviour concur with our neural patterns identified earlier?*

(f) *What neuroanatomical model of neglect and healthy spatial attention would these patterns support: Interhemispheric competition or Right hemisphere specialization?*

In the following sections we first explore the neural dynamics of spatial bias using MVPA techniques (temporal decoding) followed by regression of ERP data with behaviour based drift-diffusion model.

4.5 Methods

4.5.1 Decoding

First, we employed MVPA techniques to probe the divergent patterns in the EEG data across various conditions. Decoding (MVPA) is considered to be a form of backward model where the goal is to extract latent factors (hidden variables) from the observed data (EEG) (Haufe, Meinecke, et al. 2014). Thus, it is a method of analysing patterns of brain activity in order to predict the experimental condition (or stimuli) responsible for generating that pattern. This is in contrast to encoding which is a form of forward model wherein

arbitrary values of experimental variables (or conditions) can be used to predict patterns of brain activity (Fahrenfort, van Driel, et al. 2018). Conventional Event related potentials (ERP) analysis rely on using *a-priori* identified spatial locations or temporal segments in the data to measure the differences across conditions. However decoding techniques do not rely on *a-priori* definitions and perform much better in detecting differences across experimental conditions (Fahrenfort, van Driel, et al. 2018).

4.5.1.1 Temporal decoding

Temporal decoding involves using EEG data (X) composed of size: [Electrodes x Time points x Trials] to predict the experimental condition (Y) . The experimental condition for example could be the stimuli presented (left or right stimuli). The first step in the decoding analysis consists of fitting an estimator (w) to a subset of the data (X) called X_{train} to predict a subset of the experimental condition (Y) called Y_{train}. The second step involves using this trained estimator on another subset of the data (X) called X_{test} to predict subset of the experimental condition (Y) called Y_{test}. The third step involves evaluating the performance of this estimator using a measure (e.g. accuracy) by comparing the prediction $\hat{Y}_{test}$ with the actual label Y_{test}. The following are the steps that need to be followed in fitting a temporal decoding model to the data.

Estimator construction:

Before fitting the estimator (w) to the data (X), it needs to be standardised. Firstly, the EEG data is subjected to a standard scaler (using StandardScaler() from scikit-learn) that removes the mean of the data and scales it by its variance. This procedure is useful for normalising data, which is a standard requirement for many machine-learning estimators. Secondly, we used the logistic regression to estimate the model parameters for finding the hyperplane that can maximally separate categories in the experimental condition (Y). Thirdly, we implemented the temporal decoding by using the sliding estimator (SlidingEstimator() from scikit-learn) to fit the logistic regression model per time-point.

Cross-validation:

Next, the EEG data was down sampled to 100 Hz. Further to which we defined the categories to classify (classes in Y). For example, we can classify the stimuli that was presented ('left' or 'right') when the participant was 'alert' (to further refine this, we can only choose trials where the participant made the correct decision). In this case, the binary classification was performed between these two conditions ('left' and 'right'). Additionally, the classification was only run if the participant had at least 25 trials under each condition. This ensured that only participants that had a sufficient number of trials were used for classification. Further n-fold cross validation was performed such that (n-1)/n th of the trials were used as training set and 1/n th of the trials were used as testing set. Usually the number of folds 'n' was set to 5 unless mentioned otherwise.

Validation measure:

Next, the classifier performance was evaluated using the Area Under the Curve (AUC) of the receiver-operating characteristic (ROC). The ROC curve is obtained by plotting the true-positive rate against the false-positive rate. The AUC of this curve represents the degree of separability of the various classes. When AUC is about 0.5 the classifier performs at chance, while the AUC score of 1 has a very good separability across classes. In our case, we computed the AUC-ROC score per participant (implemented using 'roc_auc' in the sliding estimator function in scikit-learn) as the average of the score across all the cross-validation folds.

Group statistics:

Next, we performed a cluster permutation test on the AUC score of each participant (dimensions of Participants x Time points) using MNE (spatio_temporal_cluster_1samp_test) (Gramfort, Luessi, et al. 2013). This produces p-values per time point at the group level, from which we can identify the time points where the AUC score is significantly different from chance (0.5) at the group level.

Coefficients of patterns:

Next, we need to identify the patterns in the data that is being used by the estimator to produce reliable classifier performance. The parameters of the decoding model are not neurophysiologically interpretable in a straightforward way (Haufe, Meinecke, et al. 2014).

Hence it is necessary to produce a transformation that changes the backward model parameters into forward model. This is done by obtaining the coefficients of the estimator model per participant using 'get_coef' function from MNE('_patterns'). Further, the coefficients are averaged at the group level to obtain the EEG patterns in the data that help discriminate between conditions.

Source reconstruction of patterns:

Finally, the coefficients (patterns) created from the estimator model are projected in the source space as follows. Source reconstruction was done primarily using Freesurfer (Fischl 2012) and MNE (Gramfort, Luessi, et al. 2013) with the following steps. First, we used the default ICBM152 template for the structural magnetic resonance images (MRIs). We reconstructed the surface using 'recon-all' from Freesurfer. We then created the Boundary element model (BEM) using 'make_watershed_bem' from MNE. Next, we created scalp surfaces for the different element boundaries using 'make_scalp_surface' from MNE. Second, we performed the registration of the scalp surface (generated in the previous step) with the default EEG channel locations manually using 'coregistration' from MNE with the help of fiducials. Third, forward solution was computed using 'make_bem_model' from MNE with conductivity = [0.3, 0.006, 0.3]. In order to test if the source reconstruction of the sensor data is accurate we projected the ERP data of a sample participant into source space and analysed data from different regions of interest to confirm its validity (See Appendix - I). The classifier patterns (coefficients created above) of each participant (32) were used for projecting into source space. Fourth, we computed the noise covariance using the baseline data from -0.2 to 0 ms. Fifth, we used the forward solution (8196 vertices) and the noise covariance to create inverse operator using 'minimum_norm.make_inverse_operator' from MNE (loose=0.2). Sixth, we used the individual classifier pattern per subject and applied the inverse operator on it (method = dSPM, SNR = 5, lambda2 = 0.08) to produce the source reconstruction of the classifier patterns per subject. Seventh, we averaged the source reconstructed patterns per subject to produce the average pattern in the source space.

4.6 Results

4.6.1 Neural machinery

Spatial localization across alert and drowsy periods:

First, we were specifically interested in identifying the neural mechanisms involved in performing the spatial attention task during alert conditions and how the mechanisms involved in this task are modulated as participants become drowsy. For this analysis only those trials wherein the participant had made correct decision was taken into account. This was mainly done to understand the mechanisms behind spatial attention under conditions of optimal response (where the participant has detected the tone direction accurately), while avoiding noise from erroneous trials (where participant made an incorrect response).

For the right-handers, when the participant was 'alert' the decoding of stimuli that was presented ('left' or 'right') started from 160 ms after the stimulus was presented and lasted till 720 ms (reliably significant, $p < 0.05$) as shown in Figure 4.1(A). Peak Area Under Curve (AUC) of 0.61 was achieved at 280 ms. The average AUC between 200-300ms was 0.58 ± 0.007, $p < 0.05$. The average AUC between 300-400 ms was 0.56 ± 0.002, $p < 0.05$.
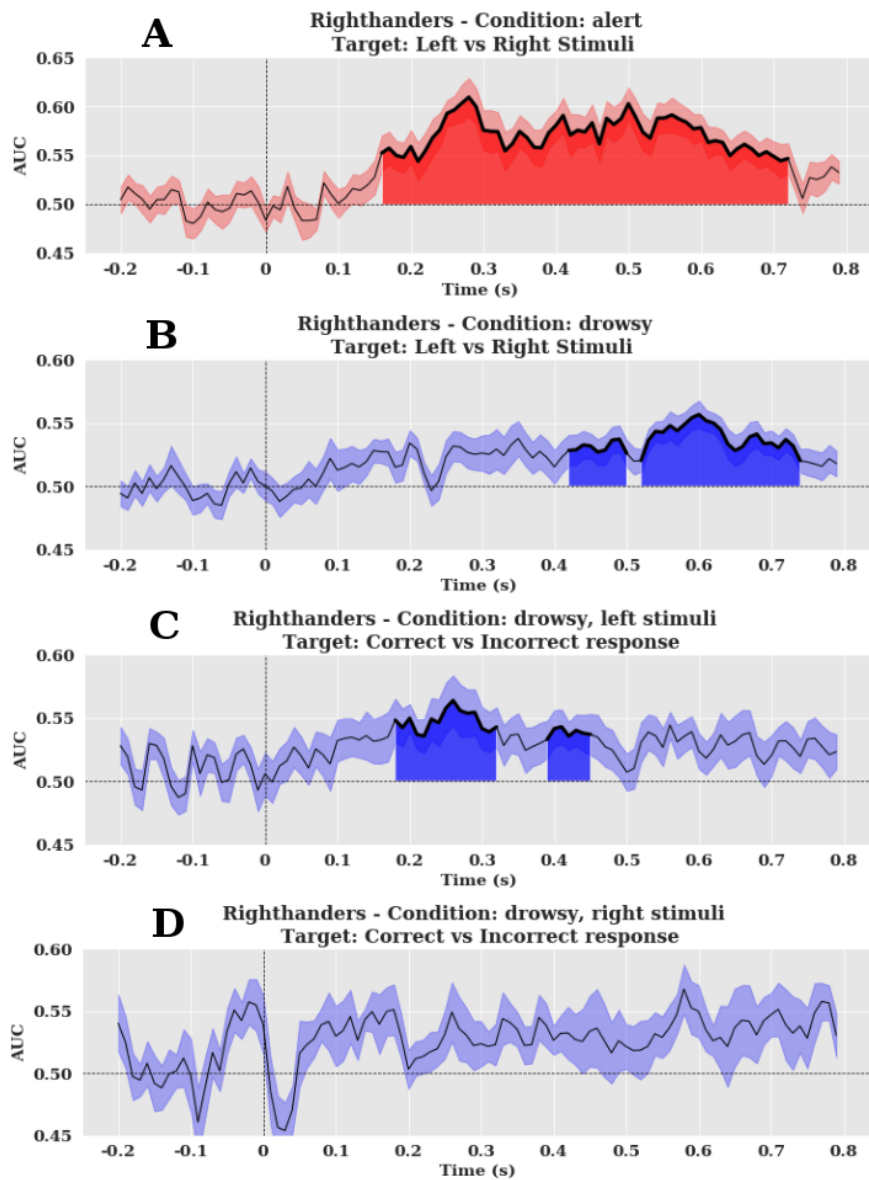
Figure 4.1: Classifier performance across time (temporal decoding) indicated by Area Under Curve (AUC). A) AUC of right-handers under alert condition, where the classifier was trained to discriminate between targets of left and right stimuli. B) AUC of right-handers under drowsy condition, where the classifier was trained to discriminate between targets of left and right stimuli. C) AUC of right-handers under drowsy condition when left stimuli were presented, where the classifier was trained to discriminate between targets of correct and incorrect responses. D) AUC of right-handers under drowsy condition when right stimuli were presented, where the classifier was trained to discriminate between targets of correct and incorrect responses.

Correspondingly we also plotted the coefficients of the classifier patterns in the sensor space which are neurophysiologically interpretable (Haufe, Meinecke, et al. 2014) for every 40 ms between 180 ms to 500 ms as shown in Figure 4.2(A). The topography between 180-

220 ms indicates strong response in the fronto-central electrodes. The topography of the patterns shifts to more posterior regions (centro-parietal electrodes in the right side of the scalp) between 220 ms to 260 ms. Further, the topography of the patterns shifts to more parietal and occipital electrodes from 260 ms to 300 ms.

When the right-handers become drowsier, the decoding of the stimuli (reliably significant, $p < 0.05$) only started from 420 ms and lasted until 740 ms as shown in Figure 4.1(B). This is very well reflected in the slower average reaction times in drowsy condition (1181.05 ms in drowsy compared to 695.15 ms in alert). Peak AUC of 0.55 was achieved at 590 ms. The average AUC between 400-500 ms was 0.53 ± 0.001, $p < 0.05$. The average AUC between 500-600 ms was 0.54 ± 0.003, $p < 0.05$. Correspondingly we also plotted the coefficients of the classifier patterns in the sensor space for every 40 ms between 180 ms to 500 ms in Figure 4.2(B). The topography between 180-220 ms indicates the strong response in the frontal electrodes (though not reliably significant to decode) compared to the more fronto-central electrodes in the alert condition. Interestingly the topography from 220-260 ms shifts again to more frontal electrodes (not reliably significant) compared to the central-parietal electrodes in the alert condition. The topography of the patterns shifts to more posterior regions (centro-parietal electrodes, reliably significant) from 380 ms to 420 ms. Further, the topography of the patterns shifts to more parietal and occipital electrodes between 420 ms to 460 ms.

To summarise, this indicates that when the right-handed participant becomes drowsy, the decoding shifts later (moves from 160 ms in alert to 420 ms in drowsy). This could possibly indicate that the process of evidence accumulation to take a decision is slower under drowsy conditions. The main reasons for this could be again noise driven by sensory level processing or noise in evidence accumulation itself (driven by attentional processes). Further central-parietal electrode pattern, which is visible in alert condition, disappears in the drowsy condition. In the drowsy condition, the temporal electrodes are activated more in the 260-300 ms compared to the alert condition; as well the temporal electrode patterns last till 500 ms. It is also interesting to note that the topography from 180-300 ms in the drowsy condition is not sufficient to decode the stimuli presented and also different compared to the alert condition.
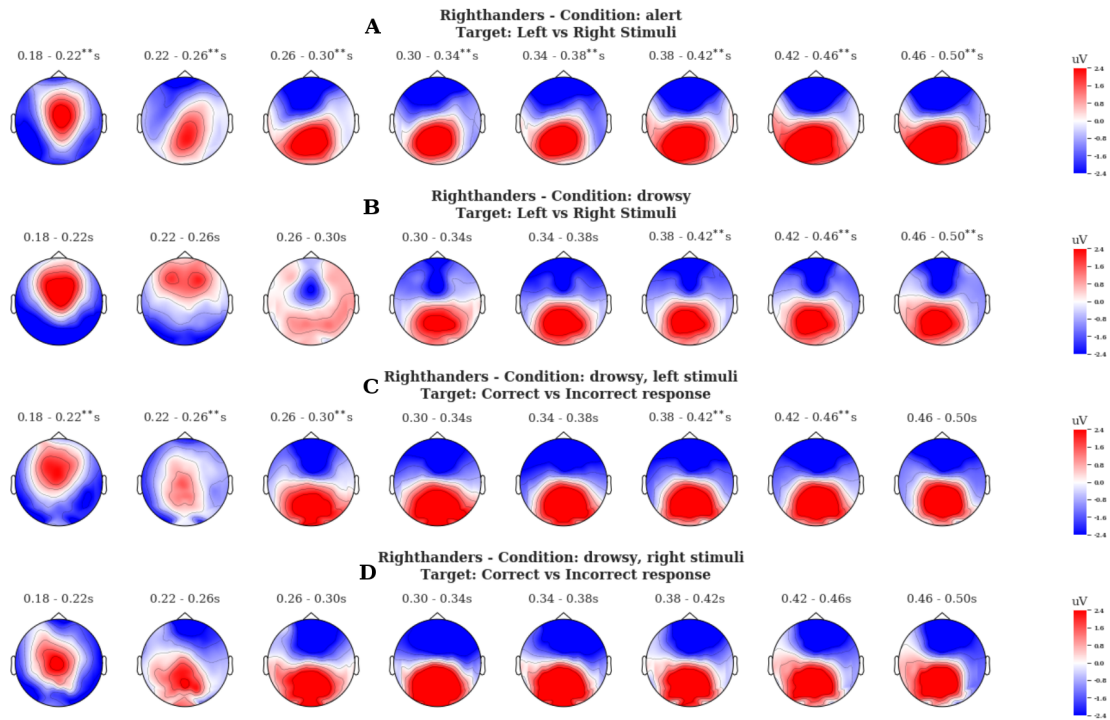
Figure 4.2: Coefficients of classifier patterns in right-handers. A) Coefficients of classifier patterns of right-handers under alert condition, where the classifier was trained to discriminate between targets of left and right stimuli. B) Coefficients of classifier patterns of right-handers under drowsy condition, where the classifier was trained to discriminate between targets of left and right stimuli. C) Coefficients of classifier patterns of right-handers under drowsy condition when left stimuli were presented, where the classifier was trained to discriminate between targets of correct and incorrect responses. D) Coefficients of classifier patterns of right-handers under drowsy condition when right stimuli were presented, where the classifier was trained to discriminate between targets of correct and incorrect responses. ** indicates reliably significant time periods, the topographical plot was averaged between the time intervals mentioned.

To further confirm the location of the brain regions involved, we decided to project the classifier patterns from the sensor space to the source space using source reconstruction techniques (as explained previously). We first found that the decoding pattern under the alert condition (target decoding of left versus right stimuli) was mainly predominant in the right hemisphere. Between 300-400 ms the right temporal regions were mainly involved classifying the stimuli. From 400-500 ms the right inferior parietal regions contribute most to the classifier patterns and this continues till 500-600 ms as shown in Figure 4.3(A).

Next under the drowsy condition, the decoding of left versus right stimuli was predominantly in the left hemisphere. Between 300-400 ms the left temporal regions were mainly

recruited by the classifier patterns. From 400-500 ms the left inferior parietal cortex along with left pre and post-central cortex regions and left lateral occipital seem to be involved. From 500-600 ms the pattern is much more localized in the left inferior parietal cortex regions as shown in Figure 4.3(B).

To summarise, this shows that for right-handers the right inferior parietal regions were mostly involved in alert condition, whereas the left inferior parietal regions were mostly involved in drowsy condition for classifying the left versus right stimuli.

Spatial localization errors in drowsy periods:

Next, we were interested in identifying the neural mechanisms involved in producing the localization errors across the left and right side of the space under drowsy conditions.

Left-stimuli:

For the right-handers, when the participant was 'drowsy' the decoding of responses (correct, incorrect responses) when left stimuli was presented started from 180 ms after the stimulus was presented and lasted till 320 ms (reliably significant, $p<0.05$), again from 390 ms to 450 ms (reliably significant, $p<0.05$) as shown in Figure 4.1(C). Peak AUC of 0.56 was achieved at 260 ms. The average AUC between 180-320ms was 0.54 ± 0.002, $p<0.05$. The average AUC between 390-450 ms was 0.53 ± 0.001, $p<0.05$. Correspondingly we also plotted the coefficients of the classifier patterns in the sensor space which are neurophysiologically interpretable for every 40 ms between 180 ms to 500 ms (Figure 4.2(C)). The topography between 180-220 ms indicates strong response in the frontal electrodes. The topography of the patterns shifts to more posterior regions (centro-parietal electrodes in the left side of the scalp) between 220 ms to 260 ms. Further, the topography of the patterns shifts to more parietal and occipital electrodes between 260 ms to 300 ms. Source localization confirmed that activity in the left SPL regions (300-500 ms), left IPL regions (500-600 ms), left frontal regions (200-500 ms), right pre-central gyrus (300-600 ms) were involved in the classifier patterns (Figure 4.3(C)). It is interesting to note that many of these regions that decode for the error in left stimuli are located in the left hemisphere indicating that the processing of information has been taken over by the left hemisphere from the right hemisphere. Areas in the ventral processing stream like right IPL, right STG

which are mainly affected in neglect patients (Mort, Malhotra, et al. 2003; Corbetta, Kincade, et al. 2005) do not show up in the classifier patterns, which clearly indicate the lack of information present in these right hemispheric regions for processing the stimuli under conditions of low alertness.

Right-stimuli:

When the right-handers became 'drowsy', the decoding of responses (correct, incorrect response) when right stimuli was presented was not reliably significant across any time point (Figure 4.1(D)). However, we decided to plot the coefficient of the classifier patterns in the sensor space to explore the electrode locations involved.

For the right-handers, we plotted the coefficients of the classifier patterns in the sensor space for every 40 ms between 180 ms to 500 ms (Figure 4.2(D)). The topography between 180-220 ms indicates strong response in the central electrodes. The topography of the patterns shifts to more posterior regions (centro-parietal electrodes in the left side of the scalp) between 220 ms to 260 ms. Further, the topography of the patterns shifts to more parietal and occipital electrodes between 260 ms to 300 ms. To further confirm the location of the brain regions involved, we decided to project the classifier patterns from the sensor space to the source space (Figure 4.3(D)). We found that the decoding pattern was located in temporal cortex (200-600 ms), left and right parietal cortex (300-600 ms), left and right pre and post-central gyrus (300-600 ms).
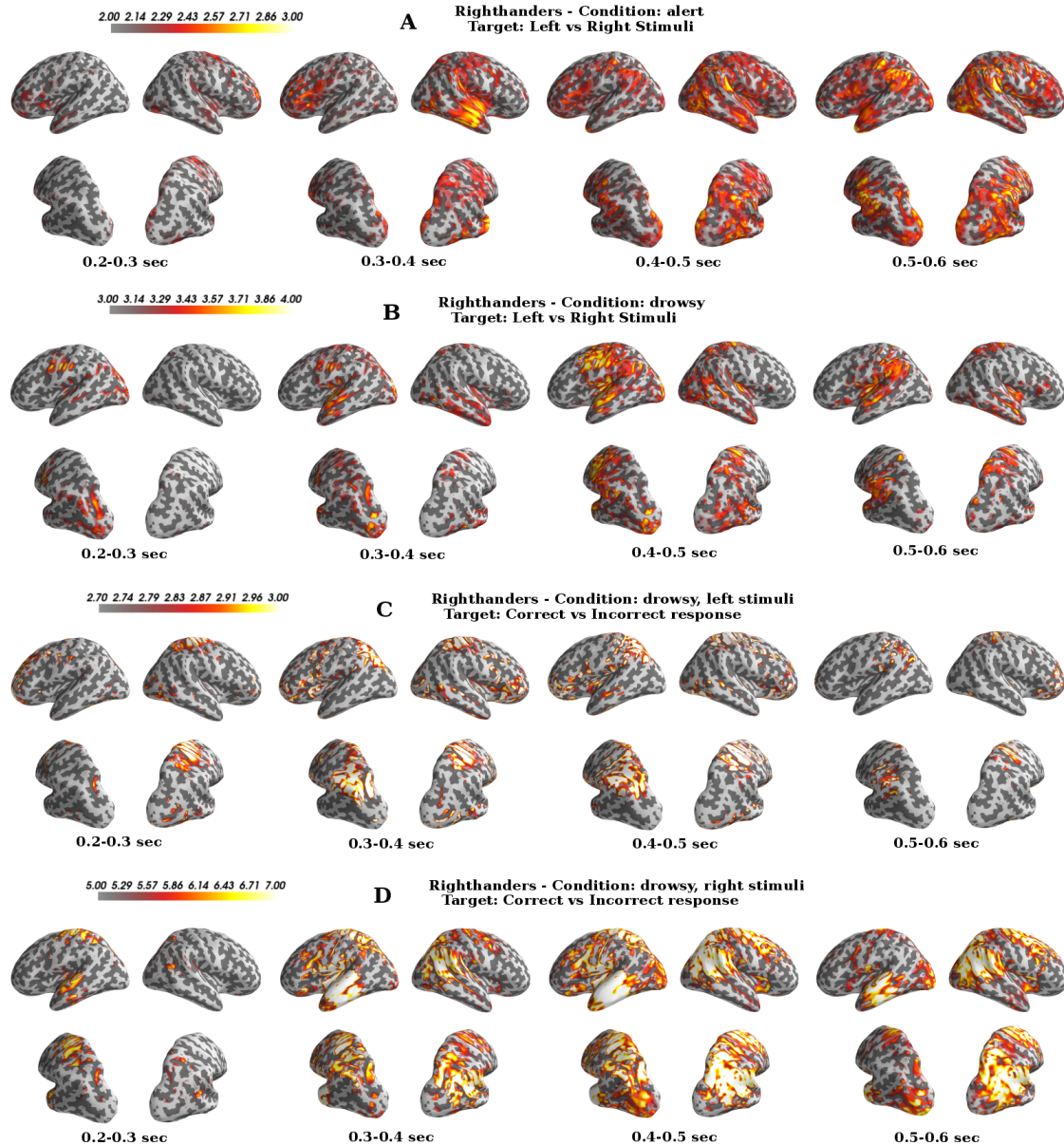
Figure 4.3: Classifier patterns projected in source space for right-handers. A) Decoding patterns (for target classification of left vs right stimuli) is more prevalent in the right hemispheric regions. B) Under drowsy conditions the decoding patterns (for left vs right stimuli) start later only at 400 ms and it more prevalent in the left hemispheric regions. C) Decoding patterns under drowsy conditions (for left stimuli with target classification of correct vs incorrect response) is present in left hemispheric regions like SPL,IPL . D) Decoding patterns under drowsy conditions (for right stimuli with target classification of correct vs incorrect response) are distributed in a more bilateral fashion across both hemispheres. ** indicates reliably significant time periods.

4.6.2 Connecting behavioural model with neural markers

Next we connected the computational model (drift-diffusion) with the neural data by performing a regression of the model with the Event related potential (ERP) data, which was z-scored to obtain the regression coefficient. This was performed in the following steps. First, the ERP data (post trial epochs) were z-scored per electrode per trial. Second, the ERP data was baseline corrected with pre-trial data from -200 ms to 0 ms. Third, the ERP data was averaged every 50 ms per electrode per trial to create 20 time points (-200 ms to 800 ms) per electrode per trial. Fourth, the ERP data was entered into regression with trial by trial estimate of the drift rate using the model HDDMRegressor from the HDDM toolbox (Wiecki, Sofer, et al. 2013).

We fitted the Stimulus-coding model ('left' or 'right') responses as earlier and estimated the drift rate (V) as a function of ERP data per trial per electrode per time point.

$$V \sim \beta_0 + \beta_1(ERP) \tag{4.1}$$

The above equation can be written in patsy[1]form as below.

$$V \sim \text{ERP} : C(state, Treatment('Alert')) : C(stim, Treatment('Right')) \tag{4.2}$$

Where, V represents the drift rate, ERP represents the z-scored ERP data computer per trial per time point, state represents 'alert' or 'drowsy', stim represents 'left' or 'right'. The bias point (z) was made to vary with the stimulus as before. This analysis elucidates the variation of drift rate with the ERP data across stimulus and alertness levels. The difference in the drift rate between the left and right stimulus in alert and drowsy conditions can then be plotted per electrode per time point (Figure 4.4). The difference in drift rates indicate the ability of the particular electrode location to differentiate between different stimuli (analogous to the MVPA and implies encoding of evidence accumulation rate).

---

[1]patsy is a Python package for describing statistical models
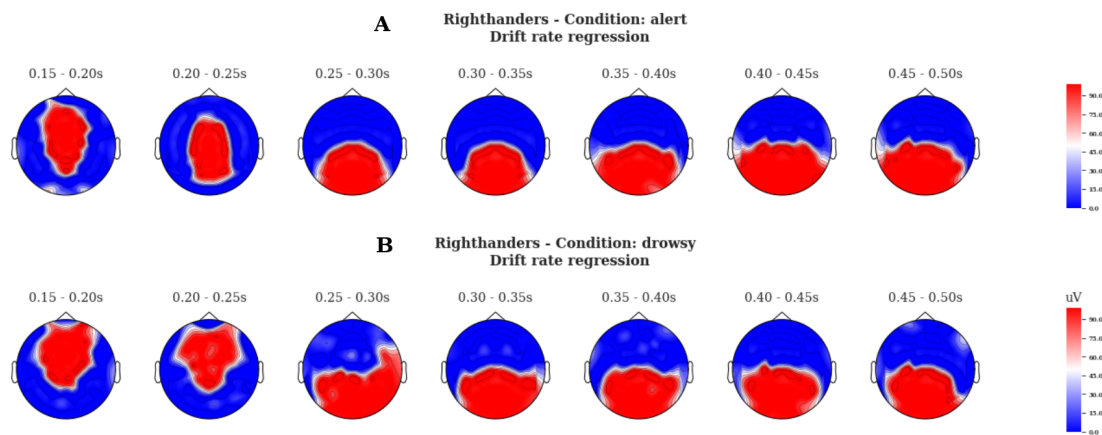
Figure 4.4: Drift rate regression across conditions in righthanders. A) Proportion of overlap between drift rates across left and right stimuli in right-handers in alert condition across different time points. B) Proportion of overlap between drift rates across left and right stimuli in right-handers in drowsy condition across different time points.

We first plotted the difference in drift rate (proportion of overlap in the posterior distribution across stimuli) in the alert condition in time steps of 50 ms. For the right-handers (Figure 4.4A), the topography of the sensor plot shows that electrodes in the fronto-central region (150-200 ms) shows higher differences in drift rate (implying the encoding of evidence accumulation rate). Followed by which the topography shifts to central and parietal electrodes (200-250 ms). Further after 250 ms the topography shifts to more posterior regions in the central and parietal electrodes.

Next we plotted the difference in drift rate in the drowsy condition. For the right-handers, the topography of the sensor plot shows that more frontal and central electrodes show differences in drift rate from 150-250 ms (Figure 4.4B). Further the topography shifts to more central, parietal, right temporal electrodes in 250-300 ms. The topography then moves to more posterior regions in the parietal and central electrodes from 350 ms onwards.

It is interesting to note that the central-parietal pattern present from 200-250 ms under alert condition disappears in the drowsy condition and is replaced by more fronto-central pattern. This clearly indicates difference in activity across sensors in parietal regions (in sensor space), which encode evidence accumulation rate.

4.7 Discussion

In this chapter, I decided to investigate the neural dynamics of spatial biases with low alertness. This follows up on the behavioural dynamics investigated in the previous chapter.

I used multivariate pattern analysis techniques to uncover the regions of the brain that are different across conditions. The first analysis involved decoding the direction stimuli ('left', 'right') under 'alert' conditions. This will help understand the brain regions involved in performing the auditory spatial attention task under baseline conditions. We found that mainly regions in the right hemisphere were involved. Chiefly regions like right temporal regions, right inferior parietal regions were involved. This agrees with findings on brain regions (right temperoparietal) detected by spatial attention task in (Corbetta&Shulman 2002). The concentration of decoding patterns in the right hemispherical regions provides more evidence for right hemispheric specialization model. The second analysis involved in decoding the direction of stimuli under 'drowsy' conditions. This will help us understand how the brain compensates to perform this task under conditions of low alertness. We found that mainly activity shifts to the left hemisphere. Primarily regions like left temporal, left inferior-parietal regions were involved. This could potentially explain the origin of the left errors in the drowsy condition. As the left hemisphere is highly active, it directs attention to the contra-lateral side (right side of space) and hence leads to misclassification of left tones as coming from the right. It is interesting to note that invasive studies performed by (Szczepanski&Kastner 2013) using transcranial magnetic stimulation where activation of dorsal regions leads to attention being shifted to the ipsilateral side. Potentially further studies involving activation in the ventral regions could possibly provide evidence for attention being shifted to the contra-lateral side. Also studies (Sturm, de Simone, et al. 1999) involving the neural correlates of alertness have shown that activity in the right hemisphere increased under conditions of high alertness, which broadly agrees with our findings. Further the location of lesions (right hemispherical regions like TPJ,IPL) present in neglect patients (Mort, Malhotra, et al. 2003) which tends to produce lack of attention in the left side of space, also broadly agrees with our findings. The third

analysis involved in decoding the responses ('correct','incorrect') in the drowsy condition on the presentation of left stimuli. Primarily regions in left superior parietal, left inferior parietal regions were involved. This is in agreement with regions reported in neglect as mentioned above (Mort, Malhotra, et al. 2003).

Next, I used trial-by-trial regression to identify regions in the sensor space that have differential drift rates across left and right stimuli. In the 'alert' condition more central and parietal electrodes were involved which are similar to the classifier patterns in the sensor space (where I decode direction of stimuli presented in the alert condition). While in the 'drowsy' condition, the activation was more in the frontal and central electrodes. It is interesting to note that activity in the parietal electrodes (in sensor space) was less informative in the drowsy condition, which agrees with neglect studies implicating damage in the parietal regions (Mort, Malhotra, et al. 2003).

As decoding of stimuli ('left', 'right') in the alert condition happens only in the right hemisphere, suggesting that the right hemisphere is activated more by the spatial attention task. This indicates evidence for the support of right hemisphere dominance model under alert condition. On the other hand, if the decoding were to occur in both hemispheres, this would indicate the activation of both left and right hemispheres. Hence would provide support a model where attention is dominant in both hemispheres, mainly inter-hemispheric competition (under the specific case of balance of both hemispheres). However as only the right hemisphere is activated in the alert condition it provides support for right hemisphere dominance model of attention.

Under drowsy condition the same decoding ('left','right') shifts to left hemisphere, indicating that the left hemisphere is dominating the spatial attention processing required on the task (though AUC being low indicates lower efficiency as left hemisphere is not specialized for this task). This indicates support for the inter-hemispheric competition model under the specific case where in the balance is tilted in favour of the left hemisphere. This imbalance pushes the attention to the right side of the space.

Similarly, the decoding of response ('correct','incorrect') for the left stimuli under drowsy

conditions primarily happens in the parietal cortex of the left hemisphere indicating that information processing has shifted to the left hemisphere again. This again indicates evidence for the inter-hemispheric competition model where in the left hemisphere now has taken over the processing of spatial attention.

5

Handedness aspects of transitions

5.1 Brief introduction

Recent studies (Bareham et al., 2014, 2015) have provided first evidence that handedness along with variation in alertness levels produces a modulation of behaviour in a auditory spatial attention task. In these studies, left and right-handed individuals performed an auditory tone localization task while falling asleep. Both left and right-handers showed a slight bias (misclassification of tones) originating from the left (more left errors) when they were fully alert. But when right-handers began to fall asleep they produced more left-errors. This is similar to a debilitating clinical condition called unilateral spatial neglect where patients find difficulty in paying attention (detection or discrimination) to information coming from the space opposite to the lesion (Corbetta and Shulman, 2011; Karnath and Fetter, 1995). On the other hand, left-handers begin to fall asleep produced a slight bias in the opposite direction by producing more errors in tones originating from the right direction.

The above mentioned auditory spatial attention task provides an interesting example to explore the effect of handedness on attention while being modulated by alertness. The

modulation of alertness levels (by falling asleep) provides an active task wherein the brain is causally manipulated by the arousal systems that differently affect the corresponding attention systems based on the handedness of the individual. We advanced this spatial attention task, by first creating a baseline task (where participants are instructed to stay alert). Further in the drowsy session (where alertness modulates attention), participants are allowed to fall asleep while performing this task. By this way we can make a direct comparison between brain dynamics involved in individual participants while they perform this task when under both conditions.

To understand how spatial attention is modulated by alertness while being constrained by handedness, we investigated with electroencephalography (EEG) the neural mechanisms involved in performing an auditory tone localization task. We first describe the behavioural dynamics of the processes involved followed by computational modelling of the behaviour. Next we describe the neural dynamics involved using multivariate pattern analysis (temporal decoding). Finally, we connect the parameters of the computational behavioural model with neural dynamics to provide convergent evidence of brain dynamics modulated by alertness and constrained by handedness.

5.2 Declaration of contribution of co-authors

The following paper is in the process of being submitted to a journal for peer-review. The spatial attention experiment was designed by me along with Dr. Tristan Bekinschtein and Dr. Corinne Bareham. I collected the data of left-handers on my own and received help from research assistants for the data collection of right-handers. The data analysis for both behaviour and neural dynamics was performed by me. I also created the figures and wrote the initial version of this manuscript which underwent revisions based on comments by co-authors.

5.3 Manuscript, *bioRxiv*

Does Handedness matter?
Mechanics of Spatial attention modulated by alertness

Sridhar R. Jagannathan[1], Corinne A. Bareham[3], Tristan A. Bekinschtein[1,2]

[1] Department of Psychology, University of Cambridge, Cambridge, United Kingdom
[2] Cognition and Brain Sciences Unit, Medical Research Council, Cambridge, United Kingdom
[3] Department of Clinical Neurosciences, University of Cambridge, Cambridge, United Kingdom

ABSTRACT:

The ability to direct attention to a specific location in space is a fundamental feature of cognition and is crucial for an organism to survive in the environment. Spatial attention is thought to be right hemisphere specialised. Most of the evidence of this specialisation (both in the patient and healthy population) comes from studies involving right-handed individuals. However, we know that approximately 10% of the population is left-handed. Here, using an auditory spatial attention task, we show that left and right-handers perform similarly when they are alert. However, when they become drowsy, right-handers tend to show deficits in attention only on the left side of space while left-handers show deficits in both the left and right side of space. To dissect the brain-behavioural dynamics we took a multipronged approach. First, we used multilevel modelling and psychophysics to quantify the change in behaviour. Second, we used drift-diffusion modelling to analyse the computational parameters behind this behaviour. Third, we used multivariate pattern analysis (decoding) to understand the neural dynamics of spatial bias with drowsiness and identified key spatial and temporal signatures. Finally, we connected the computational parameters generated in the drift-diffusion model with the neural dynamics to provide converging evidence for the spatial and temporal signatures. These findings provide evidence that key brain networks supporting spatial attention differ across left and right-handed individuals.

INTRODUCTION:

The ability to direct attention to a specific location in space is a fundamental feature of cognition and is crucial for an organism to survive in an external environment. One of the models of Spatial attention in humans proposes that the right hemisphere is specialised for attention (Bowers and Heilman, 1980; Siman-Tov et al., 2007; Vallar, 1998). Evidence for this specialization has come from stroke patients diagnosed with spatial neglect, a condition that is characterised by failure to detect and respond to stimuli from the contralateral side of the lesion. Left spatial neglect following damage to the right hemisphere is much more persistent and difficult to recover (Becker and Karnath, 2007; Bowen et al., 1999; Heilman et al., 1985; Ringman et al., 2004) compared to the right spatial neglect (with left hemisphere damage). Healthy individuals also display neglect like behaviour referred to as

'pseudoneglect'. When asked to bisect a straight line, most healthy participants tend to locate the centre of the line to the left of the veridical centre, thereby paying more attention to the left (Benwell et al., 2013; Bowers and Heilman, 1980; Harvey et al., 2000; Jewell and McCourt, 2000; Mesulam, 1999; Schenkenberg et al., 1980; Thiebaut de Schotten et al., 2005)

Two most dominant neuroanatomical models provide explanations for neglect. A) Right hemisphere dominance model: In this model, the right hemisphere can direct attention to both sides of the space, whereas the left hemisphere can only direct attention to the right side of space (Heilman and Van Den Abell, 1980; Mesulam, 1981). Hence, in case of damage to left hemisphere, the intact right hemisphere can still direct attention to both sides of space. However any damage to the right hemisphere makes the brain unable to direct attention to the left side of space. B) Interhemispheric competition model: In this model, attention is directed to the contralateral space through inhibition of the ipsilateral hemisphere (Kinsbourne, 1977). This inhibition could be achieved via cortico-cortical interactions between the parietal cortex and superior colliculus (Sprague, 1966). Here neglect, occurs due to imbalance created by damage to one of the hemispheres thereby reducing the ability to direct attention to the contralateral side of space.

In general, in any task that involves allocating attention to a specific location in space a) If it activates the right hemispheric regions irrespective of attended location (left or right space), would support the right hemisphere dominance model. B) If it activates the left hemispheric region on attending right space, right hemispheric region on attending left space; thereby producing bilateral activation across both left or right space would support interhemispheric competition model. In this context, several studies have provided evidence for right hemisphere dominant model (Benwell et al., 2014; Dietz et al., 2014) whereas others for interhemispheric competition model (Szczepanski et al., 2010). To explain this discrepancy (Corbetta and Shulman, 2011) proposed that attentional system is composed of two parts: a) Dorsal attention system composed of the frontal eye fields and intraparietal sulcus is involved in voluntary shifts of attention and is activated bilaterally. Whereas the Ventral attention system composed of temporoparietal junction and ventral frontal cortex is highly right lateralised due to its interaction with the arousal system. Thus the right lateralized ventral attention system biases the bilateral dorsal attention system to produce neglect (inattention) in the left side of space.

However, all of the above mentioned studies have predominantly used right-handed individuals (either patients or healthy participants) or in some cases handedness was not reported. Despite handedness being one of the main asymmetries in both human brain organisation and associated behaviours, it's role in attentional networks has not been extensively researched. Thus, handedness could potentially serve as a confounding factor in identifying models of spatial attention. Evidence for this has come from studies involving auditory spatial attention (Bareham et al., 2014, 2015). These studies show that handedness along with variation in arousal level produces modulation of spatial attention. In these studies, left and right-handed individuals performed an auditory tone localization task while falling asleep. Both left and right-handers showed a slight bias (misclassification of tones) originating from the left (more left errors) when they were fully alert. When right-handers began to fall asleep they produced more left-errors (similar to spatial neglect). On the other

hand, left-handers produced a slight bias in the opposite direction (more errors in tones originating from the right direction) when falling asleep.

These results highlight an important issue that vast majority of cognitive neuroscience studies have, which is recruiting participants that are predominantly right-handed. Experimenters reason that excluding left-handers tend to make the sample more homogeneous, reduce inter-subject variance and increase statistical sensitivity. Recently compelling arguments have been put forward by researchers in the domain of language studies and embodied cognition to include left-handed individuals (Willems et al., 2014) in all studies. They argue to include handedness as an additional factor like gender (which is usually balanced at 50/50) and balance the same at 90/10 (right/left handers), which is similar to the population level proportions. Further, left-handers could actually be recruited in a targeted manner to study cerebral lateralization, which is already practised in domains like embodied cognition and language processing. However, studies that did use both left and right-handed individuals for comparing the differences in brain dynamics could not connect it to differences in behaviour. This is mainly because in majority of those studies (Hauk and Pulvermuller, 2011; Willems et al., 2009, 2010), the specific cognitive tasks did not generate any differences in behaviour and only generated differences in brain regions being activated. In contrast lesion studies (Hécaen et al., 1981; Jackson et al., 1956; Quadfasel and Goodglass, 1954) have been influential in proving or disproving theories of cerebral lateralization by comparing left and right handed individuals that have been damaged in different brain regions while producing similar behavioural deficits.

Hence in order to truly understand how spatial attention is directed and how handedness modulates behaviour, we need tasks that can produce differences in behaviour (between left and right-handed), which can then be used to compare brain and behavioural dynamics across groups. The above mentioned auditory spatial attention task provides such a unique window to explore the effect of handedness on models of spatial attention. The modulation of alertness levels (by falling asleep) provides an active task wherein the brain is causally manipulated by the arousal systems that differently affect the corresponding attention systems based on the handedness of the individual.

Here, we advanced the spatial attention task in (Bareham et al., 2014, 2015), by first creating a baseline task (where participants are instructed to stay alert). Further in the drowsy session (where alertness modulates attention), participants are allowed to fall asleep while performing this task. By this way we can make a direct comparison between brain dynamics involved in individual participants while they perform this task when under both conditions. To understand how spatial attention is modulated by alertness and handedness, we investigated with electroencephalography (EEG) the neural mechanisms involved in this task. We first describe the behavioural dynamics of the processes involved followed by computational modelling of the behaviour. Next we describe the neural dynamics involved using multivariate pattern analysis (temporal decoding). Finally, we connect the parameters of the computational behavioural model with neural dynamics to provide convergent evidence of brain dynamics modulated by alertness and constrained by handedness.

RESULTS:

<u>Behavioural Evidence of Alertness modulating spatial attention</u>

Error-proportion modulated by alertness:

We first used multi-level modelling to understand how the proportion of errors made by each participant in an auditory tone-localization task (Figure 1A) was influenced by the stimulus presented ('left' or 'right' auditory tone) and the state of the participant ('alert' or 'drowsy'). For this purpose, we defined 4 different models where the error proportion varied with stimulus and alertness levels (see methods section). The winning model (compared with log-likelihood) was further analysed for both right and left-handed participants separately.

For the right-handers (Figure 1C) there was a significant effect of state on error-proportion with $F(1, 95.07) = 14.04$, $p<0.001$. Stimulus type also significantly affected error-proportion with $F(1,95.07) = 18.80$, $p<0.001$. The interaction between state and stimulus also significantly affected error-proportion with $F(1,95.07) = 6.88$, $p<0.05$. This indicates that as right-handers became drowsy the error proportion of some stimuli was affected more than others. Further estimated marginal means were computed for the 'simple' contrast of both left and right stimuli through which error-proportion across alert and drowsy could be compared. This revealed a significant difference between alert and drowsy conditions for left stimuli $t(98.11) = -4.45$, $p<0.0001$ (mean = -0.13, standard error = 0.03), whereas for the right stimuli there was no significant difference across alert and drowsy periods with $t(98.68) = -0.77$, $p>0.05$ (mean = -0.02 ,standard error = 0.03).

For the left-handers (Figure 1B) there was a significant effect of state on error-proportion with $F(1, 128) = 19.71$, $p < .001$. Stimulus type also significantly affected error-proportion with $F(1,128) = 8.30$, $p<0.01$. There was no significant interaction between state and stimulus on error-proportions with $F(1,128) = 1.54$, $p>0.05$. This indicates that as left-handers became drowsy the error-proportion of both left and right stimuli was affected equally. Estimated marginal means were computed for the 'simple' contrast of both left and right stimuli through which error-proportion across alert and drowsy could be compared. This revealed a significant difference between alert and drowsy conditions for left stimuli with $t(99.1) = -3.95$, $p<0.0001$ (mean = -0.11, standard error = 0.03) and for the right stimuli there was also a significant difference across alert and drowsy periods $t(99.1) = -2.24$, $p<0.05$ (mean = -0.06, standard error = 0.03).

To summarise, as right-handers become drowsier they tend to make more left errors, while left-handers make more errors in the drowsy condition but not in a spatially specific fashion.

In the next step, to provide more evidence of handedness modulating behaviour, data from both right and left-handers were combined and we used the handedness score from each participant as a parameter in the model. For this purpose, we defined 5 models (see methods section), where the error proportion was varied with state, stimulus and handedness score. The state-handedness model emerges as the winning model, indicating that error-proportion is affected by state and handedness of the participant. This shows that

handedness doesn't have an overall effect dependent on the stimuli being presented but rather has an effect dependent on the alertness level of the participant.

Subjective mid-line shifts are modulated by alertness:

Next, we aimed to quantify the change in the subjective mid-line per participant as they become drowsier. For this purpose, we decided to fit psychometric functions to the responses produced by each participant under alert and drowsy conditions (see methods section). The proportion of rightward response under each stimulus condition from -60° to +60° was fitted with a cumulative normal function using the generalized linear model. Bias (mean of the function), Sensitivity (inverse of standard deviation) was computed per participant per condition. For some participants, the bias point shifted to the left as they become drowsier (they started pressing more rightward responses and hence making more left errors) (Figure 2A). For some other participants, the bias point shifted to the right as they become drowsier (they started pressing more leftward responses and hence making more right errors) (Figure 2B). If the bias point moved leftwards, the participant is called as 'left-shifters', whereas if the bias point moved rightwards, the participant is called as 'right-shifters'.

For right-handers, 24 participants were identified as 'left-shifters' as their subjective midline shifted to the left when they became drowsy. 7 participants were identified as 'right-shifters' as their subjective midline shifted to the right when they became drowsy (Figure 2D). 1 participant was ignored from the analysis as their bias point in drowsy condition exceeded ±30°. This is consistent with analysis from multi-level modelling that most right-handers make left errors as they become drowsier.

For left-handers, 19 participants were identified as 'left-shifters' as their subjective midline shifted to the left when they became drowsy. 12 participants were identified as 'right-shifters' as their subjective midline shifted to the right when they became drowsy. 1 participant was ignored from the analysis as their bias point in drowsy condition exceeded ±30°. This is consistent with the multi-level modelling analysis (where the error proportion was significantly different for both left and right stimuli across different levels of alertness) that left-handers make both left and right errors as they become drowsier.

Finally, to understand the effect of drowsiness on the system we performed Pearson's product-moment correlation test between the bias and sensitivity. In the alert condition, both the right-handers (r(19)= -0.09, p<0.05) and left-handers (r(18) = -0.34, p<0.05) didn't show a significant relationship between bias and sensitivity. In the drowsy condition, the right-handers showed a significant correlation (r(19)= 0.45, p>0.05) between bias and sensitivity while the left-handers (r(18) = 0.29, p<0.05) did not have a significant relationship. This shows that the drowsiness has systematically altered both bias and sensitivity for right-handers under drowsy condition.
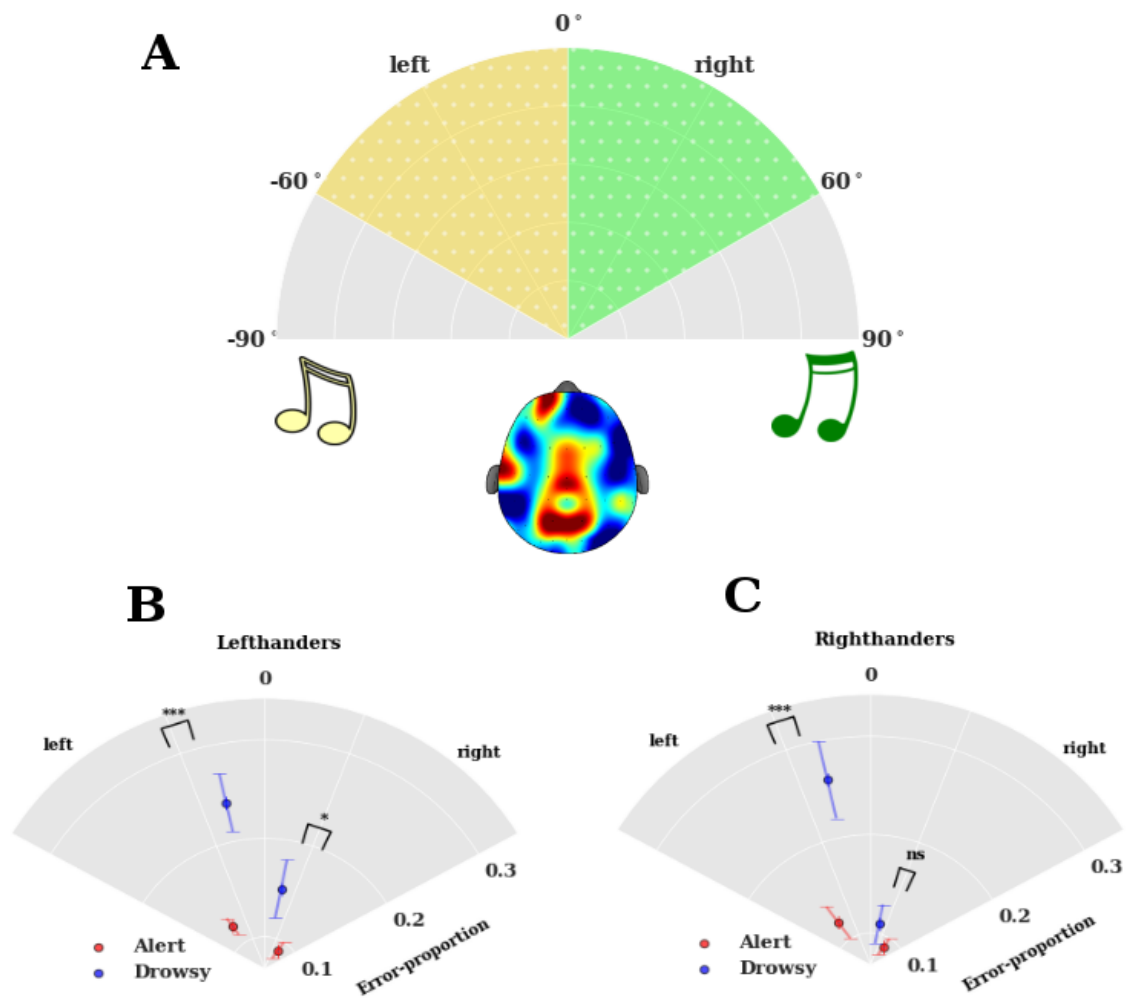
Figure 1: Auditory Spatial attention task: *A) Participants had to localize the direction of auditory tones coming from left and right side of the midline. B) Average Proportion of errors committed by left-handers in alert and drowsy periods across left and right stimuli. Error-proportion depends on stimulus type (left,right) and state of participant (alert,drowsy). Estimated marginal means indicate that error proportion is significantly different across both left and right stimuli. C) Average Proportion of errors committed by right-handers in alert and drowsy periods across left and right stimuli. Error-proportion depends on stimulus type (left,right), state of participant (alert,drowsy) and interaction between stimulus and state. Estimated marginal means indicate that error proportion is significantly different across both left stimuli, but is not significant across left stimuli. *** indicates p<0.001, ns indicates not significant, error bars indicate standard error of the mean.*
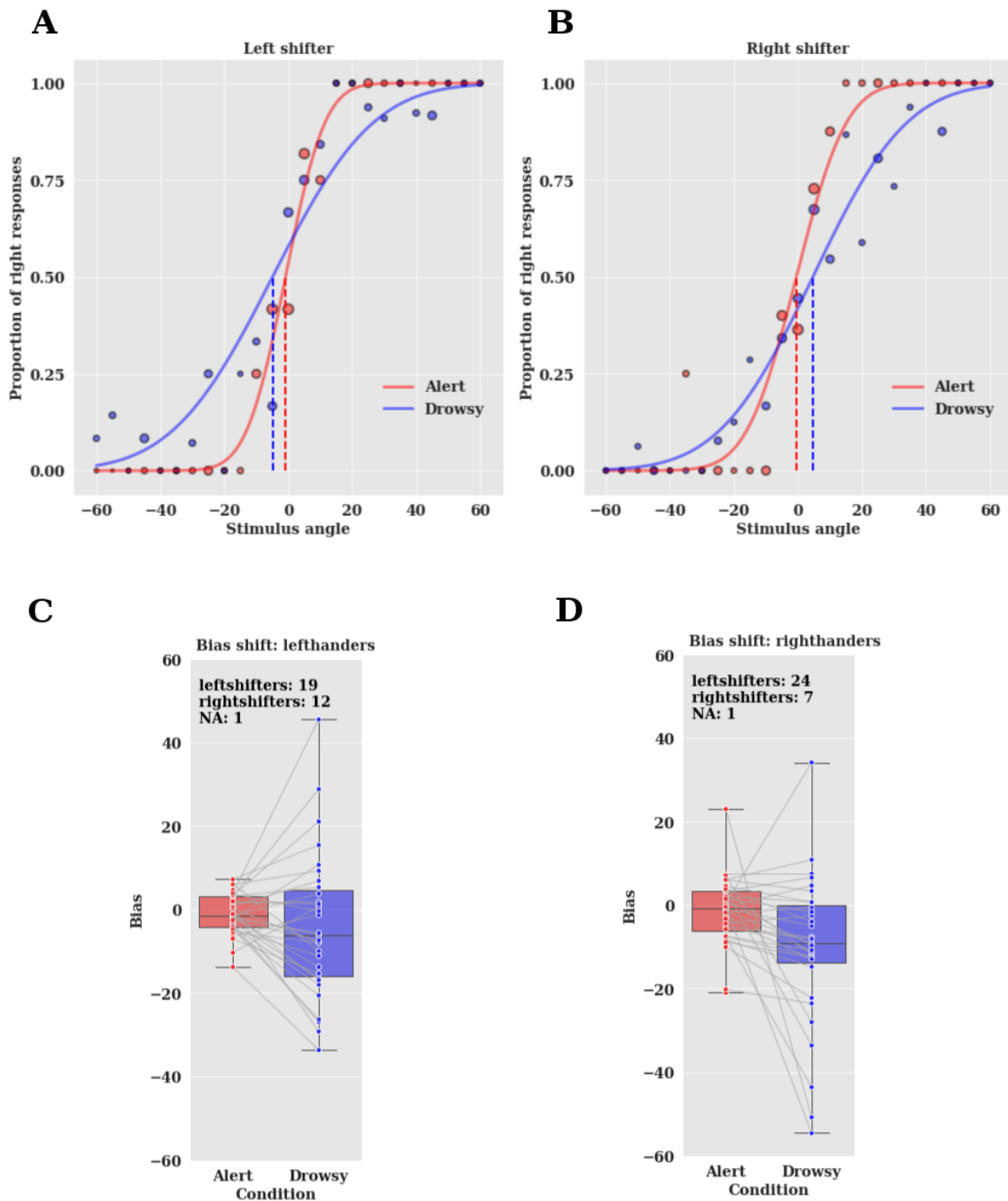
Figure 2: Psychometric fits indicating shifts in subjective mid-line. *Data from two sample participants (A,B), where proportion of right responses were fit across stimuli from -60° to +60° in both alert and drowsy periods. The mean of the fitted function ('probit') indicates the subjective midline ('bias'). A) Bias point shifts towards the left as the participant becomes drowsier. B) Bias point shifts towards the right as the participant becomes drowsier. C) Bias points across alert and drowsy periods for left-handers. The bias points move both towards the left (more negative) and towards the right (more positive) as participants become drowsier. This indicates that left-handers are more heterogeneous in terms of shift of bias and hence make both left and right errors as they become drowsier. D) Bias points across alert and drowsy periods for right-handers. The bias points move predominantly towards the left (more negative) compared to the right (more positive) as participants become drowsier. This indicates that right-handers are predominantly left-shifters and hence make more left errors as they become drowsier.*
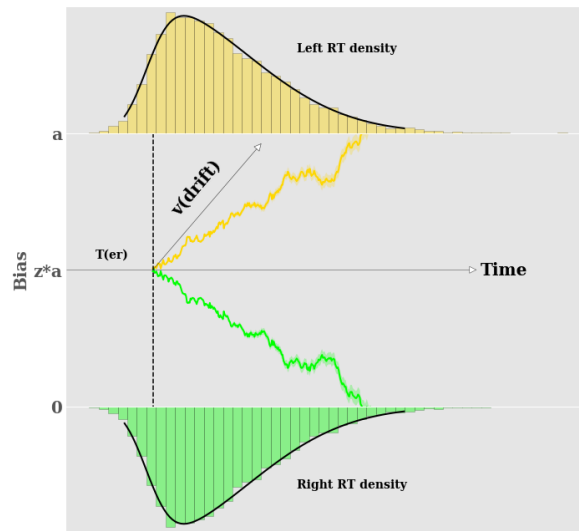
Figure 3: Drift-diffusion model. *Schematic indicating evidence accumulation expressed by drift-diffusion model. The model accounts for the reaction time distributions of responses across left and right stimuli ('Stimulus Coding'). 'V(drift)' indicates the drift rate (evidence accumulation rate), 'a' indicates the boundary separation across left and right responses, 'z' indicates the bias point, usually z = 0.5 for unbiased responses.*

Computational modelling of decision making by drift-diffusion process:

Next, we aimed to quantify the different elements of the decision-making process on the tone localization task using the drift-diffusion model. The drift-diffusion model captures the optimal procedure involved in performing a 2-alternative forced choice (2AFC) task. It assumes that the observer accumulates evidence for one or other alternative in every other time step, until that integrated evidence reaches a threshold to make a decision (Figure 3). This model is known to describe accuracy and reaction time distributions in 2-choice tasks (Ratcliff et al., 2016). The localization of tones to 'left' and 'right' side of space is in essence a 2-choice task with the participant always forced to make a decision on the direction of tone and hence the usage of the drift-diffusion model here is appropriate.

The drift diffusion model was implemented using a hierarchical Bayesian procedure using hierarchical drift diffusion model (HDDM) (See methods section). For the HDDM we fit the response of each participant ('left' or 'right') instead of accuracy ('correct' or 'incorrect'). This procedure is referred to as Stimulus-coding and is critical to uncover response bias (de Gee et al., 2017) in the decision making process.

For this purpose, we examined 8 different variants of the DDM where each model varies the following: drift-rate (v) depending on state ('alert', 'drowsy) or stimulus ('left', 'right') or a combination of both. Bias-point (z) was also varied depending on state ('alert', 'drowsy) or stimulus ('left', 'right') or a combination of both. The winning model in each case was chosen by the lowest deviance information criterion (DIC). For both the left and right-handers the

winning model composed of: Drift-rate (v) varied according to state ('alert','drowsy') and stim ('left','right'). Bias-point (z) varied according to stim ('left','right') (See methods section).

In the next step, the winning model (#8) was analysed for the comparison of posterior densities. The traditional way to compare the distribution of population of two groups is using hull-hypothesis testing (frequentist methods). However, we used Bayesian estimate which is fundamentally more informative and avoids the arbitrary choices like significance level and specific statistical tests used by the frequentist based methods (Kruschke, 2013).

For the right-handers it was found that the proportion of posterior overlap (between left and right stimuli) in the bias point was 23.8% (Figure 4B). In comparison, for the left-handers it was found that the proportion of posterior overlap in the bias point was 9.1% (Figure 4A). This indicates that the left-handers have a higher difference in bias point (between left and right stimuli) compared to the right-handers. For the right-handers, it was found that the proportion of posterior overlap (between left and right stimuli) in the drift rate under alert condition was 14.8% this reduces to 3.4% under drowsy condition (Figure 4D,F). This indicates a change in drift-rate (evidence accumulation) between left and right stimuli as right-handers become drowsier. For the left-handers, it was found that the proportion of posterior overlap (between left and right stimuli) in the drift rate under alert condition was 5.1% this changes to 9.3% under drowsy condition (Figure 4C,F). This indicates a change in drift-rate (evidence accumulation) between left and right stimuli as left-handers become drowsier. However, it is interesting to note that the change in drift-rate is higher in right-handers compared to the left-handers and in the opposite direction.

To summarise, as right-handers become drowsier the difference in rates of evidence accumulation between left and right stimuli increases compared to the left-handers. The difference in drift-rates provides a potential explanation of why right-handers make more left-errors as they become drowsier while left-handers make both left and right-errors as they become drowsier.
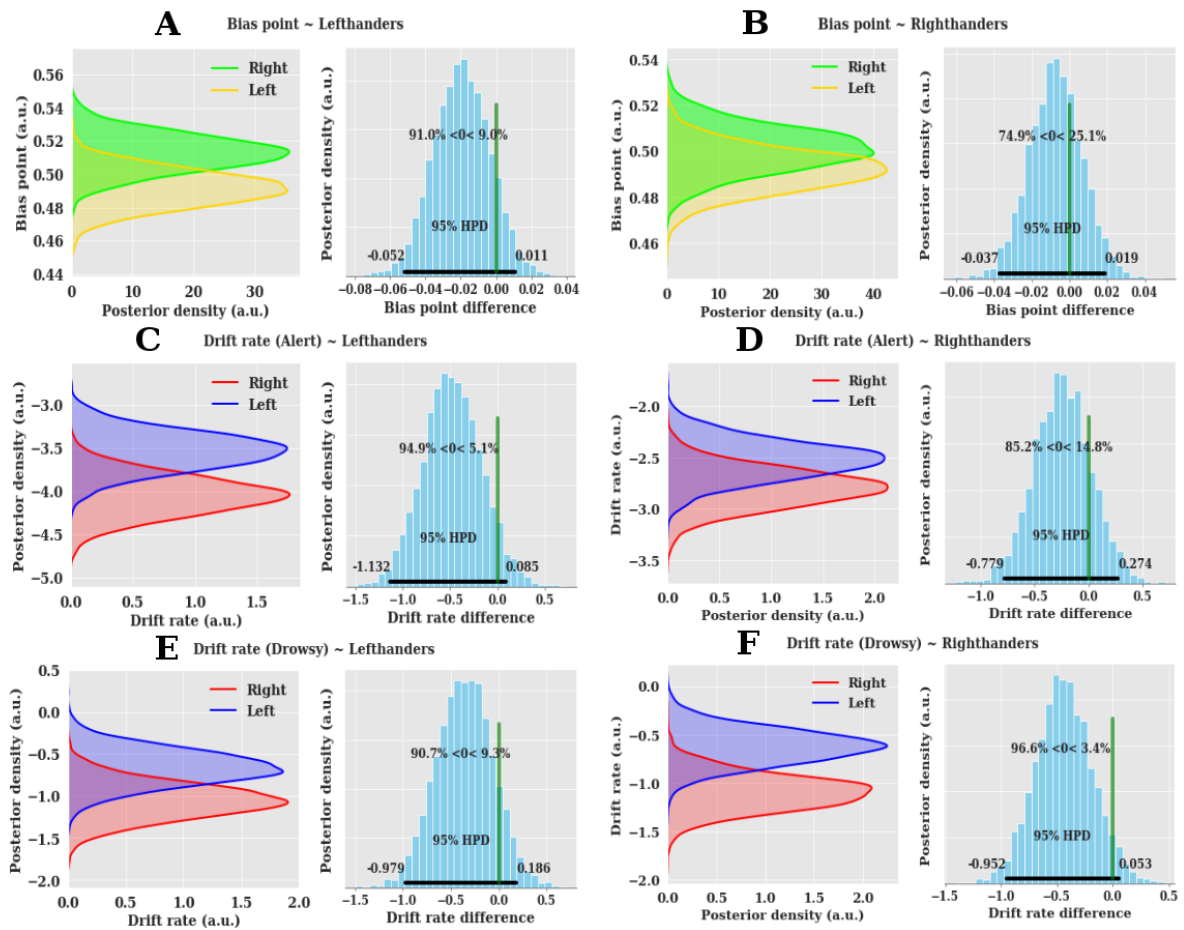
Figure 4: Posterior distributions of drift-diffusion model parameters. *A,B) Group-level posterior distributions for biaspoint (z) across left and right stimuli A) In left-handers, the difference of traces is plotted on the right indicating proportion of overlap between estimates is 9%. B) In right-handers, the difference of traces is plotted on the right indicating proportion of overlap between estimates is 25%. C,D) Group-level posterior distributions for drift-rate (v) across left and right stimuli in in alert trials. C) In left-handers, the difference of the traces is plotted on the right indicating proportion of overlap between estimates is 5.1%. D) In right-handers, the difference of the traces is plotted on the right indicating proportion of overlap between estimates is 14.8%. E,F) Group-level posterior distributions for drift-rate (v) across left and right stimuli in drowsy trials. E) In left-handers, the difference of the traces is plotted on the right indicating proportion of overlap between estimates is 9.3%. F) In right-handers, the difference of the traces is plotted on the right indicating proportion of overlap between estimates is 3.4%. HPD stands for highest posterior density representing credible interval for a particular parameter.*

<u>Neural Evidence of Alertness modulating spatial attention while constrained by handedness</u>

Next we employed multivariate pattern analysis (MVPA) techniques to probe the divergent patterns in the EEG data across various conditions. We used decoding techniques to uncover the brain activity patterns that differ across experimental conditions. Conventional ERP (Event related potentials) analysis rely on using *a-priori* identified spatial locations or temporal segments in the data to measure the differences across conditions. However decoding techniques do not rely on *a-priori* definitions and perform much better in detecting differences across experimental conditions (Fahrenfort et al., 2018). We used temporal decoding (see methods section) to understand the differences in EEG patterns across different conditions.

Neural mechanisms involved in spatial localization across alert and drowsy periods:

First, we were interested in identifying the neural mechanisms involved in performing the spatial attention task during alert conditions and how the mechanisms involved in this task are modulated as the participants become drowsy.

For the right-handers, when the participant was 'alert' the decoding of stimuli that was presented ('left' or 'right') started from 160 ms after the stimulus was presented and lasted until 720 ms (reliably significant, $p<0.05$) (Figure 5B). Peak discriminatory power computed from area under the curve (AUC) analysis was achieved at 280ms (AUC = 0.61). The average AUC between 200-300ms was 0.58 ± 0.007, $p<0.05$. The average AUC between 300-400ms was 0.56 ± 0.002, $p<0.05$. Correspondingly we also plotted the coefficients of the classifier patterns in the sensor space which are neurophysiologically interpretable (Haufe et al., 2014) for every 40ms between 180 ms to 500 ms (Figure 6A). The topography between 180-220 ms indicates strong response in the fronto-central electrodes. The topography of the patterns shifts to more posterior regions (centro-parietal electrodes in the right side of the scalp) between 220 ms to 260 ms. Further, the topography of the patterns shifts to more parietal and occipital electrodes from 260 ms to 300 ms.

When the right-handers become drowsier, the decoding of the stimuli (reliably significant, $p<0.05$) only started from 420 ms and lasted until 740 ms (Figure 5D). This is also reflected in the slower reaction times in drowsy condition (1181.05 ms in drowsy compared to 695.15 ms in alert). Peak AUC of 0.55 was achieved at 590 ms. The average AUC between 400-500 ms was 0.53 ± 0.001, $p<0.05$. The average AUC between 500-600 ms was 0.54 ± 0.003, $p<0.05$. Correspondingly we also plotted the coefficients of the classifier patterns in the sensor space for every 40 ms between 180 ms to 500 ms (Figure 6B). The topography between 180-220 ms indicates the strong response in the frontal electrodes (though not reliably significant to decode) compared to the more fronto-central electrodes in the alert condition. Interestingly the topography from 220-260 ms shifts again to more frontal electrodes (not reliably significant) compared to the central-parietal electrodes in the alert condition. The topography of the patterns shifts to more posterior regions (centro-parietal electrodes, reliably significant) from 380 ms to 420 ms. Further, the topography of the patterns shifts to more parietal and occipital electrodes between 420 ms to 460 ms.

To summarise, this indicates that when the right-handed participant becomes drowsy, the decoding shifts later (moves from 160 ms in alert to 420 ms in drowsy). Further central-parietal electrode pattern, which is visible in alert condition, disappears in the drowsy condition. In the drowsy condition, the temporal electrodes are activated more in the 260 – 300 ms compared to the alert condition; as well the temporal electrode patterns last till 500 ms. It is also interesting to note that the topography from 180-300 ms in the drowsy condition is not reliable to decode the stimuli presented and also different compared to the alert condition.
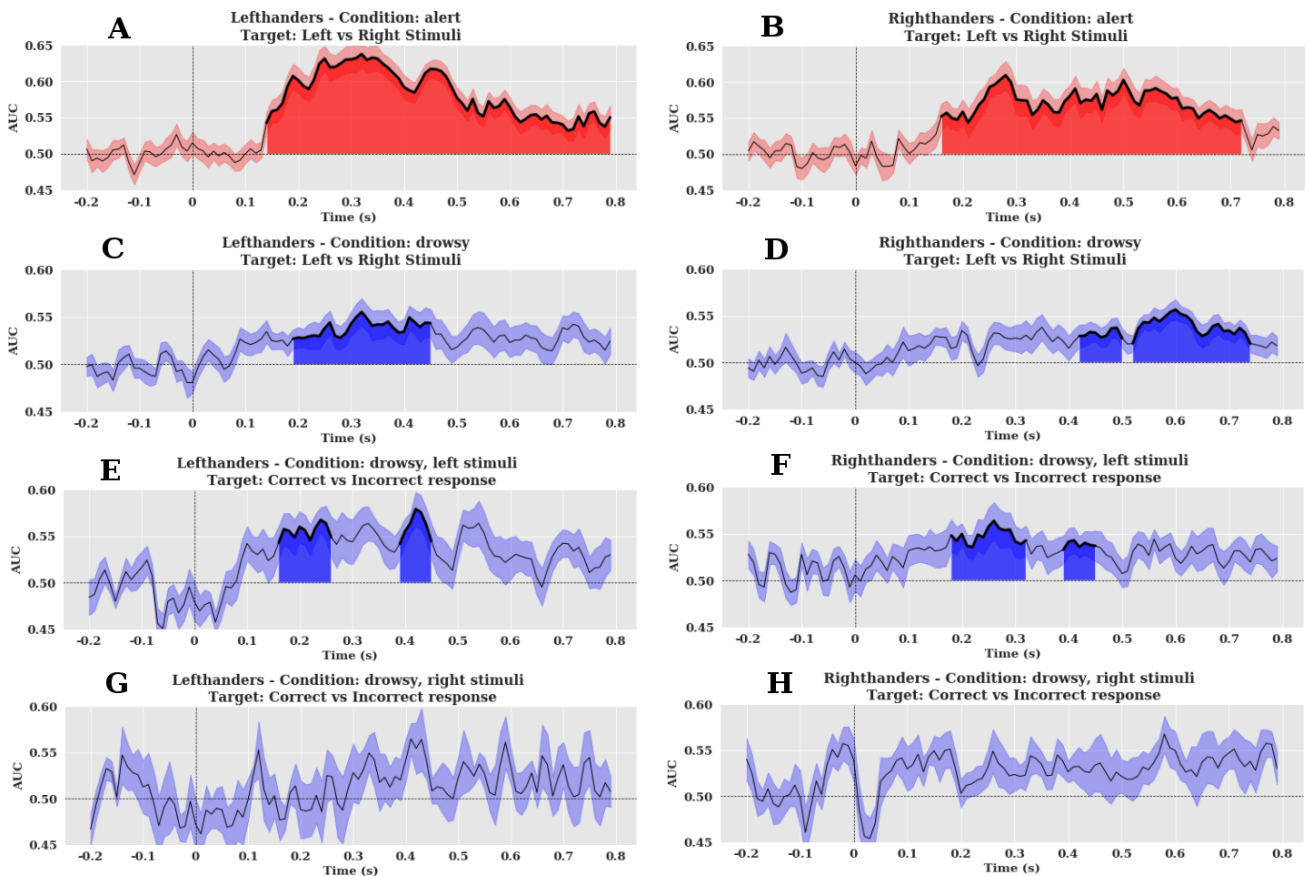
Figure 5: Classifier performance across time (temporal decoding) indicated by Area Under Curve (AUC). A) AUC of left-handers under alert condition, where the classifier was trained to discriminate between targets of left and right stimuli. B) AUC of right-handers under alert condition, where the classifier was trained to discriminate between targets of left and right stimuli. C) AUC of left-handers under drowsy condition, where the classifier was trained to discriminate between targets of left and right stimuli. D) AUC of right-handers under drowsy condition, where the classifier was trained to discriminate between targets of left and right stimuli. E) AUC of left-handers under drowsy condition when left stimuli were presented, where the classifier was trained to discriminate between targets of correct and incorrect responses. F) AUC of right-handers under drowsy condition when left stimuli were presented, where the classifier was trained to discriminate between targets of correct and incorrect responses. G) AUC of left-handers under drowsy condition when right stimuli were presented, where the classifier was trained to discriminate between targets of correct and incorrect responses. H) AUC of right-handers under drowsy condition when right stimuli were presented, where the classifier was trained to discriminate between targets of correct and incorrect responses.

To further confirm the location of the brain regions involved, we decided to project the classifier patterns from the sensor space to the source space using source reconstruction techniques (see methods section). We first found that the decoding pattern under the alert condition (target decoding of left vs right stimuli) was mainly predominant in the right hemisphere. Between 300-400 ms the right temporal regions were mainly involved classifying the stimuli. From 400-500 ms the right inferior parietal regions contribute most to the classifier patterns and this continues till 500-600 ms (Figure 7A). Next under the drowsy condition, the decoding of left vs right stimuli was predominantly in the left hemisphere. Between 300-400 ms the left temporal regions were mainly recruited by the classifier patterns. From 400-500 ms the left inferior parietal cortex along with left pre and post-central cortex regions and left lateral occipital seem to be involved. From 500-600 ms the pattern is much more localized in the left inferior parietal cortex regions (Figure 7B). This shows that for right-handers the right inferior parietal regions were mostly involved in alert condition, whereas the left inferior parietal regions were mostly involved in drowsy condition for classifying the left vs right stimuli.

For the left-handers, when the participant was 'alert' the decoding of stimuli that was presented ('left' or 'right') started from 140ms after the stimulus was presented and lasted till 790ms (reliably significant, $p<0.05$) (Figure 5A). Peak AUC of 0.64 was achieved at 320ms. The average AUC between 200-300 ms was 0.61 ± 0.004, $p<0.05$. The average AUC between 300-400 ms was 0.62 ± 0.004, $p<0.05$. Correspondingly we also plotted the coefficients of the classifier patterns in the sensor space, which are neurophysiologically interpretable (as above) for every 40 ms between 180 ms to 500 ms (Figure 8A). The topography between 180-220 ms indicates strong response in the centro-parietal electrodes. The topography of the patterns shifts to more posterior regions (parietal electrodes in the right side of the scalp) between 220 ms to 260 ms. Further, the topography of the patterns shifts to more parietal and occipital electrodes between 260ms to 300ms.

When the left-handers become drowsier, the decoding of the stimuli (reliably significant, $p<0.05$) started from 190 ms (50 ms later compared to alert condition) and lasted until 450 ms (Figure 5C). This is also reflected in the slower reaction times in drowsy condition (933.33 ms in drowsy compared to 451.75 ms in alert). Peak AUC of 0.56 was achieved at 320 ms. The average AUC between 200-300 ms was 0.53 ± 0.001, $p<0.05$. The average AUC between 300-400 ms was 0.54 ± 0.001, $p<0.05$. Correspondingly we also plotted the coefficients of the classifier patterns in the sensor space for every 40 ms between 180 ms to 500 ms (Figure 8B). The topography between 180-220 ms indicates the strong response in the frontal electrodes (reliably significant, $p<0.05$) compared to the more centro-parietal electrodes in the alert condition. Interestingly the topography from 220-260 ms shifts again to more frontal electrodes (reliably significant, $p<0.05$) compared to the central-parietal electrodes in the alert condition. The topography of the patterns shifts to more temporal regions (tempero-parietal electrodes, reliably significant) between 260 ms to 300 ms. Further, the topography of the patterns shifts to more parietal electrodes (on the left side of the scalp) between 300 ms to 340 ms.

To summarise, this indicates that when the left-handed participant becomes drowsy, the decoding shifts later (moves from 140 ms in alert to 190 ms in drowsy). Further central-parietal electrode pattern, which is visible in alert condition, disappears in the drowsy condition. In the drowsy condition, the temporal electrodes are activated more in the 260 – 300 ms compared to the alert condition. It is also interesting to note that the topography from 180-300 ms in the drowsy condition is reliable to decode the stimuli presented and even though the topography is different compared to the alert condition.

Next, we projected the classifier patterns from the sensor space to the source space using source reconstruction techniques. We first found that the decoding pattern under the alert condition (target decoding of left vs right stimuli) was mainly predominant in the right hemisphere. Between 300-400 ms the left temporal regions along with right post-central and pre-central regions were mainly involved classifying the stimuli. From 400-500 ms the right inferior parietal regions along with right post-central, pre-central regions contribute most to the classifier patterns. From 500-600 ms the pattern is much more localized in the pre and post-central regions in the right hemisphere (Figure 9A).

Next under the drowsy condition, the decoding of left vs right stimuli was present in both hemispheres. Between 300-400ms the left temporal regions along with right temporal regions, right inferior parietal regions were mainly recruited by the classifier patterns. From 400-500 ms the left temporal cortex along with right temporal regions, right inferior parietal regions along with right pre and post-central regions were involved. From 500-600 ms the pattern is much more localized in the left inferior parietal cortex regions along with right and left temporal cortex regions (Figure 9B). This shows that for left-handers the right inferior parietal regions, left temporal regions were mostly involved in alert condition, whereas the left inferior parietal regions, right and left temporal regions along with pre and post-central regions in the right hemisphere were mostly involved in drowsy condition for classifying the left vs right stimuli.

Neural mechanisms involved in spatial localization errors in drowsy periods:

Next, we were interested in identifying the neural mechanisms involved in producing the localization error across the left and right side of the space under drowsy conditions.

Left-stimuli:

For the right-handers, when the participant was 'drowsy' the decoding of responses (correct, incorrect responses) when left stimuli was presented started from 180 ms after the stimulus was presented and lasted till 320 ms (reliably significant, p<0.05), again from 390 ms to 450 ms (reliably significant, p<0.05) (Figure 5F). Peak AUC of 0.56 was achieved at 260 ms. The average AUC between 180-320 ms was 0.54 ± 0.002, p<0.05. The average AUC between 390-450 ms was 0.53 ± 0.001, p<0.05. Correspondingly we also plotted the coefficients of the classifier patterns in the sensor space for every 40 ms between 180 ms to 500 ms (Figure 6C). The topography between 180-220 ms indicates strong response in the frontal electrodes. The topography of the patterns shifts to more posterior regions (centro-parietal

electrodes in the left side of the scalp) between 220 ms to 260 ms. Further, the topography of the patterns shifts to more parietal and occipital electrodes between 260 ms to 300 ms. Source localization confirmed that activity in the left superior parietal cortex regions (300-500 ms), left inferior parietal cortex regions (500-600 ms), left frontal regions (200-500 ms), right pre-central gyrus (300-600 ms) were involved in the classifier patterns (Figure 7C).

For the left-handers, when the participant was 'drowsy' the decoding of responses (correct, incorrect responses) when left stimuli was presented started from 160 ms after the stimulus was presented and lasted till 260 ms (reliably significant, $p<0.05$), again from 390 ms to 450 ms (reliably significant, $p<0.05$) (Figure 5E). Peak AUC of 0.58 was achieved at 420ms. The average AUC between 160-260 ms was 0.55 ± 0.002, $p<0.05$. The average AUC between 390-450 ms was 0.56 ± 0.005, $p<0.05$. Correspondingly we also plotted the coefficients of the classifier patterns in the sensor space for every 40 ms between 180ms to 500ms (Figure 8C). The topography between 180-220 ms indicates strong response in the frontal electrodes. The topography of the patterns shifts to more posterior regions (centro-temporal electrodes in the right side of the scalp) between 220 ms to 260 ms. Further, the topography of the patterns shifts to more right parietal and right temporal electrodes between 260 ms to 300 ms. Source localization of the classifier patterns confirmed that activity in the left temporal cortex (300-400 ms), left inferior parietal cortex (300-600 ms), right precentral gyrus (400-600 ms) (Figure 9C).

Right-stimuli:

When both the right and left-handers became 'drowsy', the decoding of responses (correct, incorrect response) when right stimuli was presented was not reliably significant across any time point (Figure 5H,G). However, we decided to plot the coefficient of the classifier patterns in the sensor space to explore the electrode locations involved.

For the right-handers, we plotted the coefficients of the classifier patterns in the sensor space for every 40 ms between 180 ms to 500 ms (Figure 6D). The topography between 180-220 ms indicates strong response in the central electrodes. The topography of the patterns shifts to more posterior regions (centro-parietal electrodes in the left side of the scalp) between 220 ms to 260 ms. Further, the topography of the patterns shifts to more parietal and occipital electrodes between 260 ms to 300 ms. To further confirm the location of the brain regions involved, we decided to project the classifier patterns from the sensor space to the source space (Figure 7D). We found that the decoding pattern was located in temporal cortex (200-600 ms), left and right parietal cortex (300-600 ms), left and right pre and post-central gyrus (300-600 ms).

For the left-handers, we plotted the coefficients of the classifier patterns in the sensor space for every 40 ms between 180 ms to 500 ms (Figure 8D). The topography between 180-220 ms indicates strong response in the fronto-central electrodes. The topography of the patterns shifts to more posterior regions (fronto-central electrodes) between 220 ms to 260 ms. Further, the topography of the patterns shifts to more parietal and occipital electrodes between 260 ms to 300 ms. To further confirm the location of the brain regions involved, we decided to project the classifier patterns from the sensor space to the source space (Figure

9D). We found that the decoding pattern was located in left frontal regions (300-600 ms), left inferior parietal regions (400-600 ms), left pre-central gyrus (300 – 600 ms), right parietal cortex regions (500 – 600 ms).
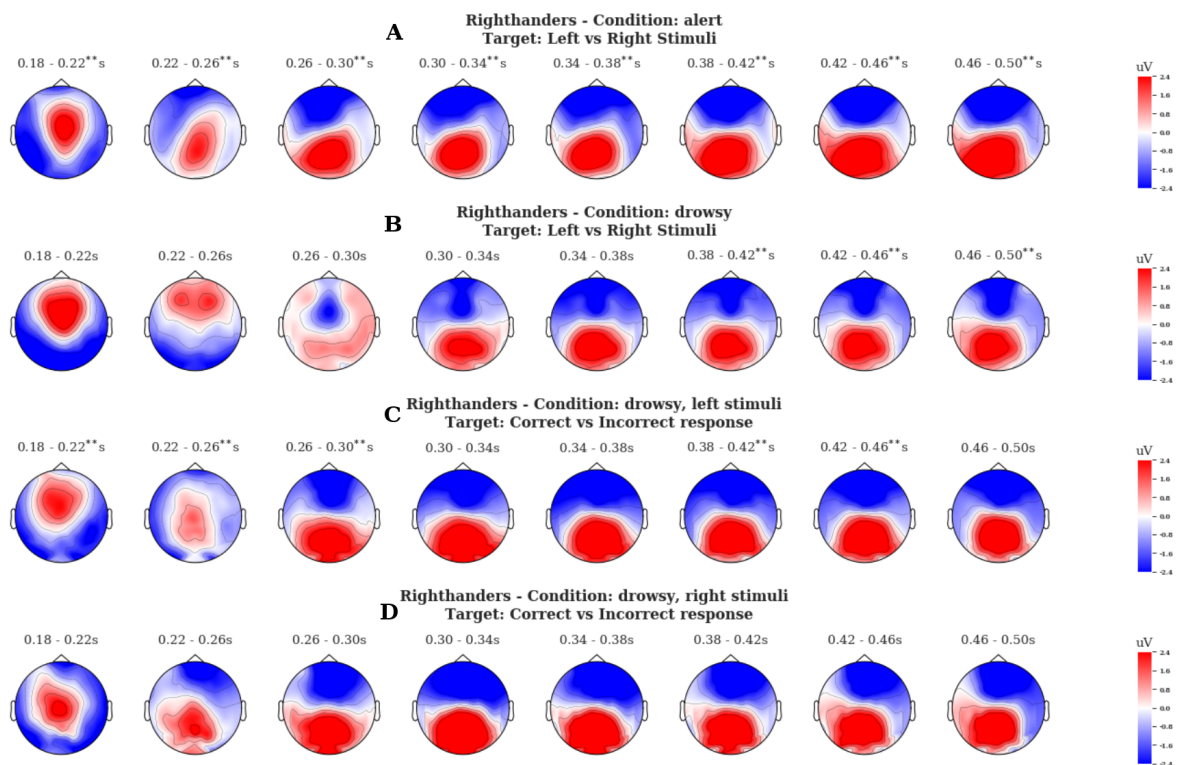
Figure 6: Coefficients of classifier patterns in right-handers. *A) Coefficients of classifier patterns of right-handers under alert condition, where the classifier was trained to discriminate between targets of left and right stimuli. B) Coefficients of classifier patterns of right-handers under drowsy condition, where the classifier was trained to discriminate between targets of left and right stimuli. C) Coefficients of classifier patterns of right-handers under drowsy condition when left stimuli were presented, where the classifier was trained to discriminate between targets of correct and incorrect responses. D) Coefficients of classifier patterns of right-handers under drowsy condition when right stimuli were presented, where the classifier was trained to discriminate between targets of correct and incorrect responses. ** indicates statistically significant time periods, the topographical plot was averaged between the time intervals mentioned.*

Figure 7: Classifier patterns projected in source space for right-handers. *A) Decoding patterns (for target classification of left vs right stimuli) starts in the left parietal regions first (280 ms), followed by right parietal regions (400 ms). B) Under drowsy conditions the decoding patterns (for left vs right stimuli) start later only at 400 ms and it more prevalent in the temporal regions, followed by parietal regions at 540-590ms. C) Decoding patterns under drowsy conditions (for left stimuli with target classification of correct vs incorrect response) starts in the regions closer to the Inferior frontal gyrus from 260ms and lasts till 410 ms. D) Decoding patterns under drowsy conditions (for right stimuli with target classification of correct vs incorrect response) starts in the temporal regions from 320 ms followed by more parietal and motor regions at 410 ms. ** indicates statistically significant time periods.*
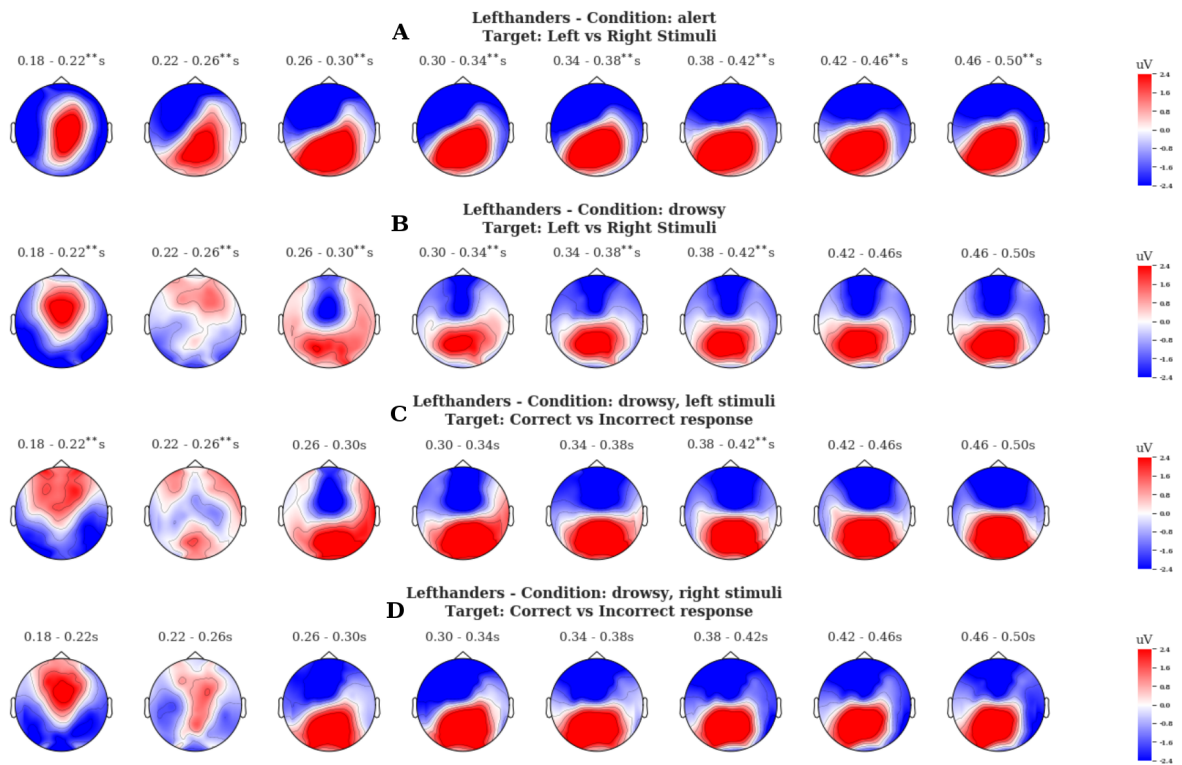
Figure 8: Coefficients of classifier patterns in left-handers. A) Coefficients of classifier patterns of left-handers under alert condition, where the classifier was trained to discriminate between targets of left and right stimuli. B) Coefficients of classifier patterns of left-handers under drowsy condition, where the classifier was trained to discriminate between targets of left and right stimuli. C) Coefficients of classifier patterns of left-handers under drowsy condition when left stimuli were presented, where the classifier was trained to discriminate between targets of correct and incorrect responses. D) Coefficients of classifier patterns of left-handers under drowsy condition when right stimuli were presented, where the classifier was trained to discriminate between targets of correct and incorrect responses. ** indicates statistically significant time periods, the topographical plot was averaged between the time intervals mentioned.

Figure 9: Classifier patterns projected in source space for left-handers. *A) Decoding patterns (for target classification of left vs right stimuli) starts in the right hemisphere regions first (240 ms), followed by left temporal regions (350 ms). B) Under drowsy conditions the decoding patterns (for left vs right stimuli) start later only at 260 ms and it more prevalent in the left temporal regions, followed by right inferior regions at 370 ms. C) Decoding patterns under drowsy conditions (for left stimuli with target classification of correct vs incorrect response) starts in the regions closer to the left frontal, temporal regions, right parietal regions from 400ms and lasts till 420 ms. D) Decoding patterns under drowsy conditions (for right stimuli with target classification of correct vs incorrect response) starts in left temporal, left parietal regions from 400 ms followed by more left frontal and motor regions at 420 ms. ** indicates statistically significant time periods.*

Connecting Behaviour with Neural signatures

Next, we were interested in identifying the neural signatures that are related directly to the process of evidence accumulation. Using this analysis, we can compute the sensor locations that reliably encode the difference in drift rates (across stimuli and alertness conditions), which could further be used to provide evidence to specific sensor location computed with the MVPA methods earlier. For this purpose, we used the parameters from the drift diffusion model constructed earlier. To summarise from the earlier findings, it was found that the rate of evidence accumulation (drift-rate) was different between left and right stimuli in right-handers as they become drowsy. To assess the trial-by-trial variation of the behavioural parameters with the neural signatures we fitted a regression model using the HDDM toolbox (Wiecki et al., 2013)

We fitted the Stimulus-coding model ('left' or 'right') responses as earlier and estimated the drift rate (v) as a function of ERP data per trial per electrode per time point (See methods section)

$$V \sim \beta_0 + \beta_1(ERP)$$

The above equation can be written in patsy form as below.

$$V \sim ERP : C\big(state, Treatment('Alert')\big) : C\big(stim, Treatment('Right')\big)$$

Where, V represents the drift rate, ERP represents the z-scored ERP data computer per trial per time point, state represents 'alert' or 'drowsy', stim represents 'left' or 'right'. The bias point (z) was made to vary with the stimulus as before. From this analysis we can find out how the drift rate varied with the ERP data across stimulus and alertness levels. The difference in the drift rate between the left and right stimulus in alert and drowsy conditions can then be plotted per electrode per time point (Figure 10).

We first plotted the difference in drift rate (proportion of overlap in the posterior distribution across stimuli) in the alert condition in time steps of 50 ms. For the right-handers (Figure 10A), the topography of the sensor plot shows that electrodes in the fronto-central region (150-200 ms) shows higher differences in drift rate (implying the encoding of evidence accumulation rate). Followed by which the topography shifts to central and parietal electrodes (200-250 ms). Further after 250 ms the topography shifts to more posterior regions in the central and parietal electrodes. For the left-handers, we plotted the difference in drift rate in the alert condition in time steps of 50 ms (Figure 10B). The topography of the sensor plot shows that electrodes in the fronto-central region (150-200ms) shows higher differences in drift rate. Followed by which the topography shifts to more posterior regions

in central and parietal electrodes (200-250 ms). Further after 250 ms the topography shifts to more posterior regions in the central and parietal electrodes.

Next we plotted the difference in drift rate in the drowsy condition. For the right-handers, the topography of the sensor plot shows that more frontal and central electrodes show differences in drift rate from 150 – 250 ms (Figure 10C). Further the topography shifts to more central, parietal, right temporal electrodes in 250-300 ms. The topography then moves to more posterior regions in the parietal and central electrodes from 350 ms onwards. For the left-handers, the topography of the sensor plot shows that more frontal and central electrodes show differences in drift rate from 150 – 250 ms (Figure 10D). Further the topography shifts to more central, parietal, right temporal, right frontal electrodes in 250-300 ms. The topography then moves to more posterior regions in the parietal and central electrodes from 350 ms onwards.
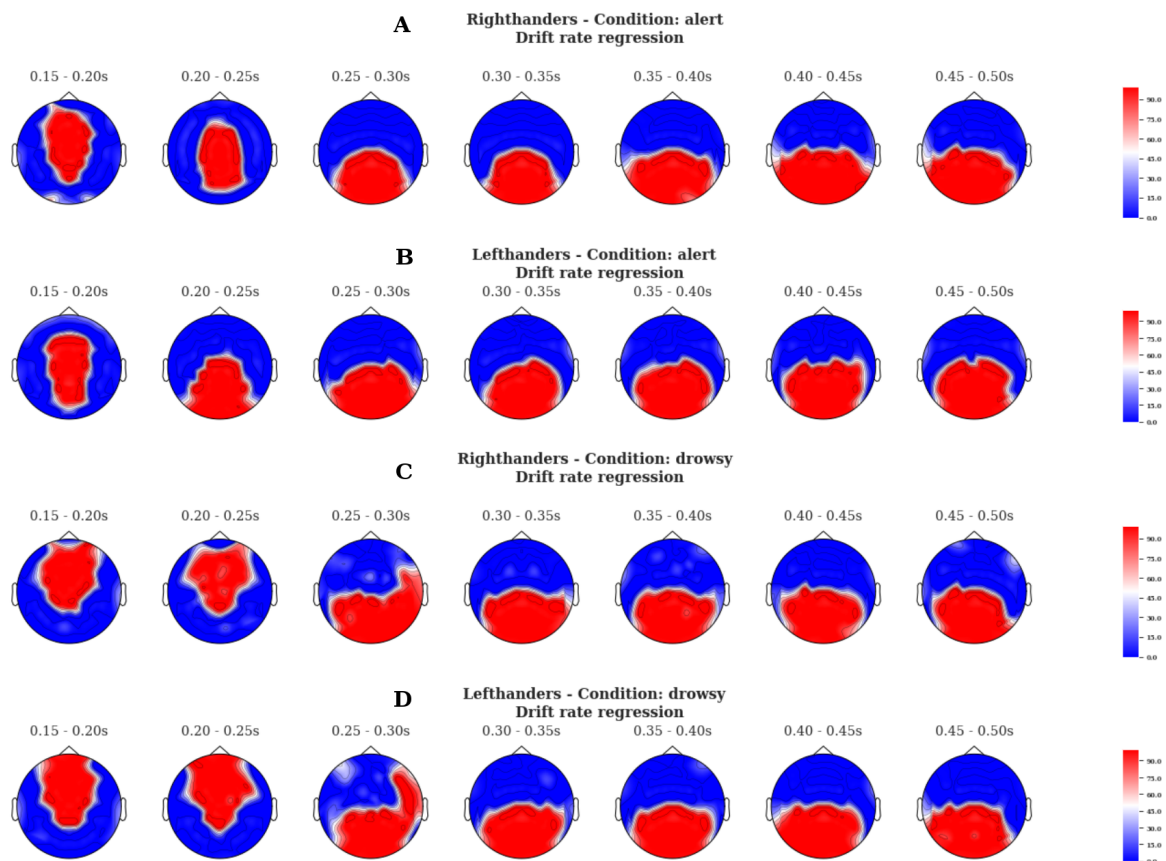
Figure 10: Regression of drift rate across different conditions in right and left-handers. A) Proportion of overlap between drift rates across left and right stimuli in right-handers in alert condition across different time points. B) Proportion of overlap between drift rates across left and right stimuli in left-handers in alert condition across different time points. C) Proportion of overlap between drift rates across left and right stimuli in right-handers in drowsy condition across different time points. D) Proportion of overlap between drift rates across left and right stimuli in left-handers in drowsy condition across different time points.

DISCUSSION:

We investigated how the brain of right and left-handed individuals is differentially affected by varying levels of alertness while performing an auditory spatial attention task.

Our results from behavioural analysis confirm the differences in performance of right and left-handed individuals.

First, multilevel modelling shows that for both right and left-handed individuals the proportion of error is dependent on a combination of alertness level ('alert' or 'drowsy') and stimuli ('left' or 'right') being presented. For right-handers we also observe that the error proportion of left stimuli is markedly increased when compared to right stimuli, thereby producing a typical neglect-like effect. However, the left-handers do not show any such effect and the error proportion of both left and right stimuli increase when left-handers become drowsy. The performance of right-handers replicate previous studies (Bareham et al., 2014) and further show evidence for left neglect as in (Fink et al., 2001; Jewell and McCourt, 2000). While those of left-handers contradict previously published results (Bareham et al., 2015). This could be due to more accurate measurement of trial-by-trial alertness levels using micro-measures algorithm (Jagannathan et al., 2018), increased trial numbers (as well as more uniform sampling of the space from -59.31° to +59.31°) and separate baseline 'alert' session providing more statistical power in the present study. We also further use the handedness score of individual participants along with alertness levels to show how they can explain the behaviour of both right and left-handed participants.

Second, we used psychophysics to show how the subjective mid-lines of individual participants vary as they become drowsy. We then show how most of the right-handed participants have their subjective midlines shifted to the left (thereby making more left errors). These results again replicate the error bias metric computed in (Bareham et al., 2014) and further show evidence of mid-line shift similar to observation in patient studies (Karnath and Fetter, 1995; Vallar, 1998). Comparatively, the left-handers are much more heterogeneous with individuals shifting to the left and right as well. We further show in right-handers; the sensitivity of the system is highly correlated with the mid-line shift as participants become drowsier. In other words, a common factor (alertness) seems to modulate both the sensitivity and the midline shift. However, left-handers do not show any such correlation, thereby providing further evidence for lack of alertness related modulation in behaviour (on one side of space).

Third, we decided to use a computational model to dissect the various parameters involved in the decision making process. We used hierarchical drift-diffusion model to show that as right-handers became drowsy the drift-rate (evidence accumulation rate) changes for the left stimuli and not for the right stimuli. Using the same model in left-handers reveals that the evidence accumulation rate doesn't change when the participants become drowsier. We also show that for both right and left-handed participants the bias point (starting point) of the decision making process doesn't change as they become drowsier. This clearly points to the elements of evidence accumulation (and not response bias) in explaining the behaviour

as the participants become drowsier. Further it has been shown that trial to trial variation in drift rate is directly linked to attentional processes (Nunez et al., 2017), thereby clearly establishing the behavioural effect as linked to attention rather than to sensory dysfunction.

Our results from EEG analysis also confirm the differential processing of information by right and left-handed individuals in the tone localization task.

First, decoding analyses in sensor space from EEG data show that during the alert condition the decoding (target: left versus right stimuli) uncovered regions in the brain that are involved in performing this task under baseline conditions. For the right-handers, we found that mainly putative regions in the right hemisphere were involved. Chiefly regions like right temporal cortex, right inferior parietal regions were present in the decoding patterns. These regions broadly correspond to findings from (Shulman et al., 2010) implicating right temporo-parietal cortex. As mentioned in the introduction, this activation of right hemispheric regions adds evidence to right hemisphere dominance model in right-handers under alert conditions. For the left-handers, we found regions in right hemisphere were involved. Chiefly regions like right inferior parietal regions were present in the decoding patterns. This activation adds evidence to right hemispheric dominance model in left-handers under alert conditions.

Second, the decoding analysis in sensor space from EEG data shows that during the drowsy condition the decoding (target: left versus right stimuli) uncovered the following regions in the brain. For the right-handers, we found that activity mainly shifts to the left hemisphere. Primarily regions like left temporal, left inferior parietal were involved. This shows that under conditions of low alertness, the left hemisphere is highly active in performing this task. Under these conditions the left hemisphere pulls attention to the right side of the space, thereby explaining neglect like effects. This again adds evidence to the right hemispheric dominance model. Further evidence from invasive studies performed by (Szczepanski and Kastner, 2013) using transcranial magnetic stimulation of dorsal attention regions leads to attention being shifted to the ipsilateral side. Potentially further studies involving activation in the ventral regions could possibly provide evidence for attention being shifted to the contralateral side. Also studies (Sturm et al., 1999) involving the neural correlates of alertness have shown that activity in the right hemisphere increased under conditions of high alertness, which broadly agrees with our findings. For the left-handers, we found that activity is bilateral in both the right and left hemisphere. Primarily regions like left temporal, left inferior parietal, right temporal, right inferior parietal were involved. This shows that under conditions of low alertness, both the right and left hemisphere is highly active in performing this task, however the locations move more ventral compared to the alert condition. This bilateral activation adds evidence to interhemispheric competition model in left-handers under drowsy conditions.

Third, the decoding analysis in sensor space from EEG data shows that during the drowsy condition on the presentation of left stimuli (target: correct versus incorrect response) uncovered the following regions in the brain. For the right-handers, primarily regions in left superior parietal, left inferior parietal were involved. These regions broadly agreed with the

inferior parietal regions found in (Mort et al., 2003). For the left-handers, primarily regions in left superior parietal, left inferior parietal were involved.

This conclusion of the differential brain regions involved was derived from qualitatively comparing the decoding patterns under different conditions. Hence the involvement of the above mentioned brain regions should be further confirmed by performing statistical analysis either in the source or the sensor space across different conditions.

Overall, these analyses putatively suggest that when undertaking a spatial attention task: the right-handers rely on the right hemisphere (posterior parietal regions) when alert, the left-handers also show such hemispheric preference in the posterior parietal regions. The right-handers shift their reliance to the left hemisphere (posterior parietal regions) when drowsy, while the left-handers maintain a balanced decoding profile in both hemispheres. These findings support the evidence for right hemisphere dominance in right-handers while supporting interhemispheric completion model in left-handers.

These findings call for inclusion of left-handers in spatial experiments in order to provide further evidence to evaluate neuroanatomical models of spatial attention.

EXPERIMENTAL PROCEDURES:

Stimuli and Protocol

Right-handers:
Forty-one healthy self-described right-handers participated in this study. Data from nine subjects had to be discarded due to a) technical problems with the headphone amplifier (8). b) Not following instructions (1). Hence data from 32 participants (24.46 ± 3.72 years old, 14 males) was considered for further analysis. Only self-described easy sleepers were recruited, further on the day of the experiment they were administered with the Epworth Sleepiness scale (Johns, 1991), Edinburgh Handedness Scale (Oldfield, 1971). 29 participants had a sleepiness score >= 7 (easy sleepers) and 3 of them had a sleepiness score >=4. All participants had handedness score of above 0 (right-handed) with mean 80.26 ± 23.59.

Left-handers:
Thirty-five healthy self-described left-handers participated in this study. Data from three subjects had to be discarded due to a) technical problems with the headphone (1). b) Not following instructions (2). Hence data from 32 participants (24.40 ± 5.89 years old, 16 males) was considered for further analysis. Only self-described easy sleepers were recruited, further on the day of the experiment they were administered with the Epworth Sleepiness scale (Johns, 1991). 30 participants had a sleepiness score >= 7 (easy sleepers) and 2 of them had a sleepiness score >=4. Handedness was assessed using Edinburgh Handedness Scale (Oldfield, 1971) with handedness scores of -57.96 ± 29.01 (score of below 0 is considered left handed).

All participants had no auditory, neurological, psychiatric abnormalities. They were also asked not to consume stimulants like Coffee/Tea on the day of the experiment. Further, they

gave written informed consent and were compensated with 30£ for the study. Each participant underwent two sessions a) Awake b) Drowsy.

Awake session:
Participants were presented with 124 complex harmonic tones (created from guitar picks) that fell on the left or right of their midline (0°) varying from -59.31° to +59.31°. The tones were recorded previously in free-field using in ear microphones (Bareham et al., 2014). Six tones from -59.31° to -39.26° were presented two times each; twelve tones from -35.24° to -1.86° were presented four times each. The same pattern was repeated on the right side with twelve tones from 1.86° to 35.24° were presented four times each, six tones from 39.26° to 59.31° presented two times each. The tones in the midline (0°) were presented four times. This resulted in a total of 124 tones. The order of stimulus presentation was randomized per participant. Participants were instructed to keep their eyes closed and respond (as quickly and as accurately as possible) with a button press (by left/right thumb) indicating the direction of the tone (left or right). Each trial began after a random interval of 2-3 seconds and if participant did not respond for 5 seconds, the next trial was started. The participants were also instructed to stay awake throughout the task.

Drowsy session:
Participants were presented with 740 complex harmonic tones (as above) that fell on the left or right of their midline (0°) varying from -59.31° to +59.31°. Six tones from -59.31° to -39.26° were presented twenty times each; twelve tones from -35.24° to -1.86° were presented twenty times each. The same pattern was repeated on the right side with twelve tones from 1.86° to 35.24° were presented twenty times each, six tones from 39.26° to 59.31° presented twenty times each. The tone in the midline (0°) was presented twenty times. This resulted in a total of 740 tones. The order of stimulus presentation was randomized per participant as above. Participants were instructed to keep their eyes closed and respond (as quickly and as accurately as possible) with a button press (by left/right thumb) indicating the direction of the tone (left or right). Each trial began after a random interval of 4-5 seconds and if participant did not respond for 5 seconds, the next trial was started. The participants were allowed to fall asleep (and become drowsy) and were woken up if they didn't respond to more than 3 trials continuously.

Before the awake and drowsy session, the participants were allowed a practise session to familiarise with the task.

Preprocessing

EEG data was acquired using 129 Ag/AgCl electrodes (Electrical Geodesics Inc) with Cz as reference. The electrode impedances were kept below 100 KΩ and signal was acquired at a sampling rate of 500 Hz. EEG data was pre-processed with custom made scripts in MATLAB (MathWorks Inc. Natick, MA, USA) using EEGLAB toolbox (Delorme and Makeig, 2004). First, the peripheral channels in the EEG that covered the regions of forehead, cheeks and neck were removed to minimise eye and muscle related artifacts, thus retaining only 92 channels that covered the scalp. Second, the data was bandpass filtered with zero phase shift between 1 and 40 Hz using hamming windowed-sinc FIR filter and was then resampled

to 250 Hz. Third, pre-trial and post-trial epochs were created as follows. For the pre-trial epochs, the data was epoched from -4000ms to 0ms to the onset of the stimuli in the Drowsy session. Pre-trial epochs were not created in the Awake session (details below). For the post-trial epochs, the data was epoched from -200ms to 800ms to the onset of the stimuli for both the Awake and Drowsy sessions. Fourth, the trials that exceed the amplitude threshold of ±250 μV were removed in a semi-automatic fashion. Fifth, the bad channels were detected in two steps: a) channels are considered bad if channel variance is below 0.5. b) The normalized power spectrum of the remaining channels is computed and any channel that exceeds the mean power spectrum by ±3 standard deviations was marked bad. Sixth, Independent component analysis (ICA) was performed on the channels not marked as bad in the previous step. ICA components that correspond to artifacts (eye-blinks, muscle) were rejected by manual inspection. Seventh, the bad channels were now interpolated using spherical interpolation. Eighth, the bad trials detection was performed again (amplitude threshold of ±250 μV) and bad electrodes in such trials interpolated in a trial-by-trial fashion. Ninth, the post-trial epochs were re-referenced to the average of all channels (pre-trial epochs were maintained with the same Cz reference).

Alertness levels

The first step in the analysis involved classifying periods of the experimental session into 'awake' and 'drowsy'. The pre-trial period before each tone was used in classifying the corresponding trial as awake or drowsy. However, in the awake session all participants were explicitly asked to stay awake. Hence the pre-trial epochs were not computed in the awake session and all 124 trials in the awake session in each participant were classified as 'awake'. In the drowsy session, the participants were allowed to fall asleep and hence in some trials they would be alert and in some they would be drowsy. Pre-trial epochs in the drowsy session (computed from the previous section) were analysed using the micro-measures algorithm (Jagannathan et al., 2018) and each trial was classified was 'alert', 'drowsy(mild)', 'drowsy(severe)'. Only trials that were classified as 'drowsy(mild)' were used as 'drowsy' trials. The other trials were ignored because usually participants don't respond when under 'drowsy(severe)' trials and we also wanted to compare the drowsy trials of the drowsy session to the alert session, so we ignored the 'alert' trials in the drowsy session.

Behavioural analysis

Multi-level modelling:

We first computed the proportion of errors made by each subject under each condition ('awake', 'drowsy') under each stimulus ('left', 'right' to the midline). If the number of trials for any participant under a particular condition is less than 5 then the corresponding error proportion is ignored in the analysis. Next we investigated whether the proportion of error is influenced by state of the participant ('awake' or 'drowsy'), stimulus ('left' or 'right') or an interaction of both. For this purpose, we defined 4 models. In the null model, the error proportion depends only on its mean (fixed effect) and the individual participant (participant id is used a random effect). In the second model (state model), the error proportion

depends only on the state of the participant ('awake' or 'drowsy' as fixed effect) and individual participant (participant id is used as random effect). In the third model (stimulus model), the error proportion depends only on the stimulus being presented ('left' or 'right' as fixed effect) and individual participant (participant id is used as random effect). In the fourth model (state-stimulus model), the error proportion depends on a combination of state of participant ('awake' or 'drowsy') and the stimulus being presented ('left' or 'right'), both used as fixed effects and individual participant (participant id is used as random effect). These 4 models are fit separately for left and right-handers using the 'lmer' function in R (Bates et al., 2015b, 2015a) and the winning model is identified as the one with the highest log-likelihood by comparing it with the null model and performing a likelihood ratio chi-square test ($\chi 2$). Finally the top two winning models are compared against each other using 'anova' function in R (Fox and Weisberg, 2011), to validate whether the winning model (if it is more complex) is actually better than the loosing model (if it is simpler).

The models for left and right-handers along with log-likelihood values are shown below. In both cases the state-stimulus model was the winning model.

Right-handers:

Model	Parameters	Log-likelihood	Pr(>$\chi 2$)
Null	Fixed: mean, Random: subject id	61.24	-
State	Fixed: state, Random: subject id	66.62	<0.001
Stimulus	Fixed: stimulus, Random: subject id	68.45	<0.001
State-Stimulus	Fixed: state*stimulus, Random: subject id	77.98	<0.001

Left-handers:

Model	Parameters	Log-likelihood	Pr(>$\chi 2$)
Null	Fixed: mean, Random: subject id	78.12	-
State	Fixed: state, Random: subject id	86.68	<0.001
Stimulus	Fixed: stimulus, Random: subject id	81.59	<0.01
State-Stimulus	Fixed: state*stimulus, Random: subject id	91.42	<0.001

The winning model of state-stimulus was further analysed with the 'anova' function to quantify the relationship between error-proportion and state and stimulus. Estimated marginal means were computed using 'emmeans' package in R.

In the next step to provide more evidence of handedness modulating behaviour, data from both right and left-handers were combined and we used the handedness score from Edinburgh Handedness Scale as a parameter in the model.

For this purpose, we defined 5 models. In the null model, the error proportion depends only on its mean (fixed effect) and the individual participant (participant id is used a random effect). In the second model (state model), the error proportion depends only on the state of the participant ('awake' or 'drowsy' as fixed effect) and individual participant (participant id is used as random effect). In the third model (stimulus model), the error proportion depends only on the stimulus being presented ('left' or 'right' as fixed effect) and individual participant (participant id is used as random effect). In the fourth model (state-handedness

model), the error proportion depends on a combination of state of participant ('awake' or 'drowsy' as fixed effect) and the handedness score of the participant (as random effect – slope) and individual participant (participant id is used as random effect - intercept). In the fifth model (stimulus-handedness model), the error proportion depends on a combination of stimulus being presented ('left' or 'right' as fixed effect) and the handedness score of the participant (as random effect – slope) and individual participant (participant id is used as random effect - intercept). The interaction effect was avoided because of two reasons. First, the handedness score is not a binary value but a continuous value from -100 to +100 and hence it is difficult to interpret the interaction effect (if any). Second, left-handers showed no interaction while the right-handers showed interaction between stimulus and state in the previous analysis and hence only factors that showed effect for left and right-handers were chosen.

The models for handedness score along with log-likelihood values are shown below. The state-handedness model emerges as the winning model.

Model	Parameters	Log-likelihood	Pr(>χ2)
Null	Fixed: mean, Random: id	138	-
State	Fixed: state, Random: id	150.94	<0.001
Stimulus	Fixed: stimulus, Random: id	148.07	<0.001
State-handedness	Fixed: state, Random: handedness, id	152.77	<0.001
Stimulus-handedness	Fixed: stimulus, Random: handedness, id	149.47	<0.001

Psychometric function fits:

The change in subjective midline was quantified by fitting psychometric functions to the responses produced by each participant under alert and drowsy conditions. The proportion of rightward response under each stimulus condition from -60° to +60° was fitted with a cumulative normal function using the generalized linear model 'glm' function in R. The link function used for the fit was 'probit' which asymptotes to 0 (Knoblauch, 2014). The mean of the cumulative normal function (the point where the curve cross 0.5 in the y-axis) is referred to as the subjective midline ('bias'). This is because the subjective midline is the stimulus where the participant performs at chance (0.5). The Bias was calculated separately per participant per condition (alert, drowsy). The standard deviation of the curve (slope or steepness of the curve) represents the 'sensitivity' of the system. Increase in standard deviation reduces the sensitivity of the system. Participants that had a bias point (mean) of more than 60° were ignored in the drowsy condition (this is because overall stimulus angle varied from -60° to +60°).

Drift diffusion model:

Next, we aimed to quantify the different elements of decision-making process using the drift-diffusion model. The primary elements of this model include i) drift-rate - 'v' which is the evidence accumulation rate ii) bias point - 'z' indicating the starting point of the decision making process iii) boundary separation distance – 'a' which is the distance between the two

decision boundaries. iv) non-decision time –'Ter' usually accounting for processes like stimulus encoding (prior to evidence accumulation), time for response execution (after evidence accumulation). We decided to use the hierarchical drift diffusion model (HDDM) to provide for a hierarchical Bayesian procedure to estimate the model parameters involved in our task (Wiecki et al., 2013) (version 0.6.0). It is important to note that different participants would have differing levels of alertness, this would mean that we have varying number of trials per condition per participant. Hence it is crucial to use an approach that would provide a robust estimation of model parameters with the limited amount of trials available (Zhang et al., 2016).

For the HDDM we fit the response of each participant ('left' or 'right') instead of accuracy ('correct' or 'incorrect'). This procedure is referred to as Stimulus-coding. For this purpose, we examined 8 different variants of the DDM (see below).

For individual models, we created 15000 samples from the posterior distribution of the model parameters using Markov chain Monte Carlo methods. Further 5000 samples were discarded as burn-in to reduce the effect of initial values on the estimation of the posterior.

The winning model in each case was chosen by the lowest deviance information criterion (DIC). The DIC provides a measure for the accuracy of the model, while penalising for model complexity (Spiegelhalter et al., 2002). To check the convergence of the winning model, Gelman-Rubin statistic was compared for 5 model runs and the winning model was found to have values close to 1 and not larger than 1.2 thus indicating convergence (Gelman, 2013).

The DIC scores along with model specifications are given below for right and left-handers separately.

Right-handers:

Model#	Drift-rate(v)	Bias-point(z)	DIC score
1	'state'	'state'	22515.22
2	'state'	'stim'	22474.04
3	'state'	'state', 'stim'	22274.47
4	'stim'	'state'	24057.05
5	'stim'	'stim'	23903.25
6	'stim'	'state', 'stim'	22112.33
7	'state', 'stim'	'state'	21712.48
8	**'state', 'stim'**	**'stim'**	**21698.74**

Left-handers:

Model#	Drift-rate(v)	Bias-point(z)	DIC score
1	'state'	'state'	15312.62
2	'state'	'stim'	15282.13
3	'state'	'state', 'stim'	15004.32
4	'stim'	'state'	18059.01
5	'stim'	'stim'	17778.83
6	'stim'	'state', 'stim'	15120.32

7	'state', 'stim'	'state'	14425.01
8	'state', 'stim'	'stim'	14303.69

Decoding

Next we employed multivariate pattern analysis (MVPA) techniques to probe the divergent patterns in the EEG data across various conditions. Decoding is considered to be a form of backward model where the goal is to extract latent factors (hidden variables) from the observed data (EEG) (Haufe et al., 2014). Thus, decoding is the method of analysing patterns of brain activity in order to predict the experimental condition (or stimuli) responsible for generating that pattern. This is in contrast to encoding which is a form of forward model wherein arbitrary values of experimental variables (or conditions) can be used to predict patterns of brain activity (Fahrenfort et al., 2018). Conventional ERP (Event related potentials) analysis rely on using a-priori identified spatial locations or temporal segments in the data to measure the differences across conditions. However decoding techniques do not rely on a-priori definitions and perform much better in detecting differences across experimental conditions (Fahrenfort et al., 2018).

Temporal decoding:

Temporal decoding involves using EEG data (X) composed of size: [Electrodes x Time points x Trials] to predict the experimental condition (Y) . The experimental condition for e.g. could be the stimuli presented (for e.g. left or right stimuli). The first step in the decoding analysis consists of fitting an estimator (w) to a subset of the data (X) called X_{train} to predict a subset of the experimental condition (Y) called Y_{train}. The second step involves using this trained estimator on another subset of the data (X) called X_{test} to predict subset of the experimental condition (Y) called Y_{test}. The third step involves evaluating the performance of this estimator using a measure (e.g. accuracy) by comparing the prediction $\hat{Y}_{test}$ with the actual label Y_{test}.

Estimator construction:

Before fitting the estimator (w) to the data (X), it needs to be standardised. Firstly, the EEG data is subjected to a standard scaler (using *StandardScaler()* from scikit-learn) that removes the mean of the data and scales it by its variance. This procedure is useful for normalising data, which is a standard requirement for many machine-learning estimators. Secondly, we used the logistic regression to estimate the model parameters for finding the hyperplane that can maximally separate categories in the experimental condition (Y). Thirdly, we implemented the temporal decoding by using the sliding estimator (*SlidingEstimator()* from scikit-learn) to fit the logistic regression model per time-point.

Cross-validation:

Next, the EEG data was down sampled to 100 Hz. Further to which we defined the categories to classify (classes in Y). For example, we can classify the stimuli that were presented ('left' or 'right') when the participant was 'alert' (to further refine this, we can only

choose trials where the participant made the correct decision). In this case, the binary classification was performed between these two conditions ('left' and 'right'). Additionally, the classification was only run if the participant had at least 25 trials under each condition. This ensured that only participants that had a sufficient number of trials were used for classification. Further n-fold cross validation was performed such that $(n-1)/n^{th}$ of the trials were used as training set and $1/n^{th}$ of the trials were used as testing set. Usually the number of folds 'n' was set to 5 unless mentioned otherwise.

Validation measure:

Next, the classifier performance was evaluated using the Area Under the Curve (AUC) of the receiver-operating characteristic (ROC). It is implemented using *'roc_auc'* in the sliding estimator function in scikit-learn. The ROC curve is obtained by plotting the true-positive rate against the false-positive rate. The AUC of this curve represents the degree of separability of the various classes. When AUC is about 0.5 the classifier performs at chance, while the AUC score of 1 has a very good separability across classes. In our case, we computed the AUC-ROC score per participant as the average of the score across all the cross-validation folds.

Group statistics:

Next, we performed a cluster permutation test on the AUC score of each participant (dimensions of Participants x Time points) using MNE (*spatio_temporal_cluster_1samp_test*) (Gramfort et al., 2013). This produces p-values per time point at the group level, from which we can identify the time points where the AUC score is significantly different from chance (0.5) at the group level.

Coefficients of patterns:

Next, we need to identify the patterns in the data that is being used by the estimator to produce reliable classifier performance. The parameters of the decoding model are not neurophysiologically interpretable in a straightforward way (Haufe et al., 2014). Hence it is necessary to produce a transformation that changes the backward model parameters into forward model. This is done by obtaining the coefficients of the estimator model per participant using *'get_coef'* function from MNE(*'_patterns'*). Further, the coefficients are averaged at the group level to obtain the EEG patterns in the data that help discriminate between conditions.

Source reconstruction of patterns:

Finally, the coefficients (patterns) created from the estimator model are projected in the source space as follows. Source reconstruction was done primarily using Freesurfer (Fischl, 2012) and MNE (Gramfort et al., 2013). Firstly, we used the default ICBM152 template for the structural magnetic resonance image (MRIs). We reconstructed the surface using 'recon-all' from Freesurfer. We then created the Boundary element model (BEM) using *'make_watershed_bem'* from MNE. Next, we created scalp surfaces for the different element boundaries using *'make_scalp_surface'* from MNE. Secondly, we performed the registration of the scalp surface (generated in the previous step) with the default EEG channel locations manually using *'coregistration'* from MNE with the help of fiducials. Thirdly, forward solution was computed using *'make_bem_model'* from MNE with conductivity = [0.3, 0.006, 0.3]. In

order to test if the source reconstruction of the sensor data is accurate we projected the ERP data of a sample participant into source space and analysed data from different regions of interest to confirm its validity (See Supplementary information).

The classifier patterns (coefficients created above) of each participant (32) were used for projecting into source space. Fourthly, we computed the noise covariance using the baseline data from -0.2 to 0 ms. Fifthly, we used the forward solution (8196 vertices) and the noise covariance to create inverse operator using '*minimum_norm.make_inverse_operator*' from MNE (loose=0.2). Sixthly, we used the individual classifier pattern per subject and applied the inverse operator on it (method = dSPM, SNR = 5, lambda2 = 0.08) to produce the source reconstruction of the classifier patterns per subject. Seventhly, we average the source-reconstructed patterns per subject to produce the average pattern in the source space.

Regression of Drift diffusion parameters with Neural Dynamics

Next we used the model parameters generated by the drift diffusion model and regressed the same with the ERP data, which was z-scored to obtain the regression coefficient. This was performed in the following steps. First, the ERP data (post trial epochs) were z-scored per electrode per trial. Second, the ERP data was baseline corrected with pre-trial data from -200ms to 0ms. Third, the ERP data was averaged every 50ms per electrode per trial to create 20 time points (-200ms to 800ms) per electrode per trial. Fourth, the ERP data was entered into regression with trial by trial estimate of the drift rate using the model HDDMRegressor from the HDDM toolbox (Wiecki et al., 2013). The Stimulus-coding model ('left' or 'right' responses) was used as earlier and the drift rate was allowed to vary per trial based on the ERP data per state ('alert' or 'drowsy') per stimuli ('left' or 'right'). Fifth, the traces were computed per condition (state and stimuli combination). Sixth, the differences in drift rate (between 'left' and 'right' stimuli) per time point per electrode were computed in both 'alert' and 'drowsy' condition.

Author contributions:

Conceptualization: SRJ, TAB.
Data Curation: SRJ.
Formal Analysis: SRJ.
Investigation: SRJ, CAB.
Funding Acquisition: TAB.
Methodology: SRJ.
Project Administration: SRJ.
Resources: SRJ, CAB, TAB.
Software: SRJ.
Supervision: TAB.
Validation: SRJ.
Visualization: SRJ.
Writing – original draft: SRJ.
Writing – review & editing: SRJ, CAB, TAB.

Acknowledgements:

SUPPLEMENTAL INFORMATION:

Verification of source reconstruction:

In order to verify the source localization procedure, we performed the following steps. First, We used the EEG data from a sample participant and computed the noise covariance from -0.2sec to 0sec using the 'shrunk' method. Further the covariance was regularized. Second, the forward solution was computed using the transformation file, source space, beamformer solution computed earlier. Third, the inverse operator was computed by using the noise covariance and the forward solution. Fourth, the inverse operator was applied on the data from the sample participant (snr = 3, lambda2 = 1.0 / snr ^{2}, method = 'MNE'). The MNE method was used instead of the dSPM used earlier as we wanted to have positive and negative amplitude for the source signals and only normal orientations were picked further. Fifth, we used the labels from the left hemisphere in the regions of auditory, occipital, middle temporal and frontal pole regions to extract signals from these ROIs using the mode of 'mean_flip'. Sixth, we compute the mean across these ROIs to extract a single time course per ROIs in the left hemisphere which is plotted in Figure s1. It is evident from the figure that N100 amplitude is highly localized in the auditory regions compared to other regions which serves to validate the source localization used.
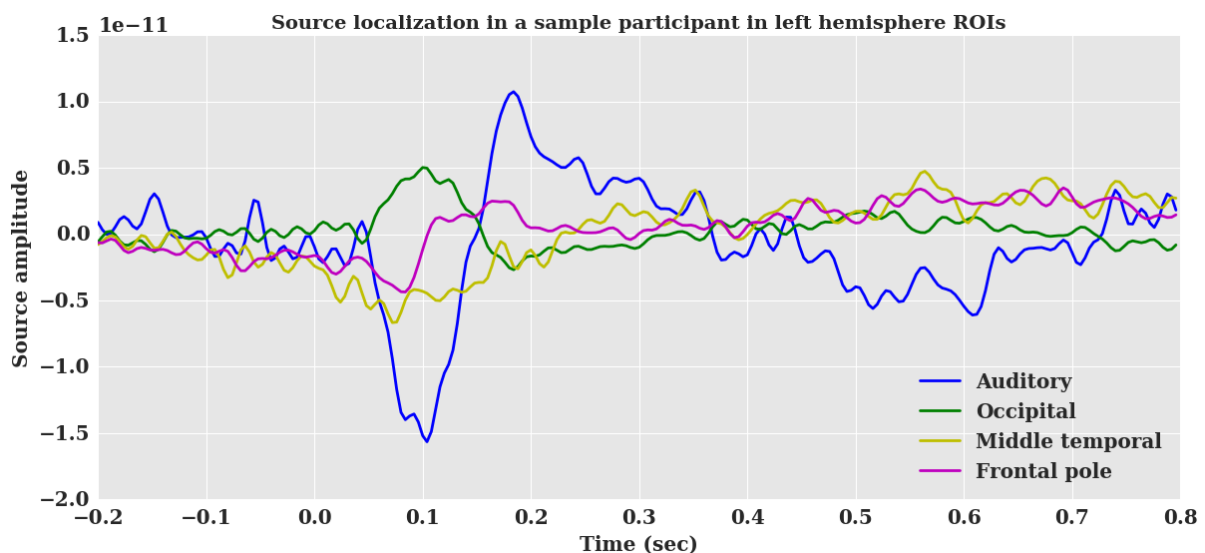
Figure s1: Source localization performed in a sample participant in specific left hemisphere ROIs. N100 amplitude is clearly visible in the auditory regions, whereas it is diminished in the other regions clearly indicating the validity of the source localization procedure.

REFERENCES:

Bareham, C.A., Manly, T., Pustovaya, O. V., Scott, S.K., and Bekinschtein, T.A. (2014). Losing the left side of the world: Rightward shift in human spatial attention with sleep onset. Sci. Rep. *4*, 1–5.

Bareham, C.A., Bekinschtein, T.A., Scott, S.K., and Manly, T. (2015). Does left-handedness confer resistance to spatial bias? Sci. Rep. *5*, 9162.

Bates, D., Maechler, M., Bolker, B., and Walker, S. (2015a). lme4: Linear mixed-effects models using Eigen and S4.

Bates, D., Maechler, M., Bolker, B.M., and Walker, S. (2015b). Fitting Linear Mixed-Effects Models using lme4.

Becker, E., and Karnath, H.O. (2007). Incidence of visual extinction after left versus right hemisphere stroke. Stroke *38*, 3172–3174.

Benwell, C.S.Y., Thut, G., Learmonth, G., and Harvey, M. (2013). Spatial attention: Differential shifts in pseudoneglect direction with time-on-task and initial bias support the idea of observer subtypes. Neuropsychologia *51*, 2747–2756.

Benwell, C.S.Y., Harvey, M., and Thut, G. (2014). On the neural origin of pseudoneglect: EEG-correlates of shifts in line bisection performance with manipulation of line length. Neuroimage *86*, 370–380.

Bowen, A., McKenna, K., and Tallis, R.C. (1999). Reasons for variability in the reported rate of occurrence of unilateral spatial neglect after stroke. Stroke *30*, 1196–1202.

Bowers, D., and Heilman, K.M. (1980). Pseudoneglect: effects of hemispace on a tactile line bisection task. Neuropsychologia *18*, 491–498.

Corbetta, M., and Shulman, G.L. (2011). Spatial neglect and attention networks.

Delorme, A., and Makeig, S. (2004). EEGLAB: an open source toolbox for analysis of single-trial EEG dynamics including independent component analysis. J. Neurosci. Methods *134*, 9–21.

Dietz, M.J., Friston, K.J., Mattingley, J.B., Roepstorff, A., and Garrido, M.I. (2014). Effective Connectivity Reveals Right-Hemisphere Dominance in Audiospatial Perception : Implications for Models of Spatial Neglect. *34*, 5003–5011.

Fahrenfort, J.J., van Driel, J., van Gaal, S., and Olivers, C.N.L. (2018). From ERPs to MVPA using the Amsterdam Decoding and Modeling toolbox (ADAM). Front. Neurosci. *12*.

Fink, G.R., Marshall, J.C., Weiss, P.H., and Zilles, K. (2001). The neural basis of vertical and horizontal line bisection judgments: an fMRI study of normal volunteers. Neuroimage *14*, 59–67.

Fischl, B. (2012). FreeSurfer. Neuroimage *62*, 774–781.

Fox, J., and Weisberg, S. (2011). An R Companion to Applied Regression (Thousand Oaks {CA}: Sage).

de Gee, J.W., Colizoli, O., Kloosterman, N.A., Knapen, T., Nieuwenhuis, S., and Donner, T.H. (2017). Dynamic modulation of decision biases by brainstem arousal systems. Elife *6*, 1–36.

Gelman, A.J.C.H.S.D.D.A.V.D.R. (2013). Bayesian Data Analysis, Third Edition (Chapman & Hall/CRC Texts in Statistical Science): Chapman Hall/CRC; 3 Ed.

Gramfort, A., Luessi, M., Larson, E., Engemann, D., Strohmeier, D., Brodbeck, C., Goj, R., Jas, M., Brooks, T., Parkkonen, L., et al. (2013). MEG and EEG data analysis with MNE-Python. Front. Neurosci. *7*, 267.

Harvey, M., Pool, T.D., Roberson, M.J., and Olk, B. (2000). Effects of visible and invisible cueing procedures on perceptual judgments in young and elderly subjects. Neuropsychologia *38*, 22–31.

Haufe, S., Meinecke, F., Görgen, K., Dähne, S., Haynes, J.D., Blankertz, B., and Bießmann, F. (2014). On the interpretation of weight vectors of linear models in multivariate neuroimaging. Neuroimage *87*, 96–110.

Hauk, O., and Pulvermuller, F. (2011). The Lateralization of Motor Cortex Activation to Action-Words. Front. Hum. Neurosci. *5*, 149.

Hécaen, H., Agostini, M. De, and Monzon-Montes, A. (1981). Cerebral organization in left-handers. Brain Lang. *12*, 261–284.

Heilman, K.M., and Van Den Abell, T. (1980). Right hemisphere dominance for attention: the mechanism underlying hemispheric asymmetries of inattention (neglect). Neurology *30*, 327–330.

Heilman, K.M., Bowers, D., Coslett, H.B., Whelan, H., and Watson, R.T. (1985). Directional hypokinesia: prolonged reaction times for leftward movements in patients with right hemisphere lesions and neglect. Neurology *35*, 855–859.

Jackson, C. V, Ettlinger, G., and Zangwill, O.L. (1956). Cerebral dominance in Sinistrals. Brain *79*, 569–588.

Jagannathan, S.R., Ezquerro-Nassar, A., Jachs, B., Pustovaya, O. V., Bareham, C.A., and Bekinschtein, T.A. (2018). Tracking wakefulness as it fades: Micro-measures of alertness. Neuroimage *176*, 138–151.

Jewell, G., and McCourt, M.E. (2000). Pseudoneglect: a review and meta-analysis of performance factors in line bisection tasks. Neuropsychologia *38*, 93–110.

Johns, M.W. (1991). A New Method for Measuring Daytime Sleepiness: The Epworth Sleepiness Scale. Sleep *14*, 540–545.

Karnath, H.-O., and Fetter, M. (1995). Ocular space exploration in the dark and its relation to subjective and objective body orientation in neglect patients with parietal lesions. Neuropsychologia *33*, 371–377.

Kinsbourne, M. (1977). Hemi-neglect and hemisphere rivalry. Adv Neurol *18*, 41–49.

Knoblauch, K. (2014). psyphy: Functions for analyzing psychophysical data in R.

Kruschke, J.K. (2013). Bayesian estimation supersedes the t test. J. Exp. Psychol. Gen. *142*, 573–603.

Mesulam, M.M. (1981). A cortical network for directed attention and unilateral neglect. Ann. Neurol. *10*, 309–325.

Mesulam, M.M. (1999). Spatial attention and neglect: parietal, frontal and cingulate contributions to the mental representation and attentional targeting of salient extrapersonal events. Philos. Trans. R. Soc. Lond., B, Biol. Sci. *354*, 1325–1346.

Mort, D.J., Malhotra, P., Mannan, S.K., Rorden, C., Pambakian, A., Kennard, C., and Husain, M. (2003). The anatomy of visual neglect. Brain *126*, 1986–1997.

Nunez, M.D., Vandekerckhove, J., and Srinivasan, R. (2017). How attention influences perceptual decision making: Single-trial EEG correlates of drift-diffusion model parameters.

J Math Psychol *76*, 117–130.

Oldfield, R.C. (1971). The assessment and analysis of handedness: The Edinburgh inventory. Neuropsychologia *9*, 97–113.

Quadfasel, F.A., and Goodglass, H. (1954). Language laterality in left-handed aphasiscs. Brain *77*, 521–548.

Ratcliff, R., Smith, P.L., Brown, S.D., and McKoon, G. (2016). Diffusion Decision Model: Current Issues and History. Trends Cogn. Sci. *20*, 260–281.

Ringman, J.M., Saver, J.L., Woolson, R.F., Clarke, W.R., and Adams, H.P. (2004). Frequency, risk factors, anatomy, and course of unilateral neglect in an acute stroke cohort. Neurology *63*, 468–474.

Schenkenberg, T., Bradford, D.C., and Ajax, E.T. (1980). Line bisection and unilateral visual neglect in patients with neurologic impairment. Neurology *30*, 509–517.

Shulman, G.L., Pope, D.L., Astafiev, S. V, McAvoy, M.P., Snyder, A.Z., and Corbetta, M. (2010). Right hemisphere dominance during spatial selective attention and target detection occurs outside the dorsal frontoparietal network. J Neurosci *30*, 3640–3651.

Siman-Tov, T., Mendelsohn, A., Schonberg, T., Avidan, G., Podlipsky, I., Pessoa, L., Gadoth, N., Ungerleider, L.G., and Hendler, T. (2007). Bihemispheric leftward bias in a visuospatial attention-related network. J. Neurosci. *27*, 11271–11278.

Spiegelhalter, D.J., Best, N.G., Carlin, B.P., and Van Der Linde, A. (2002). Bayesian measures of model complexity and fit. J. R. Stat. Soc. Ser. B (Statistical Methodol. *64*, 583–639.

Sprague, J.M. (1966). Interaction of cortex and superior colliculus in mediation of visually guided behavior in the cat. Science (80-.). *153*, 1544–1547.

Sturm, W., de Simone, A., Krause, B.J., Specht, K., Hesselmann, V., Radermacher, I., Herzog, H., Tellmann, L., Muller-Gartner, H.W., and Willmes, K. (1999). Functional anatomy of intrinsic alertness: evidence for a fronto-parietal-thalamic-brainstem network in the right hemisphere. Neuropsychologia *37*, 797–805.

Szczepanski, S.M., and Kastner, S. (2013). Shifting attentional priorities: control of spatial attention through hemispheric competition. J. Neurosci. *33*, 5411–5421.

Szczepanski, S.M., Konen, C.S., and Kastner, S. (2010). Mechanisms of Spatial Attention Control in Frontal and Parietal Cortex. J. Neurosci. *30*, 148–160.

Thiebaut de Schotten, M., Urbanski, M., Duffau, H., Volle, E., Lévy, R., Dubois, B., and Bartolomeo, P. (2005). Direct evidence for a parietal-frontal pathway subserving spatial awareness in humans. Science *309*, 2226–2228.

Vallar, G. (1998). Spatial hemineglect in humans. Trends Cogn. Sci. (Regul. Ed.) *2*, 87–97.

Wiecki, T. V, Sofer, I., Frank, M.J., and Hanke, M. (2013). HDDM: Hierarchical Bayesian estimation of the Drift-Diffusion Model in Python.

Willems, R., Toni, I., Hagoort, P., and Casasanto, D. (2009). Body-specific motor imagery of hand actions: neural evidence from right- and left-handers. Front. Hum. Neurosci. *3*, 39.

Willems, R.M., Hagoort, P., and Casasanto, D. (2010). Body-Specific Representations of Action Verbs: Neural Evidence From Right- and Left-Handers. Psychol. Sci. *21*, 67–74.

Willems, R.M., Der Haegen, L. Van, Fisher, S.E., and Francks, C. (2014). On the other hand: Including left-handers in cognitive neuroscience and neurogenetics. Nat. Rev. Neurosci. *15*, 193–201.

Zhang, J., Rittman, T., Nombela, C., Fois, A., Coyle-Gilchrist, I., Barker, R.A., Hughes, L.E., and Rowe, J.B. (2016). Different decision deficits impair response inhibition in progressive supranuclear palsy and Parkinson's disease. Brain *139*, 161–173.

6

Transitions in a Model system
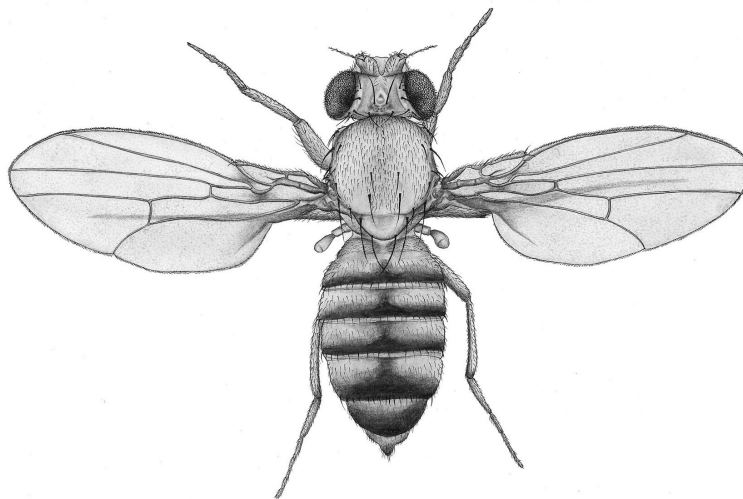
Figure 6.1: Drosophila Melanogaster[1]

6.1 Brief introduction

In this chapter, I investigate the alertness transitions in the fruit fly (*Drosophila melanogaster*). Specifically, I explore the neural and behavioural dynamics in spontaneous sleep using local field potentials (LFP) recorded from the fly brain. For this

purpose, I first introduce the experimental set ups for recording two-channel differential and multi channel local field potentials. Next, I provide a data driven approach of identifying changes in spectral patterns in the LFP (two-channel differential) data using support vector machines. Thereby establishing the ability of the LFP to differentiate across awake and sleep conditions in a systematic manner. Further, I probe the period of transition to sleep to understand its dynamics. Next, to identify the spatial locations in the brain that track alertness fluctuations, I collect LFP recordings from multi channel probes inserted half way into the fly brain. Further, I identify regions in the fly brain that differ across awake and sleep periods using changes in the power spectrum. Finally, I show evidence from induced sleep (thermogenetic manipulation of dorsal fan shaped body dFSB) to provide converging evidence for the spatial regions identified in the previous step.

6.2 Shortcomings

As mentioned in the introduction chapter, a fly is considered to be asleep if it does not move for more than 5 minutes. In this context, recent studies (van Alphen, Yap, et al. 2013; Yap, Grabowska, et al. 2017) have shown using LFP recorded from the fly brain, that flies possibly sleep in different stages associated with distinct electrophysiological patterns and different arousal thresholds.

Though these studies were pioneering in many ways, they however ignored interesting aspects in the dynamics of transition to sleep. First, the transition to sleep (period from 0 minute to 5th minute) was not investigated. The transitory period is one of the prime focus of this dissertation. Second, the sleep in flies (Yap, Grabowska, et al. 2017) was categorized based on the time of sleep induction (day or night). However it is well known that the depth of the sleep (sleep duration) modulates arousal threshold (Huber, Hill, et al. 2004) and hence it would be interesting to dissect the changes in frequency patterns across sleep of different depths. Third, the changes in frequency spectrum across awake and sleep periods were not characterised to identify important elements in the spectrum that can generalize the findings to a new fly (this could be done by building classifiers

based on frequency spectrum to identify 'awake' and 'sleep' periods). Fourth, the data (two channel differential LFP) from flies falling asleep in a spontaneous manner, is not able to provide spatial information on how distinct regions in the brain differ across 'awake' and 'sleep' periods.

6.3 Research Question

This sets us up for the fourth research question to understand the process of transition to spontaneous sleep in fruit flies.

(a) *Can we build a data driven approach based on elements of the frequency spectrum (as done in micro-measures algorithm) to differentiate between 'awake' and 'sleep' patterns. For example this could be a classifier (with features like frequency spectrum) based on SVM. Could such a classifier generalise to new data and identify 'awake' and 'sleep' periods independent of movement data?*

(b) *What happens to the frequency spectrum elements (or classifier patterns) when the fly is transitioning into sleep (period from 0 to 5 minutes)?*

(c) *How do the classifier patterns depend on the sleep depth, does longer sleep duration (deep sleep) differ from smaller sleep duration (light sleep)?*

(d) *What regions of the fly brain change (and in what frequency bands) across awake and sleep periods?. This could be uncovered using multichannel recordings as in (Paulk, Zhou, et al. 2013).*

(e) *How does the spontaneous sleep measured with multichannel recordings differ from artificially inducing sleep. For example thermogenetically activating the dFSB as in (Yap, Grabowska, et al. 2017)?*

6.4 Methods

6.4.1 Experimental Set-up

In the next section, I briefly describe the experimental set-up and description of flies that I have used for studying spontaneous sleep and its corresponding transition at the individual level (fly on tethered ball as described in Introduction). I also provide a brief overview of the preparation needed to set up the fly on the tethered ball.

6.4.1.1 Animals

Female flies (*Drosophila melanogaster*) used for this study were reared in an incubator maintained under a 12-hour light and 12-hour dark cycle while being fed on a standard yeast-based medium. The temperature in the incubator was maintained at 22-24°C and humidity at 40-60% to mimic the daily variation in the experimental rig. Wild-type Canton-S (CS) flies which were at most 7 days post-eclosion of the were used for the recordings.

6.4.1.2 Preparation

The preparation of the flies in the tethered ball set-up consists of the following steps (van Alphen, Yap, et al. 2013; Paulk, Zhou, et al. 2013). First, flies were anesthetized using a thermoelectric-cooled block (1-2 °C). Second, the dorsal surface of the thorax of the fly was attached to a tungsten rod using dental cement (Coltene Whaledent Synergy D6 Flow A3.5/ B3). The cement was then cured by exposing it to high intensity blue light (Radii Plus, Henry Scheinn Dental). Finally, the head of the fly was also attached to the thorax and cured with blue light as before. This is mainly to make sure that the head of the fly does not get dislodged during electrode insertion (as the neck of the fly is fragile)

6.4.1.3 Two channel differential LFP

Author Contributions

This dataset was acquired as a part of the study (Yap, Grabowska, et al. 2017) by Melvyn H.W. Yap. I analysed the data with advice from Bruno van Swinderen and developed classifiers based on LFP patterns which was presented in (Jagannathan, Jeans, et al. 2018).

Electrode holder preparation

The electrode holders used for measuring LFPs in this set-up consisted of pulled borosilicate micro-pipettes. The micro-pipettes were first cut out leaving only the tip (about 6mm in length with $\sim 3M\Omega$ resistance), which was further filled with extracellular fluid (ECF) containing electrolytes like Sodium chloride, glucose, sucrose etc. Then, the cut micro-pipettes were inserted into each brain hemisphere to a depth of about $100\mu m$ through the dorsal eye rim using a mechanical micro manipulator. Finally, the implanted micro-pipettes were secured using dental cement.

Electrode insertion

Fine tungsten wires (which were used as electrodes) were then inserted into each micro-pipette and then sealed with electrical insulators. The prepared files were then carefully placed on the air-supported ball as shown in Figure 6.2.

Local field potential recordings

Local field potentials (LFPs) were recorded after 1-2 hour post the electrode insertion procedure. Field-effect transistors (FETs) (NB Labs, Denison, TX) were used for recording the electrical potentials. LFP signal was recorded as a differential of the voltage from the two glass electrodes at a sampling rate of 291 Hz and amplified with a differential amplifier (gain = 10,000) to increase the signal to noise ratio. The entire electrophysiology rig was placed in a light-shielded enclosure that mimicked the 12-h light and 12-h dark cycle as in the incubator.

Behavioural recordings

Infra-red LEDs were used for illumination (as this would not disturb the natural circadian rhythm of the fly unlike visible light). The behaviour of the fly on the ball was recorded using an infra-red enabled web camera with a frame rate of 3 frames per second. The video recorded by this set-up was essentially composed of monochromatic low-resolution images (27x34 pixels), thus well suited for long recordings.

Further details of this set-up and step by step instructions are available at (Yap, Grabowska, et al. 2017).
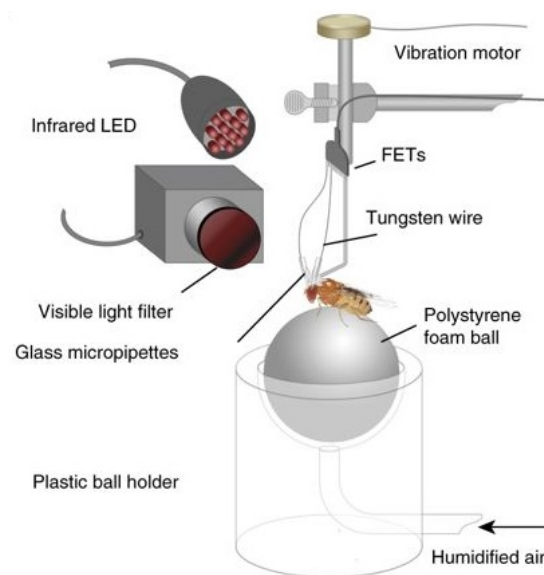
Figure 6.2: Two channel differential recording [2]. Here LFPs were recorded in-vivo for 24 hours. The locomotion activity of the fly was recorded with a web camera under infra red lighting conditions. The entire set-up was housed in a shielded box with 12-hour light and 12-hour dark cycle.

6.4.1.4 Multi channel

This dataset was acquired by Rhiannon Jeans and me as part of the study (Jagannathan, Jeans, et al. In prep). The data for 8 flies was acquired by Rhiannon Jeans, while I designed the calibration procedure, developed tools for collecting hourly LFP, video data (for about 12 hours per fly) and collected data from 2 flies. Data analysis was primarily performed by

---

[2]adapted from (Yap, Grabowska, et al. 2017)

me with code for LFP data extraction provided by Rhiannon Jeans. The entire study was designed by me and Rhiannon Jeans along with Bruno van Swinderen.

Electrode insertion

To record from multiple locations in the fly brain, we used a 16-channel electrode array. This was composed of a linear silicon probe (model no. A1 x 16-3 mm50-177) made by NeuroNexus Technologies.

The prepared flies (see section 6.4.2) were first inserted with a sharpened, fine tungsten wire (0.25mm; A-M systems) superficially in the thorax. This tungsten wire served as the reference electrode in the recording. The flies were then carefully placed on the air-supported ball. The electrodes were then inserted laterally into the eyes, perpendicular to the eye's curvature using a micro manipulator (Merzhauser, Wetzlar, Germany) as shown in Figure 6.3. The location of the inserted electrodes was then verified with a calibration procedure (see below) to make sure that each fly had the electrodes inserted in approximately the same location. The electrodes were only inserted in one hemisphere of the fly brain and hence this recording is also referred to as half-brain probe.
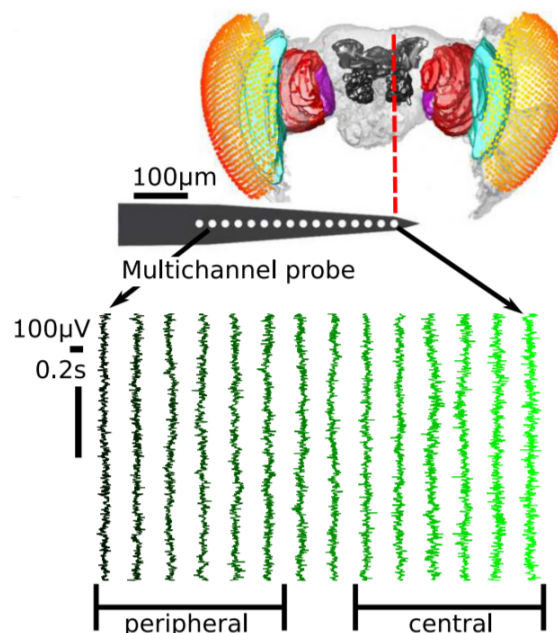
Figure 6.3: Multi channel LFP recording [3]. The electrode contacts (not to scale) are represented by white dots.

[3]adapted from (Cohen, Zalucki, et al. 2016)

An example fly with the reference electrode along with the tethering rod and reference electrode is shown in Figure 6.4.

Figure 6.4: Example fly in the multichannel set-up. The dark spot visible in the eye of the fly was the location in which the electrode was inserted. The reference electrode can be seen here inserted in the thorax of the fly.

Local field potential recordings

Electrophysiological recordings were made using equipment from Tucker-Davis Technologies. The data was acquired at a sampling rate of 25 kHz using a RZ5 Bioamp processor and RP2.1 enhanced real-time processor.

Calibration procedure

Before explaining the calibration procedure, it would be prudent to understand the motivation behind this procedure. The previous recordings made using multichannel probes (Paulk, Zhou, et al. 2013) inserted electrodes in an arbitrary manner especially in the dorsal-ventral axis. Those studies relied on evoked potentials (with higher signal to noise ratio) based on visual stimuli, and hence any deviation in electrode locations can be tolerated. However as we aim to measure spontaneous activity for the first time with multi channel set up, we need to have consistency in the location of electrode insertion. This would ensure lower variances among flies and hence a robust group analysis can then be performed. To achieve this objective, we designed a calibration procedure in the

following steps. First, we inserted the electrode step by step (in steps of 2 electrodes) using the micro manipulator. Second, we use flickering blue lights (spectral peak at 470 nm with 30 mn half-peak width, square wave with 50% duty cycle) to trigger a steady state visual evoked potential (SSVEP). Third, the SSVEP is monitored at each channel as the electrode is inserted in steps. Fourth, in some channels the SSVEP is positive while in some other the SSVEP is negative in the leading edge of the square wave as shown in Figure 6.5. The exact location of this reversal of polarity depends on the angle, insertion depth of the electrodes. Fifth, we stop the electrode insertion when the reversal of polarity happens between channels 10-13. This makes sure that the insertion depth and insertion angle are consistent across flies, as any change in one of them would cause no polarity reversal in the SSVEPs. The calibration procedure for an example fly is shown in Figure 6.5.
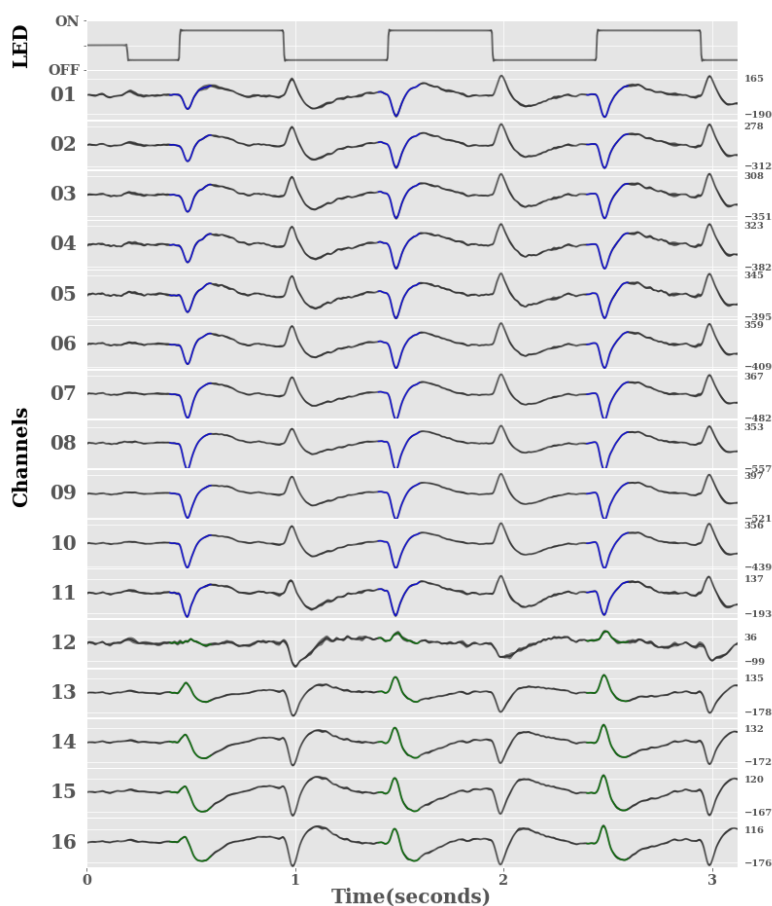
Figure 6.5: .Calibration procedure for multichannel recordings.The SSVEP values are displayed in μV, it can be seen here that the polarity reversal happens in the 12th electrode.

Behavioural recordings

The movement of the fly on the ball was recorded with DCM130 microscope CMOS camera at 30 frames/s and Infra-red LEDs were used for illumination (as before). The video recorded by this set-up composed of high-resolution colour images (640x480 pixels) recorded 30 times a second. Example screen shot of the video capture with this set up is shown in Figure 6.6
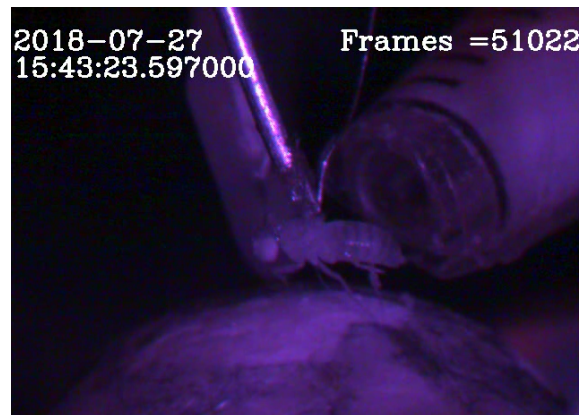
Figure 6.6: Screen grab of video recorded in multichannel recording. Apart from the video, we also captured time stamps and frame numbers of video in separate files for further analysis.

6.5 Results

6.5.1 Behavioural & Neural dynamics

6.5.1.1 Two channel differential LFP

Selection of flies

10 flies survived the 24-hour period and hence only data from those flies was considered for further analysis in the two channel differential recordings.

Movement analysis

The main goal of the behavioural analysis is to define periods of 'sleep' and 'awake' based on the immobility periods. As mentioned before more than 5 minutes of immobility is considered as sleep. To achieve this goal, index of movement needs to be

computed from the video recordings. For this, we used the pixel subtraction technique to quantify the movement across frames (van Alphen, Yap, et al. 2013). Here the change in pixel value between subsequent frames was quantified by subtracting the adjacent frames in a video to create a difference image (Δ pixels) across time (Figure 6.7). The change in pixels is then summed to create a movement value. The fly is said to have moved only if this movement value exceeds a certain threshold (which was determined manually for each recording based on noise levels in the image).

Figure 6.7: Pixel subtraction for movement detection [4]. The difference of images between consecutive frames provides a proxy for movement.

Using the pixel subtraction technique we can identify time segments with more than 5 minutes or more of inactivity (sleep is counted as starting from the +5th minute onwards). Thus the period from +5th minute to the start of locomotion activity again is considered as 'sleep', while the period from 0 to +5 minutes is considered as 'transition' and every other period is considered as 'awake'.

Local field potential analysis

The main goal of this LFP analysis is to understand how the changes in behaviour ('awake', 'sleep' as computed above) is reflected in the power spectrum. First, we computed the morlet wavelet transformation on the LFP data using the function 'ft_specest_wavelet' from the Fieldtrip toolbox (Oostenveld, Fries, et al. 2011). We set the width of the wavelet at 30 and the standard deviations as 3 (gwidth). Second, we computed the absolute value of the wavelets computed in the previous step. Third, we time-matched the LFP data to the behaviour data (which consists of periods in time reflecting immobility). Fourth, we computed the 'awake', 'sleep' periods from the immobility periods and plotted the power spectrum for the entire period. Figure 6.8 shows an example data from a fly

---

[4]adapted from (van Alphen, Yap, et al. 2013)

recorded with two channel differential set up for a period of 24 hours. The red dots in the figure indicate periods of time where the fly was immobile for more than 5 minutes and hence considered as sleep. From the figure it is clear that power in the low frequency bands (<10 Hz) changes when the fly falls asleep. This led us to ask if we can design a automated method to track the changes in the power spectrum and thereby track the changes in the alertness levels from the LFP data.
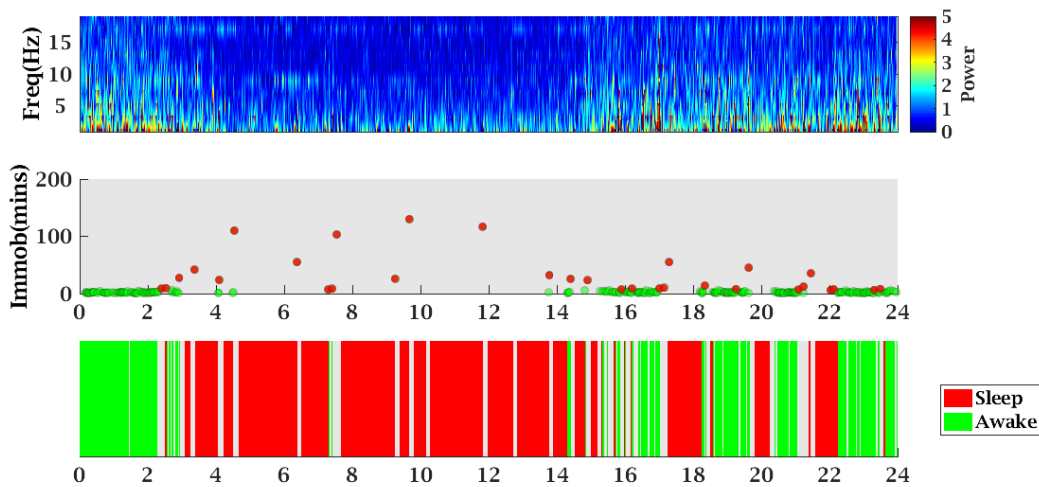
Figure 6.8: Two channel differential LFP recordings. The red dots indicate periods of time where the fly was immobile for more than 5 minutes, the green dots represent other periods of immobility (less than 5 minutes). The activity in the frequency bands (<10 Hz) are clearly modulated depending on whether the fly was 'awake' or 'sleep'.

6.5.1.2 Tracking wakefulness with machine learning

From the previous section it is clear that information in the frequency spectrum of the LFP is potentially sufficient to categorize the data into 'awake' or 'sleep'. Hence we need an objective method to track the alertness levels based on the frequency spectrum of LFP data. This problem is conceptually similar to the one encountered in Chapter 2, wherein I developed the micro-measures algorithm to track trial-by-trial alertness levels with EEG data. Hence I decided to follow a similar approach to design a classifier based on a class of supervised learning algorithms called Support Vector Machines (SVM).

Support Vector Machine

Before we decide to use SVMs to build our classifier a brief overview on the concept of the SVMs would be useful (for detailed overview refer to Chapter 2). The main aim of the SVMs is to build a hyperplane or set of hyperplanes capable of separating two classes (in our case 'awake', 'sleep') based on features in the data (in our case LFP frequency spectrum). The SVMs aim to maximise the distance of separation between the closest data point (in training set) of any class (which is referred to as the functional margin). The idea behind this is that once the optimal choice of such a functional margin is found it would also produce lower generalization error (in the testing set). The main reason to map the data onto higher dimension is driven by the fact that at lower dimensions most classes are inseparable. Such a mapping onto higher dimensional space is achieved by using a kernel function $k(x, y)$. As in the micro-measures method we choose the radial basis function (RBF) as our kernel function.

Gold standard labels

First, we define the gold standard labels (or ground truth labels) that the classifier can learn and be tested on. For this purpose we use the behavioural classification based on video data (see previous section on movement analysis using pixel subtraction technique) to classify segments of data into 'awake' or 'sleep'. Thus the main goal of the classifier is to perform binary classification of the LFP data into 'awake' or 'sleep'. Second, we segmented the LFP data based on these ground truth labels. The segmented data were then binned into 1 minute segments and further down sampled to 250 Hz. The length of the LFP data into 1 minute segments was based on changes observable in power spectrum based on 1 minute bins in previous studies (van Alphen, Yap, et al. 2013; Yap, Grabowska, et al. 2017). Third, we computed the continuous wavelet transform based on the morlet wavelet from the 'cwt' function in MATLAB. We further extract the wavelet coefficients only from frequencies 1 to 40 Hz. Fourth, we then normalized the wavelet amplitude by its power and compute the mean of the coefficients across the entire 1 minute period. This results in 131 coefficients per 1 minute bin which will be used as features for the SVM.

Parameter selection

The process of training the SVM could be considered as the process of identifying

the optimal value of the hyper-parameters (γ, C). Here γ controls the curvature of the hyperplane and C represents the penalty parameter for the soft-margin. Parameter selection for the SVM was achieved by performing a grid search in (γ, C) in the space $(2^{-1}, 2^5)$ and $(2^{-1}, 2^{25})$ respectively.

Parameter optimization

Next, we will use the features computed per 1 minute bin and feed it into the SVM for classifying the data segments (similar procedures to micro-measures algorithm in Chapter 2). For this purpose we perform the following steps. First, the data from all flies was collated and divided into 5 disjoint subsamples, chosen randomly but with equal size. This process was achieved using the 'cvpartition' function in MATLAB. Each subsample consists of four folds grouped into a train set and the fifth fold considered as the test set. Each of the folds within a subsample was made using stratified sampling such that the overall representation of subclasses remained similar in each fold. This will avoid the problems of over-representation prevalent while using random-sampling. In the second step, one of the subsamples is selected. In the third step, half of the trails were randomly chosen from the train set of this subsample and these trials are used for parameter optimization. In the third step, half of the trails were randomly chosen from the train set of this subsample and these trials are used for parameter optimization. In the fourth step, we performed a 3-fold nested cross-validation for choosing the optimal parameters from the grid space. Nested cross-validation ensures that parameter selection and validation are independent, thus preventing the over fit of tuning the parameters to the train set. In the fifth step, the best parameter pair is now used and the best model is trained based on the train set. Further a five-fold cross validation is used for estimating the validation metrics for the train set and the best model is used on the test set to produce validation metrics on the same. In the sixth step, the same procedures from the second to the fifth step are repeated on the next subsample. Thus, 5 different subsamples yield 5 separate test and train set validation metrics.

Validation metrics

The definition of the validation metrics used for evaluating the performance of the classifier are as follows:

(a) Sensitivity: This refers to the ability of a classifier to correctly detect the true class among the classifications made. It is obtained by the (TP/TP + FN). It is also known as recall. TP: True Positives, FN: False Negatives.

(b) Specificity: This refers to the ability of a classifier to correctly ignore the classes that don't belong to the true condition. It is obtained by (TN/TN + FP). TN: True Negatives, FP: False Positives.

(c) F1-score: This is the harmonic mean between precision and recall. Precision refers to measure of exactness of classifier. It is obtained by (TP/TP + FP). Recall refers to the sensitivity of the classifier

Validation

The validation metrics for the different classes ('awake', 'sleep') are shown in Figures 6.9, 6.10. These metrics (>0.8) indicate that the classifier reliably detects awake/sleep periods in train sets and generalizes to new test sets.
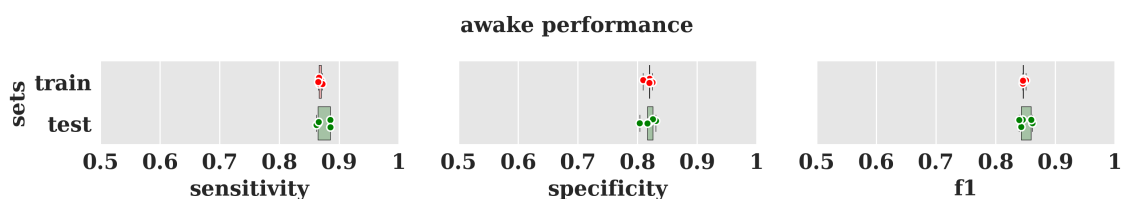
Figure 6.9: Classifier performance metrics for 'awake' class.
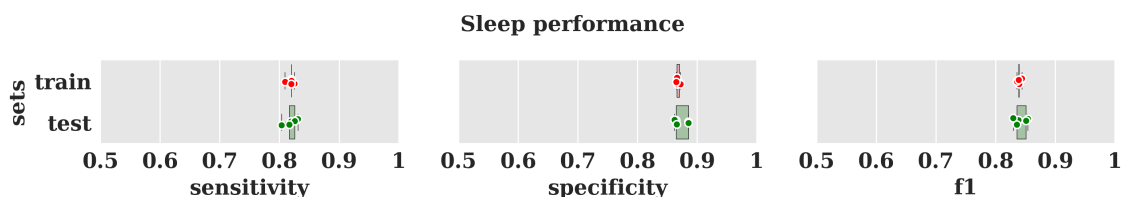
Figure 6.10: Classifier performance metrics for 'sleep' class.

Thus we have designed a classifier based on LFP data for detecting wakefulness levels which can now be used independent of movement (behavioural) parameters.

Predicting transition to Sleep

Next, we were interested in understanding the transition to sleep and thus predict-

ing the occurrence of transition to sleep itself. As mentioned in the previous section, LFP data from 0 to +5minutes is regarded as transition to sleep (where 0 minute is the period when the fly actually stops moving). Usually the LFP data in these segments is ignored. We decided to train the classifier as in the previous section, but this time we considered the time segments from -2 minutes to +5 minutes as transition (with 0 minute being the actual time when the fly stopped moving) and the classifier considered the remaining periods as 'awake' or 'sleep' correspondingly. Next we decided to convert the classifier output from binary prediction ('awake' or 'sleep) into a probabilistic prediction where 0 means highly probable to be 'sleep' and 1 means highly probable to 'awake'. Further we also decided to divide the transition into two types based on the depth of the sleep after the +5minute period. If the fly sleeps only for 5 more minutes or less i.e. if it still sleeps till +10minutes or less, then it is considered as 'light sleep'. Whereas if the fly sleeps for 15 more minutes or more i.e. if it sleeps till +20minutes or above, then it is considered to be 'deep sleep'. This classification is based on (van Alphen, Yap, et al. 2013). For the control analysis, we also took contiguous 7 minutes of data where in the fly was 'awake' and provided the same to the probabilistic classifier. The Figure 6.11, shows that the 'awake' data were all classified well above 0.8 (meaning highly probable to be 'awake'). Further we can see that in the transition, both the 'light sleep' and 'deep sleep' start to move toward 0 (beginning to drift towards the 'sleep' class). Interestingly we can find that at -2 minutes (when the fly is behaviourally active) we can detect that the fly would begin to fall asleep using the classifier. Furthermore we can also detect the depth of the sleep at -2 minutes from the probabilistic classifier.
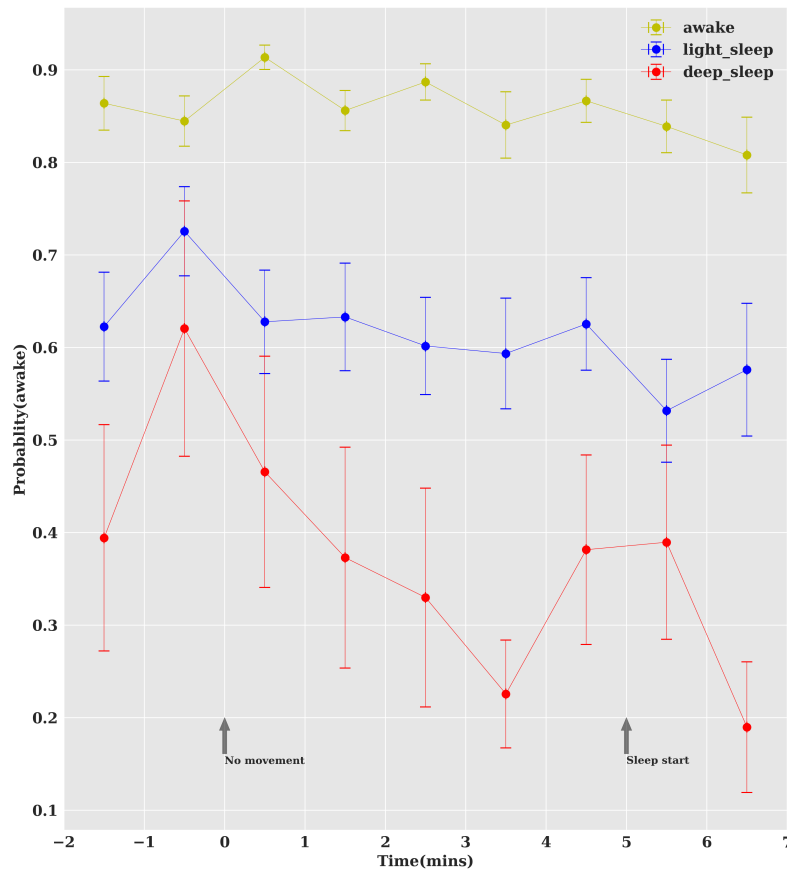
Figure 6.11: Probabilistic classifier predicting sleep and its depth [5]. Transition to sleep in flies can be predicted at 2 minutes before the cessation of movement itself.

6.5.1.3 Multi channel

Selection of flies

As the multichannel experiments were much more invasive (due to insertion of reference electrode and deeper brain probe) we analysed only flies that survived for more than 12 hours in this experiment. 10 flies again survived the 12-hour period and we considered them for further analysis.

Movement analysis

The main goal of this behavioural analysis again was to define periods of 'sleep' and 'awake' based on the immobility periods. As the video output in this experiment (640x480

---

[5](Jagannathan, Jeans, et al. 2018)

pixels) was of much higher quality than the previous two channel differential LFP experiment (27x34 pixels), we decided to not use the pixel subtraction technique. Instead we decided to use the computer vision toolbox OpenCV for quantifying movement from frame to frame. The frame movement detection algorithm consists of the following steps. First, the colour frames were converted to grey scale values. Second, a part of the main scene with the fly at its centre was cropped and used for further analysis. Third, absolute difference was computed between this frame and the previous frame. Fourth, if the difference in each pixel is above a certain threshold value, then the pixel value is set to 255. Fifth, the thresholded image is dilated to fill in the holes in the image. Sixth, contours were detected in the dilated image of the previous step. Seventh, the area occupied by each contour was computed and only if they exceeded a certain threshold then movement is detected. Figure 6.12(A) shows a frame capture used for motion detection, Figure 6.12(B) shows the same frame with green boxes indicating where movement has happened with respect to the previous frame.

As before, fly sleep is defined as immobility of more than 5 minutes. Using the above method we can identify time segments with more than 5 mins or more of inactivity (sleep is counted as starting from the +5th minute onwards). Thus the period from +5th minute to the start of activity again is considered as 'sleep', while the period from 0 to +5 minutes is considered as 'transition' and every other period is considered as 'awake'.
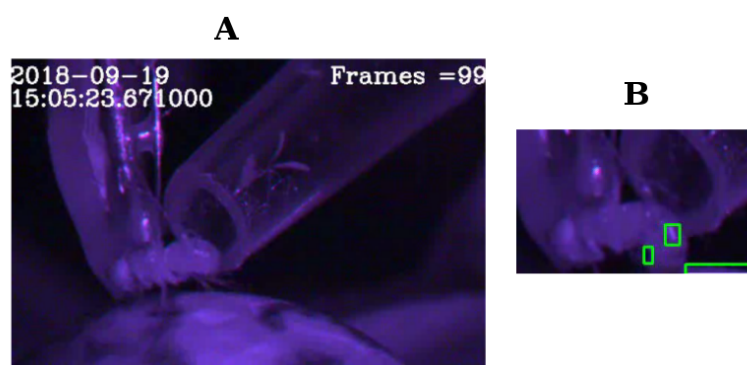
Figure 6.12: Computer vision for movement detection. (A) represents input to the movement detection algorithm. (B) green boxes represent regions where movement is deemed to have taken place when compared to the previous frame.

LFP data

The preprocessing of the LFP data consisted of the following steps. First, raw LFP data in tucker-davis format (tank files) was down sampled to 250 Hz. Second, data was filtered with zero phase shift between 0.5 and 40 Hz using hamming windowed-sinc FIR filter. Third, the timing data in real world format was also added along with the LFP data to make it easier for comparison with the movement analysis. Fourth, the movement data ('1' representing moved, '0' representing not moved) from the analysis in the above section was time-matched and added to each LFP segment. Fifth, LFP data was re-referenced to a neutral electrode among the 16 electrodes. The neutral electrode was chosen using the Calibration procedure from the previous sections. The electrode in which the polarity reversal of the SSVEP occurs is considered to be the neutral electrode for that fly (usually it is electrode #10 or #11).

6.5.1.4 Power spectrum analysis

The main goal of this power spectrum analysis is to understand how different regions of the fly brain change across 'awake' and 'sleep' periods. The power spectrum of individual flies across different conditions ('awake','sleep') is computed as follows. First, data was epoched into segments of 1 minute duration. Second, data was filtered with zero phase shift between 5 and 40 Hz using hamming windowed-sinc FIR filter. Third, the power spectrum was computed per 1 minute bin using the 'spectopo' function in EEGLAB toolbox (Delorme&Makeig 2004) (which computes the mean log spectrum). Fourth, the mean power spectrum per state ('awake', 'sleep') was computed per fly. Sixth, the difference between the states was computed separately per fly. Seventh, we conducted a one sample t-test on this difference (to find if it is statistically different from zero) using the function 'stats.ttest_1sam' from the MNE toolbox (Gramfort, Luessi, et al. 2013). Eighth, the p-value from the previous test was corrected for multiple comparison using the False Discovery rate (FDR) method . The correction was performed using the function 'fdr_correction' from the MNE toolbox. The median differences across 'awake' and 'sleep' states at the group level is plotted in Figure 6.13(A). Further the negative logarithm of the uncorrected p-values are shown in Figure 6.13(B). Further, Figure 6.13(C) shows the

negative logarithm of the p-values corrected by the FDR method where values above 1.30 indicate statistically significant (p<0.05)
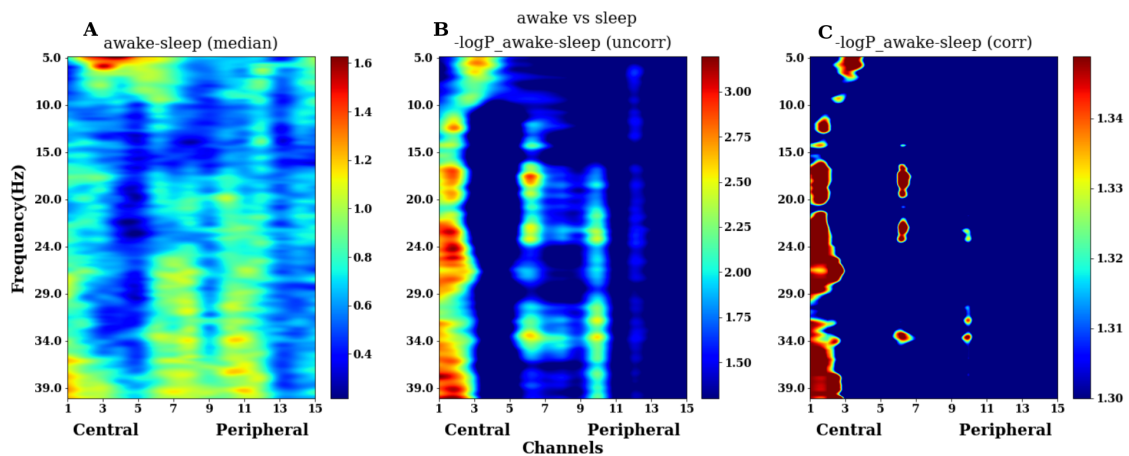
Figure 6.13: Differences in Power spectrum across awake and sleep states. It can be seen from the figure that at central and middle channels. the frequency spectrum changes dependent on the state ('awake', 'sleep') of the fly.

From figure 6.13(C), it is clear that spectral changes in the central channels(#1,#2,#3) are the most prominent when the fly falls asleep. While some middle channels (#6) also show changes between 'awake' and 'sleep' patterns. These changes indicate putative regions in the fly brain that show significant differences in electrophysiology across 'awake' and 'sleep' states.

Thermogenetically induced sleep

The next logical step would be to validate our findings from spontaneous sleep. In this context, we considered data from previously published studies (Yap, Grabowska, et al. 2017) on multi channel recordings. In this study, sleep was induced by thermogenetically manipulating the fly brain. Thermogenetics is the process of activating a group of neurons using heat-activated cation channels from the transient receptor potential (TRP) family (Bernstein, Garrity, et al. 2012). Thermogenetic manipulation were made to induce sleep in flies by activating a group of neurons in the dorsal Fan shaped body (dFSB). The dFSB forms a part of the core network of neurons involved in regulating and triggering sleep in flies (mentioned in detail in the Introduction chapter). In this study, while the flies fell asleep using thermally activated methods, the LFP data was recorded for the whole of the brain using multi-channel recordings (referred to as full-brain probe that

extend to both hemispheres). It was found that activity in the central channels (possibly near the dFSB) increased as the fly fell asleep. Figure 6.14(A) shows the location of the electrodes in the full-brain probe set-up, while Figure 6.14(B) shows the change in power spectrum in the central channels in the range from 2-40 Hz at the group level (n = 7 flies). This causal manipulation indeed validates our findings from the multichannel recordings where the flies were made to fall asleep in a spontaneous manner.
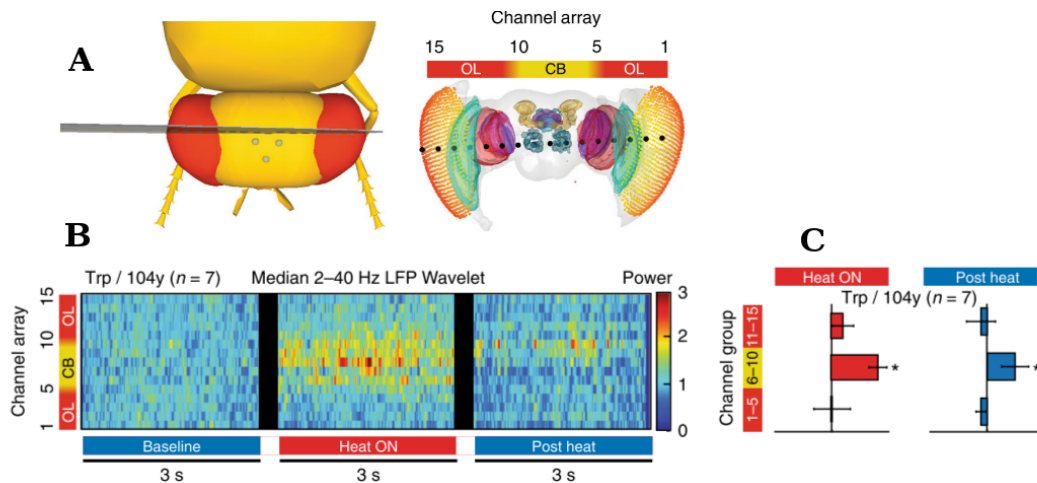
Figure 6.14: Sleep induction through thermogenetics [6]. (A) represents the dorsal view of the electrode insertion, followed by the frontal view of putative locations in the fly brain targeted by the channel array. (B,C) shows that the central channels in the fly brain show the most changes in the frequency spectrum (2-40 Hz) when sleep is triggered by activating the dFSB with thermogenetic methods.

6.6 Summary

In this chapter, we first established a method to track the fly sleep using machine learning methods based on LFP data from the two channel differential set-up. The classifier based on the LFP power spectrum was shown to detect fly sleep in test datasets independent of any behavioural measure (like fly locomotion). This represents an important advancement in the field of drosophila sleep, as it moves the sleep measures from the current behaviour based technique (immobility of more than 5 minutes) to more brain related measures. This has the chance to create an impact much like the EEG studies in the early 1960s (of Recht-shaffen and Kales) that established the presence of different sleep stages in humans. The

---

[6] adapted from (Yap, Grabowska, et al. 2017)

ability to predict sleep before the occurrence of any behavioural change (no movement start) using probabilistic classifiers points to mechanisms in the brain (possibly related to homoeostatic pressure) that are already present even when the fly is completely active. Also the ability of the classifier to predict sleep depth indicates that fly sleep may not be homogeneous and adds further evidence of different sleep stages indicated by other studies (van Alphen, Yap, et al. 2013; Yap, Grabowska, et al. 2017).

Next, we used multi-channel recordings to understand the contribution of different areas in the fly brain in the 'awake' and 'sleep' periods. We showed that the central regions (channels) of the fly brain displayed significant differences in the LFP power spectrum across 'awake' and 'sleep' periods. Further we validated our findings in spontaneous sleep recordings with data from another study (Yap, Grabowska, et al. 2017). In (Yap, Grabowska, et al. 2017) multi-channel recordings (full brain probes) were used to record LFP data across the fly brain while sleep was triggered by activating the dFSB using thermogenetics. We could potentially infer that the central channels in our study were measuring LFPs from the regions around dFSB. Thus providing direct validation and evidence of spontaneous sleep in our data. However in the future, we could use dyes in electrodes and perform dissections of the brain (post insertion) to identify the locations of individual electrodes. Currently, we are in the process of refining this dye based method which could provide direct evidence of the regions from where the LFPs are measured. Also the development of a calibration procedure would enable easier replication of studies with multi channel recordings.

7

General discussion

Every 24-hours we undergo a remarkable transformation and slip into a state of inactivity and become unaware of our surroundings. This process of behavioural quiescence is commonly referred to as sleep. About a third of us will be affected by sleep disorders at some point in our lives[1]. These disorders could range from relatively common problems like insomnia [2] to severely debilitating ones like narcolepsy[3]. Economic costs associated with sleep deprivation in the UK alone are estimated at £40 billion a year[4]. Further, people that sleep less than six hours a day are also 13% more likely to die earlier than their well sleeping counterparts. Thus sleep is an important public health issue that needs utmost attention. Most of the research in sleep has targeted processes that occur after the onset of sleep stage N2. However, we are aware that most of the issues in sleep are also closely related to the process of falling asleep itself and thus the transition from wakefulness to N2 could provide useful insights into sleep disorders.

Tangentially, understanding how the brain loses consciousness in a reversible manner during general anaesthesia is a major challenge in neuroscience. Every year millions of pa-

---

[1]https://www.sleepassociation.org/sleep-disorders/
[2]Refers to inability to falling or staying asleep
[3]Refers to uncontrollable or excessive tendency to sleep
[4]https://www.rand.org/randeurope/research/projects/the-value-of-the-sleep-economy.html

tients around the world undergo surgery with general anaesthesia. About 1% of patients wake up during surgery or are able to recollect events that occurred during surgery which is commonly referred to as anaesthesia with recall (AWR) (Errando, Sigl, et al. 2008). This experience could be particularly traumatic if pain was experienced by the patient but was not detected by doctors during the operation. Though the risk factors associated with AWR are known (drug or alcohol usage etc), the exact mechanisms through which such wakefulness periods occur during general anaesthesia are not fully known. This is mainly because the neural dynamics during induction and recovery from general anaesthesia have not been fully characterised. Recently researchers have shown using mutant flies (Kottler, Bao, et al. 2013) that resistance to anaesthetics like isoflurane are linked with the sleep duration. This further adds evidence to the hypothesis that anaesthetics work through activating the endogenous sleep pathways like dorsal fan shaped body (dFSB). Thus the process of induction to sleep could help us understand the process of induction to anaesthesia and therefore understand the process of AWR.

Both the aforementioned problems, motivated us to understand the process of falling asleep i.e. to understand the behavioural and neural dynamics of transitions of alertness.

7.1 Micro measures algorithm

We first developed a method (micro-measures algorithm) for objectively measuring alertness using EEG in a trial-by-trial manner. Our approach to this problem has been to use machine learning algorithms (SVM) to identify features in the data that can help classify states of alertness. Though this approach is not new in EEG based studies (Tagliazucchi, von Wegner, et al. 2012; Crisler, Morrissey, et al. 2008; Stein 2007), For example, (Tagliazucchi, von Wegner, et al. 2012) implemented a method for tracking alertness fluctuations with a temporal resolution of 30 seconds. While (Crisler, Morrissey, et al. 2008) have implemented similar measures in animals using sleep scoring techniques with temporal resolution similar to 30 seconds. Other methods with temporal resolutions as low

as 1 second have validated their algorithm (Stein 2007) against measures like heart-rate variability (which are indirect measures of drowsiness). This is the first time alertness levels have been measured with a automated technique in temporal resolution as low as 4 seconds and have been directly validated against a well established scale of drowsiness (Hori scale).

The following are the strengths and limitations of our approach in the development of micro-measures algorithm.

7.1.1 Strengths

One of the main advantages of our method is that it has been validated against a reliable system like Hori. Though Hori scoring in practise depends on the expertise of the individual scorer, it has been shown to systematically correlate with behavioural measures like variation in reaction times, cessation of responses etc. Second, the ability of the algorithm to also provide with features like spindle detection, vertex sharp waves, K-complex detection is bound to be useful to sleep researchers. Particularly in closed loop experiments wherein specific stimulus could be delivered based on the sleep state of the participant. Using this approach can extend those experiments to specific graphical features (spindles etc). Third, the ability of the algorithm to track alertness fluctuations in a scale as low as 4-seconds is much more suitable to investigate the dynamic nature of the transitions in the human brain. Fourth, the ability of the algorithm to generalise to independent datasets is most useful to the general neuroscience community, who could use this as a tool to control for alertness in their experiments.

7.1.2 Limitations

The main limitations of this method arise from the usage of Hori scale itself. First, there is a proportion of participants that do not show alpha like patterns in the EEG and in those participants the algorithm could perform poorly. Second, the training dataset for the algorithm is composed of very few trials in certain conditions like Hori level 4 (which is an

intermediate stage, not known to occur in all participants), hence the algorithm will be biased against classifying those trials in the proper category. Third, we have validated the algorithm only against 3 sub classes, however interesting behavioural changes also happen at individual levels in the Hori scale and hence this algorithm would not be sensitive enough to capture those changes. Fourth, the algorithm so far has only been developed for eyes-closed condition however it is well known that participants can sleep or become drowsy even with active tasks like driving. Fifth, the validation metric for the drowsy(severe) class was low, this is mainly because in our dataset, we didn't have enough participants falling asleep with k-complex and spindles etc.

7.2 Mechanisms of alertness induced spatial bias

Spatial attention is considered to be a right hemisphere specialised function (Vallar 1998; Bowers&Heilman 1980; Siman-Tov, Mendelsohn, et al. 2007). Evidence for this specialization has mainly come from studies with stroke patients displaying inattention to the left hemi-field (neglect) (Driver&Mattingley 1998; Halligan, Fink, et al. 2003; Harvey&Rossit 2012; Mort, Malhotra, et al. 2003; Vallar 1998; Karnath 1997). Healthy populations have also been reported to consistently favour the left hemi-field in line bisections tasks, where participants bisect a straight line to the left of the veridical centre (pseudoneglect) (Jewell&McCourt 2000; Bowers&Heilman 1980; Voyer, Voyer, et al. 2012). The most common model accounting for such biases is the right hemisphere dominance model (Mesulam 1981). In this model, spatial attention is lateralised in the right hemisphere and hence right hemisphere is highly dominant under base-line conditions which explains the bias towards the contra-lateral side (left visual field) in the line bisection tasks. Patients that have lesions in the right hemisphere lose such dominance resulting in inattention of the left hemi-field.

Several studies in the past have also reported shift in the bias (due to time-on-task effect) in such line bisection tasks, wherein at the beginning of the task participants display a bias to the left hemi-field which shifts to the right hemi-field over a prolonged duration (Benwell,

Thut, et al. 2013; Manly, Cornish, et al. 2005; Dufour, Touzalin, et al. 2007). Also a minority of participants have a rightward bias and shift in the opposite direction. These findings have led to the suggestion that differences in bias (at baseline) and shift direction is only meaningful, if they underlie genuine observer subtypes (a reliable and stable trait within individuals). Evidence from (Benwell, Thut, et al. 2013) has suggested with line bisection task that indeed such traits (both left and right bias) are reliable (even when tested after days) and hence represent a subtype rather than those that occur due to variation in the sampling process in selecting participants from a homogeneous group (those with right hemisphere dominance). However the same study (Benwell, Thut, et al. 2013) did not find any effect of vigilance or arousal in bias shift across participants using subjective alertness ratings. Thus raising questions over the validity of the right hemisphere dominance model in pseudoneglect.

For the first time using a auditory spatial attention task, we have established the existence of genuine observer subtypes using a baseline session (where participants are alert) followed by a drowsy session (where arousal is modulated). Also we have established the main modulator of the observer subtype as handedness, using not only behavioural measures like multi-level modelling but also with a direct evaluation of bias (with midline shift) using psychophysical techniques. Furthermore, we also used a computational model of decision making in the form of drift diffusion process and showed the difference in drift rates (indicating attentional processes) between left and right-handers to further strengthen handedness as a main modulator of this observer subtype.

Neural mechanisms of bias in visuo-spatial attention has been evaluated by studies (O'Connell, Schneider, et al. 2011; Benwell, Harvey, et al. 2014) with line bisection tasks. Using EEG, they found an increased engagement of right hemispheric regions (specifically ventral attention network). TPJ is shown to be the pivot point in this task that connects the dorsal and ventral attention systems and is shown to be reliably activated in the right hemisphere. Further, using increased perceptual load to bias the attentional system they show that activity in the right TPJ is attenuated resulting in shift of spatial bias in the line bisection task. Finally, several studies (Foxe, McCourt, et al. 2003; Benwell, Harvey, et al. 2014) have also reported the existence of a two stage processing model using ERP anal-

ysis, wherein early activity is localised in the right TPJ, while the later activity located in the right SPL. The initial processing has been isolated to N100[5]which is associated with accumulation of sensory evidence. While the later stages were associated with memory rehearsal or decisional stages.

However, in our study we used MVPA methods for model-free estimation of spatial and temporal signatures and identified the putative neural correlates involved in the generation of alertness induced spatial bias. Using right-handers (under 'alert' conditions) we showed that the direction of stimuli can be reliably decoded from the right hemispheric regions (mainly right parietal, right tempero-parietal). Thus providing more evidence to the right hemispheric model of spatial attention (Mesulam 1981). The spatial locations are also in broad agreement with (Foxe, McCourt, et al. 2003; Benwell, Harvey, et al. 2014). Under drowsy conditions though, the decoding shifts to the left hemisphere. This provides direct evidence of arousal modulated shift in spatial attention which was not found in studies investigating time on task effect on line bisection task (Benwell, Harvey, et al. 2014). Furthermore, our shift in decoding areas provides support for the model of interaction between spatial and non-spatial aspects of attention proposed by (Corbetta&Shulman 2011). Here the dorsal fronto-parietal network responsible for deployment of attention is bilaterally distributed in both hemispheres, while the ventral network responsible for arousal in right lateralised. Under conditions of low alertness, the right hemisphere gets attenuated resulting in bias towards the left side of space. Using left-handers (under 'alert' conditions) we showed that the direction of stimuli can be reliably decoded from the right hemispheric regions. However under drowsy conditions, the decoding of the direction of stimuli is much more bilateral involving regions like both left and right inferior parietal, left and right temporal regions. This provides evidence for the inter-hemispheric competition model of spatial attention (Kinsbourne 1970). Here attention is shifted towards the contra-lateral hemi-field through inhibition of the ipsilateral hemisphere. Under 'alert' conditions, the right hemisphere holds a slight advantage compared to the left hemisphere and hence pulls (biases) the attention towards the right hemi

---

[5]N100 is a negative deflection in event related potential (ERP) recorded with EEG, which occurs around 100 ms of stimulus presentation.

field. Under 'drowsy' conditions, the balance is tilted in favour of the left hemisphere, though the right hemisphere is still active and hence the decoding profile is balanced.

As mentioned earlier, the conclusion of the differential brain regions involved was derived from qualitatively comparing the decoding patterns under different conditions. Hence the involvement of the above mentioned brain regions should be further confirmed by performing statistical analysis either in the source or the sensor space across different conditions.

The following are the strengths and limitations of our approach to understand the behavioural dynamics of alertness induced spatial bias.

7.2.1 Behavioural dynamics of alertness induced spatial bias

7.2.1.1 Strengths

One of the main strengths of this study is the usage of the multilevel modelling to estimate the relationship between error proportion and alertness levels. This is because traditional regression techniques (like rmANOVA) treat every participant in the same manner. However it is well known that in our study different participants fell asleep in different ways, thus producing different number of trials per condition. Hence using such a method that estimates parameters at both the subject and group level helps to produce a better estimation of model parameters. Second, in previous studies (Bareham, Manly, et al. 2014; Bareham, Bekinschtein, et al. 2015) bias shift was quantified by using measures like ($lefterrors-righterrors/totalerrors$), this ignores variability produced by the direction of the stimuli from -59.31° to +59.31°. Using a psychophysical method to approach this problem produces a much more systematic measure of bias (mean of the pscyhometric function). Third, previous studies (Bareham, Bekinschtein, et al. 2015) have used signal detection theory (SDT) to estimate the sensitivity of the observer performing this task. In SDT observer makes a decision based on a single sample of information available. However, the decision making process in a drift diffusion model is much more dynamic and

is drawn from a sequence of samples. Further, the SDT only considers correct and incorrect responses, whereas drift diffusion model considers the shape of the reaction time distributions apart from the response proportion itself. Finally, in drift diffusion model the criteria (boundary separation etc.) is disentangled from the ability (sensitivity).

7.2.1.2 Limitations

In the multilevel models in the study, I made multiple assumptions like assigning a random intercept to the participant id (meaning participants are chosen at random), and assigning a fixed effect to the stimulus type. This could bias the findings because for example, the categorization of the stimuli as 'left', 'right' is arbitrary as the stimulus varies from -59.31° to +59.31° and hence it could also be assigned to the random intercept type. However this is an inherent defect associated with multilevel models. Second the choice of the psychometric function could actually bias the estimates of the mean thereby biasing the estimate the of the subjective mid-line itself. I chose the *'probit'* function based on previous studies involving a 2-choice task. However a better approach would be to systematically choose a link function based on the fit to a group of subjects (like goodness of fit measure etc). Third, I have ignored the 'alert' trials in the drowsy session to systematically to compare across the two extremes (comparing alert session versus drowsy(mild) in drowsy session). This could potentially bias the findings and additional analysis needs to be done to make sure that the difference in the 'alert' trials across sessions are minimal. Fourth, the Deviance information criterion (DIC) is used as a measure to choose the best model in the HDDM, however DIC is known to be biased towards more complex models.

The following are the strengths and limitations of our approach to understand the neural dynamics of alertness induced spatial bias.

7.2.2 Neural dynamics of alertness induced spatial bias

7.2.2.1 Strengths

One of the main advantages of using decoding to understand the neural mechanisms is that we do not impose *a-priori* definitions of temporal or spatial signatures involved in this task. This allows for a model-free approach where the differences across conditions is obtained by the patterns that can discriminate across conditions in a reliable manner. Second, the AUC (as classifier performance measure) can be thought of as a proxy for effect size, and a higher AUC indicates greater discriminability and possibly larger effect size. Third, the electrodes that differ in drift rates, when regressed against trial by trial variation in ERP value concurs with the locations produced by the classifier patterns. This connects the computational model of decision making developed in the previous chapter with the neural markers (identified with decoding) thus providing convergent evidence.

7.2.2.2 Limitations

One of the main limitations in this study is that when right stimuli was presented to right-handers under 'drowsy' conditions, the decoding of responses (correct, incorrect response) was not reliably significant across any time point. This could be due to less number of subjects (10) satisfying the criteria to perform classification. Second the *HD-DMregression* model (for regressing drift diffusion with ERP data) can only produce one regression coefficients per time point at the group level in the sensor space. However to move to source space we need multiple such coefficients, and if we have a higher number of subjects (>60) we could have partitioned the subjects into sub-groups to produce separate regression coefficient per group and further perform source localization. Third, the source localization of patterns was performed without the use of structural information (MRIs) from individual subjects which make the source space interpretations less reliable. Fourth, as the participants were asked to respond as accurately and as quickly as possible, the reaction times are very variable in the drowsy condition, thus motor regions are invariably involved in multiple time points (in decoding) which could confound the analysis.

Fifth, though the neural markers were assessed using the decoding on the sensor data, connectivity measures would be much more useful in directly measuring the information exchange between frontal and parietal regions which are known to change as participants become drowsy (Noreika, Kamke, et al. 2017; Goupil&Bekinschtein 2012).

The following are the strengths and limitations of our approach to understand the dynamics of alertness induced spatial bias modulated by handedness.

7.2.3 Alertness induced spatial bias modulated by handedness

7.2.3.1 Strengths

First, we included left-handers and performed a direct comparison between left and right-handers in terms of behaviour as well as decoding patterns. Second, most studies investigating the effect of handedness do not show any differences in behaviour and only show differences in activation patterns in the brain (for example language studies). Thus claiming different mechanisms for left and right-handers in the brain. However in our study, we have a clear dissociation of behaviour between left and right-handers under drowsy condition. Thus providing us with clinching evidence of the effect of handedness on alertness induced spatial bias.

7.2.3.2 Limitations

The main disadvantage with using left-handers is that they are very heterogeneous (handedness score); as observed from the mid-line shifts wherein nearly equal number of participants shift to the left side and nearly equal number shift to the right side. This makes group analysis of neural patterns more noisy due to divergent patterns being produced by different participants in the same group.

7.3 Transitions in fruit-flies

Evidence for sleep in invertebrates has been far and few in between (van Alphen, Yap, et al. 2013; Eban-Rothschild&Bloch 2008). The initial excitement when fly sleep was discovered about 20 years ago (Hendricks, Finn, et al. 2000; Shaw, Cirelli, et al. 2000) has mainly faded away. This is mainly because the initial expectation was that with the diverse and powerful genetic tools available for *Drosophila*, it would be possible to map the circuits responsible for generating sleep. Further, it was expected that we can identify functional roles of specific kinds of sleep based on the neuroanatomy and specific electrophysiological signatures associated with them. This was mainly driven from possible functions associated with sleep like synaptic homoeostasis (Tononi&Cirelli 2003; Tononi&Cirelli 2006). According to the hypothesis of synaptic homoeostasis(Tononi&Cirelli 2006), sleep essentially serves to downscale synaptic strengths proportionally across the different regions of the brain. This is essential to decrease energy consumption while the rescaling preserves learning and plasticity. It was further proposed that slow wave sleep (0.5- 4 Hz) in mammals may serve this functional purpose. However these expectations of uncovering functional roles have fallen short mainly because researchers have been unable to identify sleep in flies with such slow wave signatures (van Swinderen 2007). This led to the belief that sleep in flies is homogeneous and essentially bimodal in nature.

These views of bimodal sleep started to change when a study (van Alphen, Yap, et al. 2013) discovered that flies indeed sleep in stages. They concluded that duration of sleep in flies does not necessarily equate with the intensity of fly sleep (which is directly measured by levels of arousal threshold). They further hypothesised that sleep in the range of 11-40 Hz would be the most suitable candidate signature that could possibly be associated with synaptic downscaling. Our results with two-channel differential LFP differs from them in several ways. First, we show using probabilistic classifiers designed with support vector machines that sleep duration (sleep depth as per our definition) already has an effect on the transition period (from 0 to 5 minutes), further we show that the sleep depth again can be captured at 2 minutes prior to initiation of no movement activity. These findings indicate that sleep depth is in essence a modulator of sleep intensity and that

sleep of different durations have distinct electrophysiological signatures. It is interesting to note that in the study of (van Alphen, Yap, et al. 2013) arousal threshold experiments were done separately from electrophysiological experiments which could explain the discrepancies.

Further another study (Yap, Grabowska, et al. 2017) decided to compare spontaneous sleep with sleep induction by artificial ways. They primarily activated the so-called sleep switch (dFSB) in the fly brain (Pimentel, Donlea, et al. 2016; Donlea, Thimgan, et al. 2011) by using thermogenetic techniques which produced an increase in 2-40 Hz oscillation. As the two-channel differential LFP in the same study resulted in modulations of frequencies in the range of 1-100 Hz, they concluded that the fly sleep associated with dFSB may be unique and different from the spontaneous sleep. One of the main criticisms of this conclusion is that in the recording set up of the dFSB activated sleep, electrodes covered the full regions of the fly brain (full-brain probe). Hence, they cannot be directly compared to the data from two-channel differential LFP setup. We overcame this limitation and conducted a spontaneous sleep study for the first time with multi-channel recordings (albeit half brain probe). We found that spontaneous sleep was associated with change in frequencies in the range of 2-40 Hz in the central and middle channels. Currently fly dissection protocols are being performed to idenfity the actual target locations in the fly brain. But from previous studies we are confident that the region of the central channels is actually the dFSB in the central complex in the fly brain. This contradicts findings from (Yap, Grabowska, et al. 2017) as we show that indeed spontaneous sleep has spatial and temporal signatures similar to the dFSB based artificial sleep induction.

The following are the strengths and limitations of our approach to understand the dynamics of sleep in *Drosophila*.

7.3.1 Strengths

First, one of the main advantages of using fruit flies is the ability to causally manipulate putative circuits to show how sleep is triggered. I used multichannel spontaneous sleep

recordings to show that central channels (possibly located near the dorsal fan shaped body) differ across 'awake' and 'sleep' conditions. Second, the fruit fly as a sleep model has a distinct advantage of being able to record data for long hours (12-24 hrs) which is difficult with other species.

7.3.2 Limitations

First, the location of multichannel electrodes has not been verified in the current study. They need to be verified with dissection using a dye on the electrode tip to reliably identify the locations being measured. These locations can then be compared with known fly atlases to identify the circuits involved. Second, the arousal threshold in the multichannel sleep settings has not been verified by using a periodic stimuli that disturbs the sleep of the animal. This is crucial as this determines if the fly actually displays increased arousal threshold (one of the hallmarks of sleep) under this set up. Third, the location of electrodes (insertion depth, location) in the two channel differential set up may not be same across flies. This can produce a systematic noise in the recordings which could contribute to noise in very specific frequencies. Fourth, so far we have studied only flies that were alive for atleast 12 hours on the ball (multichannel), however the flies that survived 12 hours could be starving and hence lack of movement that is attributed to sleep could actually be due to tiredness or hunger.

8

Future directions

8.1 Tracking alertness transitions

The micro-measures algorithm could be improved in many ways. First, in the current study the only kernel that was evaluated with the SVM was the Radial Basis function (RBF), we could potentially evaluate other kernels like polynomial functions to make the optimal choice. Second, the algorithm should be checked with varying measures of signal to noise ratio. As EEG data collection methods are highly variable this can cause problems if the algorithm was run with different quality data. Though in our study we only performed minimal preprocessing to ensure that the specifics of preprocessing pipeline does not bias the algorithm. Third, the current epoch duration in the algorithm has been fixed at 4 seconds, however there could be fast paced tasks that lack graphical elements (spindles, k-complex etc.) as participants don't dwell into deeper levels of drowsiness and hence it is important to modify the algorithm for such needs. Fourth, the algorithm needs to be developed for eyes-open condition, this can make it widely applicable in many areas including the industry wherein applications that can track the alertness levels of users (for example truck drivers) are in great demand. Fifth, the algorithm could be trained on large datasets that have large number of individual hori ratings that are verified by

multiple scorers resulting in a large sample of gold standard ratings that can improve the reliability of the algorithm.

8.2 Behavioural dynamics of alertness transitions

The auditory spatial attention task used to measure the behavioural dynamics of transition could be improved in several ways. First, the range of the stimuli can be expanded to include the full spectrum of -90° to +90° to observe the full range of the behavioural effects. Though this can lead to a possible ceiling effect it would be highly informative in the estimate of subjective mid-line with psychometric fits (possibly helpful in choosing the optimal link function). Second, auditory task can be expanded to a visual modality task wherein the participants are made to perform a line bisection task a) while being alert, b) while falling asleep, this could confirm if the spatial bias across sessions also change in a different modality. Third, this task could be modified to include a warning cue which produces temporary improvements in alertness, this can help us understand how phasic alertness impacts the spatial bias. Fourth, the next step in this procedure is to perform this spatial attention task on patients that show typical neglect-like effects and see if a temporary amelioration of alertness using warning cues (like above) improves the performance in this task, thereby confirming neglect as primarily a deficit of alertness that in turn causes deficits in attention. Fifth, we can identify putative regions in the brain (like right superior parietal cortex etc.) and target them with invasive techniques like TMS to study this phenomenon in a causal manner.

8.3 Neural dynamics of alertness transitions

The analysis of neural dynamics in alertness transition can be improved in several ways First, the decoding could be applied on connectivity measures like weighted phase lag index, weighted symbolic mutual information etc. which can reveal how the connectivity patterns help differentiate across different behavioural conditions. Second, following

the previous point we can further connect the trial-by-trial drift rate regression with the change in connectivity values instead of the ERP data. This can show how information flow between regions can be connected to parameters in the computational model.

8.4 Handedness aspects of transitions

First, The analysis of the neural dynamics of both right and left-handers could be tagged to responses (instead of the current way of tagging to stimuli). This could make the response related process uniform across trials and possibly highlight mechanisms which are responsible for generating errors in the right sided stimuli. Second, the trial-by-trial connectivity parameters could be computed that can be correlated with trial-by-trial drift parameters. Further in this model we can again explain the correlation with a continuous parameter (handedness score). This could highlight that handedness is not a binary variable but a continuous variable that reflects on the neural patterns in this spatial attention task in a systematic manner.

8.5 Transitions in fruit-flies

First, the data in the multichannel recordings have so far only been analysed for the electrophysiological correlates of sleep and wake states. However the fly performs a range of activity on the ball like grooming, proboscis extension etc. If the video data was annotated by automated software like *DeeplabCut* (Mathis, Mamidanna, et al. 2018). Further this dataset could be used for investigating the electrophysiological correlates of such natural behaviour, which could further open doors to other questions. Second, the experiment to study spontaneous sleep could be adapted and instead of LFP we can record calcium signals (tagged with GFP) from the whole brain of the fruit-flies. This can provide us with detailed information on connectivity between different structures in the fly brain in different depths of sleep. Furthermore, the recording with calcium imaging is compar-

atively less invasive and hence we can eliminate the higher rate of fly deaths associated with LFP experiments.

Concluding remarks

In summary, this research investigated the neural and behavioural dynamics of alertness transitions across humans and fruit flies. I developed a novel method that can track alertness levels across human participants with EEG in a trial-by-trial manner. Next, I used behavioural tools like multilevel modelling, psychophysics and computational model of the decision making process (drift-diffusion model) to quantify and track these behavioural changes. I next used machine learning tools like decoding to identify temporal and spatial signatures that can drive the differences in behaviour in the previous step. Further, I use handedness as an element of variability to show how different neural signatures can produce differences in behaviour across alertness levels. Finally, I ventured into the fruit fly model to develop classifier that can track sleep and further showed evidence of spontaneous sleep in flies.

A

Appendix - I

A.1 Verification of Source Localisation

In order to verify the source localisation procedure, we performed the following steps. First, We used the EEG data from a sample participant and computed the noise covariance from 0.2 seconds to 0 seconds using the 'shrunk' method. Further the covariance was regularised. Second, the forward solution was computed using the transformation file, source space, beamformer solution computed earlier. Third, the inverse operator was computed by using the noise covariance and the forward solution. Fourth, the inverse operator was applied on the data from the sample participant (snr = 3, lambda2 = 1.0 / snr 2, method = 'MNE'). The MNE method was used instead of the dSPM used earlier as we wanted to have positive and negative amplitude for the source signals and only normal orientations were picked further.
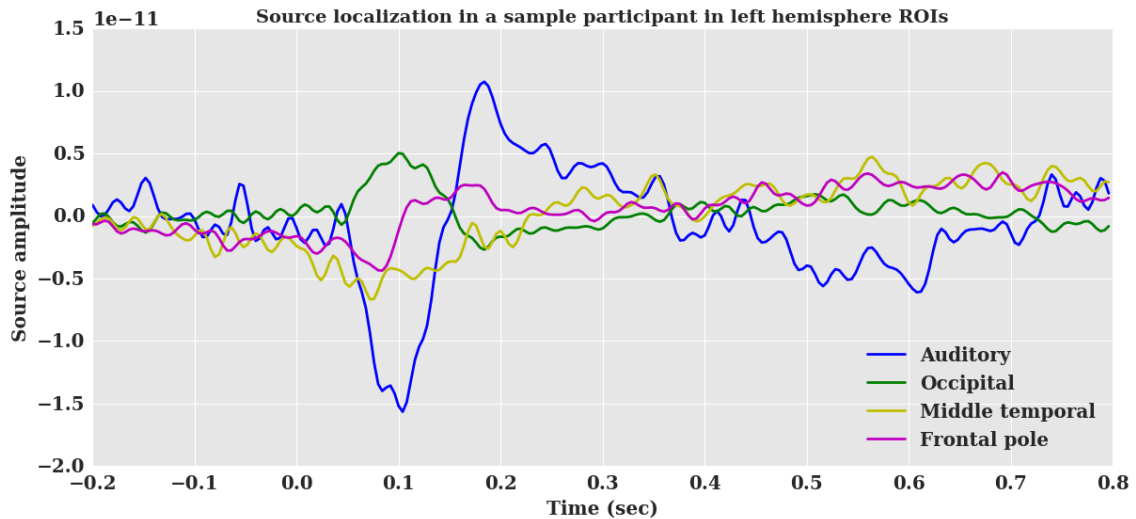
Figure A.1: Source localisation performed in a sample participant in specific left hemisphere regions of interest (ROI). N100 amplitude is clearly visible in the auditory regions, whereas it is diminished in the other regions clearly indicating the validity of the source localisation procedure.

Fifth, we used the labels from the left hemisphere in the regions of auditory, occipital, middle temporal and frontal pole regions to extract signals from these ROIs using the mode of 'mean_flip'. Sixth, we compute the mean across these ROIs to extract a single time course per ROIs in the left hemisphere which is plotted in Figure A.1. It is evident from the figure that N100 amplitude is highly localised in the auditory regions compared to other regions which serves to validate the source localisation used.

Agosto, J., Choi, J. C., Parisky, K. M., Stilwell, G., Rosbash, M., & Griffith, L. C. (2008). Modulation of GABAA receptor desensitization uncouples sleep onset and maintenance in Drosophila. *Nat. Neurosci. 11*(3), 354–359.

Alekoumbides, A. (1978). Hemispheric dominance for language: quantitative aspects. *Acta Neurol. Scand. 57*(2), 97–140.

Alertness Etymology. (1714). https://www.etymonline.com/word/alert?ref=etymonline_crossreference. Accessed: 2019-03-25.

Ali, M. A., Ghoneim, M. M., Ping, S. T. S., & Block, R. I. (1991). Human Learning during General Anaesthesia and Surgery. *BJA: British Journal of Anaesthesia*, *66*(2), 170–178.

Alkire, M. T., Gruver, R., Miller, J., McReynolds, J. R., Hahn, E. L., & Cahill, L. (2008). Neuroimaging analysis of an anesthetic gas that blocks human emotional memory. *Proceedings of the National Academy of Sciences*, *105*(5), 1722–1727.

Andretic, R. & Shaw, P. J. (2005). Essentials of sleep recordings in drosophila: Moving beyond sleep time. Methods in Enzymology, *393*, 759–772.

Annett, M. (1975). Hand preference and the laterality of cerebral speech. *Cortex*, *11*(4), 305–328.

Antognini, J. F. & Schwartz, K. (1993). Exaggerated anesthetic requirements in the preferentially anesthetized brain. *Anesthesiology: The Journal of the American Society of Anesthesiologists*, *79*(6), 1244–1249.

Baharav, A., Kotagal, S., Gibbons, V., Rubin, B. K., Pratt, G., Karin, J., & Akselrod, S. (1995). Fluctuations in autonomic nervous activity during sleep displayed by power spectrum analysis of heart rate variability. *Neurology*, *45*(6), 1183–1187.

Bareham, C. A., Bekinschtein, T. A., Scott, S. K., & Manly, T. (2015). Does left-handedness confer resistance to spatial bias? *Scientific reports*, *5*, 9162.

Bareham, C. A., Manly, T., Pustovaya, O. V., Scott, S. K., & Bekinschtein, T. A. (2014). Losing the left side of the world: Rightward shift in human spatial attention with sleep onset. *Scientific Reports*, *4*, 1–5.

Bartolomeo, P., Thiebaut de Schotten, M., & Doricchi, F. (2007). Left unilateral neglect as a disconnection syndrome. *Cereb. Cortex*, *17*(11), 2479–2490.

Bates, D., Maechler, M., Bolker, B., & Walker, S. (2015a). *lme4: Linear mixed-effects models using Eigen and S4*. Retrieved from https://cran.r-project.org/package=lme4

Bates, D., Maechler, M., Bolker, B. M., & Walker, S. (2015b). Fitting Linear Mixed-Effects Models using lme4.

Baxter, D. M. & Warrington, E. K. (1986). Ideational agraphia: a single case study. *J. Neurol. Neurosurg. Psychiatry*, *49*(4), 369–374.

Becker, E. & Karnath, H. O. (2007). Incidence of visual extinction after left versus right hemisphere stroke. *Stroke*, *38*(12), 3172–3174.

Bekinschtein, T., Cologan, V., Dahmen, B., & Golombek, D. (2009). You are only coming through in waves: wakefulness variability and assessment in patients with impaired consciousness. *Progress in Brain Research*, *177*(C), 171–189.

Bennett, H., Davis, H., & Giannini, J. (1985). Non-verbal response to intraoperative conversation. *British Journal of Anaesthesia*, *57*(2), 174–179.

Benwell, C. S., Thut, G., Learmonth, G., & Harvey, M. (2013). Spatial attention: differential shifts in pseudoneglect direction with time-on-task and initial bias support the idea of observer subtypes. *Neuropsychologia*, *51*(13), 2747–2756.

Benwell, C. S. Y., Harvey, M., & Thut, G. (2014). On the neural origin of pseudoneglect: Eeg-correlates of shifts in line bisection performance with manipulation of line length. *NeuroImage*, *86*, 370–380.

Bernstein, J. G., Garrity, P. A., & Boyden, E. S. (2012). Optogenetics and thermogenetics: Technologies for controlling the activity of targeted cells within intact neural circuits. *Current Opinion in Neurobiology*, *22*(1), 61–71. Neurotechnology.

Berry, R. B., Budhiraja, R., Gottlieb, D. J., Gozal, D., Iber, C., Kapur, V. K., … Tangredi, M. M. (2012). Rules for scoring respiratory events in sleep: Update of the 2007 AASM manual for the scoring of sleep and associated events.

Biebuyck, J. F., Ghoneim, M. M., & Block, R. I. (1992). Learning and Consciousness during General Anesthesia. *Anesthesiology: The Journal of the American Society of Anesthesiologists*, *76*(2), 279–305.

Binder, J., Marshall, R., Lazar, R., Benjamin, J., & Mohr, J. P. (1992). Distinct syndromes of hemineglect. *Arch. Neurol. 49*(11), 1187–1194.

Bishop, D. (1990). *Handedness and developmental disorder*.

Bisiach, E. & Luzzatti, C. (1978). Unilateral neglect of representational space. *Cortex*, *14*(1), 129–133.

Borbély, A. A. (1982). A two process model of sleep regulation. *Human Neurobiology*, *1*(3), 195–204.

Botvinick, M. M., Braver, T. S., Barch, D. M., Carter, C. S., & Cohen, J. D. (2001). Conflict monitoring and cognitive control. *Psychological Review*, *108*(3), 624–652.

Bowen, A., McKenna, K., & Tallis, R. C. (1999). Reasons for variability in the reported rate of occurrence of unilateral spatial neglect after stroke. *Stroke*, *30*(6), 1196–1202.

Bowers, D. & Heilman, K. M. (1980). Pseudoneglect: effects of hemispace on a tactile line bisection task. *Neuropsychologia*, *18*(4-5), 491–498.

Brain, W. R. (1941). Visual disorientation with special reference to lesions of the right cerebral hemisphere. *Brain*, *64*(4), 244–272.

Brown, J. (1970). Get up.

Bryden, M. P., Hecaen, H., & DeAgostini, M. (1983). Patterns of cerebral organization. *Brain Lang*, *20*(2), 249–262.

Buckingham, G. & Carey, D. P. (2009). Rightward biases during bimanual reaching. *Exp Brain Res*, *194*(2), 197–206.

Busch, S., Selcho, M., Ito, K., & Tanimoto, H. (2009). A map of octopaminergic neurons in the Drosophila brain. *J. Comp. Neurol. 513*(6), 643–667.

Chennu, S. & Bekinschtein, T. A. (2012). Arousal modulates auditory attention and awareness: Insights from sleep, sedation, and disorders of consciousness. *Frontiers in Psychology*, *3*, 1–9.

Chokron, S. & De Agostini, M. (1995). Reading habits and line bisection: a developmental approach. *Brain Res Cogn Brain Res*, *3*(1), 51–58.

Chokron, S. & Imbert, M. (1993). Influence of reading habits on line bisection. *Brain Res Cogn Brain Res*, *1*(4), 219–222.

Chung, B. Y., Kilman, V. L., Keath, J. R., Pitman, J. L., & Allada, R. (2009). The GABA(A) receptor RDL acts in peptidergic PDF neurons to promote sleep in Drosophila. *Curr. Biol. 19*(5), 386–390.

Cohen, D., Zalucki, O. H., van Swinderen, B., & Tsuchiya, N. (2016). Local Versus Global Effects of Isoflurane Anesthesia on Visual Processing in the Fly Brain. *eNeuro, 3*(4).

Cohen, J. D., Romero, R. D., Servan-Schreiber, D., & Farah, M. J. (1994). Mechanisms of spatial attention: the relation of macrostructure to microstructure in parietal neglect. *J Cogn Neurosci, 6*(4), 377–387.

Committeri, G., Pitzalis, S., Galati, G., Patria, F., Pelle, G., Sabatini, U., … Pizzamiglio, L. (2007). Neural bases of personal and extrapersonal neglect in humans. *Brain, 130*(Pt 2), 431–441.

Connolly, K. J. & Bishop, D. V. (1992). The measurement of handedness: a cross-cultural comparison of samples from England and Papua New Guinea. *Neuropsychologia, 30*(1), 13–26.

Corbetta, M., Kincade, M. J., Lewis, C., Snyder, A. Z., & Sapir, A. (2005). Neural basis and recovery of spatial attention deficits in spatial neglect. *Nat. Neurosci. 8*(11), 1603–1610.

Corbetta, M. & Shulman, G. L. (2002). Control of goal-directed and stimulus-driven attention in the brain. *Nat. Rev. Neurosci. 3*(3), 201–215.

Corbetta, M., Akbudak, E., Conturo, T. E., Snyder, A. Z., Ollinger, J. M., Drury, H. A., … Shulman, G. L. (1998). A common network of functional areas for attention and eye movements. *Neuron, 21*(4), 761–773.

Corbetta, M. & Shulman, G. L. (2011). Spatial neglect and attention networks. *Annual Review of Neuroscience, 34*(1), 569–599.

Cote, K. A., de Lugt, D. R., & Campbell, K. B. (2002). Changes in the scalp topography of event-related potentials and behavioral responses during the sleep onset period. *Psychophysiology, 39*(1), 29–37.

Coull, J., Frith, C., Büchel, C., & Nobre, A. (2000). Orienting attention in time: Behavioural and neuroanatomical distinction between exogenous and endogenous shifts. *Neuropsychologia, 38*(6), 808–819.

Crisler, S., Morrissey, M. J., Anch, A. M., & Barnett, D. W. (2008). Sleep-stage scoring in the rat using a support vector machine. *Journal of Neuroscience Methods*, *168*(2), 524–534.

Crocker, A. & Sehgal, A. (2008). Octopamine regulates sleep in drosophila through protein kinase A-dependent mechanisms. *J. Neurosci. 28*(38), 9377–9385.

Crocker, A., Shahidullah, M., Levitan, I. B., & Sehgal, A. (2010). Identification of a neural circuit that underlies the effects of octopamine on sleep:wake behavior. *Neuron*, *65*(5), 670–681.

Danckert, J. & Ferber, S. (2006). Revisiting unilateral neglect. *Neuropsychologia*, *44*(6), 987–1006.

Davidson, M. C. & Marrocco, R. T. (2000). Local infusion of scopolamine into intraparietal cortex slows covert orienting in rhesus monkeys. *Journal of Neurophysiology*, *83*(3), 1536–1549.

de Gee, J. W., Colizoli, O., Kloosterman, N. A., Knapen, T., Nieuwenhuis, S., & Donner, T. H. (2017). Dynamic modulation of decision biases by brainstem arousal systems. *eLife*, *6*(Lc), 1–36

Dellatolas, G., Coutin, T., & De Agostini, M. (1996). Bisection and perception of horizontal lines in normal children. *Cortex*, *32*(4), 705–715.

Delorme, A. & Makeig, S. (2004). EEGLAB: an open source toolbox for analysis of single-trial EEG dynamics including independent component analysis. *Journal of Neuroscience Methods*, *134*(1), 9–21.

Diekelmann, S. & Born, J. (2010). The memory function of sleep. *Nat. Rev. Neurosci. 11*(2), 114–126.

Dissel, S., Angadi, V., Kirszenblat, L., Suzuki, Y., Donlea, J., Klose, M., … Shaw, P. A. (2015). Sleep restores behavioral plasticity to drosophila mutants. *Current Biology*, *25*(10), 1270–1281.

Donlea, J. M., Thimgan, M. S., Suzuki, Y., Gottschalk, L., & Shaw, P. J. (2011). Inducing sleep by remote control facilitates memory consolidation in drosophila. *Science*, *332*(6037), 1571–1576.

Doricchi, F. & Tomaiuolo, F. (2003). The anatomy of neglect without hemianopia: a key role for parietal-frontal disconnection? *Neuroreport*, *14*(17), 2239–2243.

References

Driver, J. & Mattingley, J. B. (1998). Parietal neglect and visual awareness. *Nat. Neurosci. 1*(1), 17–22.

Dufour, A., Touzalin, P., & Candas, V. (2007). Time-on-task effect in pseudoneglect. *Exp Brain Res*, *176*(3), 532–537.

Dylan, B. (1970). When you gonna wake up?

Eban-Rothschild, A. D. & Bloch, G. (2008). Differences in the sleep architecture of forager and young honeybees (Apis mellifera). *J. Exp. Biol. 211*(Pt 15), 2408–2416.

Enell, L., Hamasaka, Y., Kolodziejczyk, A., & Nassel, D. R. (2007). gamma-Aminobutyric acid (GABA) signaling components in Drosophila: immunocytochemical localization of GABA(B) receptors in relation to the GABA(A) receptor subunit RDL and a vesicular GABA transporter. *J. Comp. Neurol. 505*(1), 18–31.

Errando, C. L., Sigl, J. C., Robles, M., Calabuig, E., Garcia, J., Arocas, F., … Garcia-Aguado, R. (2008). Awareness with recall during general anaesthesia: a prospective observational evaluation of 4001 patients. *Br J Anaesth*, *101*(2), 178–185.

Fahrenfort, J. J., van Driel, J., van Gaal, S., & Olivers, C. N. (2018). From ERPs to MVPA using the Amsterdam Decoding and Modeling toolbox (ADAM). *Frontiers in Neuroscience*, *12*(JUL).

Fan, J., McCandliss, B. D., Sommer, T., Raz, A., & Posner, M. I. (2002). Testing the efficiency and independence of attentional networks. *J Cogn Neurosci*, *14*(3), 340–347.

Fan, J., McCandliss, B. D., Fossella, J., Flombaum, J. I., & Posner, M. I. (2005). The activation of attentional networks. *NeuroImage*, *26*(2), 471–479.

Farne, A., Buxbaum, L. J., Ferraro, M., Frassinetti, F., Whyte, J., Veramonti, T., … Ladavas, E. (2004). Patterns of spontaneous recovery of neglect and associated disorders in acute right brain-damaged patients. *J. Neurol. Neurosurg. Psychiatry*, *75*(10), 1401–1410.

Faville, R., Kottler, B., Goodhill, G. J., Shaw, P. J., & Van Swinderen, B. (2015). How deeply does your mutant sleep? Probing arousal to better understand sleep defects in Drosophila. *Scientific Reports*, *5*.

Fimm, B., Willmes, K., & Spijkers, W. (2006). The effect of low arousal on visuo-spatial attention. *Neuropsychologia*, *44*(8), 1261–1268.

Fink, G. R., Marshall, J. C., Weiss, P. H., & Zilles, K. (2001). The neural basis of vertical and horizontal line bisection judgments: an fMRI study of normal volunteers. *Neuroimage*, *14*(1 Pt 2), 59–67.

Fischl, B. (2012). FreeSurfer. *NeuroImage*, *62*(2), 774–781

Floel, A., Buyx, A., Breitenstein, C., Lohmann, H., & Knecht, S. (2005). Hemispheric lateralization of spatial attention in right- and left-hemispheric language dominance. *Behav. Brain Res. 158*(2), 269–275.

Fox, J. & Weisberg, S. (2011). *An R Companion to Applied Regression* (Second). Thousand Oaks {CA}: Sage.

Foxe, J. J., McCourt, M. E., & Javitt, D. C. (2003). Right hemisphere control of visuospatial attention: line-bisection judgments evaluated with high-density electrical mapping and source analysis. *Neuroimage*, *19*(3), 710–726.

Friggi-Grelin, F., Coulom, H., Meller, M., Gomez, D., Hirsh, J., & Birman, S. (2003). Targeted gene expression in Drosophila dopaminergic cells using regulatory sequences from tyrosine hydroxylase. *J. Neurobiol. 54*(4), 618–627.

Gelman, A. J. C. H. S. D. D. A. V. D. R. (2013). Bayesian Data Analysis, Third Edition (Chapman & Hall/CRC Texts in Statistical Science): London: Chapman and Hall/CRC.

Gilestro, G. F. (2012). Video tracking and analysis of sleep in drosophila melanogaster. *Nature Protocols*, *7*(5), 995–1007.

Goupil, L. & Bekinschtein, T. A. (2012). Cognitive processing during the transition to sleep. *Archives Italiennes de Biologie*, *150*, 140–154.

Gramfort, A., Luessi, M., Larson, E., Engemann, D., Strohmeier, D., Brodbeck, C., … Hämäläinen, M. (2013). MEG and EEG data analysis with MNE-Python. *Frontiers in Neuroscience*, *7*, 267

Halligan, P. W., Fink, G. R., Marshall, J. C., & Vallar, G. (2003). Spatial cognition: evidence from visual neglect. *Trends Cogn. Sci. (Regul. Ed.) 7*(3), 125–133.

Hampton, A. N. & O'Doherty, J. P. (2007). Decoding the neural substrates of reward-related decision making with functional mri. *Proceedings of the National Academy of Sciences*, *104*(4), 1377–1382.

Hardyck, C. & Petrinovich, L. F. (1977). Left-handedness. *Psychol Bull*, *84*(3), 385–404.

Harvey, M. & Rossit, S. (2012). Visuospatial neglect in action. *Neuropsychologia*, *50*(6), 1018–1028.

Haufe, S., Meinecke, F., Görgen, K., Dähne, S., Haynes, J. D., Blankertz, B., & Bießmann, F. (2014). On the interpretation of weight vectors of linear models in multivariate neuroimaging. *NeuroImage*, *87*, 96–110.

Haynes, P. R., Christmann, B. L., & Griffith, L. C. (2015). A single pair of neurons links sleep to memory consolidation in Drosophila melanogaster. *Elife*, *4*.

He, B. J., Snyder, A. Z., Vincent, J. L., Epstein, A., Shulman, G. L., & Corbetta, M. (2007). Breakdown of functional connectivity in frontoparietal networks underlies behavioral deficits in spatial neglect. *Neuron*, *53*(6), 905–918.

Hendricks, J. C., Finn, S. M., Panckeri, K. A., Chavkin, J., Williams, J. A., Sehgal, A., & Pack, A. I. (2000). Rest in drosophila is a sleep-like state. *Neuron*, *25*(1), 129–138.

Hillis, A. E., Newhart, M., Heidler, J., Barker, P. B., Herskovits, E. H., & Degaonkar, M. (2005). Anatomy of spatial attention: insights from perfusion imaging and hemispatial neglect in acute stroke. *J. Neurosci. 25*(12), 3161–3167.

Huber, R., Hill, S. L., Holladay, C., Biesiadecki, M., Tononi, G., & Cirelli, C. (2004). Sleep homeostasis in Drosophila melanogaster. *Sleep*, *27*(4), 628–639.

Huber, R., Felice Ghilardi, M., Massimini, M., & Tononi, G. (2004). Local sleep and learning. *Nature*, *430*, 78.

Hussey, E. & Novick, J. (2012). The benefits of executive control training and the implications for language processing. *Frontiers in Psychology*, *3*, 158.

Iselin-Chaves, M., Irène A., Willems, P., Sylvie J., Jermann, D. P., Françoise C., Forster, M., Alain, Adam, P., Stéphane R., & Van der Linden, P., Martial. (2005). Investigation of Implicit Memory during Isoflurane Anesthesia for Elective Surgery Using the Process Dissociation Procedure. *Anesthesiology: The Journal of the American Society of Anesthesiologists*, *103*(5), 925–933.

Jagannathan, S. R., Ezquerro-Nassar, A., Jachs, B., Pustovaya, O. V., Bareham, C. A., & Bekinschtein, T. A. (2018). Tracking wakefulness as it fades: Micro-measures of alertness. *NeuroImage*, *176*(April), 138–151.

Jagannathan, S. R., Jeans, R., Yap, M. H. W., Troup, M., Bekinschtein, T. A., & van Swinderen, B. (In prep). Tracking wakefulness in the fly brain. *In prep*.

Jagannathan, S. R., Jeans, R., Yap, M. H. W., Troup, M., Bekinschtein, T. A., & van Swinderen, B. (2018). Tracking wakefulness in the fly brain. *The International Congress of Neuroethology*.

Jewell, G. & McCourt, M. E. (2000). Pseudoneglect: a review and meta-analysis of performance factors in line bisection tasks. *Neuropsychologia*, *38*(1), 93–110.

Johns, M. W. (1991). A New Method for Measuring Daytime Sleepiness: The Epworth Sleepiness Scale. *Sleep*, *14*(6), 540–545

Joiner, W. J., Crocker, A., White, B. H., & Sehgal, A. (2006). Sleep in Drosophila is regulated by adult mushroom bodies. *Nature*, *441*(7094), 757–760.

Kandel, E. R. (2001). The molecular biology of memory storage: A dialogue between genes and synapses. *Science*, *294*(5544), 1030–1038.

Karnath, H. O. (1997). Spatial orientation and the representation of space with parietal lobe lesions. *Philos. Trans. R. Soc. Lond., B, Biol. Sci. 352*(1360), 1411–1419.

Karnath, H. O. (2007). Pusher syndrome–a frequent but little-known disturbance of body orientation perception. *J. Neurol. 254*(4), 415–424.

Karnath, H. O., Christ, K., & Hartje, W. (1993). Decrease of contralateral neglect by neck muscle vibration and spatial orientation of trunk midline. *Brain*, *116 (Pt 2)*, 383–396.

Karnath, H. O., Fruhmann Berger, M., Kuker, W., & Rorden, C. (2004). The anatomy of spatial neglect based on voxelwise statistical analysis: a study of 140 patients. *Cereb. Cortex*, *14*(10), 1164–1172.

Kaufmann, C., Wehrle, R., Wetter, T. C., Holsboer, F., Auer, D. P., Pollmächer, T., & Czisch, M. (2005). Brain activation and hypothalamic functional connectivity during human non-rapid eye movement sleep: an EEG/fMRI study. *Brain*, *129*(3), 655–667.

King, B. S. & Rampil, I. J. (1994). Anesthetic depression of spinal motor neurons may contribute to lack of movement in response to noxious stimuli. *Anesthesiology: The Journal of the American Society of Anesthesiologists*, *81*(6), 1484–1482.

Kinomura, S., Larsson, J., Gulyas, B., & Roland, P. E. (1996). Activation by attention of the human reticular formation and thalamic intralaminar nuclei. *Science*, *271*(5248), 512–515.

Kinsbourne, M. (1970). A model for the mechanism of unilateral neglect of space. *Trans Am Neurol Assoc*, *95*, 143–146.

Kinsbourne, M. (1977). Hemi-neglect and hemisphere rivalry. *Adv Neurol*, *18*, 41–49.

Kirszenblat, L. & van Swinderen, B. (2015). The Yin and Yang of Sleep and Attention. *Trends in Neurosciences*, *38*(12), 776–786.

Kleinman, J. T., Newhart, M., Davis, C., Heidler-Gary, J., Gottesman, R. F., & Hillis, A. E. (2007). Right hemispatial neglect: frequency and characterization following acute left hemisphere stroke. *Brain Cogn*, *64*(1), 50–59.

Knecht, S., Drager, B., Deppe, M., Bobe, L., Lohmann, H., Floel, A., … Henningsen, H. (2000). Handedness and hemispheric language dominance in healthy humans. *Brain*, *123 Pt 12*, 2512–2518.

Knoblauch, K. (2014). *psyphy: Functions for analyzing psychophysical data in R*. Retrieved from https://cran.r-project.org/package=psyphy

Kopp Lugli, A., Yost, C. S., & Kindler, C. H. (2009). Anaesthetic mechanisms: update on the challenge of unravelling the mystery of anaesthesia. *European Journal of Anaesthesiology*, *26*(10), 807–820.

Kottler, B., Bao, H., Zalucki, O., Imlach, W., Troup, M., van Alphen, B., … van Swinderen, B. (2013). A sleep/wake circuit controls isoflurane sensitivity in drosophila. *Current Biology*, *23*(7), 594–598.

Kouider, S., Andrillon, T., Barbosa, L. S., Goupil, L., & Bekinschtein, T. A. (2014). Inducing task-relevant responses to speech in the sleeping brain. *Current Biology*, *24*(18), 2208–2214.

Kruschke, J. K. (2013). Bayesian estimation supersedes the t test. *Journal of Experimental Psychology: General*, *142*(2), 573–603.

Kume, K., Kume, S., Park, S. K., Hirsh, J., & Jackson, F. R. (2005). Dopamine is a regulator of arousal in the fruit fly. *J. Neurosci. 25*(32), 7377–7384.

Lamb, M. R. (1998). The two sides of perception. *Trends in Cognitive Sciences*, *2*(5), 200–201.

Liu, C., Haynes, P. R., Donelson, N. C., Aharon, S., & Griffith, L. C. (2015). Sleep in Populations of Drosophila Melanogaster. *eNeuro*, *2*(4).

Liu, C., Placais, P. Y., Yamagata, N., Pfeiffer, B. D., Aso, Y., Friedrich, A. B., … Tanimoto, H. (2012). A subset of dopamine neurons signals reward for odour memory in Drosophila. *Nature*, *488*(7412), 512–516.

Liu, S., Liu, Q., Tabuchi, M., & Wu, M. N. (2016). Sleep drive is encoded by neural plastic changes in a dedicated circuit. *Cell*, *165*(6), 1347–1360.

Lundell, M. J. & Hirsh, J. (1994). Temporal and spatial development of serotonin and dopamine neurons in the Drosophila CNS. *Dev. Biol. 165*(2), 385–396.

Ly, S., Pack, A. I., & Naidoo, N. (2018). The neurobiological basis of sleep: Insights from drosophila. *Neuroscience Biobehavioral Reviews*, *87*, 67–86.

Magnin, M., Rey, M., Bastuji, H., Guillemant, P., Mauguière, F., & Garcia-Larrea, L. (2010). Thalamic deactivation at sleep onset precedes that of the cerebral cortex in humans. *Proceedings of the National Academy of Sciences*, *107*(8), 3829–3833.

Makos, M. A., Kim, Y. C., Han, K. A., Heien, M. L., & Ewing, A. G. (2009). In vivo electrochemical measurements of exogenously applied dopamine in Drosophila melanogaster. *Anal. Chem. 81*(5), 1848–1854.

Malhotra, P., Coulthard, E., & Husain, M. (2006). Hemispatial neglect, balance and eye-movement control. *Curr. Opin. Neurol. 19*(1), 14–20.

Manly, T., Cornish, K., Grant, C., Dobler, V., & Hollis, C. (2005). Examining the relationship between rightward visuo-spatial bias and poor attention within the normal child population using a brief screening task. *J Child Psychol Psychiatry*, *46*(12), 1337–1344.

Mao, Z. & Davis, R. L. (2009). Eight different types of dopaminergic neurons innervate the Drosophila mushroom body neuropil: anatomical and physiological heterogeneity. *Front Neural Circuits*, *3*, 5.

Marchant, L., Mcgrew, W., & Eibl-Eibesfeldt, I. (1995). Is human handedness universal? ethological analyses from three traditional cultures. *Ethology*, *101*, 239–258.

Marshall, J. C. & Halligan, P. W. (1988). Blindsight and insight in visuo-spatial neglect. *Nature*, *336*(6201), 766–767.

Mathis, A., Mamidanna, P., Cury, K. M., Abe, T., Murthy, V. N., Mathis, M. W., & Bethge, M. (2018). DeepLabCut: markerless pose estimation of user-defined body parts with deep learning. *Nat. Neurosci. 21*(9), 1281–1289.

McIntosh, R., Brodie, E., & MacDonald, J. (1997). Heterogeneity Amongst Patients with Visual Neglect Issues for Diagnosis. *Age and Ageing*, *26*(suppl$_1$), P44-b-P44.

McManus, I. C. (1980). Handedness in twins: a critical review. *Neuropsychologia*, *18*(3), 347–355.

Mesulam, M. M. (1981). A cortical network for directed attention and unilateral neglect. *Ann. Neurol. 10*(4), 309–325.

Mort, D. J., Malhotra, P., Mannan, S. K., Rorden, C., Pambakian, A., Kennard, C., & Husain, M. (2003). The anatomy of visual neglect. *Brain*, *126*(Pt 9), 1986–1997.

Moser, D., Anderer, P., Gruber, G., Parapatics, S., Loretz, E., Boeck, M., … Dorffner, G. (2009). Sleep classification according to AASM and Rechtschaffen Kales: effects on sleep scoring parameters. *Sleep*, *32*(2), 139–149.

Mosidze, V. M., Mkheidze, R. A., & Makashvili, M. A. (1994). Disorders of visuo-spatial attention in patients with unilateral brain damage. *Behav. Brain Res. 65*(1), 121–122.

Nässel, D. R. (1988). Serotonin and serotonin-immunoreactive neurons in the nervous system of insects. *Prog. Neurobiol. 30*(1), 1–85.

Nässel, D. R. (1999). Histamine in the brain of insects: a review. *Microsc. Res. Tech. 44*(2-3), 121–136.

Noreika, V., Canales-Johnson, A., Harrison, W. J., Johnson, A., Arnatkeviciute, A., Koh, J., … Bekinschtein, T. A. (2017). Wakefulness state modulates conscious access: Suppression of auditory detection in the transition to sleep. *bioRxiv*, 1–34.

Noreika, V., Kamke, M. R., Canales-Johnson, A., Chennu, S., Mattingley, J. B., & Bekinschtein, T. A. (2017). Neurobehavioral dynamics of drowsiness. *bioRxiv*, 1–36.

Nunez, M. D., Vandekerckhove, J., & Srinivasan, R. (2017). How attention influences perceptual decision making: Single-trial EEG correlates of drift-diffusion model parameters. *J Math Psychol*, *76*(Pt B), 117–130.

O'Connell, R. G., Schneider, D., Hester, R., Mattingley, J. B., & Bellgrove, M. A. (2011). Attentional load asymmetrically affects early electrophysiological indices of visual orienting. *Cereb. Cortex*, *21*(5), 1056–1065.

Ogilvie, R. D. (2001). The process of falling asleep. *Sleep Medicine Reviews*, *5*(3), 247–270.

Oh, Y., Jang, D., Sonn, J. Y., & Choe, J. (2013). Histamine-HisCl1 receptor axis regulates wake-promoting signals in Drosophila melanogaster. *PLoS ONE*, *8*(7), e68269.

Ojemann, G. A. (1991). Cortical organization of language. *J. Neurosci. 11*(8), 2281–2287.

Okada, R., Awasaki, T., & Ito, K. (2009). Gamma-aminobutyric acid (GABA)-mediated neural connections in the Drosophila antennal lobe. *J. Comp. Neurol. 514*(1), 74–91.

Oken, B., Salinsky, M., & Elsas, S. (2006). Vigilance, alertness, or sustained attention: Physiological basis and measurement. *Clinical Neurophysiology*, *117*(9), 1885–1901.

Oldfield, R. C. (1971). The assessment and analysis of handedness: The Edinburgh inventory. *Neuropsychologia*, *9*(1), 97–113

Oostenveld, R., Fries, P., Maris, E., & Schoffelen, J. M. (2011). FieldTrip: Open source software for advanced analysis of MEG, EEG, and invasive electrophysiological data. *Comput Intell Neurosci*, *2011*, 156869.

Parisky, K. M., Agosto, J., Pulver, S. R., Shang, Y., Kuklin, E., Hodge, J. J., … Griffith, L. C. (2008). PDF cells are a GABA-responsive wake-promoting component of the Drosophila sleep circuit. *Neuron*, *60*(4), 672–682.

Paulk, A. C., Zhou, Y., Stratton, P., Liu, L., & van Swinderen, B. (2013). Multichannel brain recordings in behaving Drosophila reveal oscillatory activity and local coherence in response to sensory stimulation and circuit activation. *Journal of Neurophysiology*, *110*(7), 1703–1721.

Peschel, N. & Helfrich-Förster, C. (2011). Setting the clock–by nature: circadian rhythm in the fruitfly Drosophila melanogaster. *FEBS Lett. 585*(10), 1435–1442.

Petersen, S. E. & Posner, M. I. (2012). The attention system of the human brain: 20 years after. *Annu Rev Neurosci*, *35*, 73–89.

Pimentel, D., Donlea, J. M., Talbot, C. B., Song, S. M., Thurston, A. J. F., & Miesenböck, G. (2016). Operation of a homeostatic sleep switch. *Nature*, *536*, 333.

Pitman, J. L., McGill, J. J., Keegan, K. P., & Allada, R. (2006). A dynamic role for the mushroom bodies in promoting sleep in Drosophila. *Nature*, *441*(7094), 753–756.

Pivik, R. & Busby, K. (1996). Heart rate associated with sleep onset in preadolescent. *Journal of Sleep Research*, *5*(1), 33–36.

Pollack, I. & Hofbauer, A. (1991). Histamine-like immunoreactivity in the visual system and brain of Drosophila melanogaster. *Cell Tissue Res. 266*(2), 391–398.

Porzgen, P., Park, S. K., Hirsh, J., Sonders, M. S., & Amara, S. G. (2001). The antidepressant-sensitive dopamine transporter in Drosophila melanogaster: a primordial carrier for catecholamines. *Mol. Pharmacol. 59*(1), 83–95.

References

Pujol, J., Deus, J., Losilla, J. M., & Capdevila, A. (1999). Cerebral lateralization of language in normal left-handed people studied by functional MRI. *Neurology*, *52*(5), 1038–1043.

Qian, Y., Cao, Y., Deng, B., Yang, G., Li, J., Xu, R., … Rao, Y. (2017). Sleep homeostasis regulated by 5HT2b receptor in a small subset of neurons in the dorsal fan-shaped body of drosophila. *Elife*, *6*.

Raizen, D. M., Zimmerman, J. E., Maycock, M. H., Ta, U. D., You, Y.-j., Sundaram, M. V., & Pack, A. I. (2008). Lethargus is a caenorhabditis elegans sleep-like state. *Nature*, *451*, 569.

Rampil, I. J., Mason, P., & Singh, H. (1993). Anesthetic potency (mac) is independent of forebrain structures in the rat. *Anesthesiology: The Journal of the American Society of Anesthesiologists*, *78*(4), 707–712.

Rampil, I. J. & M.S., M. (1994). Anesthetic potency is not altered after hypothermic spinal cord transection in rats. *Anesthesiology: The Journal of the American Society of Anesthesiologists*, *80*(3), 606–610.

Ratcliff, R., Smith, P. L., Brown, S. D., & McKoon, G. (2016). Diffusion Decision Model: Current Issues and History. *Trends in Cognitive Sciences*, *20*(4), 260–281.

Robertson, I. H., Manly, T., Andrade, J., Baddeley, B. T., & Yiend, J. (1997). 'Oops!': performance correlates of everyday attentional failures in traumatic brain injured and normal subjects. *Neuropsychologia*, *35*(6), 747–758.

Robertson, I. H., Mattingley, J. B., Rorden, C., & Driver, J. (1998). Phasic alerting of neglect patients overcomes their spatial deficit in visual awareness. *Nature*, *395*, 169.

Shaw, P. J., Cirelli, C., Greenspan, R. J., & Tononi, G. (2000). Correlates of sleep and waking in drosophila melanogaster. *Science*, *287*(5459), 1834–1837.

Shulman, G. L., Pope, D. L., Astafiev, S. V., McAvoy, M. P., Snyder, A. Z., & Corbetta, M. (2010). Right hemisphere dominance during spatial selective attention and target detection occurs outside the dorsal frontoparietal network. *J. Neurosci. 30*(10), 3640–3651.

Silver, M. A. & Kastner, S. (2009). Topographic maps in human frontal and parietal cortex. *Trends Cogn. Sci. (Regul. Ed.) 13*(11), 488–495.

Siman-Tov, T., Mendelsohn, A., Schonberg, T., Avidan, G., Podlipsky, I., Pessoa, L., … Hendler, T. (2007). Bihemispheric leftward bias in a visuospatial attention-related network. *J. Neurosci. 27*(42), 11271–11278.

Sinakevitch, I. & Strausfeld, N. J. (2006). Comparison of octopamine-like immunoreactivity in the brains of the fruit fly and blow fly. *J. Comp. Neurol. 494*(3), 460–475.

Sitaraman, D., Zars, M., Laferriere, H., Chen, Y. C., Sable-Smith, A., Kitamoto, T., … Zars, T. (2008). Serotonin is necessary for place memory in Drosophila. *Proc. Natl. Acad. Sci. U.S.A. 105*(14), 5579–5584.

Spiegelhalter, D. J., Best, N. G., Carlin, B. P., & Van Der Linde, A. (2002). Bayesian measures of model complexity and fit. *Journal of the Royal Statistical Society: Series B (Statistical Methodology)*, *64*(4), 583–639.

Stein, M. (2007). Visual and computer-aided identification of vigilance differences in resting eeg between patients with obsessive-compulsive disorder, patients with borderline personality disorder and healthy controls. [german original title: Visuelle und computergestützt]. *Ludwig-Maximilians-University Munich, Munich. Med. Fac.*

Sturm, W., de Simone, A., Krause, B. J., Specht, K., Hesselmann, V., Radermacher, I., … Willmes, K. (1999). Functional anatomy of intrinsic alertness: evidence for a fronto-parietal-thalamic-brainstem network in the right hemisphere. *Neuropsychologia*, *37*(7), 797–805.

Šušmáková, K. & Krakovská, A. (2008). Discrimination ability of individual measures used in sleep stages classification. *Artificial Intelligence in Medicine*, *44*(3), 261–277.

Szczepanski, S. M. & Kastner, S. (2013). Shifting attentional priorities: control of spatial attention through hemispheric competition. *J. Neurosci. 33*(12), 5411–5421.

Tagliazucchi, E. & Laufs, H. (2014). Decoding wakefulness levels from typical fmri resting-state data reveals reliable drifts between wakefulness and sleep. *Neuron*, *82*(3), 695–708.

Tagliazucchi, E., von Wegner, F., Morzelewski, A., Borisov, S., Jahnke, K., & Laufs, H. (2012). Automatic sleep staging using fmri functional connectivity data. *NeuroImage*, *63*(1), 63–72.

Tanaka, H., Hayashi, M., & Hori, T. (1996). Statistical Features of Hypnagogic EEG Measured by a New Scoring System. *Sleep*, *19*(9), 731–738.

Thiebaut de Schotten, M., Urbanski, M., Duffau, H., Volle, E., Levy, R., Dubois, B., & Bartolomeo, P. (2005). Direct evidence for a parietal-frontal pathway subserving spatial awareness in humans. *Science*, *309*(5744), 2226–2228.

Thompson, K. G., Biscoe, K. L., & Sato, T. R. (2005). Neuronal basis of covert spatial attention in the frontal eye field. *Journal of Neuroscience*, *25*(41), 9479–9487.

Tononi, G. & Cirelli, C. (2003). Sleep and synaptic homeostasis: a hypothesis. *Brain Res. Bull. 62*(2), 143–150.

Tononi, G. & Cirelli, C. (2006). Sleep function and synaptic homeostasis. *Sleep Med Rev*, *10*(1), 49–62.

Ueno, T., Tomita, J., Tanimoto, H., Endo, K., Ito, K., Kume, S., & Kume, K. (2012). Identification of a dopamine pathway that regulates sleep and arousal in Drosophila. *Nat. Neurosci. 15*(11), 1516–1523.

Usher, M., Cohen, J. D., Servan-Schreiber, D., Rajkowski, J., & Aston-Jones, G. (1999). The role of locus coeruleus in the regulation of cognitive performance. *Science*, *283*(5401), 549–554.

Vallar, G. (1998). Spatial hemineglect in humans. *Trends Cogn. Sci. (Regul. Ed.) 2*(3), 87–97.

Vallar, G., Guariglia, C., Nico, D., & Bisiach, E. (1995). Spatial hemineglect in back space. *Brain*, *118 (Pt 2)*, 467–472.

Vallar, G. & Perani, D. (1986). The anatomy of unilateral neglect after right-hemisphere stroke lesions. A clinical/CT-scan correlation study in man. *Neuropsychologia*, *24*(5), 609–622.

Vallar, G. (2003). Spatial disorders. In L. Nadel (Ed.), *Encyclopedia of cognitive science*. Nature Publishing Group.

Valles, A. M. & White, K. (1988). Serotonin-containing neurons in Drosophila melanogaster: development and distribution. *J. Comp. Neurol. 268*(3), 414–428.

Van den Heuvel, C. J., Noone, J. T., Lushington, K., & Dawson, D. (1998). Changes in sleepiness and body temperature precede nocturnal sleep onset: Evidence from a polysomnographic study in young men. *Journal of Sleep Research*, *7*(3), 159–166.

van Alphen, B., Yap, M. H., Kirszenblat, L., Kottler, B., & van Swinderen, B. (2013). A dynamic deep sleep stage in drosophila. *Journal of Neuroscience*, *33*(16), 6917–6927.

van Swinderen, B. (2007). 1.28 - sleep in invertebrates. In J. H. Kaas (Ed.), *Evolution of nervous systems* (pp. 451–456). Oxford: Academic Press.

Voyer, D., Voyer, S. D., & Tramonte, L. (2012). Free-viewing laterality tasks: a multilevel meta-analysis. *Neuropsychology*, *26*(5), 551–567.

Walter, W. G. (1964). The convergence and interaction of visual, auditory, and tactile responses in human nonspecific cortex. *Annals of the New York Academy of Sciences*, *112*(1), 320–361.

Watanabe, M., Cheng, K., Murayama, Y., Ueno, K., Asamizuya, T., Tanaka, K., & Logothetis, N. (2011). Attention but not awareness modulates the BOLD signal in the human V1 during binocular suppression. *Science*, *334*(6057), 829–831.

Whitehouse, A. J. & Bishop, D. V. (2008). Cerebral dominance for language function in adults with specific language impairment or autism. *Brain*, *131*(Pt 12), 3193–3200.

Whitehouse, A. J. & Bishop, D. V. (2009). Hemispheric division of function is the result of independent probabilistic biases. *Neuropsychologia*, *47*(8-9), 1938–1943.

Wiecki, T. V., Sofer, I., Frank, M. J., & Hanke, M. (2013). HDDM: Hierarchical Bayesian estimation of the Drift-Diffusion Model in Python

Yap, M. H. W., Grabowska, M. J., Rohrscheib, C., Jeans, R., Troup, M., Paulk, A. C., … van Swinderen, B. (2017). Oscillatory brain activity in spontaneous and induced sleep stages in flies. *Nature Communications*, *8*(1), 1815.

Yuan, Q., Joiner, W. J., & Sehgal, A. (2006). A sleep-promoting role for the Drosophila serotonin receptor 1A. *Curr. Biol. 16*(11), 1051–1062.

Zhang, J., Rittman, T., Nombela, C., Fois, A., Coyle-Gilchrist, I., Barker, R. A., … Rowe, J. B. (2016). Different decision deficits impair response inhibition in progressive supranuclear palsy and Parkinson's disease. *Brain*, *139*(1), 161–173.